NASA CR-174814

ANALYSIS AND TEST EVALUATION OF THE DYNAMIC RESPONSE AND STABILITY OF THREE ADVANCED TURBOPROP MODELS

By
P.N. Bansal, P.J. Arseneaux, A.F. Smith,
J.E. Turnberg and B.M. Brooks

Hamilton Standard Division
United Technologies Corporation
Windsor Locks, Connecticut 06096

August 1985

National Aeronautics and Space Administration
Lewis Research Center
Cleveland, Ohio 44135

Contracts
NAS3-22393
NAS3-22755

1. Report No.	2. Government Accession No.	3. Recipient's Catalog No.
NASA CR-174814		

4. Title and Subtitle	5. Report Date
Analysis and Test Evaluation of the Dynamic Response and Stability of Three Advanced Turboprop Models	August 1985
	6. Performing Organization Code

7. Author(s)	8. Performing Organization Report No.
P.N. Bansal, P.J. Arseneaux, A.F. Smith, J.E. Turnberg and B.M. Brooks	HSER 8945
	10. Work Unit No.

9. Performing Organization Name and Address	11. Contract or Grant No. NAS3-22393 And NAS3-22755. Task I
Hamilton Standard Division United Technologies Corporation Windsor Locks, CT 06096	13. Type of Report and Period Covered Contractor Report

12. Sponsoring Agency Name and Address	14. Sponsoring Agency Code
National Aeronautics and Space Administration Washington, D.C. 20546	

15. Supplementary Notes

Final report. Project Technical Monitor, O. Mehmed
NASA Lewis Research Center, Cleveland, Ohio 44135

16. Abstract

Results of dynamic response and stability wind tunnel tests of three 62.2 cm (24.5 in) diameter models of the Prop-Fan, advanced turboprop, are presented. Measurements of dynamic response were made with the rotors mounted on an isolated nacelle, with varying tilt for non-uniform inflow. One model was also tested using a semi-span wing and fuselage configuration for response to realistic aircraft inflow. Stability tests were performed using tunnel turbulence or a nitrogen jet for excitation. Measurements are compared with predictions made using beam analysis methods for the model with straight blades, and finite element analysis methods for the models with swept blades.

Correlations between measured and predicted rotating blade natural frequencies for all the models are very good. The 1P dynamic response of the straight blade model is reasonably well predicted. The 1P response of the swept blades is underpredicted and the wing induced response of the straight blade is overpredicted. Two models did not flutter, as predicted. One swept blade model encountered an instability at a higher RPM than estimated, showing predictions to be conservative.

17. Key Words (Suggested by Author(s))		18. Distribution Statement
Advanced Turboprop	Flutter	[redacted]ntil September 30, 1987
Aeroelastic Test	Propeller	
Prop-Fan	Wind Tunnel Test	
Energy Efficient		
Structural Response		

19. Security Classif. (of this report)	20. Security Classif. (of this page)	21. No. of Pages	22. Price*
Unclassified	Unclassified	169	

* For sale by the National Technical Information Service, Springfield, Virginia 22161

NASA-C-168 (Rev. 10-75)

PRECEDING PAGE BLANK NOT FILMED

FOREWORD

All of the testing reported herein was performed at NASA facilities under the direction of NASA personnel. Testing of the SR-2C, SR-3 and SR-5 Prop-Fan models in the isolated nacelle configuration was performed at the NASA/Lewis Research Center 8 x 6 foot wind tunnel. Testing of the SR-2C model Prop-Fan in the installed nacelle/wing/fuselage configuration was performed at the NASA/Ames Research Center 14 x 14 foot wind tunnel.

TABLE OF CONTENTS

TABLE OF CONTENTS (Continued)

TABLE OF CONTENTS (Continued)

SUMMARY

Hamilton Standard under contract to NASA/Lewis has completed an evaluation of the dynamic response and stability of three 62.2 cm (24.5 inch) diameter models of the Prop-Fan, an advanced turbopropeller design for future energy efficient transport aircraft which cruise at flight speeds up to 0.8 Mach number. The Prop-Fan has many thin, swept blades which provide for high aerodynamic performance efficiency with low noise.

Wind tunnel tests were conducted on three Prop-Fan models, designated SR-2C, SR-3 and SR-5. The SR-2C model has eight blades of graphite-epoxy composite construction with no sweep. It serves as a base reference configuration since it has unswept blades like conventional propellers. The SR-3 model has eight solid titanium blades with moderate sweep and the SR-5 model has ten solid titanium blades with a larger amount of sweep at the tip. The three models were designed using low thickness ratio blading with varying sweep to operate at 0.8 flight Mach number cruise at 10.667 km (35,000 ft). They each have a nominal diameter of 62.2 cm (24.5 in).

The objective of this program was to determine the vibrational dynamic response and stability characteristics of the three Prop-Fan models operating at a variety of flight conditions, and to compare these test results with analytical predictions. Testing was performed during three different test series. Dynamic 1P response tests were conducted in the NASA/Lewis 8 x 6 foot tunnel, operating the models on an isolated nacelle and varying the rotor centerline tilt angle to provide angular inflow excitation. Stability tests were also conducted at NASA/Lewis with the isolated nacelle at zero tilt angle, and with excitation provided by either natural tunnel turbulence (SR-2C) or by a nitrogen gas jet located behind the rotor (SR-3, SR-5). Additionally, a test was conducted in the NASA/Ames 14 x 14 foot wind tunnel with the SR-2C blades installed on a semi-span fuselage/wing/nacelle model to provide realistic inflow excitation. The isolated nacelle testing at the NASA/Lewis 8 x 6 foot tunnel with the SR-2C blades furnished baseline data for the comparison with the Ames testing.

The analytical methods used included both beam type and finite element analyses for the determination of blade critical speeds, mode shapes and 1P response. The Hamilton Standard developed BESTRAN code and the MSC/NASTRAN code were used for finite element analysis. For analysis of the semi-span wing tests, two flow field analysis methods were used. These are the NASA/Ames HESS code panel method, and the Hamilton Standard HS/H039 code which uses a lifting line wing and Rankine solid nacelle/fuselage. Stability predictions were made using four different aeroelastic methods with varying degrees of sophistication for modeling coupled blade modes and the unsteady, compressible aerodynamics of swept blades.

Early attempts at correlation between experimental results and theoretical results indicated the need for improvement. Therefore, during the course of this study, improvements were made to the various computerized analytical methods used. Comparisons that were made later during this study, with the improved methodology, indicate better correlation.

Results of the analytical studies showed that beam analysis methods can adequately predict the vibratory stresses of long, slender, beam-like blades, such as the SR-2C. However, for the swept blades of the SR-3 and SR-5 models, the beam methods may not adequately model the coupling between the flatwise bending, edgewise bending and torsion modes. Finite element representations are needed to model these blades.

Measured trends for a once-per-revolution (1P) blade response for the three rotor models show a conventional linear increase with airspeed squared (excitation factor). Correlations between measured and predicted 1P stresses for the SR-2C model are reasonable. For the SR-3 and SR-5 models, the 1P stress is considerably underpredicted. The calculated 1P stress is very sensitive to the assumed chordwise and spanwise distributions of aerodynamic loading. By contrast, the measured 1P and 2P stresses for the SR-2C model wing and fuselage tests are overpredicted, although the stress levels are not high. This may be due, in part to extrapolations necessary to match the pretest predictions done for operating conditions differing from those tested.

Predicted values for rotating blade natural frequencies showed good correlation with the measured values for all of the rotor models.

It was found that the natural turbulence of the wind tunnel was insufficient to excite the Prop-Fan models for subcritical modal damping determination. A gas jet was marginally acceptable for exciting the SR-3 and SR-5 models. Using a moving-block analysis, realistic values for modal damping for these rotors were obtained.

The SR-2C and SR-3 models did not flutter during these tests, as was predicted. However, the SR-5 model did encounter an instability threshold over a range of RPM and Mach numbers. The instability threshold rotational speed for the SR-5 decreases with increasing Mach number, blade angle and number of blades on the rotor. The SR-5 model, however, was stable to higher rotational speeds than indicated by analysis, showing the prediction methods to be conservative.

SYMBOLS AND ABBREVIATIONS

b	Blade semi-chord, m
C	Damping
C_c	Critical Damping
C_l	Lift coefficient
C_p	Power coefficient
EF	Excitation Factor = $\psi\ (V_T/644.8)^2(\rho/\rho_o)$, deg
H	Bending displacement, m
K	Stiffness, kg/m
ℓ	Length, m
m	Mass per unit length, kg/m
M	Mach number
M_N	Modal mass, kg
N	Rotational speed, RPM
N_c	Normalized blade chord
P_N	Normalized load
r	Blade radial station, m
RPM	Revolutions per minute
SHP	Shaft horsepower
t	Time, sec
V_a	Blade section axial velocity, m/s
V_t	Blade section tangential velocity, m/s
V_o	Freestream velocity, m/s
V_E	Equivalent air speed, km/hour
V_T	True airspeed, km/hour

α	Aircraft incidence angle, deg
$\beta_{.75}$	Blade angle at 3/4 radius, deg
β_{REF}	Reference blade angle, deg
γ	Sweep parameter = [tan $\Lambda/(\ell/b)$]
ε	Strain, m/m
ζ	Critical damping ratio, C/C_c
θ	Elastic twist displacement, deg
Λ	Local blade sweep angle, deg
Ω	Rotation speed, radians/sec
ρ	Air density (kg/m^3)
ρ_o	Sea level ambient air density (kg/m^3)
σ	Stress, kPa
ψ	Propeller shaft tilt, deg
ω	Frequency, Hz
ω_n	Natural frequency, Hz
1P	Frequency = one per propeller revolution
nP	Frequency = n per propeller revolution

SI units of measurement used throughout unless specified otherwise.

SECTION 1.0
INTRODUCTION

The occurrence of fuel shortages, increased fuel cost and the threat of future worsening conditions for air transportation has caused NASA to sponsor studies of new, more efficient, aircraft and propulsion systems. One of the promising concepts established by these studies is the advanced high speed turboprop, or Prop-Fan. This propulsion system differs from existing turboprops. The Prop-Fan has greater solidity than a turboprop, achieved by more blades of larger chord. The turboprop has straight blades with relatively thick airfoil sections; the Prop-Fan has swept back blades with thin airfoil sections, to enhance performance and reduce noise. The turboprop cruises at no more than 0.65 Mach number; the Prop-Fan is designed to cruise at 0.7 to 0.8 Mach number. The diameter of the Prop-Fan is about 40 to 50% smaller than that of the turboprop. For maximum performance, the Prop-Fan makes use of advanced core engines of the kind being used in modern turbofan engines. Performance is also enhanced by use of a spinner and nacelle aerodynamically contoured to reduce compressibility losses, by retarding the high velocity flow through the root sections of the prop-fan blades.

Utilizing predicted and measured aerodynamic performance data, weight estimates, and noise projections, several Government sponsored studies by both engine and airframe manufacturers have concluded that a fuel savings of approximately 20 to 40%, depending on operating Mach number, should be achieved by a Prop-Fan aircraft, as compared with a high bypass ratio turbofan aircraft. With these encouraging results, a research technology effort has been instituted to establish the design criteria for this new propulsion system.

A major objective in the development of Prop-Fan configurations is to insure the structural integrity of the rotor. Since the Prop-Fan is such a significant departure from conventional propellers, with its highly swept, thin blades, the structural demands are substantial. The high speed operation of highly swept blades imparts large forces to the limited load-bearing material inherent to the thin airfoil sections needed for efficient performance. It is imperative that the rotor be able to absorb the aerodynamic loads at all operating conditions, as well as the centrifugal loads associated with its unique shape and construction. The steady-state dynamic response of the blades must be low and flutter instabilities must be avoided, for safe operation.

In this report are summarized the results of dynamic response and stability tests of three Prop-Fan model designs. Strain gage measurements were made for these models operating on an isolated nacelle over a range of rotational and flight speeds, shaft powers, and inflow angles. Also, testing was performed on one model design installed on a simulated fuselage and wing to determine the response of the rotor to excitation from a realistic flow field. Analytical predictions of blade responses for these operating conditions were made for comparison with test results. The comparisons were used to evaluate the accuracy of the analytical prediction methods and to increase their utility and effectiveness as Prop-Fan design tools.

SECTION 2.0
TEST PROGRAM

2.1 MODEL DESCRIPTION

Three Prop-Fan model configurations, The SR-2C, SR-3, and SR-5 were used for dynamic response and stability testing on the isolated nacelle installation. Testing was also performed with the SR-2C model installed on a simulated wing and fuselage.

The Prop-Fan concept incorporates thin airfoils and blade sweep to achieve high aerodynamic efficiency with low noise generation. An envisioned Prop-Fan installation is shown in Figure 2-1. Detailed discussions of the Prop-Fan concept are given in References 1 to 3. The SR-3 model was the first to be designed specifically for low noise using an early methodology developed at Hamilton Standard, as described in References 4 and 5. The SR-2C (straight blade) model geometry was included in the program as a reference for evaluating the effect of sweep in the tip sections. The 'C' designation indicates that this model was constructed from composite materials to evaluate their structural properties. The SR-5 model was designed using improved aerodynamic and acoustic methodologies (see Reference 6), resulting in a configuration with a greater number of blades and more blade sweep than earlier models.

All three blade models were designed to operate at 0.8 flight Mach number and 10.667 km (35,000 ft) altitude. The overall characteristics of these models are compared in Figure 2-2. All the models have a nominal diameter of 62.2 cm (24.5 in.). The SR-3 and SR-5 model blades are constructed of solid titanium, whereas the SR-2C model blades are constructed of solid graphite-epoxy composite with a metal ferrule at the shank for retention purposes in the hub.

Strain gage locations for the SR-2C model blade are shown in Figure 2-3. Note in Figure 2-3 that the strain gage installation for the NASA/Lewis (isolated nacelle) tests differed from the installation for the NASA/Ames (wing/fuselage) tests. Strain gage locations for the SR-3 model are shown in Figure 2-4, and the strain gage installation for the SR-5 model is shown in Figure 2-5. A more complete description of the SR-5 model is given in Reference 6.

2.2 TEST INSTALLATIONS

This Prop-Fan model test program encompassed three different types of testing. Each test examined a separate aspect of the rotor vibrational behavior. Testing was performed at the NASA/Lewis 8 x 6 foot wind tunnel, described in Reference 7, and the NASA/Ames 14 x 14 foot wind tunnel (Reference 8).

2.2 (Continued)

One test series was conducted to determine Prop-Fan model 1P response. This was done in the NASA/Lewis tunnel, by operating the model on an axisymmetric, isolated nacelle with various angles of shaft tilt, to provide nonuniform inflow excitation. This is the same nacelle that was used for the majority of Prop-Fan testing done at NASA/Lewis. The SR-2C, SR-3 and SR-5 models were tested in this manner. A typical test installation is shown in Figure 2-6.

A second test series was performed at NASA/Lewis to determine the stability boundaries for Prop-Fan model operation. For this test, the models were operated on the isolated nacelle with zero shaft tilt angle. The models were excited by either natural tunnel turbulance (SR-2C), or by a jet pulse located behind the rotor (SR-3 and SR-5). A photograph of the jet pulse installation is shown in Figure 2-7.

The third test series was conducted at NASA/Ames using a half-span simulated fuselage, wing and nacelle installation. This was designed to provide realistic excitation to the Prop-Fan model rotor. The SR-2C model was used for this test. A photograph of the installation is shown in Figure 2-8 and the test is described schematically in Figures 2-9, and 2-10.

2.3 TEST PROCEDURE

The conditions for the three Prop-Fan model test series described above, including the ranges of operating parameters which were varied, are summarized in Table 2-I. Note that for the stability tests, the SR-3 model was tested in both the full 8 blade configuration and a 4 blade configuration. Also, the SR-5 model was tested in a full 10 blade configuration, a 5 blade configuration, and a 2 blade configuration.

The operating procedure was to set the Prop-Fan blade angle prior to tunnel startup. the wind tunnel was then brought up to operating speed with the Prop-Fan in the windmill (unpowered) condition and the model shaft tilt angle at zero degrees. Finally, the shaft tilt angle was set and the Prop-Fan was powered to the rotational speeds desired.

All of the testing at these NASA facilities was performed under the direction of NASA personnel. Hamilton Standard participated in these tests. This participation included a review of the NASA blade structural response measurement systems, calibration of the blade strain gage channels, and reviews of the test plans with NASA tunnel operating personnel. Model critical speeds and potentially hazardous operating conditions were identified, and model and tunnel operating procedures were established to ensure safe recovery from the onset of blade flutter or unexpected structural response. During the conduct of each test, blade response was monitored to ensure safe operation within the prescribed blade stress limits. Signal quality for recorded data was also monitored. A log was maintained of the conditions tested, the parameters that limited each run series, the critical speeds encountered, and the blade stress levels and frequencies associated with conditions producing significant structural response.

TABLE 2-I. TEST CONDITIONS

FACILITY & TEST TYPE	PROP-FAN MODEL	NO. BLADES	WIND TUNNEL MACH NO.	RPM	REF. BLADE ANGLE (DEG)*	SHAFT TILT ANGLE (DEG)	FUSELAGE ANGLE OF ATTACK (DEG)	APPROX. DATES OF TEST
NASA-LEWIS 1P RESPONSE (8x6 FT WIND TUNNEL)	SR-2C	8	0.36-0.90	4000-9000	38.1-59.7	0 TO 15	–	APRIL 1980
	SR-3	8	0.35-0.85	3600-90100	45.0-60.7	0 TO 15	–	DEC. 1980
	SR-5	10	0.36-0.85	2700-9000	49.1-72.9	-1 TO 15	–	AUG. 1981
NASA-LEWIS STABILITY (8x6 FT WIND TUNNEL)	SR-2C	8	– INSUFFICIENT AERODYNAMIC EXCITATION –				–	APRIL 1980
	SR-3	4	0.8-0.85	7000-9000	59.0-60.8	0	–	JUNE 1980
		8	0.8-0.85	7000-9000	57.7 61.0	0	–	APRIL 1981
	SR-5	2,5&10	0.7-0.85	4700-6750	69.0-73.0	0	–	JUNE 1981
NASA-AMES INSTALLED SR-2C RESPONSE (14x14 FT WIND TUNNEL)	SR-2C	8	0.6-0.85	6430-9000	50.7-57.0	–	-3 TO 5	NOV. 1980

* $\beta_{REF} = \beta_{.75} - 0.8$ FOR THE SR-2C AND SR-3 MODELS

$\beta_{REF} = \beta_{.75} + 0.5$ FOR THE SR-5 MODEL

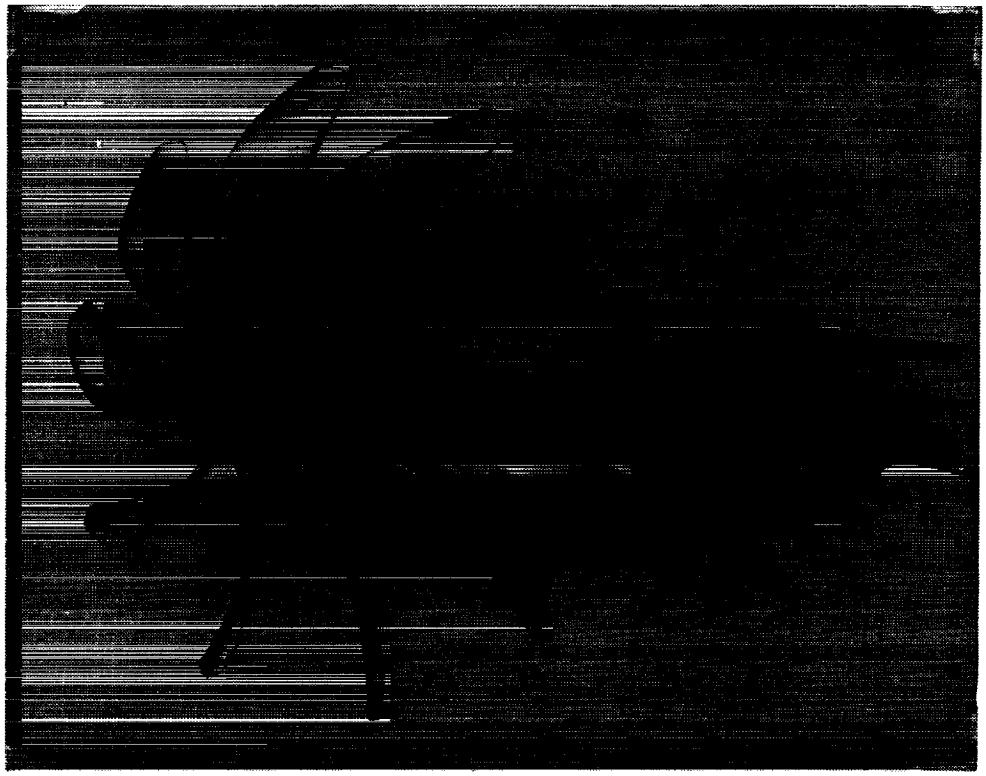

FIGURE 2-1. FUTURE PROP-FAN PROPULSION SYSTEM

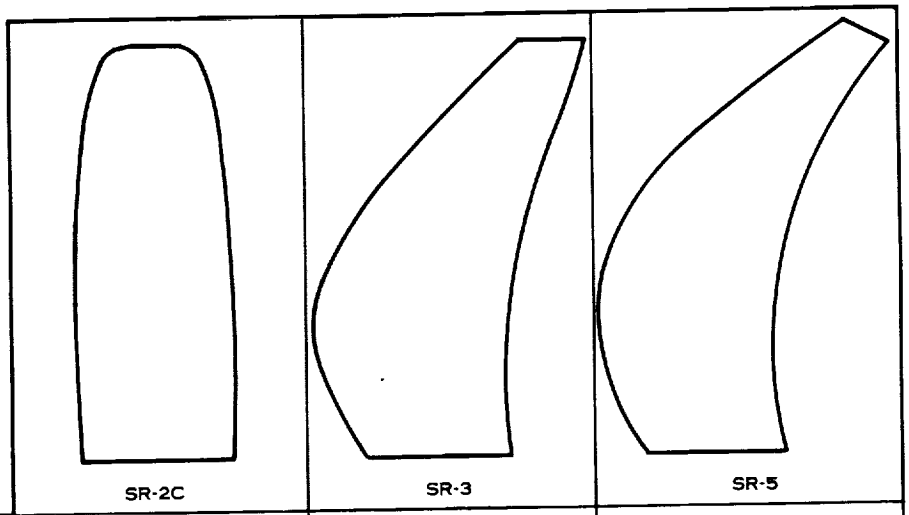

	SR-2C	SR-3	SR-5
NUMBER OF BLADES	8	8	10
ACTIVITY FACTOR/BLADE, AF	203	235	210
INTEGRATED DESIGN LIFT COEFFICIENT, C_L	0.084	0.214	0.271
BLADE AERODYNAMIC TIP SWEEP, DEGREES	0	34.5	48
POWER LOADING KW/M^2 (SHP/FT^2)	300 (37.5)	300 (37.5)	208 (26)
TIP SPEED M/S (FPS)	244 (800)	244 (800)	183 (600)
POWER COEFFICIENT, C_P	1.695	1.695	2.786
ADVANCE RATIO, J	3.056	3.056	4.075
CRUISE EFFICIENCY, PERCENT	76.4	78.4	78.6[2]
CRUISE NOISE[1], dB	150.3	144.5	136.6[2]

(1) MAXIMUM SIDELINE NOISE AT BLADE PASSAGE FREQUENCY
(2) CALCULATED FOR ELASTIC BLADES; DEFLECTIONS REDUCE CAMBER AND TWIST OF STATIC BLADES

FIGURE 2-2. COMPARISON OF OVERALL CRUISE DESIGN CHARACTERISTICS AND BLADE PLANFORMS FOR THREE PROP-FAN MODELS

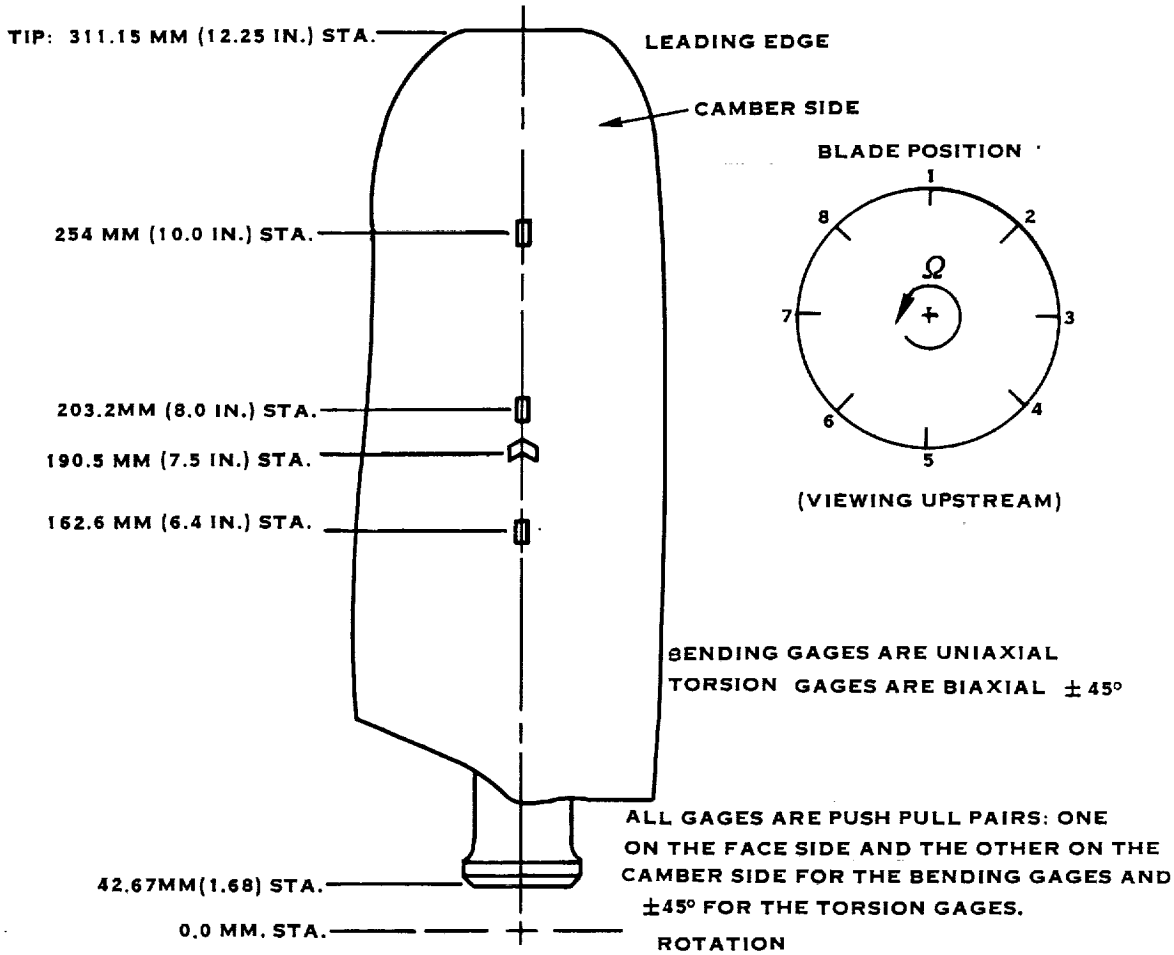

NASA/LEWIS (ISOLATED NACELLE) TESTS		
GAGE TYPE	GAGE LOCATION, MM (IN.)	BLADE NO.
FLATWISE BENDING	162.6 (6.4) IN BOARD	1
FLATWISE BENDING	162.6 (6.4) IN BOARD	3
TORSION	190.5 (7.5) VEE	3
FLATWISE BENDING	254.0 (10.0) TIP	5
TORSION	190.5 (7.5) VEE	7
NASA/AMES (WING/FUSELAGE) TESTS		
GAGE TYPE	GAGE LOCATION, MM (IN.)	BLADE NO.
FLATWISE BENDING	162.6 (6.4) IN BOARD	5
FLATWISE BENDING	203.2 (8.0) MID-BLADE	5
FLATWISE BENDING	162.6 (6.4) IN BOARD	6
TORSION	190.5 (7.5) VEE	6
FLATWISE BENDING	162.6 (6.4) IN BOARD	8
FLATWISE BENDING	254.0 (10.0) TIP	8

FIGURE 2-3. SR-2C MODEL PROP-FAN BLADE STRAIN GAGE INSTALLATIONS

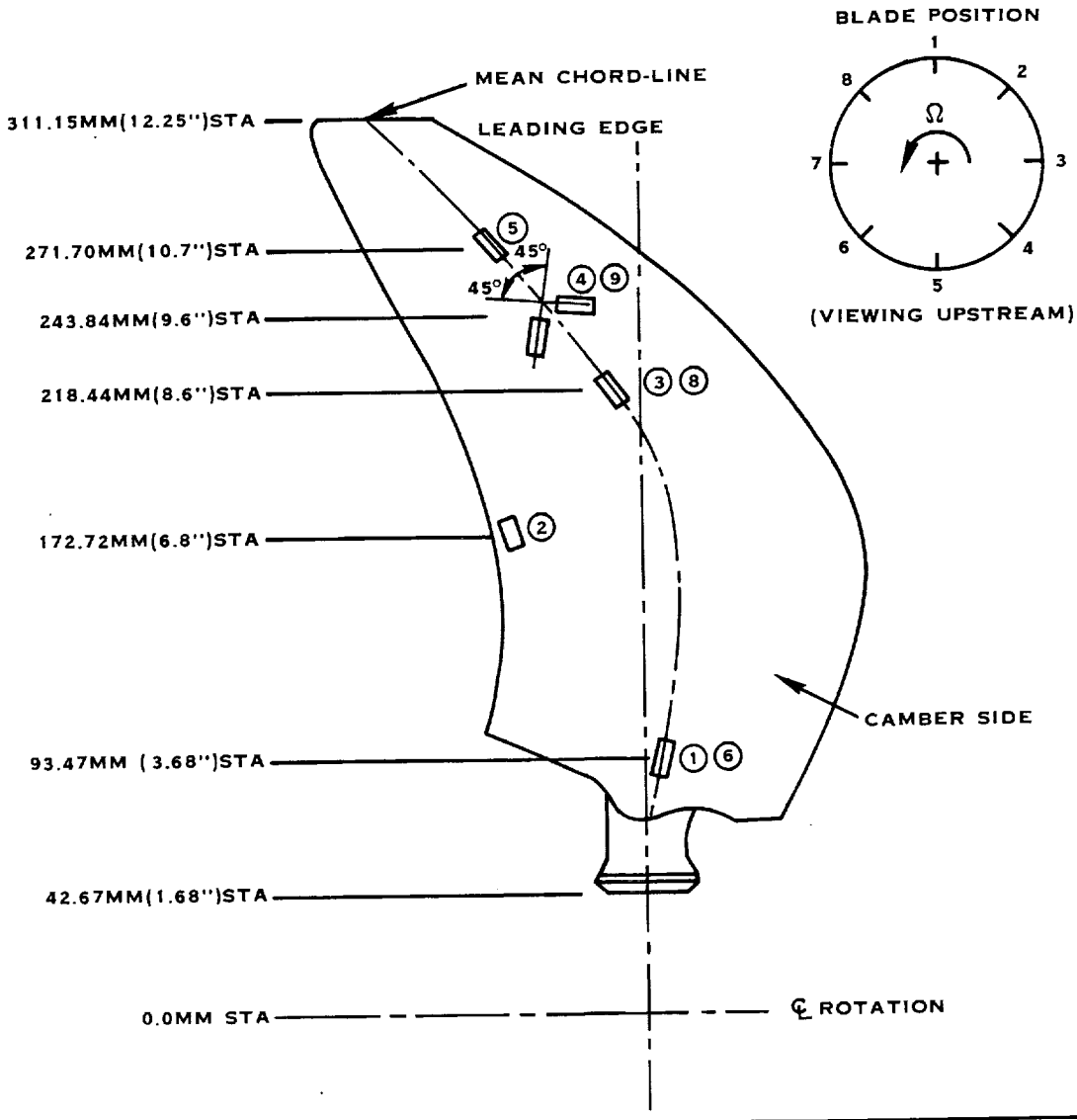

NASA/LEWIS (ISOLATED NACELLE) TESTS		
GAGE TYPE	GAGE LOCATION	DESIGNATION
INBOARD BENDING	93.47MM(3.68)STA - BLADE NO. 1	BG-1
"	93.47MM(3.68)STA - BLADE NO. 5	BG-6
TRAILING-EDGE BENDING	172.72MM(6.8")STA - BLADE NO. 1	BG-2
MID-BLADE BENDING	218.44MM(8.6")STA - BLADE NO. 1	BG-3
"	218.44MM(8.6")STA - BLADE NO. 5	BG-8
MID-BLADE TORSION	243.84MM(9.6")STA - BLADE NO. 1	BG-4
"	243.84MM(9.6")STA - BLADE NO. 5	BG-9
TIP BENDING	271.78MM(10.7")STA - BLADE NO. 1	BG-5

FIGURE 2-4. SR-3 MODEL PROP FAN BLADE STRAIN GAGE INSTALLATION

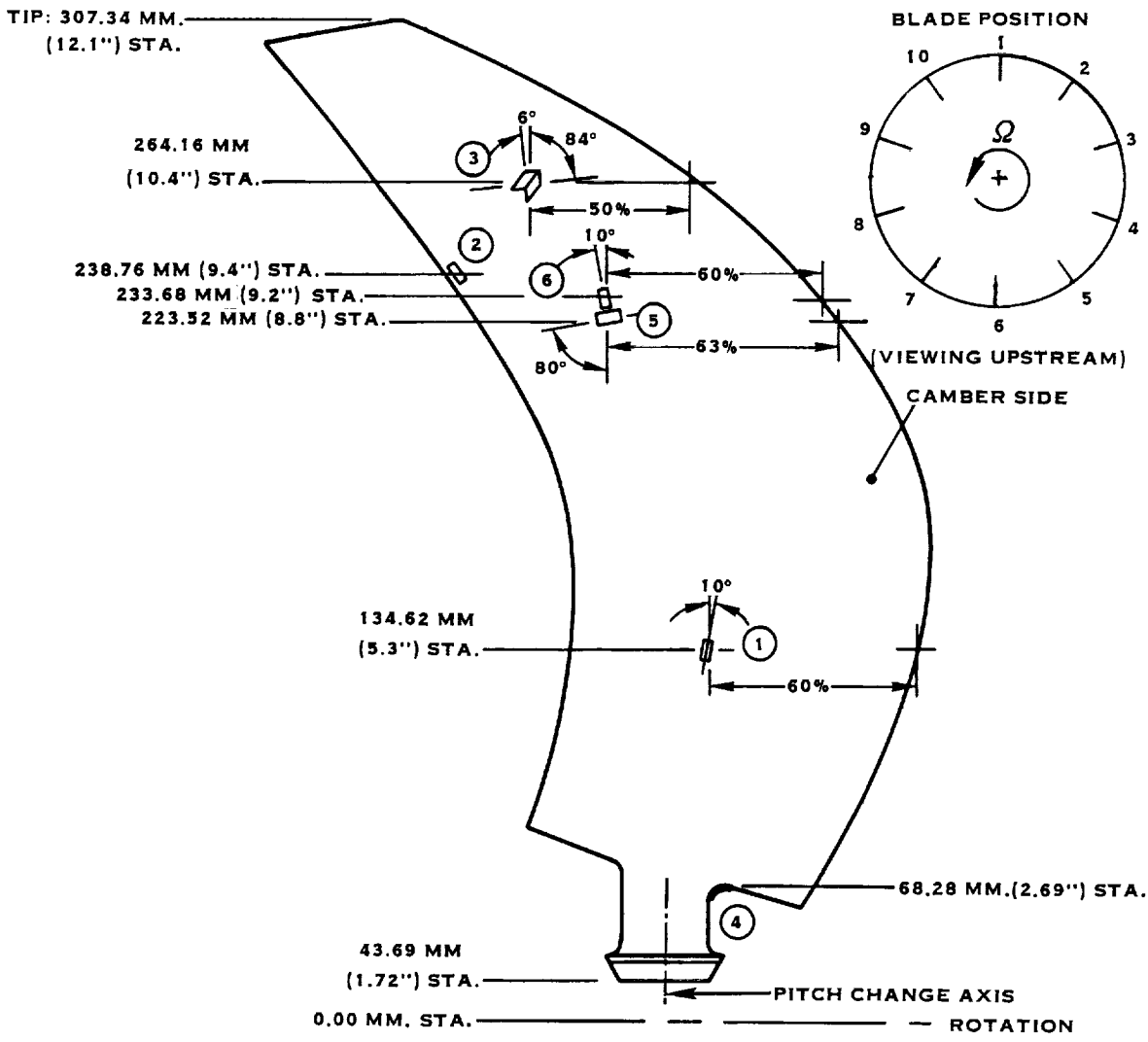

FIGURE 2-5. SR-5 MODEL PROP-FAN BLADE STRAIN GAGE INSTALLATION

NASA/LEWIS (ISOLATED NACELLE) TESTS		
GAGE TYPE	GAGE LOCATION	DESIGNATION
FLATWISE BENDING	134.62 MM.(5.3") IN BOARD	BG1-1
FLATWISE BENDING	134.62 MM.(5.3") IN BOARD	BG2-1
FLATWISE BENDING	134.62 MM.(5.3") IN BOARD	BG6-1
FLATWISE BENDING	238.76 MM.(9.4") TRAILING EDGE	BG1-2
TORSION	264.16 MM.(10.4") TIP-VEE	BG1-3
TORSION	264.16 MM.(10.4") TIP-VEE	BG6-3
EDGEWISE BENDING	68.28 MM.(2.69") SHANK	BG1-4
CHORDWISE BENDING	223.52 MM.(8.8") MID-BLADE	BG1-5
FLATWISE BENDING	233.68 MM.(9.2") MID-BLADE	BG1-6

FIGURE 2-6. SR-3 MODEL PROP-FAN INSTALLED FOR ISOLATED NACELLE TESTING IN THE NASA/LEWIS 8 X 6 FOOT WIND TUNNEL

ORIGINAL PAGE
COLOR PHOTOGRAPH

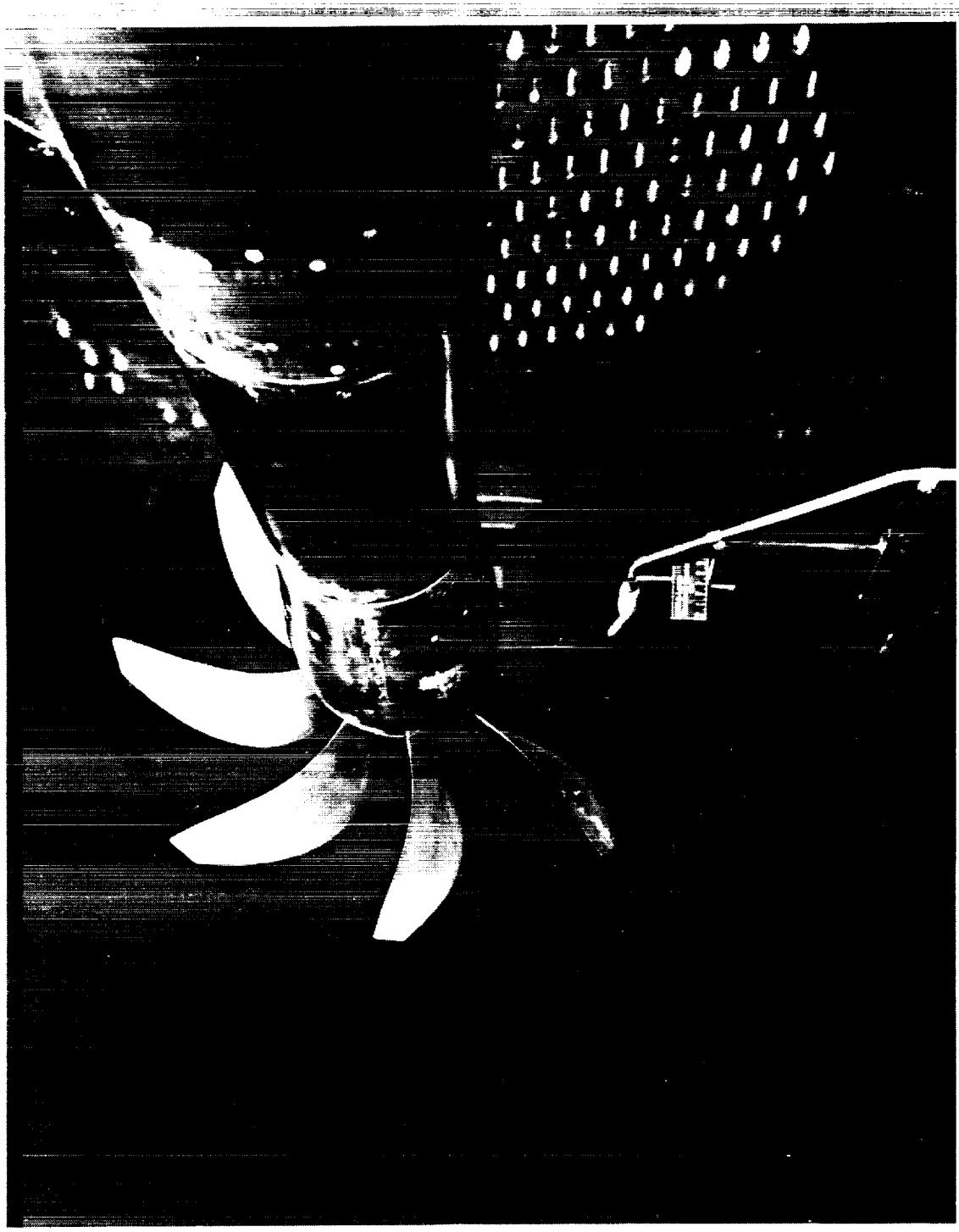

FIGURE 2-7. SR-3 PROP-FAN MODEL WITH AIR-JET EXCITATION AT NASA-LEWIS, JULY 1980

FIGURE 2-8. NASA MODEL INSTALLED IN AMES 14-FOOT TUNNEL

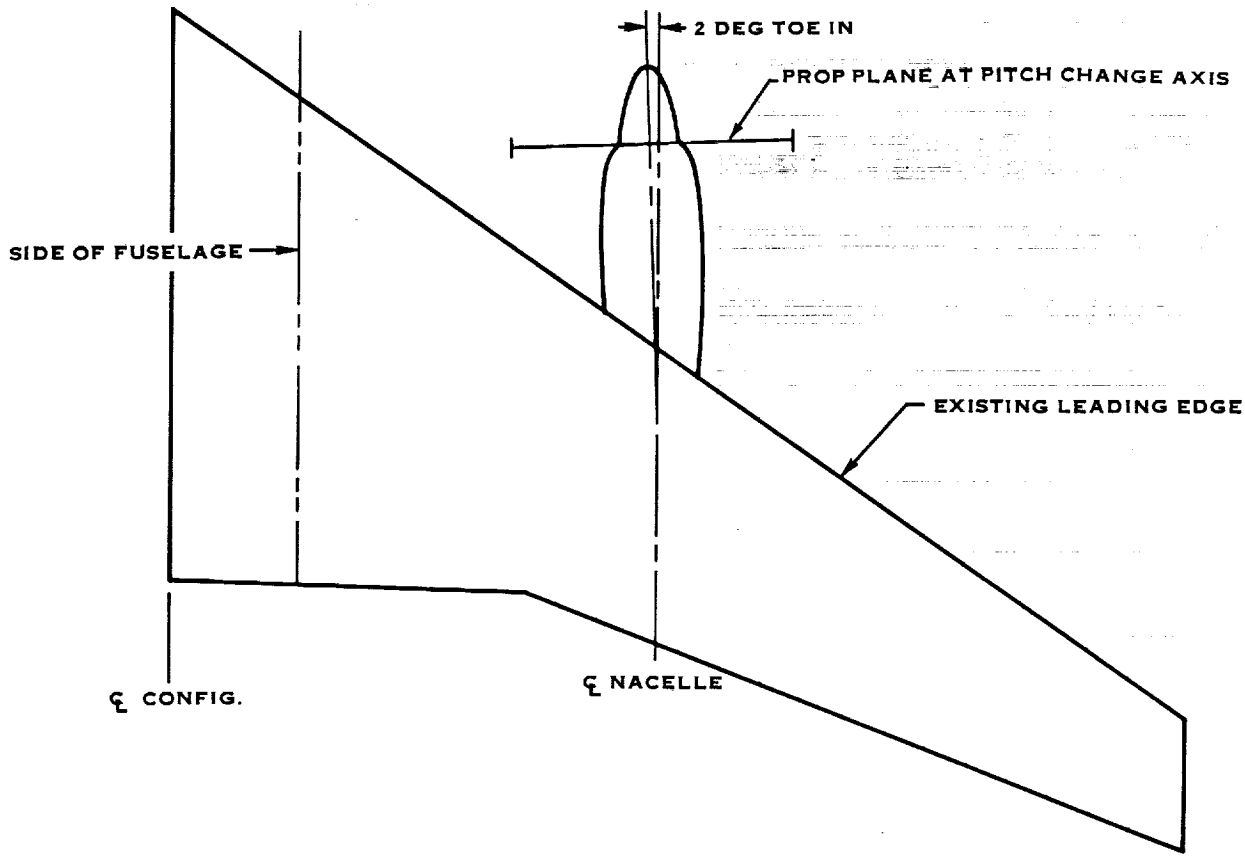

FIGURE 2-9. NASA/AMES MODEL PLANFORM

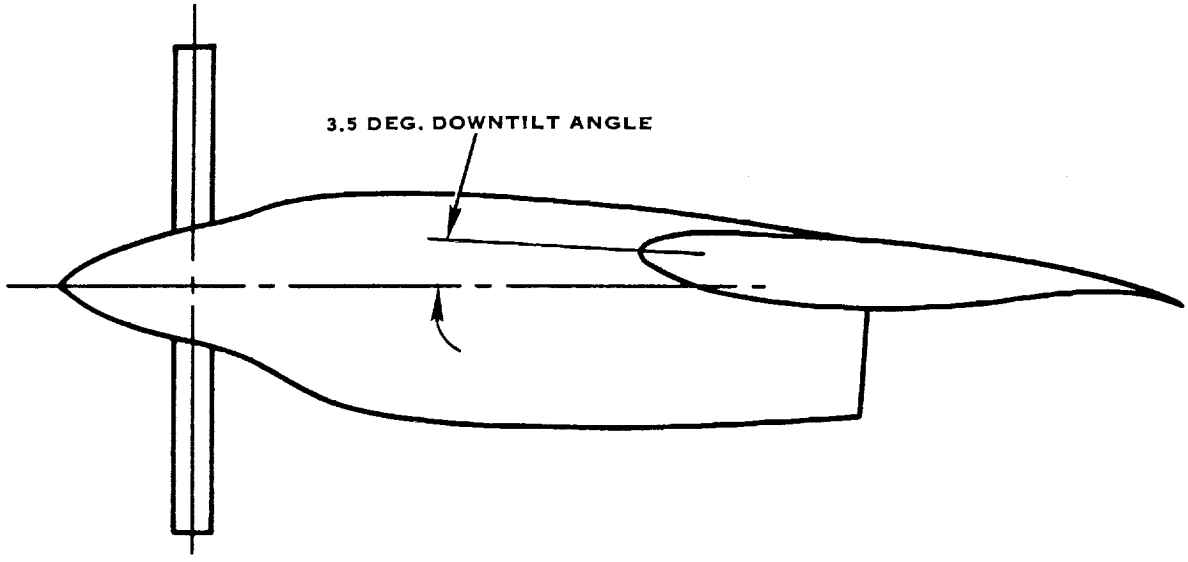

FIGURE 2-10. NASA/ AMES MODEL-SIDE VIEW OF UNDERWING NACELLE

SECTION 3.0
ANALYTICAL PREDICTIONS

3.1 DYNAMIC RESPONSE ANALYSIS

Analytical Methods

Introduction - The calculations described in the following sections were made over a period of several years. During that period of time there have been a number of refinements to the technology used in analyzing Prop-Fan blades. The discussions to follow generally pertain to procedures deemed appropriate at the time of the analyses. On-going research and development work has been directed at improving correlations between analyses and tests. In particular, efforts have been directed at accounting for the nacelle in the isolated nacelle configuration, improved modeling of the induction effects of the rotor, sensitivity studies to determine the effect of load distribution assumptions, and the study of aeroelastic effects. Use of the latest technology would be expected to improve the correlations presented here. The results discussed in this report are derived from those analyses done under the subject contract and do not necessarily incorporate the latest technology available.

The blade modal characteristics for the SR-2C blade were determined using two Hamilton Standard beam analysis programs, HS/H025 (bending modes) and HS/H027 (torsional modes). The width, sweep, and offset characteristics of the SR-3 and SR-5 blades are such that these beam analyses may not be adequate to represent the complex behavior of the higher modes observed for these blades. Finite element analyses were considered more appropriate to model these blades. A general purpose finite element code (BESTRAN) developed at Hamilton was used to calculate the modal characteristics for the SR-3 and SR-5 blades.

Aerodynamic loads for both the isolated nacelle and wing/nacelle configuration analyses were calculated using a basic Hamilton Standard strip analysis code, HS/H045. For the isolated nacelle cases the flow field was assumed to be unperturbed by the presence of the rotor or the nacelle (pure inflow). For the wing/nacelle configuration a more complicated calculation of the flow field was necessary to model the perturbations due to the interaction of the fuselage and wing. Two separate codes, the Hamilton Standard HS/H039 code and the NASA/Ames Hess code, were used to make the flow field calculations.

The SR-2C 1P dynamic response analyses for the isolated nacelle configuration were performed using the beam analysis code HS/H026 developed at Hamilton Standard. The SR-2C n-p dynamic response analyses for the wing/nacelle configuration tested at NASA/Ames were done using the Hamilton Standard developed HS/F094 code. The SR-3 and SR-5 1P dynamic response analyses were done using the MSC/NASTRAN general purpose finite element code.

3.1 (Continued)

Determination of Aerodynamic Loads - In the analyses of the isolated nacelle configuration the flow field is assumed to be only a function of the free stream velocity (V_o), the inflow angle (ψ), and the rotational speed (Ω). At any radial location (r) in the propeller plane the in-plane velocity (V_t) and out-of-plane velocity (V_a) can be calculated from:

$$V_t = \Omega r - V_o SIN\psi \cdot COS\Omega t$$

$$V_a = V_o COS\psi$$

Figure 3-1 is a schematic diagram showing the resolution of the local blade velocities. No influence of the nacelle on the flow field is assumed.

For the analysis of the SR-2C model in the wing/nacelle configuration a more sophisticated calculation of the flow field is required. Figure 3-2 shows the steps involved. Two different sets of flow fields were generated for each of the nine different operating conditions done for the study. One set was done by NASA/Ames using the HESS code, and the other was done by Hamilton Standard using an in-house flow field analysis designated HS/H039. Both procedures are 3-dimensional and utilize incompressible and inviscid flow. The HESS code used in this study is a NASA version of the McDonnell-Douglas HESS code that uses lifting surfaces to represent the fuselage and wings. The HS/H039 procedure was developed by Hamilton Standard and approximates the fuselage by utilizing a Rankine solid and replaces the wing with a lifting line. Both codes were run to see which better represented the flow field of the aircraft half-model configuration tested at NASA/Ames. Comparison of the results of using the two methods will be discussed later in this section.

The flow field, having been determined from one of the procedures discussed above, is used as input to the Hamilton Standard strip analysis HS/H045. This code determines the time variation of the loads and performs a Fourier analysis to obtain the harmonic components. It performs a quasi-static lifting line airfoil analysis, using 2-D airfoil section data for lift and drag, at a number of azimuthal and radial locations. It is often refered to as the multi-azimuth strip analysis. A 'Goldstein' type wake analysis is used to determine induced effects, via an iterative approach. Refinements have been added to the code to handle transonic aerodynamics, sweep, compressibility effects, and stall. This code produces the harmonics of the in-plane and out-of-plane aerodynamic loads at a number of radial locations. These become the input for the beam or finite element dynamic analyses.

For the SR-2C analysis with the isolated nacelle, a simplified version of HS/H045 was used. This code, designated HS/H444, assumes a 1P variation, examines aerodynamic loads 180° out of phase and determines the oscillation in load level by taking half the difference evaluated at these two extremes. This has been shown to give virtually the same result as the more complicated HS/H045 analysis if the variations are truly only 1P, as they are assumed to be for the SR-2C isolated nacelle analysis.

3.1 (Continued)

Critical Speed Analysis (Beam models) - The Hamilton Standard beam analysis program HS/H025 gives the natural frequencies in vacuum, mode shapes, and modal masses for the bending modes of a straight blade acting under the influence of a centrifugal field. Another program, HS/H027, gives the same information for the torsional modes. These decks are limited to the analysis of long, slender, i.e. beam-like, isotropic blades. In the case of the composite SR-2C blade an effective Young's modulus was chosen so that the analytically calculated non-rotating first mode natural frequency matched the value that was measured. The accuracy of the codes has been verified over a number of years with correlation of predicted and measured frequencies for many Hamilton Standard propeller blades. Critical speeds are determined from a Campbell diagram using the HS/H025 and HS/H027 calculated frequencies.

Critical Speed Analysis (Finite Element Models) - Because of the sweep, offset, and width of the SR-3 and SR-5 blades, the beam analyses may not be adequate to obtain reasonable approximations of the higher mode natural frequencies and mode shapes. Finite element analyses were considered better to model the blades. For purposes of this contract the natural frequencies in vacuum were calculated using the Hamilton Standard developed finite element code BESTRAN. The code was developed with a variable thickness triangular plate element capable of analyzing both membrane and bending stresses for either solid or composite blade construction. The effects of the centrifugal field are represented, including differential stiffness and the effect of load change with displacement.

To more accurately determine the displaced shapes under centrifugal loading, a piecewise linear option is available in order to apply the load gradually, updating the blade geometry during the process. Having determined a displaced position in space under the centrifugal and steady air loads, the natural frequencies and mode shapes about that position can be determined. The BESTRAN code uses a wavefront technique in the solution of a static problem. During this procedure the determinant of the stiffness matrix is calculated. Then, by evaluating the determinant of $[K] - \omega^2 [M]$, the natural frequencies can be identified via a frequency search. That is, the determinant is evaluated a number of times with varying frequency (ω). The determinant is plotted, and the natural frequencies occur when the determinant crosses zero. A large number of test cases and comparisons to known solutions, other finite element codes, and test results have verified the techniques involved. Critical speeds are determined from a Campbell diagram using the BESTRAN calculated frequencies.

1P Analysis (Isolated Nacelle/Beam Blade Model) - A computer code was developed at Hamilton Standard (HS/H026) for the analysis of beam-like blades (e.g. SR-2C) where only 1P response is anticipated. 1P aerodynamic loads derived from H045 and structural properties are used as inputs to the code which performs an iterative solution for the blade vibratory displacements and stresses. A direct approach to the solution of the equations of motion is used, where the effects of the centrifugal field are taken into account.

3.1 (Continued)

With the iterative techniques involved, the effects of differential stiffness and load change due to displacement are included. Stresses are predicted as a function of blade radius.

1P Analysis (Isolated Nacelle/Finite Element Blade Model) - As in the determination of critical speeds for the SR-3 and SR-5 blades, it was felt that a finite element analysis would best represent the 1P response of these wide, swept blades. For these 1P analyses the MSC/NASTRAN code was used. Finite element models were generated by converting the previously developed BESTRAN models to NASTRAN models using the NASTRAN triangular (CTRIA3) and quadrilateral (CQUAD4) elements. Figure 3-3 shows a flow chart which outlines the procedure used in the calculation of 1P vibratory stresses. Note that the inclusion of higher order vibrations could easily be incorporated into this procedure.

Using the HS/H045 calculated aerodynamic loads, centers of pressure, and blade angle ($\beta_{.75}$), a preprocessor (HS/F194) is used to distribute the harmonic loads on the finite element grids. The blade angle was adjusted to account for centrifugal twisting. The centers of pressure versus span are assumed to be independent of azimuth. They are calculated from an HS/H045 analysis with steady state conditions and zero inflow angle. The aero loads obtained from HS/H045 are expressed in terms of in-plane/out-of-plane components. The HS/F194 code converts these to components parallel and normal to any given blade section. The assumption is made that the load parallel to the blade chord (drag) is uniform across the blade. The normal loads (lift) are distributed along the chord using an analytical expression

$$P_N = A(N_c)^B[1 - (N_c)^{.25}]^2,$$

where N_c is the normalized chordwise position and A and B are chosen to match the total load and center of pressure desired. Figure 3-4 shows typical samples of this distribution function.

Before the 1P dynamic response analysis could be performed, it was necessary to do an analysis to determine the steady state position and stiffness of the blade at the rotating condition. Because of the non-linear effects of prestress (centrifugal stiffening) and large displacements (Coriolis forces), it is desirable to perform a non-linear analysis of the blade under the influence of centrifugal loading. This portion of the analysis was done using "rigid format 64" of MSC/NASTRAN, a geometric non-linear static analysis. The solution technique employs a Newton-Raphson iterative scheme to converge on a displaced shape which satisfies the equations of equilibrium. This is a more rigorous approach than employed in the previously used differential stiffness solution (rigid format 4 in COSMIC/NASTRAN). The iteration is done at full rpm and in theory would give the same solution as a piecewise linear solution, such as that employed in BESTRAN, with a 'large' number of load steps. Rigid format 64 in MSC/NASTRAN does account for the centrifugal effects including an update of the load vector with displacement.

3.1 (Continued)

It was found during the course of the iteration procedure that singularities often occurred in the structural stiffness matrix associated with the lack of plate element stiffness about its own normal. This is a feature of the NASTRAN plate elements. Removal of the singularities can be accomplished by fixing or tying affected degrees of freedom to neighboring nodes (SPCS or MPCS in NASTRAN terminology). It was also found that there exists a procedure within NASTRAN whereby the user adds artificial stiffness to the diagonal of the assembled stiffness matrix. The solution still converges to the correct answer even with an erroneous stiffness matrix. This is a feature of the Newton-Raphson iterative scheme, because the final solution is a function only of the elemental stiffness matrix and not the assembled global stiffness matrix. Both of these 'fixes' were employed during the analyses.

Upon completion of the iteration within rigid format 64 of MSC/NASTRAN, the incremental stiffness matrix was saved on magnetic tape. The incremental stiffness matrix is the stiffness matrix which is used to examine small (linear) perturbations about the steady state deflected position. It includes the basic elemental structural stiffness and the differential stiffness representing the additional stiffness due to the fact that the blade is in a centrifugal field. However the matrix output from NASTRAN does not recognize that the magnitudes of the load vectors on the model's mass points change as the points vibrate about the steady state position. This effect can be explained as follows.

Consider an element of mass under the influence of a centrifugal field. There is a radial force acting on this mass equal to '$mr\omega^2$' where 'r' is the radius from the center of rotation. If the mass is allowed to deflect outward then there will be an increase in the centrifugal force due to the increase in radius;

$$\Delta F = m\omega^2 \Delta r$$

Since the increment in force on the element is in the same direction as the displacement (instead of a restoring force) it is equivalent to a negative stiffness, thus;

$$K_{radial} = \frac{-\Delta F}{\Delta r} = - m\omega^2$$

It can also be shown that the same effect is present in the tangential direction, hence:

$$K_{tangential} = - m\omega^2$$

3.1 (Continued)

The inclusion of these terms in the stiffness matrix is necessary to produce accurate results. Since the new terms are proportional to the mass matrix, just as the inertia terms are in a vibrations problem, it is clear that their importance depends upon the relationship between the frequency of vibration and the rotational speed. The lower the frequency of vibration, the more important these terms are. At high frequencies the inertia terms dominate and the negative in-plane stiffness terms are less important. This negative in-plane stiffness matrix is added to the incremental stiffness matrix generated by MSC/NASTRAN. It is actually added using a program modification (DMAP alter) in rigid format 64, before the stiffness matrix is written to magnetic tape.

Because the stiffness matrix generated from the steady state analysis is based on the shape of the blade after deformation, it was found necessary to save the steady displacements. These displacements were added to the original grid point positions so that these 'updated' grid cards are used for the dynamic analysis. They could also be used for an eigen-value analysis. The updated grid cards are checked to verify that the steady state position is near the desired operating condition (i.e. correct $\beta_{.75}$).

With the HS/H045 generated dynamic air loads and centers of pressure as input, the HS/F194 code is used to distribute the loads on the finite element model. This is done in the same manner as for the steady loads except the loads are written to different NASTRAN bulk data cards (DAREA instead of FORCE) because the loads are harmonic.

Using the updated grid cards, the air loads, and the stiffness matrix saved on tape, the dynamic analysis is performed using rigid format 26 in MSC/NASTRAN, Direct Frequency Response. Alternately the Modal Frequency Response analysis could be used (rigid format 30). Note that DMAP alters are required to read the stiffness matrix from tape and effectively replace the stiffness matrix which would not have the differential or negative in-plane stiffness effects.

Upon completion of the NASTRAN dynamic analysis the elemental stresses are saved for postprocessing. A computer program has been written which reads the elemental stresses, interpolates for stress at any position, and calculates strains for comparison to test. Apparent stress is calculated as the strain in a given direction times Young's modulus. It is to be noted that this postprocessor accounts for the strain gage thickness by increasing the bending strain, but not membrane strain to correspond to a location at distance from the neutral axis increased by the gage thickness.

3.1 (Continued)

n-P Analysis (Wing/Nacelle/Beam Blade Model) - Due to proximity of the wing and fuselage of the SR-2C NASA/Ames test configuration, aerodynamic excitation at higher P-orders was expected. For analysis of these conditions a modal superposition analysis was used to obtain the n-p response. The procedure which was used to calculate the vibratory stresses in the blades has four major steps:

1. Determine the aerodynamic environment (flow-field).

2. Calculate the harmonic aero loads.

3. Calculate the blade modal characteristics.

4. Use a modal analysis to calculate response.

The flow field, as discussed previously, was determined from the HESS code or HS/H039. The harmonic air loads were calculated via the HS/H045 program. The HS/H025 code was used to calculate the blade modes, in the same manner as discussed for the critical speed calculations.

Once the blade modal characteristics and the excitation were determined, the response was calculated. The analysis used was based on modal theory. Response of each structural mode to each harmonic input was calculated separately. The results were then superimposed to give the total response. Hamilton Standard computer program HS/F094 did these calculations. The form of the total response, in this case blade stresses, was a series of complex time-histories representing the stress wave forms for each station on the blade. The net vibratory stress amplitude was determined by taking one-half the difference between the maximum and minimum values of the wave form at each station. Comparisons to test data were then made.

Analytical Results For NASA/Lewis Isolated Nacelle (SR-2C, SR-3, SR-5)

SR-2C 1P Critical Speed Predictions - The composite SR-2C model Prop-Fan blade was analyzed using the beam codes HS/H025 and HS/H027, as discussed earlier. The blade properties were determined from the blades' physical construction and aerodynamic considerations. The cross-sectional areas, moments of inertia, density, and twist distribution were required inputs. The blade angle was chosen as 55° for this analysis, since this is near a typical operating blade angle. Because these codes assume an isotropic material, a single value of Young's modulus was required to represent the effective stiffness of the composite model. This value, 58.6×10^6 kPa, was chosen to give a match between the measured and calculated first mode non-rotating frequency of 134 Hz. This value was measured in shake tests performed at NASA/Ames. Comparison to test for the remaining modes is made in a later section (4.1). Figure 3-5 shows the predicted Campbell diagram for the SR-2C. Also shown, for reference purposes, are curves obtained from a NASA COSMIC/NASTRAN calculation.

3.1 (Continued)

SR-3 1P Critical Speed Predictions - A BESTRAN model was set up using triangular, variable thickness elements. This model is pictured in Figure 3-6. It should be noted that since this blade was not expected to undergo significant changes in its twist distribution at speed, no attempt was made to 'pretwist' the analytical model. That is, the finite element model was built based on the desired aerodynamic shape at the 'design' operating speed of 8636 rpm. A single step, differential stiffness solution was used to determine the steady state position, about which the frequencies were evaluated using the code's frequency search option, discussed earlier. The frequencies are presented on a Campbell diagram, also shown in Figure 3-6.

SR-5 1P Critical Speed Predictions - The BESTRAN model set up for the SR-5 is pictured in Figure 3-7. It is noted that since this blade was expected to undergo significant changes in its twist distribution at speed, the model was pretwisted. That is, the finite element model was set so that untwisting at speed (7950 rpm), due to centrifugal loading, would cause the desired aerodynamic shape to be obtained. The frequencies were then calculated in the same manner as for the SR-3 model. The predictions are also presented in Figure 3-7.

SR-2C 1P Response Predictions - Predictions of 1P dynamic response were made for the SR-2C model blade using procedures outlined in previous discussions. Assuming pure angular inflow, i.e. no perturbation of the flow field due to the nacelle, the HS/H444 code was used to predict 1P aerodynamic loads. The HS/H026 code was used to predict the response. As previously noted, the blade was represented with a single value of Young's modulus. The conversion of measured strain to stress is complicated by the actual composite nature of the blade's construction. For this reason the calculations are reported in terms of predicted strain per degree of inflow, giving a more direct comparison with the measured values.

The computations were conducted in two manners. For one, the operating conditions were matched point for point with the proper input parameters for comparison with test. A second set of calculations was made in order to parametrically study a range of rotational speeds, power settings and Mach numbers. The inflow angle was adjusted as a function of forward speed in an attempt to keep the excitation factor constant for this parametric study. The results of the parametric study are given in Table 3-I. The results of the analyses made to correlate with test points are shown in Table 3-II. It should be noted that the calculations show that the strain per degree of inflow does not go up as a straight line with equivalent speed squared, but falls off at the higher speeds.

Figures 3-8 through 3-11 show strain per degree of inflow plotted as a function of equivalent airspeed on a squared scale for 6000, 7000, 8000 and 9000 rpm, respectively. Curves for four values of constant power are shown. The curves are fairly straight lines, except at the high speed where the fall off is evident. Also at high power settings and low airspeeds, the curves deviate from straight lines because of blade stall. At low airspeeds and high power setting, the high rpm fall off seems to occur earlier at the high rotational speeds.

3.1 (Continued)

The explanation for this fall off may be found in Figure 3-12 where the lift curve slope dCL/α, is plotted as a function of equivalent airspeed on a squared scale. Two curves are shown, one for 149 kW and one for 447 kW. The data were obtained from H444 calculations for 7000 rpm at the 78% radius. The 447 kW 1P curve drops off at low speeds because of stall. The rise and fall of the lift curve slope is due to compressibility effects. Note that at the high speed, the fall off is very sharp, similar to that experienced with the excitation. This is typical of the airfoils used in Prop-Fans. Generally, the change in lift curve slope increases with the inverse Prandtl-Glauert laws as section velocity is increased, but experiences a fall off in the transonic region above and below Mach 1. The one-per-rev excitation is directly proportional to lift curve slope. Therefore, it is not surprising that the blade response shows similar trends.

Comparisons of the predicted strains to measured values will be discussed in Section 4.1.

SR-3 Response 1P Predictions - The procedures discussed earlier and outlined in Figures 3-2 and 3-3 were used to determine the 1P response of the SR-3 model blade. As noted, the MSC/NASTRAN code was used. The finite element model used is pictured in Figure 3-13. It was derived from the BESTRAN model. Since the design untwist of this blade is small (less than 2°), the static blade angle was set to the desired operating blade angle without consideration of the change at speed. Because of the expense involved with these analyses, only six conditions were chosen for study.

Shown in Figure 3-14 is a plot of the calculated spanwise-in-plane and out-of-plane 1P aerodynamic loads for one of the cases. The center of pressure spanwise distributions for two of the analyzed cases are shown in Figure 3-15. As discussed earlier, the loads are distributed across the chord in a manner consistent with the center of pressure and total aerodynamic loads at a given station. The azimuthal variation of center of pressure is not considered.

The operating conditions and predicted stresses for each of five strain gages (refer to Figure 3-16 for location) are shown in Table 3-III. The stresses are normalized with respect to the excitation factor (EF) defined as:

$$EF = \psi(V_T/644.8)'\rho/\rho_o$$

where ψ is the inflow angle, V_T the true airspeed in km/H, ρ the air density, and ρ_o the air density at standard sea level conditions. It has been found analytically and experimentally that the stress is nearly linear with respect to inflow angle if there is 1P excitation only.

3.1 (Continued)

The stresses predicted for case 4 showed considerably higher stresses (per EF) at the outboard gage locations than at the others. It is noted that this case, which was for low power, had a calculated chordwise center of pressure distribution considerably aft of the other cases (see Figure 3-15). Case 4 was rerun using the same total loads but assuming the center of pressure distribution of case 6. As can be seen, the stresses become comparable to the other cases. This shows a sensitivity to the center of pressure assumption, especially at the tip.

Figure 3-16 shows a contour plot of the calculated effective stress for case 6, the design condition. The effective stress is defined as:

$$\sigma_{EFF} = \sqrt{\sigma_x^2 + \sigma_y^2 - \sigma_x\sigma_y + 3\tau_{xy}^2}$$

Note that it is not directly relatable to the apparent stress (strain times Young's modulus) predicted for comparison to test (Reference 9).

SR-5 1P Response Predictions - The MSC/NASTRAN finite element model used was derived from the BESTRAN model, which is pictured in Figure 3-15. Note that the tip of the SR-5 model was formed using quadrilateral elements. This was because it was felt that high sweep in this area could be better modeled using the more accurate (vs. trianglar elements) MSC quadrilateral elements. Since the untwist of this blade at the design speed is relatively large (greater than 5°) the static (non-rotating) blade angle was set to values greater than the desired operating blade angles for each case. In this fashion the blade angle is near the desired angle at speed. The actual blade itself is also 'pretwisted' so that the predicted deformed shape at design rpm is a reasonable approximation to the desired aerodynamic shape.

As was done for the SR-3, six operating conditions were chosen for analysis as shown in Table 3-IV. Shown in Figure 3-17 is a plot of the spanwise in-plane and out-of-plane 1P aerodynamic loads for one of the cases. Figure 3-18 shows the center of pressure distribution for two of the cases. The loads are distributed, as were the SR-3 loads, using chordwise distributions as pictured in Figure 3-4.

The predicted apparent stresses for each of five strain gages (refer to Figure 3-19 for location) are shown in Table 3-IV. It was found that the predicted stresses near the tip were very sensitive to the assumptions made as to the pressure distribution.

Figure 3-19 shows a contour plot of the effective stress for case 6 of Table 3-IV, the design condition. As previously noted, the predicted apparent stress values are not directly comparable to this plot.

3.1 (Continued)

Analytical Results For NASA/Ames Wing and Nacelle (Installed SR-2C)

Flow Field Predictions - The methods briefly described earlier were used to compute the flow fields for the NASA Ames semi-span model with the wing, nacelle, and SR-2C Prop-Fan installed. Nine analysis conditions were specified and are listed in Table 3-V.

Comparisons of the NASA/Ames HESS code calculated flow fields and the HS/H039 calculated flow fields are shown in Figures 3-20 through 3-29. Figures 3-20 through 3-24 are plots of axial velocity distribution shown as a function of azimuth for three values of non-dimensional radius. Differences between the two procedures diminish as the calculations move towards the blade tip. The same trends in axial velocity, which are exhibited in Figure 3-20, can also be observed in Figures 3-21 to 3-24.

It appears that the agreement between the two procedures improves as lift coefficient is reduced. This is possibly due to the differences in the methods between the two procedures. That is, the HESS code utilizes a lifting surface with a pressure distribution defined over it and the HS/H039 procedure uses a lifting line. It may be that as the angle of attack increases, the calculated differences are enhanced by differences in the procedures. At one particular point in the study, the discrepancy between the NASA/Ames HESS calculations and the HS/H039 calculations appeared to be caused by either wing circulation, wing cross-flow and/or nacelle cross-flow. Hand calculations, performed as a crosscheck for the HS/H039 procedure were found to be in agreement with the computer calculations.

Tangential velocity gradients calculated by both programs are compared in Figures 3-25 through 3-29, for the 5 flow fields. Agreement is apparent when the blade is below the wing but becomes less apparent when the blade moves above the wing. Lift coefficient can be seen to have only a minor effect on the differences between the tangential velocity ratio calculated by the two programs.

A comparison of efficiency levels and 1-P shaft forces and moments for the 9 operating conditions is shown in Table 3-VI. In general, the comparison of normal forces and yawing moments is favorable, although the HS/H039 program calculated pitching moments differ from those predicted by the HESS code. Again, it is likely that this may be caused by the fact that the HS/H039 procedure uses methods that are not as refined as those used in the HESS code. In order to evaluate the differences in flow fields, blade response was calculated at all the operating conditions for both flow field prediction procedures.

For both sets of flow fields, the harmonic aerodynamic loadings on the blades were calculated using the Hamilton Standard multi-azimuth strip analysis HS/H045 described previously. A summary of the resulting aerodynamic excitations is given in Table 3-VII. From this table, it can be seen that the HS

3.1 (Continued)

flow fields generate higher 1P loadings while the Ames/HESS flow fields give greater higher-order loads, particularly at 2P. Both flow fields show an increase in 2P loads with increasing Mach number. It can also be concluded that the 5P loadings can be ignored since their magnitudes are so small.

1P and Higher Order Response Predictions - Some of the results of running the HS/H025 analysis on the SR-2C Prop-Fan model, such as the critical speed diagram, were discussed earlier. The calculated natural response frequencies are tabulated in Table 3-VIII for each of the calculated operating conditions. The total vibratory response stresses were calculated using the HS/F094 response analysis, taking the loads from the HS calculated flow fields and also from the Ames/HESS code flow fields. The results are shown in Table 3-IX. These values are the n-p and total vibratory stresses and represent one half of the difference between the maximum and minimum stress values at the radial station for which the total stress is maximum.

The same trends are seen in Table 3-IX as were observed in the aerodynamic excitation, namely, that the HS predictions show higher 1P and lower 2P stresses than the HESS code predictions. The blade responses follow the basic patterns of the loadings except for cases 3 and 4 which are at rpm's close to the 2P/1st mode critical speed. For these two cases, the 2P excitations are magnified considerably, such that the resulting 2P blade stress is a large contributor to the total vibratory stress. It is also noted that the 3P, 4P and 5P stresses are generally lower than the proportions of the respective excitations would indicate. This is due to the fact that the loading patterns (spatial variations) of these higher order excitations make them less efficient at exciting the primary blade modes. It appears that excitations above 2P are only important if they are very large or if a resonant condition (critical speed) is present.

In the interest of determining the effect of changing the nacelle toe-in, operating case Number 6 was calculated with 0° of nacelle toe-in. Table 3-X is a comparison of the calculated 1P and higher order moments with 0° of nacelle toe-in and 2° of toe-in (as the Ames model was configured). The moments are slightly higher with 2° of toe-in.

Some relatively significant differences exist between the NASA/Ames HESS code and the HS/H039 predicted flow fields. The differences in the predicted flow fields and the resultant difference in the blade responses are most likely due to the inherent differences between the two flow field procedures themselves. The HESS code is a sophisticated procedure and probably more accurate than the HS/H039 code. It utilizes lifting surfaces for a definition of the fuselage and wings rather than the Rankine solid and lifting lines used by the HS/H039 procedure. However, HS/H039 is simpler and much less expensive to use as a design tool. The evaluation as to which of these two prediction techniques is the better or more useful tool must be made by each user.

3.2 AEROELASTIC STABILITY ANALYSIS

Analytical Methods

The aeroelastic stability of the model Prop-Fan blades was investigated analytically using four calculation procedures G400T2, F168, F187, and F203. Each analysis has a different approach to the stability solution and has inherent limitations in modeling the complex structure and aerodynamics of the Prop-Fan. Table 3-XI presents an overview of the features and procedures of these stability analyses. Further details concerning the aeroelastic stability analyses will be presented in the following discussions.

The G400T2 aeroelastic blade analysis is a non-linear time-history response computer program (Reference 10). Non-linear differential equations of blade motion are established to couple the uncoupled flatwise, edgewise, and torsion mode shapes structurally and aerodynamically. The unsteady aerodynamic forces take the form of non-linear quasi-steady strip equations. These non-linear equations are solved using a timestepping numerical integration scheme to determine blade response. Blade stability is evaluated by examining the predicted response growth or decay from an initial disturbance.

The F168 classical flutter program is a linearized analysis that was derived for large propeller blade angles. The analysis structurally couples three uncoupled blade modes, first flatwise bending, first edgewise bending, and first torsion. Linear quasi-steady strip aerodynamics are used to establish the aerodynamic forces. The entire solution takes the form of a complex eigen-value problem from which frequency and damping for the three modes are obtained.

The program F187 approaches the problem in a different manner. The blade is represented by fully coupled three-dimensional modes of vibration where the motions are in-plane and out-of-plane displacement and rotation about the pitch change axis. This technique eliminates many questions about the representation of a complex structure by beam modes. The aerodynamics for this analysis involve unsteady modified strip theory with aerodynamic circulation functions (Theodorsen functions) acting on the blade at the frequency of vibration. All equations are linearized about the helix angle of the blade and put into modal coordinates so that the equations reduce to a real eigen-value problem. The roots of the eigen-value problem indicate the system frequency and damping.

The F203 aeroelastic stability analysis was specifically tailored to model the structural and aerodynamic complexities of the Prop-Fan (Reference 11). The complex structure is modeled as with the F187 program, using fully coupled mode shapes. These coupled modes take the form of translation normal to the blade surface and rotation about the blade mid-chord along with the first and second spanwise derivatives of the displacements.

3.2 (Continued)

The aerodynamics for the analysis are modeled with a modified version of the unsteady sweep equations developed by Cunningham (Reference 12). These unsteady sweep equations were generalized to account for compressible isolated and/or cascade unsteady aerodynamic data in a manner similar to that of Kielb and Kaza (References 13, 14, and 15). The solution to the equations of motion takes the form of a complex eigen-value problem to give frequency, damping, and complex mode shape for the system.

Structurally the four analyses take two approaches toward modeling a blade. G400T2 and F168 use uncoupled beam mode shapes and rely on beam differential equations of motion to structurally couple the modes, whereas F187 and F203 use coupled mode shapes that are furnished by external sources for computation such as finite element analyses. The use of coupled mode shapes in F187 or F203 eliminates some of the questions about the accuracy of a beam model in representing the complex structure of a swept, low aspect ratio Prop-Fan.

The G400T2, F168, and F187 analyses use aerodynamic coefficients resolved about aerodynamic blade streamlines whereas the F203 uses the swept coordinate system approach presented by Cunningham (Reference 12). The Cunningham sweep corrections approximately account for spanwise flow due to sweep in the unsteady terms. In a quasi-steady sense all the aerodynamic equations are similar, but the Cunningham unsteady sweep corrections permit the analytical possibility of first mode bending flutter, because the unsteady spanwise derivative sweep terms permit the introduction of negative flatwise damping.

In addition to the unsteady sweep corrections in F203, cascade unsteady aerodynamic effects are included to account for the close spacing of the Prop-Fan blades and their aerodynamic influence on each other. Cascade effects generally destabilize a system.

The results generated by the use of these analytical programs on the model Prop-Fan is the topic of the section on classical flutter boundaries.

Excitation Method

For an empirical assessment of sub-critical aeroelastic stability of model Prop-Fans, it was initially proposed to measure the frequency content and vibration damping, during operation under power in the wind tunnel, using the 'Randomdec' method of analysis. This method of analysis has been used routinely by NASA, at wind tunnel facilities at Ames and Langley, for fixed wing aircraft and other non-rotating structural models. The underlying principle behind the Randomdec analysis is that tunnel airflow turbulence will cause a random response that can be sampled and averaged with previous samples until the signal is enchanced to the point where the averaged data can be spectrally analyzed for the identification of frequency content and damping.

3.2 (Continued)

After examining data samples for the SR-2C, and SR-3 model Prop-Fans, it was observed that the results from the basic Randomdec method were not satisfactory. The expected signal enhancement did not occur. It was concluded that the excitation resulting from natural inflow turbulence did not provide a sufficiently large initial impulse as was necessary. The wind tunnel turbulence was not acting on the Prop-Fan as satisfactorily as it apparently did on fixed airfoil structural models in published accounts of Randomdec investigations of flutter margin.

It was then recommended that a method be determined to impart a large enough initial impulse on the blade to obtain a response suitable for spectral decomposition. A number of methods were evaluated for excitations including ceramic gages, blade-mounted explosives, explosively-induced gas jet, jelly ball missiles, and a pulse from a gas-jet system. The gas-jet system was finally selected as the most practical impulse excitation system.

The gas-jet system consists of an gas-jet probe mounted behind the Prop-Fan that is capable of producing a short high velocity stream of nitrogen gas that will impinge on the rotor. Figure 2-7 shows the arrangement of the gas-jet system behind the SR-3 model Prop-Fan. The gas-jet system produced a blade response that was suitable for spectral decomposition.

The decay of individual data samples was studied separately, each sample being selected for its content of a single desired mode with minimal interference from other modes. When this was done, it was found with very few exceptions, that the samples having single predominant modes did not decay uniformly. Also, the exceptions did not exhibit satisfactorily similar rates of decay. These results will be presented in Section 4.2 along with further discussion of the analytical methods used to reduce the data.

Classical Flutter Boundaries

Application of the four aeroelastic stability analyses yielded differing results for the stability of the three model Prop-Fan blades. The differing results were expected due to the varying approaches to the stability solution inherent in the four applied analyses. Table 3-XII shows a summary of the stability predictions. Of these results only the SR-3 model Prop-Fan was calculated to be stable by all of the applied methods. Details of the calculations will be presented in the following discussions with an emphasis on the F203 analysis and the SR-5 model Prop-Fan. It was found that the F203 analysis best models the Prop-Fan and that the SR-5 was the most flutter-prone model.

The G400T2 analysis predicted the SR-2C and the SR-5 model Prop-Fan blades to have a band of instability in the test region corresponding to the blade tip entering a zone where the local blade relative velocity was transonic. Below and above this region the blades were predicted to be stable as shown in Figure 3-30. The SR-3 model was stable for all cases examined.

3.2 (Continued)

For both the SR-2C and the SR-5 blades, G400T2 analysis showed that the first uncoupled torsion mode controlled the system stability, as shown in Figure 3-31 for the SR-2C blade. The concept of a pure torsion mode is realistic for the straight SR-2C model, but becomes questionable for the highly swept SR-5 model.

The limit amplitude motion of the response is due to the empirical airfoil aerodynamic data used by G400T2. A limit amplitude is reached when the response drives the blade into the stalled region of the airfoil data and the lift curve slope goes to zero or changes sign. The empirical airfoil data also account for the band of instability in the predicted boundaries. As the blade relative velocity becomes supersonic, the aerodynamic center moves aft and the lift curve slope drops, resulting in an increase in stability even though a high relative velocity exists along the blade.

Neither the F168 nor F187 analysis was applied to all of the model Prop-Fan blades. The F168 analysis was applied to the SR-2C and the SR-3 model blades, because the SR-2C has no sweep and the SR-3 has moderate sweep, so that an analysis using beam equations was thought to be applicable. The SR-5 model has a high degree of sweep and a beam analysis was not considered as applicable, therefore the F187 coupled mode shape analysis was applied. The results, shown in Figure 3-32 indicate that only the SR-2C model would be unstable. The instability for this blade covers the majority of the test region. Also, the torsion mode was found to control the system stability as was the case for the G400T2 calculations.

The F203 aeroelastic stability analysis was applied to all of the model Prop-Fan configurations because the analysis was specifically tailored to the Prop-Fan structural and aerodynamic complexities and therefore best models the Prop-Fan. The previous analyses were limited to the study of a single blade so that no aerodynamic influence from the other blades could be taken into account.

Using the single isolated blade assumption, F203 was used to calculate stability boundaries to serve as a comparison to the previous analytical work and for correlation to test data on reduced blade number tests. Figure 3-33 shows the isolated blade results. Only the SR-5 was predicted to be unstable and the instability did not occur in the questionable torsion mode as indicated in G400T2. The SR-5 instability indicated by F203 occurred in the first mode. The analytical existence of first bending mode flutter in highly swept wings has been previously documented (References 16 and 17). Figure 3-34 shows the result of approximating the non-dimensional parameters in reference 16, for the SR-5 model. The blade falls in the region where a potential for first mode flutter exists, giving support to the F203 calculation. To lend more insight into the SR-5 first mode instability, the application of F203 to the SR-5 blade will be described in further detail.

3.2 (Continued)

The structural input to the F203 analysis is developed from finite element results. Typical finite element results in the form of displacement contour plots for mode shapes at 7000 RPM, shown in Figure 3-35, illustrate the complex bending torsion coupling patterns that occur in this blade. The centrifugal effects due to rotational speed are taken into account in F203 by the finite element results, external to the analysis. The analysis uses as input the computed frequency, modal mass and bending-torsion mode shapes from the finite element results. The bending-torsion mode shapes are reductions of the full finite element results to translation normal to the blade surface and rotations about the mid-chord of the blade in the swept coordinate system of Figure 3-36. The coupled bending-torsion mode shapes at 7000 RPM are shown in Figure 3-37.

The SR-5 model blade stability was initially studied as an isolated blade, eliminating any aerodynamic cascade effects from the problem. Figure 3-38 shows the computed variation in viscous damping ratio of the first four modes at 7000 RPM as the wind tunnel speed is increased. The first mode for the isolated blade configuration goes unstable at 0.85 Mach Number.

The computed flutter mode shape at 7000 RPM is given in Figure 3-39 along with a comparison to the input first structural mode shape. The flutter mode has more bending-torsion coupling than the structural mode. Also, the bending-torsion motion is not in phase. This mode shape change is caused by aerodynamic coupling of several modes. The first eight modes were included in the analysis although only the first four (4) modes are considered influential to the analysis of the SR-5 Prop-Fan.

The degree to which the higher modes of the blade contribute to the SR-5 instability was examined by using only the first structural mode in an analysis, eliminating any mode coupling. For the one-mode system, instability could not be found in the test region indicating that the instability is a multi-mode phenomenon even though the first structural mode dominates the frequency and mode shape of the instability.

The SR-5 model Prop-Fan was then studied to examine the effect that blades have on each other by using cascade unsteady aerodynamics. The rotor was assumed to be a tuned system and ten interblade phase angles for the ten bladed model were examined to determine the least stable phase angle. The root locus plot of system eigen-values in Figure 3-40 shows that 288° is the least stable interblade phase angle. This corresponds to a two-nodal-diameter system mode for the ten bladed model. Cascade aerodynamics were initially assumed to affect the full blade length. The cascade aerodynamics produced a predicted flutter point substantially below that of the isolated aerodynamics. To better account for three dimensional effects and large gap to chord ratios near the blade tips, a mixture of cascade and isolated airfoil data was then used to model the system. When the gap to chord (s/c) ratio becomes larger than 2.0, isolated data were substituted for cascade data. The resulting calculation is shown in Figure 3-41. A complete boundary using

3.2 (Continued)

cascade and isolated data for the SR-5 is shown in Figure 3-42. Additional first mode viscous damping ratio plots for the SR-5 model at 9000 RPM and 5000 RPM are shown in Figures 3-43 and 3-44.

The SR-3 and SR-2C isolated viscous damping ratio plots used to assess the blade stability shown in Figure 3-33 are presented in Figures 3-45 and 3-46 for the first four modes. The SR-3 results show a destabilizing trend in the first mode damping as was the case for the SR-5. No such first mode trend is shown by the SR-2C model. When cascade aerodynamic data are used for analysis of these models, the damping results are modified. Figure 3-47 shows that the first mode instability trend for the SR-3 model is enhanced depending on the amount of blade affected by cascade aerodynamic coefficients. This trend was also evident for the SR-2C, Figure 3-48, but the full cascade results could not be generated because supersonic flow conditions at the blade tip prohibits the use of the subsonic cascade airfoil data contained in the F203 analysis. The results of applying F203 with cascade corrections show that the SR-2C model is predicted to be stable in the test region, the SR-3 model has a tendency toward first mode instability, and that the SR-5 model has a definite flutter boundary in the test region.

Summary - The analyses show that aerodynamic sweep destabilizes the first mode stability of a Prop-Fan. To show first mode instability analytically a swept form of unsteady aerodynamics must be applied to the blade. Of the applied analyses, only the F203 analysis has this form of unsteady aerodynamic equations.

TABLE 3-I. SR-2C 1P (ISOLATED NACELLE) STRAIN PREDICTIONS
PARAMETRIC VARIATIONS OF POWER, RPM, MACH NUMBER

POWER KW (HP)	RPM	STRAIN PER DEGREE OF INFLOW AT 163MM STATION* ϵ/ψ MACH NUMBER MN=0.36	ϵ/ψ MACH NUMBER MN=0.6	ϵ/ψ MACH NUMBER MN=0.8	ϵ/ψ MACH NUMBER MN= 0.85
149 (200)	6000	60.6	149.4	228.2	219.4
149 (200)	7000	51.4	139.1	195.3	189.2
149 (200)	8000	44.2	123.8	166.1	161.0
149 (200)	9000	37.4	99.6	140.6	136.9
298 (400)	6000	69.9	169.8	241.0	225.4
298 (400)	7000	67.9	160.8	206.3	193.2
298 (400)	8000	58.2	143.0	173.4	165.0
298 (400)	9000	50.5	112.3	146.1	142.9
447 (600)	6000	71.8	186.4	253.8	233.5
447 (600)	7000	75.7	178.7	217.3	199.3
447 (600)	8000	68.9	160.9	180.7	169.1
447 (600)	9000	62.6	123.8	149.7	146.9
597 (800)	6000	93.6	166.0	266.5	239.5
597 (800)	7000	73.3	194.0	228.2	203.3
597 (800)	8000	76.7	178.7	188.0	173.1
597 (800)	9000	73.3	135.3	155.2	151.0

*REFER TO FIGURE 3-13 FOR GAGE LOCATION

STRAIN ϵ EXPRESSED AS μ-M/M

TABLE 3-II. SR-2C 1P (ISOLATED NACELLE) STRAIN PREDICTIONS PREDICTIONS TO MATCH TEST CONDITIONS

TEST RUN NUMBER	$\beta_{.75}$ BLADE ANGLE	POWER KW (HP)	RPM	MACH NUMBER	V_E EQUIVALENT VELOCITY KM/H (KNOTS)	ρ/ρ_o DENSITY RATIO	ψ INFLOW ANGLE	ϵ/ψ STRAIN PER DEGREE OF INFLOW AT 163 MM STATION *
9	45.2°	128 (172)	6000	0.351	437 (236)	1.041	8°	56.0
10	45.2°	273 (366)	7000	0.353	439 (237)	1.044	8°	63.4
34	41.3°	87 (117)	6000	0.348	435 (235)	1.069	15°	47.6
35	41.3°	210 (282)	7000	0.352	441 (238)	1.069	15°	55.4
38	38.1°	36 (48)	6000	0.358	448 (242)	1.072	15°	68.9
45	52.0°	37 (49)	6000	0.591	719 (388)	1.018	4°	127.0
46	52.0°	253 (339)	7000	0.592	723 (390)	1.024	4°	151.3
50	52.0°	48 (64)	6000	0.590	719 (388)	1.020	7°	127.7
57	48.9°	123 (165)	7000	0.591	723 (390)	1.027	7°	131.4
78	53.0°	60 (80)	6000	0.596	719 (388)	0.9828	7°	130.7
85	53.0°	81 (109)	7000	0.690	797 (430)	0.9184	3°	161.0
86	53.0°	380 (509)	8000	0.686	797 (430)	0.9243	3°	160.3
90	53.0°	383 (514)	8000	0.686	797 (430)	0.9255	5°	161.4
91	53.0°	499 (669)	8300	0.681	791 (427)	0.9268	5°	160.2
98	50.5°	170 (228)	7000	0.589	713 (385)	0.9895	4°	135.3
103	50.5°	199 (267)	7000	0.588	713 (385)	0.9916	7°	139.3
108	50.5°	227 (305)	8000	0.689	797 (430)	0.9218	5°	146.6
123	55.7°	57 (77)	7000	0.793	862 (465)	0.8317	4°	175.0
124	55.7°	346 (464)	8000	0.785	856 (462)	0.8351	4°	161.8
125	55.7°	677 (908)	8990	0.783	856 (462)	0.8363	4°	146.5
130	55.7°	171 (229)	8000	0.842	886 (478)	0.7909	4°	158.3
131	55.7°	477 (639)	9000	0.839	884 (477)	0.7951	4°	142.0
133	55.7°	53 (71)	7000	0.788	862 (465)	0.8321	2°	173.5
134	55.7°	341 (457)	8000	0.784	858 (463)	0.8338	2°	162.0
135	55.7°	684 (917)	9000	0.800	856 (462)	0.8393	2°	147.0
147	57.5°	200 (268)	7000	0.793	863 (466)	0.8355	4°	185.3
148	57.5°	532 (713)	8000	0.786	858 (463)	0.8397	4°	170.5
155	57.5°	79 (106)	7000	0.842	884 (477)	0.7930	2°	181.5
156	57.5°	366 (491)	8000	0.844	888 (479)	0.7934	2°	165.5
157	57.5°	655 (879)	9000	0.843	886 (478)	0.7913	2°	147.5
160	57.5°	81 (109)	7000	0.846	888 (479)	0.7909	4°	181.0
161	57.5°	362 (485)	8000	0.844	886 (478)	0.7922	4°	164.8
162	57.5°	669 (897)	9000	0.844	886 (478)	0.7918	4°	147.3
168	59.5°	192 (258)	7000	0.841	869 (469)	0.7400	4°	182.8
169	59.5°	471 (632)	8000	0.848	873 (471)	0.7371	4°	165.0
175	53.8°	117 (157)	8000	0.795	847 (457)	0.7728	4°	148.8
176	53.8°	403 (540)	9000	0.794	847 (457)	0.7740	4°	135.5

* REFER TO FIGURE 3-13 FOR GAGE LOCATION

STRAIN ϵ EXPRESSED AS μ-M/M

TABLE 3-III. SR-3 1P (ISOLATED NACELLE) APPARENT STRESS PREDICTIONS (REFER TO FIGURE 3-16 FOR GAGE LOCATIONS)

TEST POINT	CASE	POWER KW (HP)	RPM	MACH NUMBER	INFLOW ANGLE	ρ/ρ_O	EXCITATION FACTOR (EF)	σ/EF KPA (PSI) GAGE 1	σ/EF KPA (PSI) GAGE 2	σ/EF KPA (PSI) GAGE 3	σ/EF KPA (PSI) GAGE 4 (VEE)	σ/EF KPA (PSI) GAGE 5
215	1	225 (302)	7016	0.596	4°	0.9377	4.86	2006 (291)	1407 (204)	1751 (254)	455 (66)	745 (108)
217	2	650 (872)	8802	0.596	4°	0.9440	4.79	2799 (406)	1696 (246)	1917 (278)	690 (100)	324 (47)
245	3	195 (261)	7006	0.695	3°	0.9046	4.60	2027 (294)	1717 (249)	2000 (290)	255 (37)	1248 (181)
272	4*	148 (199)	7017	0.799	2°	0.8000	3.54	2055 (298)	2627 (381)	2799 (406)	545 (79)	3324 (482)
296	5	224 (301)	7012	0.792	4°	0.8134	7.06	2158 (313)	1889 (274)	2186 (317)	200 (29)	1517 (220)
—	6*	441 (591)	8636	0.800	3°	0.7602	5.33	2296 (333)	1552 (225)	1551 (233)	310 (45)	593 (86)
RERUN OF CASE 4 WITH CP OF CASE 6		148 (199)	7017	0.799	2°	0.8000	3.54	2103 (305)	1476 (214)	1820 (264)	400 (58)	945 (137)

CP=CENTER OF PRESSURE (SPANWISE VARIABLE)

*SEE FIGURE 3-17 FOR A PLOT OF CENTER PRESSURE VS. SPAN

TABLE 3-IV. SR-5 1P (ISOLATED NACELLE) APPARENT STRESS PREDICTIONS (REFER TO FIGURE 3-19 FOR GAGE LOCATIONS)

CASE	POWER KW (HP)	RPM	MACH NUMBER	INFLOW ANGLE	ρ/ρ_o	EXCITATION FACTOR (EF)	σ/EF KPA (PSI) GAGE 1	σ/EF KPA (PSI) GAGE 2	σ/EF KPA (PSI) GAGE 3 (VEE)	σ/EF KPA (PSI) GAGE 5	σ/EF KPA (PSI) GAGE 6
1	186 (250)	6000	0.6	7°	0.8889	7.86	4599 (667)	476 (69)	593 (86)	883 (128)	1455 (211)
2	336 (450)	6000	0.6	7°	0.8889	7.86	5033 (730)	496 (72)	662 (96)	1000 (145)	1620 (235)
3	388 (520)	7950	0.6	7°	0.8889	7.86	4695 (681)	476 (69)	524 (76)	600 (87)	1282 (186)
4	186 (250)	6000	0.8	2°	0.7976	3.49	4930 (715)	524 (76)	510 (74)	1393 (202)	1351 (196)
5	336 (450)	6000	0.8	2°	0.7976	3.49	5337 (774)	421 (61)	572 (83)	1076 (156)	1538 (223)
6	388 (520)	7950	0.8	2°	0.7976	3.49	4806 (697)	524 (76)	441 (64)	931 (135)	1131 (164)

TABLE 3-V. OPERATING CONDITIONS FOR AMES FLOW FIELD CALCULATIONS

T_T = 48.9°C
P_T = 1 ATM

		DESIGN CONDITIONS						TUNNEL CONDITIONS					
		MN	DESIGN POWER/D^2 KW/M^2	ISA ALT M	TIP SPEED M/S	J	C_P	V(TAS) (KM/HR)	N (RPM)	MN (TIP)	POWER KW	FLOW FIELD NO.	CASE NO.
HESS RUN CLIMB	C_L = 1.245 (WING) α_W = 12°	0.3	580	S.L.	244	1.316	1.0093	385.2	7846	0.717	221	1	1
		0.3	290	S.L.	244	1.316	0.5047	385.2	7846	0.717	110	1	2
		0.3	580	S.L.	183	1.755	2.3925	385.2	5883	0.538	221	1	3
		0.3	290	S.L.	183	1.755	1.1962	385.2	5883	0.538	110	1	4
	C_L = 0.815 (WING) α_W = 6°	0.3	580	S.L.	244	1.316	1.0093	385.2	7846	0.717	221	2	5
CRUISE	C_L = 0.783 (WING) α_W = 5°	0.6	302	10.668	244	2.296	1.6925	750.9	8771	0.823	454	3	6
		0.6	151	10.668	244	2.296	0.8462	750.9	8771	0.823	227	3	7
	C_L = 0.58 (WING) α_W = 2.5°	0.6	302	10.668	244	2.296	1.6925	750.9	8771	0.823	454	4	8
	C_L = 0.695 α_W = 0.3°	0.8	302	10.668	244	3.060	1.7000	976.1	8549	0.823	372	5	9

TABLE 3-VI. COMPARISON OF MULTIAZIMUTH CALCULATIONS WITH FLOW FIELDS FROM HS/H039 & AMES/HESS PROGRAMS

CASE NO.	PROGRAM	η	1P SHAFT FORCE (N)		1P SHAFT MOMENT (N-M)	
			COS (−NORMAL)	SIN (SIDE)	COS (YAW)	SIN (PITCH)
1	H039	0.680	−423	−9	−95	1
	AMES	0.693	−405	58	−89	16
2	H039	0.808	−316	9	−81	6
	AMES	0.821	−302	76	−76	22
3	H039	0.467	−512	−49	−53	−6
	AMES	0.488	−498	−4	−53	−2
4	H039	0.750	−405	−13	−75	−0.2
	AMES	0.768	−387	49	−71	11
5	H039	0.671	−187	−27	−42	−4
	AMES	0.679	−178	27	−38	8
6	H039	0.728	−596	−138	−80	−14
	AMES	0.746	−512	44	−66	12
7	H039	0.832	−498	−89	−77	−8
	AMES	0.852	−423	93	−62	19
8	H039	0.731	−200	−160	−27	−18
	AMES	0.745	−142	13	−16	5
9	H039	0.745	−374	−142	−39	−10
	AMES	0.776	−200	120	−17	17

TABLE 3-VII. AERODYNAMIC EXCITATIONS

	HS FLOW FIELDS								AMES/HESS FLOW FIELDS				
	1P SHANK MOMENT N-M	HIGHER ORDER SHANK MOMENTS – PERCENT OF 1P				MACH NO.	TIP SPEED M/S	POWER KW	1P SHANK MOMENT N-M	HIGHER ORDER SHANK MOMENTS – PERCENT OF 1P			
		2P	3P	4P	5P					2P	3P	4P	5P
CASE 1	23.8	7.9	2.9	0.9	0.3	0.3	244	221	22.7	10.5	4.4	1.8	0.7
2	19.1	9.6	3.1	1.1	0.3	0.3	244	110	18.4	11.1	4.4	1.8	0.7
3	21.9	5.7	2.9	2.3	0.8	0.3	183	221	21.0	11.3	4.6	3.4	1.8
4	20.6	8.0	2.7	0.9	0.3	0.3	183	110	19.6	10.0	4.3	1.7	0.6
5	10.7	11.8	4.4	1.5	0.5	0.3	244	221	9.7	20.3	7.9	3.3	1.4
6	27.1	11.0	4.8	1.5	0.5	0.6	244	454	21.8	22.3	9.2	3.5	1.5
7	23.3	13.2	5.0	1.6	0.5	0.6	244	227	19.2	23.1	9.1	3.5	1.6
8	10.8	21.5	8.4	2.8	1.1	0.6	244	454	5.6	70.5	29.2	12.3	5.1
9	15.5	20.1	8.1	2.9	1.0	0.8	244	372	8.8	55.4	21.0	9.3	4.0

TABLE 3-VIII. CALCULATED NATURAL FREQUENCIES FOR SR-2C

CASE NO.	RPM	$\beta_{.75R}$-DEG.	NATURAL FREQUENCIES – HZ			
			MODE 1	MODE 2	MODE 3	MODE 4
1 & 5	7843	42.1	219	573	1117	1308
2	7843	36.1	223	574	1117	1308
3	5883	57.7	183	522	1074	1286
4	5883	47.7	187	523	1074	1286
6 & 8	8771	53.8	226	596	1138	1323
7	8771	49.1	229	598	1138	1322
9	8549	59.6	219	589	1133	1318

TABLE 3-IX. PREDICTED VIBRATORY BLADE RESPONSE STRESSES (kPa) FOR THE SR-2C PROP-FAN INSTALLED ON THE SEMI-SPAN MODEL AT AMES

	HS/H039 FLOW-FIELDS						AMES/HESS FLOW-FIELDS					
CASE NO.	1P	2P	3P	4P	5P	TOTAL	1P	2P	3P	4P	5P	TOTAL
1	45645	5130	310	62	14	46610	42404	7171	710	269	165	42749
2	34268	5537	276	48	7	35785	32407	6695	586	200	138	32820
3	55712	14342	710	69	110	61503	51575	26959	1158	531	496	64675
4	47162	26753	572	55	7	64124	43439	34958	931	221	165	64537
5	20409	3606	214	34	7	21512	18065	5516	531	214	117	19237
6	52678	4764	448	572	34	53574	41163	8136	1379	3448	248	40543
7	43025	5254	538	462	41	44473	35302	7998	1172	3241	248	34544
8	20961	3751	372	538	62	21581	10067	6343	1379	2689	200	12894
9	30269	5102	462	159	41	31855	16824	7791	758	483	145	20409

TABLE 3-X. THE EFFECT OF TOE-IN ON THE HIGHER ORDER BENDING MOMENTS FOR THE SR-2C PROP-FAN MODEL INSTALLED ON THE SEMI-SPAN MODEL AT AMES - OPERATING CASE NO. 6

	2° TOE-IN		0° TOE-IN	
	MOMENT N-M	% OF 1P	MOMENT N-M	% OF 1P
1P	27.3	100.0	26.9	100.0
2P	3.0	11.0	2.6	9.6
3P	1.3	4.8	1.1	3.9
4P	0.4	1.5	0.3	1.2
5P	0.1	0.5	0.1	0.3

TABLE 3-XI. A COMPARISON OF THE FEATURES INCORPORATED IN THE AEROELASTIC STABILITY ANALYSES USED TO EVALUATE MODEL PROP-FAN STABILITY

ANALYSIS	STRUCTURAL MODEL	SOLUTION TECHNIQUE	AERODYNAMIC MODEL		
			UNSTEADY FORMULATION	SWEEP CORRECTIONS	CASCADE CORRECTIONS
G400T2	UNCOUPLED BEAM MODES	NON-LINEAR TIME HISTORY	EMPIRICAL QUASI-STEADY	NONE	NONE
F168	UNCOUPLED BEAM MODES	LINEAR EIGENVALUE	EMPIRICAL QUASI-STEADY	NONE	NONE
F187	COUPLED BLADE MODES	LINEAR EIGENVALUE	THEORETICAL UNSTEADY INCOMPRESSIBLE THEODORSEN	COSINE CORRECTION	NONE
F203	COUPLED BLADE MODES	LINEAR EIGENVALUE	THEORETICAL UNSTEADY COMPRESSIBLE	CUNNINGHAM CORRECTION	SMITH COMPRESSIBLE SUBSONIC

TABLE 3-XII. CLASSICAL FLUTTER STABILITY PREDICTION SUMMARY FOR THE MODEL PROP-FANS

ANALYSIS	SR-2C	SR-3	SR-5
G400T2	UNSTABLE 1ST TORSION MODE	STABLE	UNSTABLE "1ST TORSION MODE"
F168	UNSTABLE 1ST TORSION MODE	STABLE	———
F187	———	———	STABLE
F203	STABLE	STABLE (POTENTIAL 1ST MODE INSTABILITY)	UNSTABLE 1ST MODE

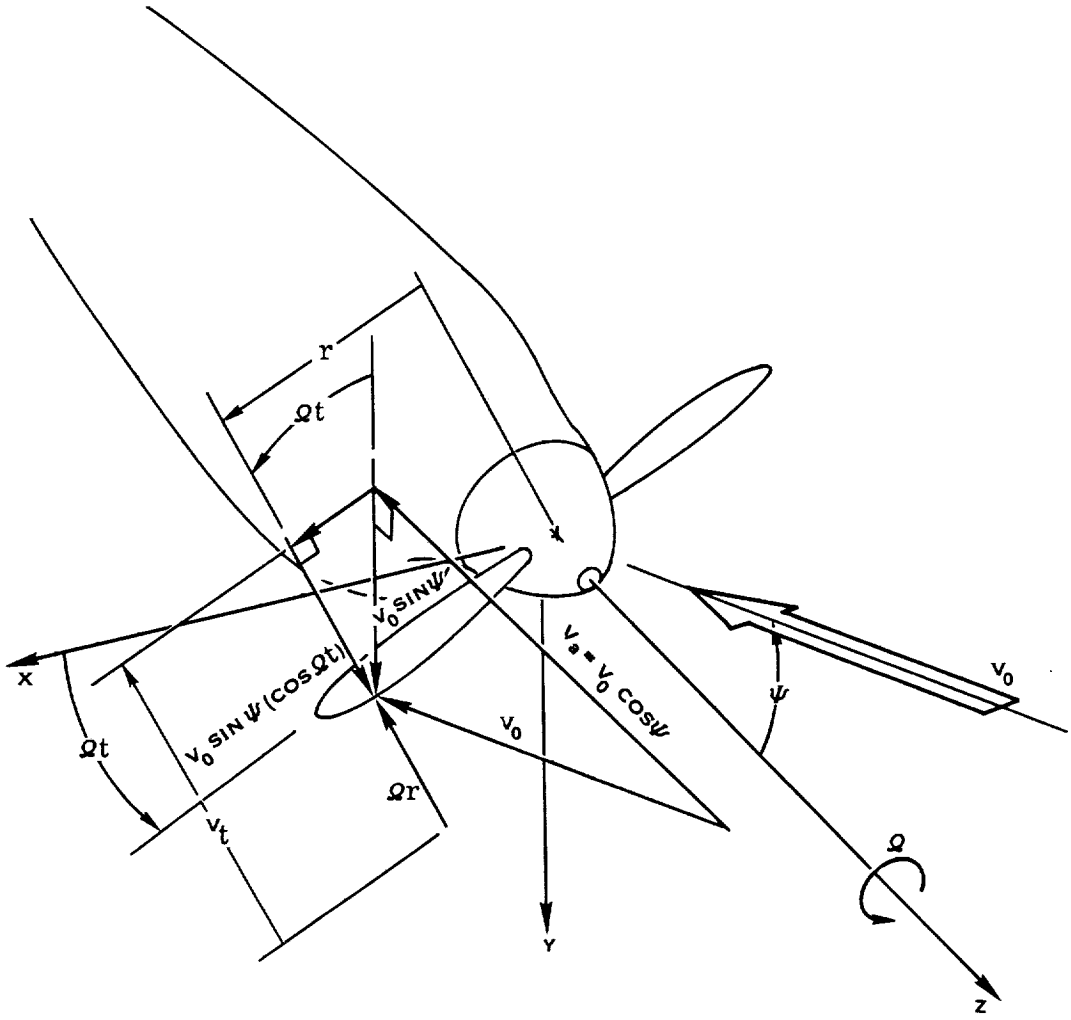

PROP-FAN VELOCITY DEFINITIONS

AXIAL $V_a = V_O \cos\psi$

TANGENTIAL $V_t = \Omega r - V_O \sin\psi (\cos\Omega t)$

FREE STREAM = V_O

FIG. 3-1 ISOLATED NACELLE SHOWING LOCAL BLADE ELEMENT VELOCITY VECTORS DUE TO AN ANGULAR FLOW FIELD.

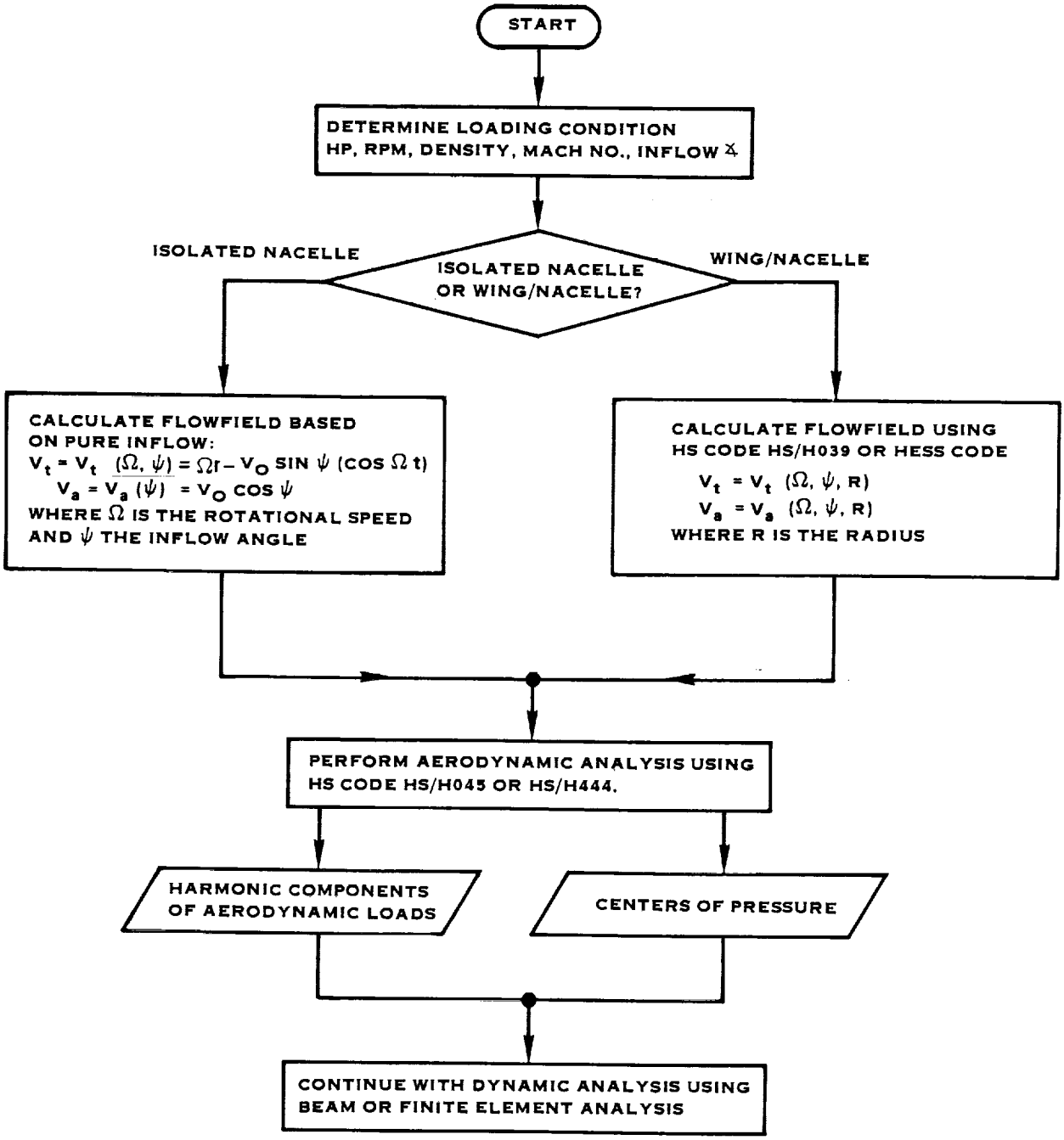

FIGURE 3-2. PROP-FAN MODEL BLADE ANALYSIS - FLOWCHART FOR AERODYNAMIC LOAD CALCULATION (DYNAMIC ANALYSIS)

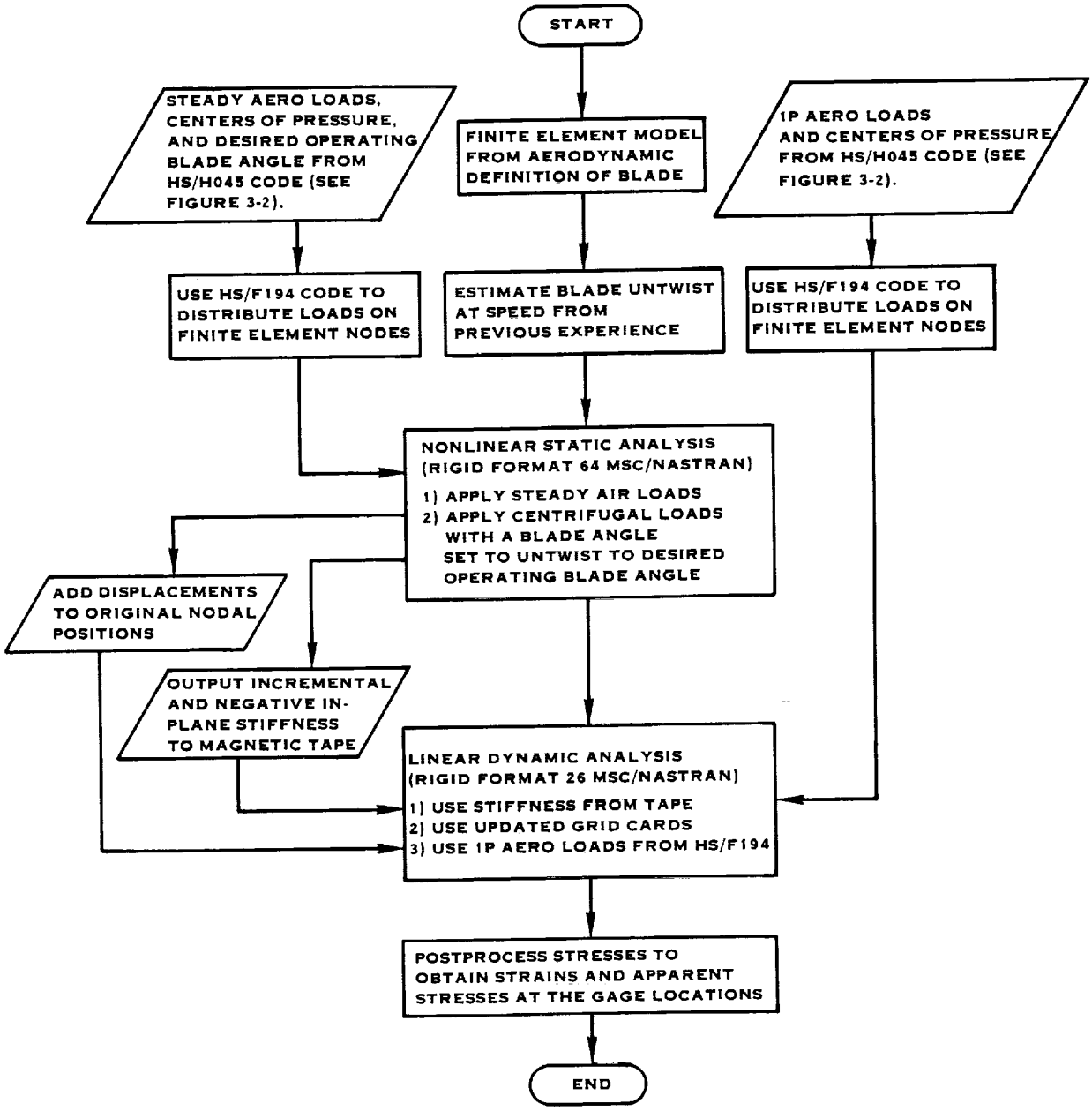

FIGURE 3-3 PROP-FAN MODEL BLADE ANALYSIS - 1P DYNAMIC ANALYSIS USING MSC/NASTRAN

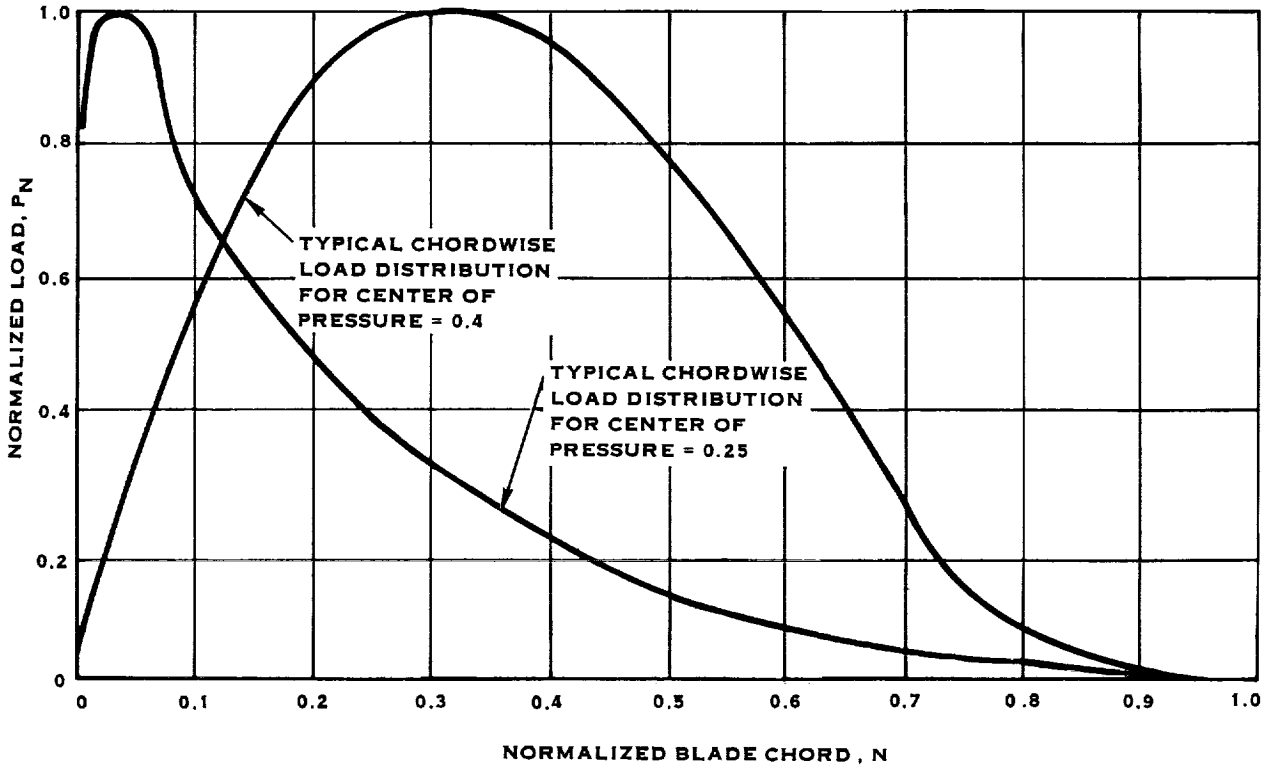

TYPICAL CHORDWISE 1P LOAD DISTRIBUTION BASED ON THE ANALYTICAL FUNCTION $P_N = A(N_C)^B (1-(N_C)^{.25})^2$ WHERE N_C IS THE NORMALIZED BLADE CHORD AND A AND B ARE CHOSEN TO GIVE THE CALCULATED TOTAL LOAD AND TO MATCH THE CALCULATED CENTER OF PRESSURE.

FIGURE 3-4. SR-3 AND SR-5 MODEL PROP-FAN 1P ANALYSES

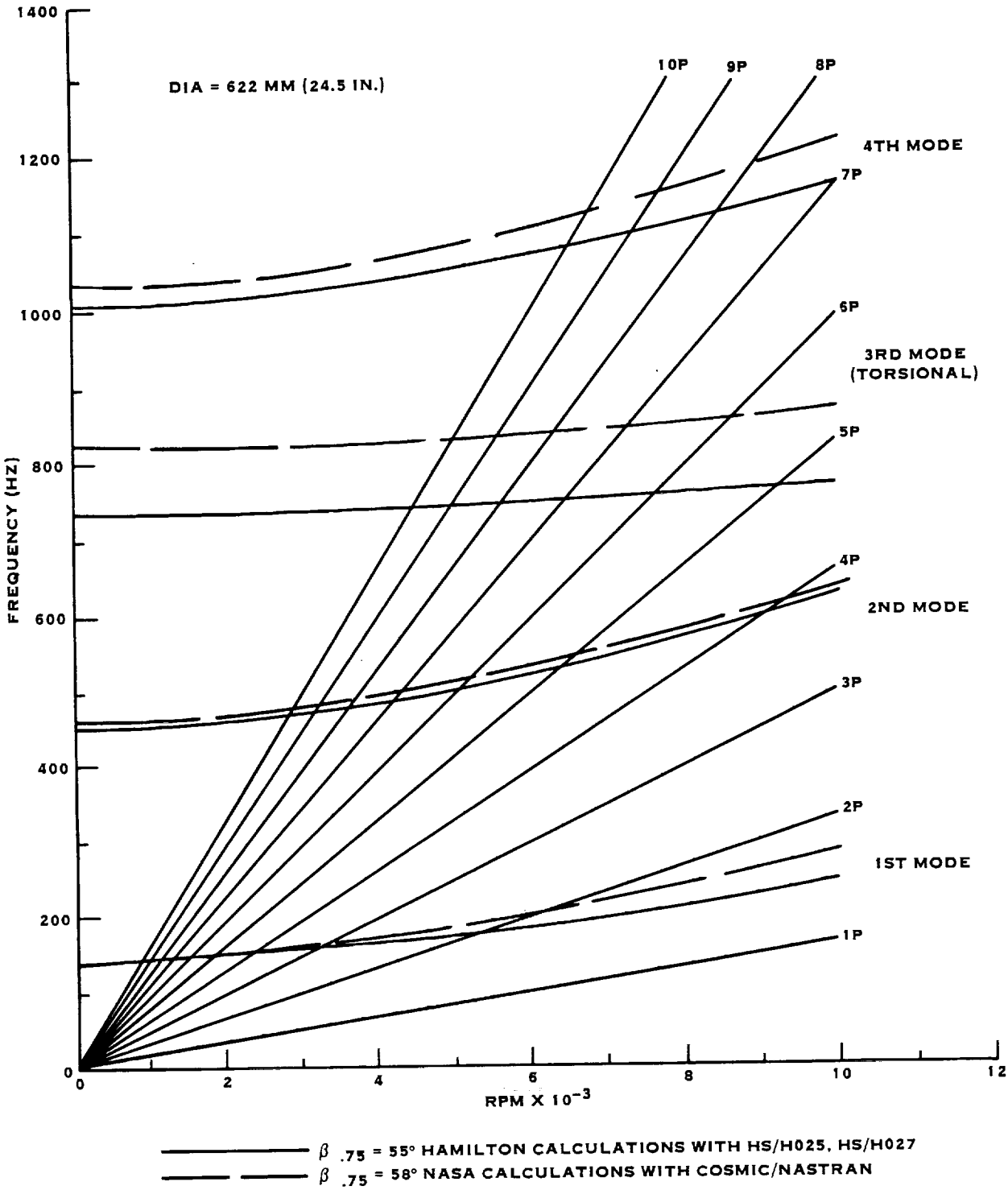

FIGURE 3-5 SR-2C PROP-FAN MODEL CAMPBELL DIAGRAM

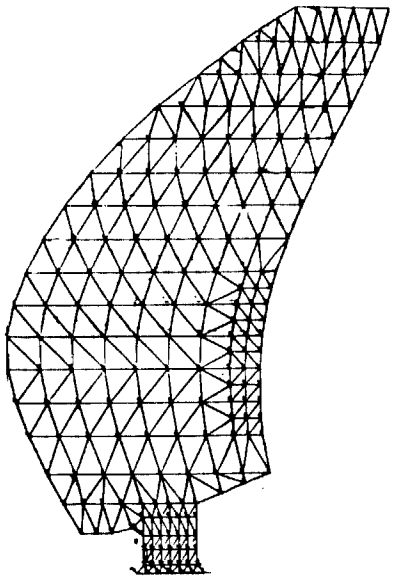

DIA = 622 MM (24.5 IN.)
$\beta_{.75}$ = 57°
(CALCULATIONS WITH BESTRAN)

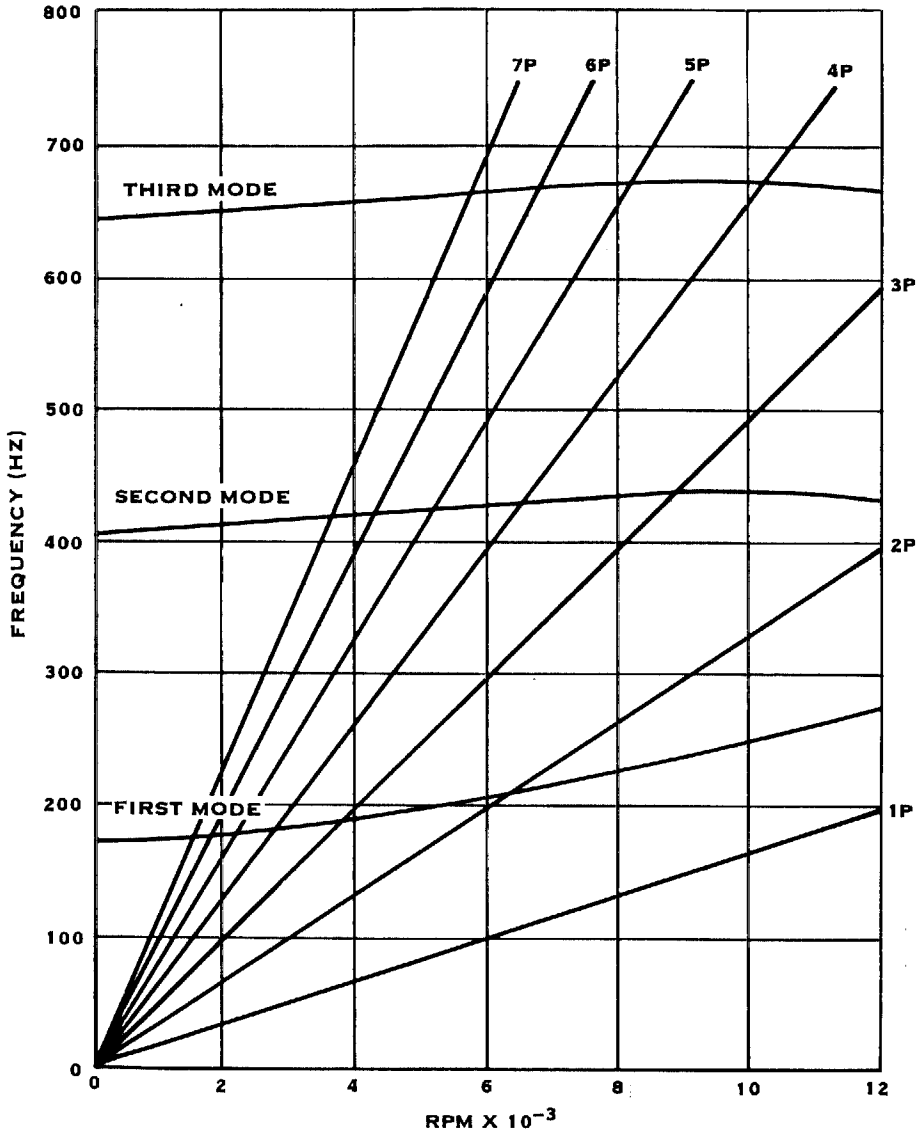

FIGURE 3-6 SR-3 PROP-FAN MODEL CAMPBELL DIAGRAM

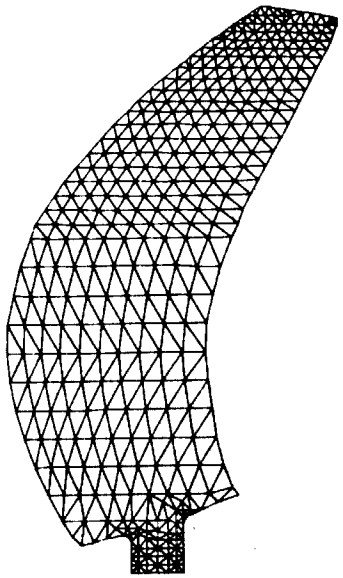

NOTE: MODEL USED WAS PRETWISTED TO OBTAIN AN APPROXIMATION TO DESIRED AERODYNAMIC SHAPE AT 7950 RPM ($\beta_{.75}$ AT ZERO RPM IS 66.7°)

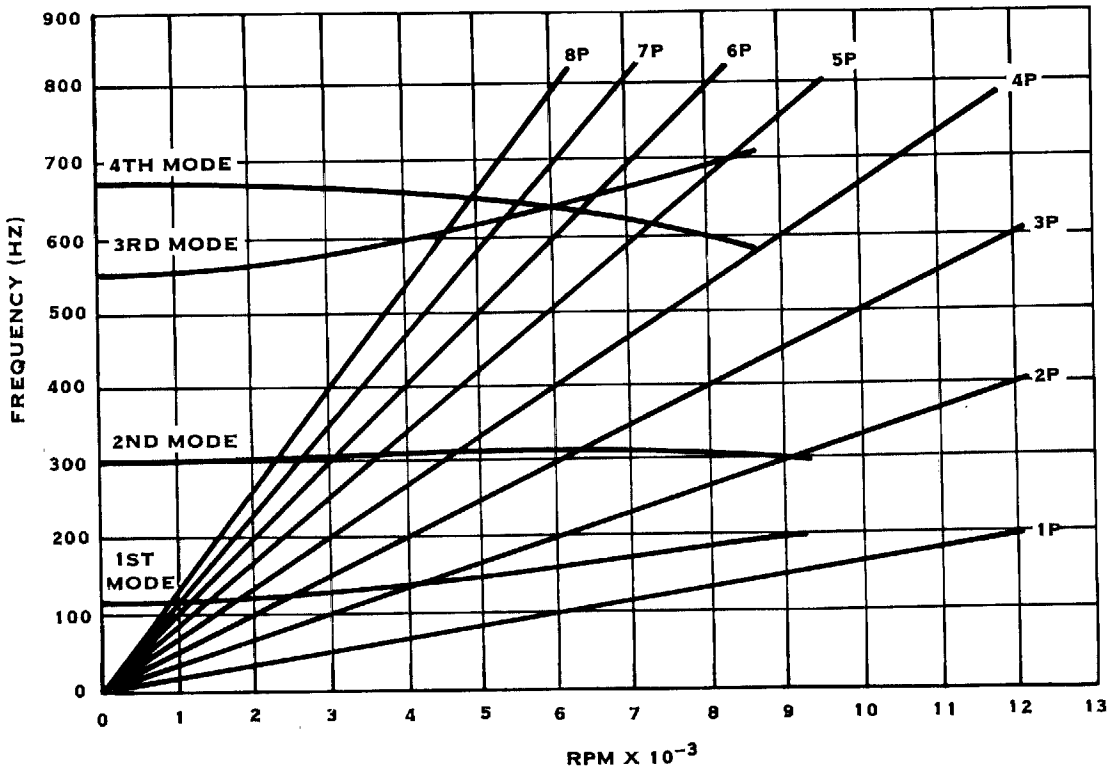

FIGURE 3-7 SR-5 PROP-FAN MODEL CAMPBELL DIAGRAM, DIA = 622 MM (24.5 IN.)
$\beta_{.75}$ = 61.1° CALCULATIONS WITH BESTRAN

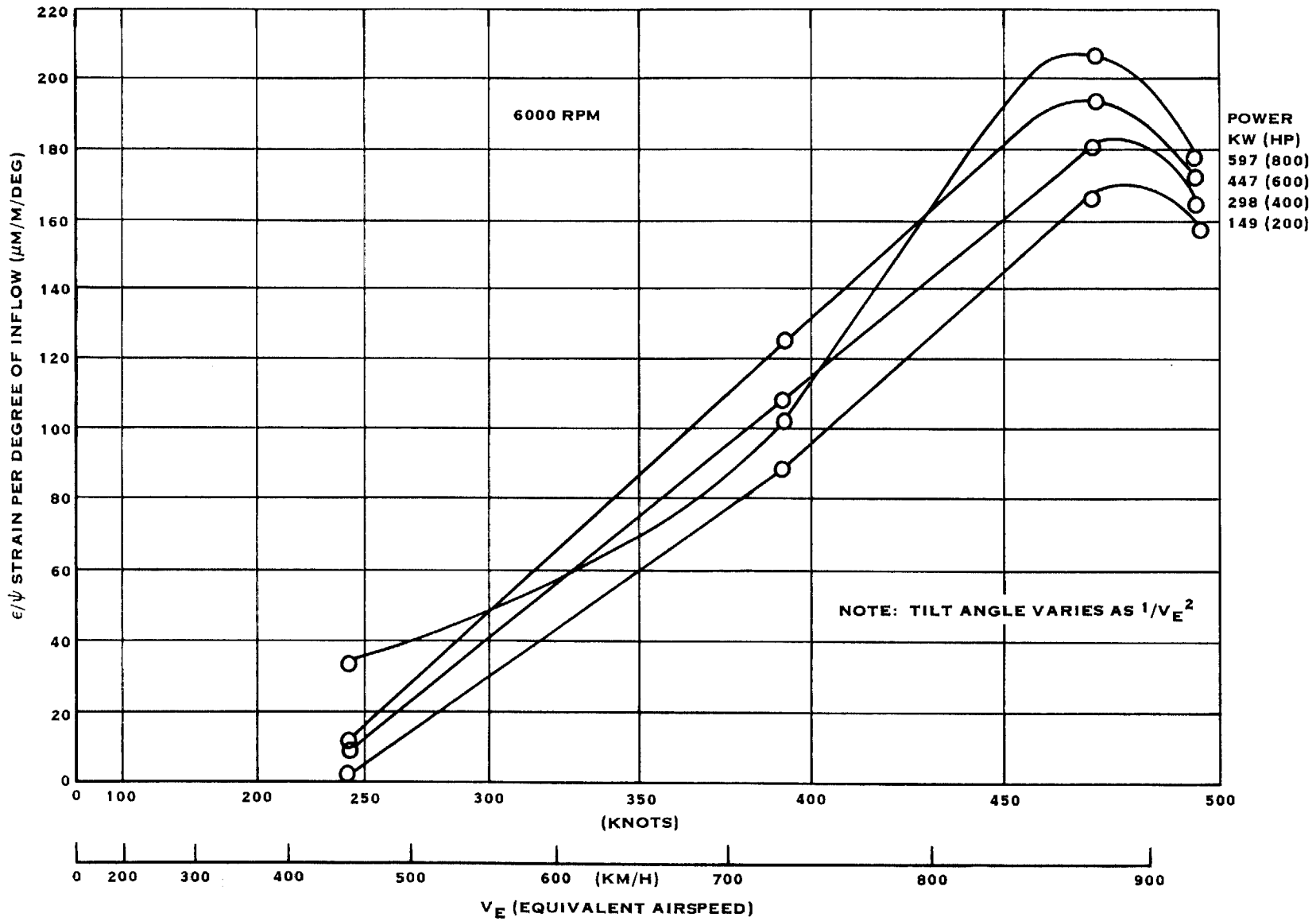

FIGURE 3-8 SR-2C MODEL PROP-FAN 1P CALCULATIONS, STRAIN GAGE 1 (ISOLATED NACELLE) USING HS CODES HS/H444, HS/H026 (6000 RPM)

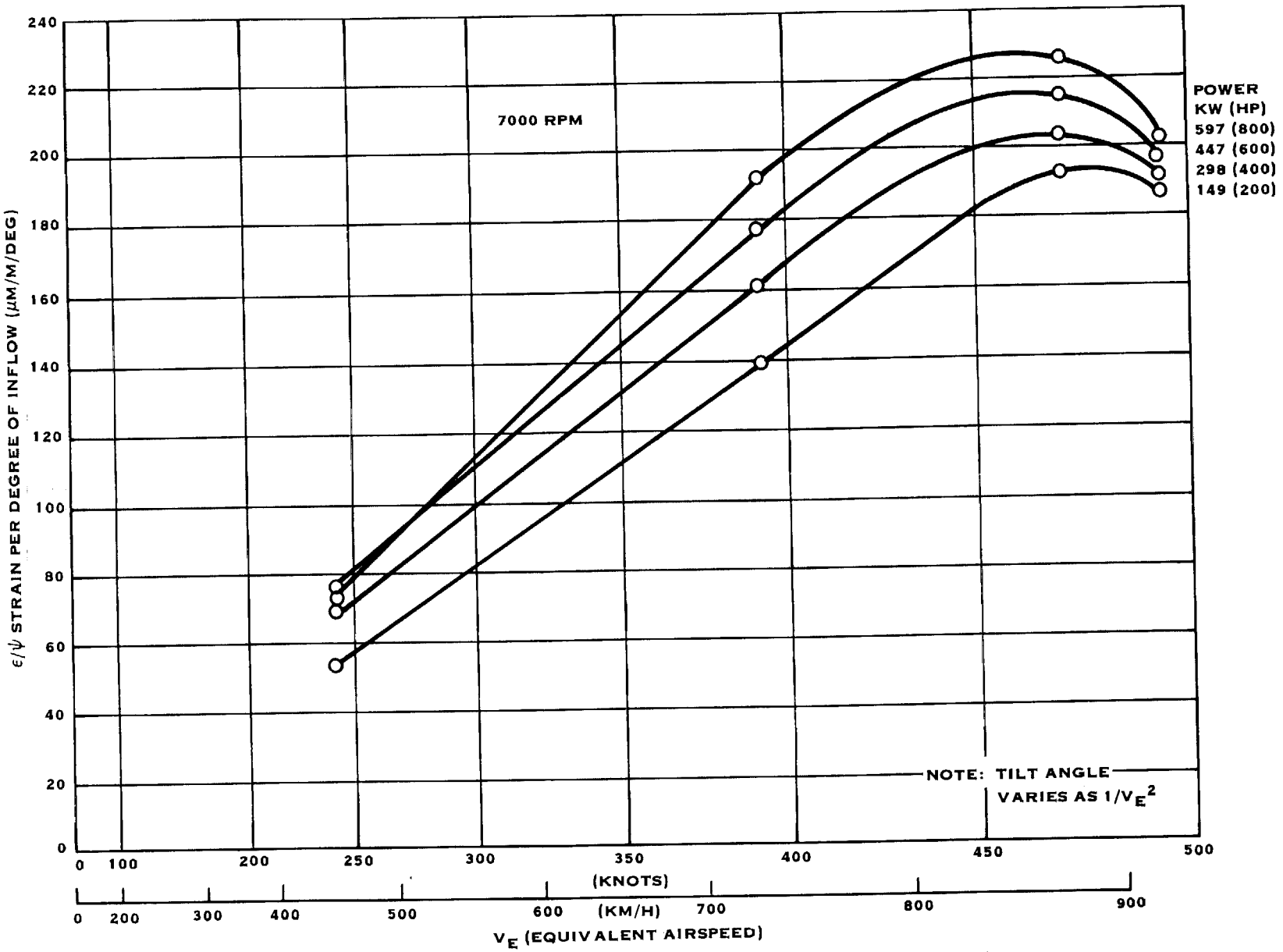

FIGURE 3-9 SR-2C MODEL PROP-FAN 1P CALCULATIONS, STRAIN GAGE 1 (ISOLATED NACELLE) USING HS CODES HS/H444, HS/H026 (7000 RPM)

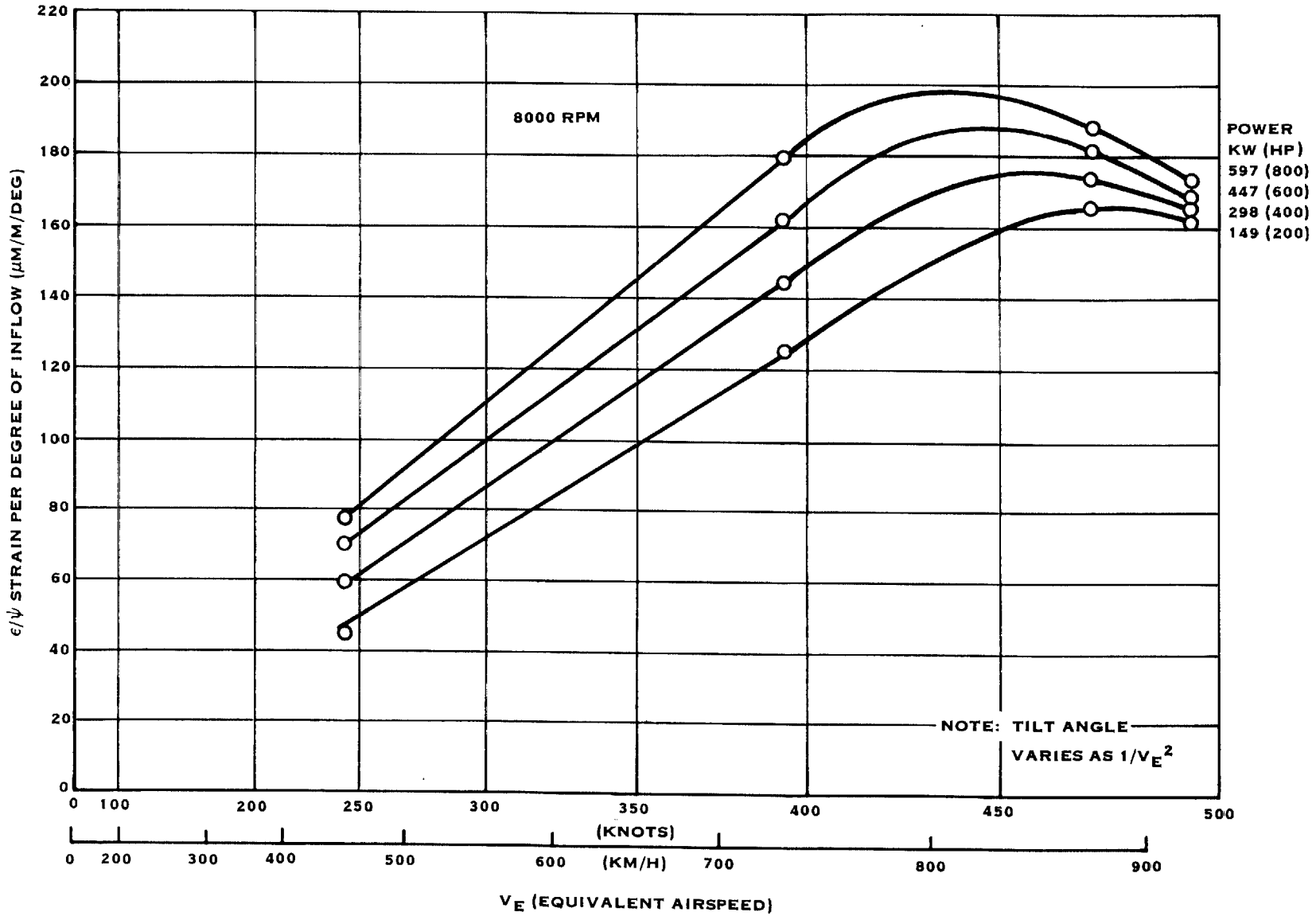

FIGURE 3-10. SR-2C MODEL PROP-FAN 1P CALCULATIONS, STRAIN GAGE 1 (ISOLATED NACELLE) USING HS CODES HS/H444, HS/H026 (8000 RPM)

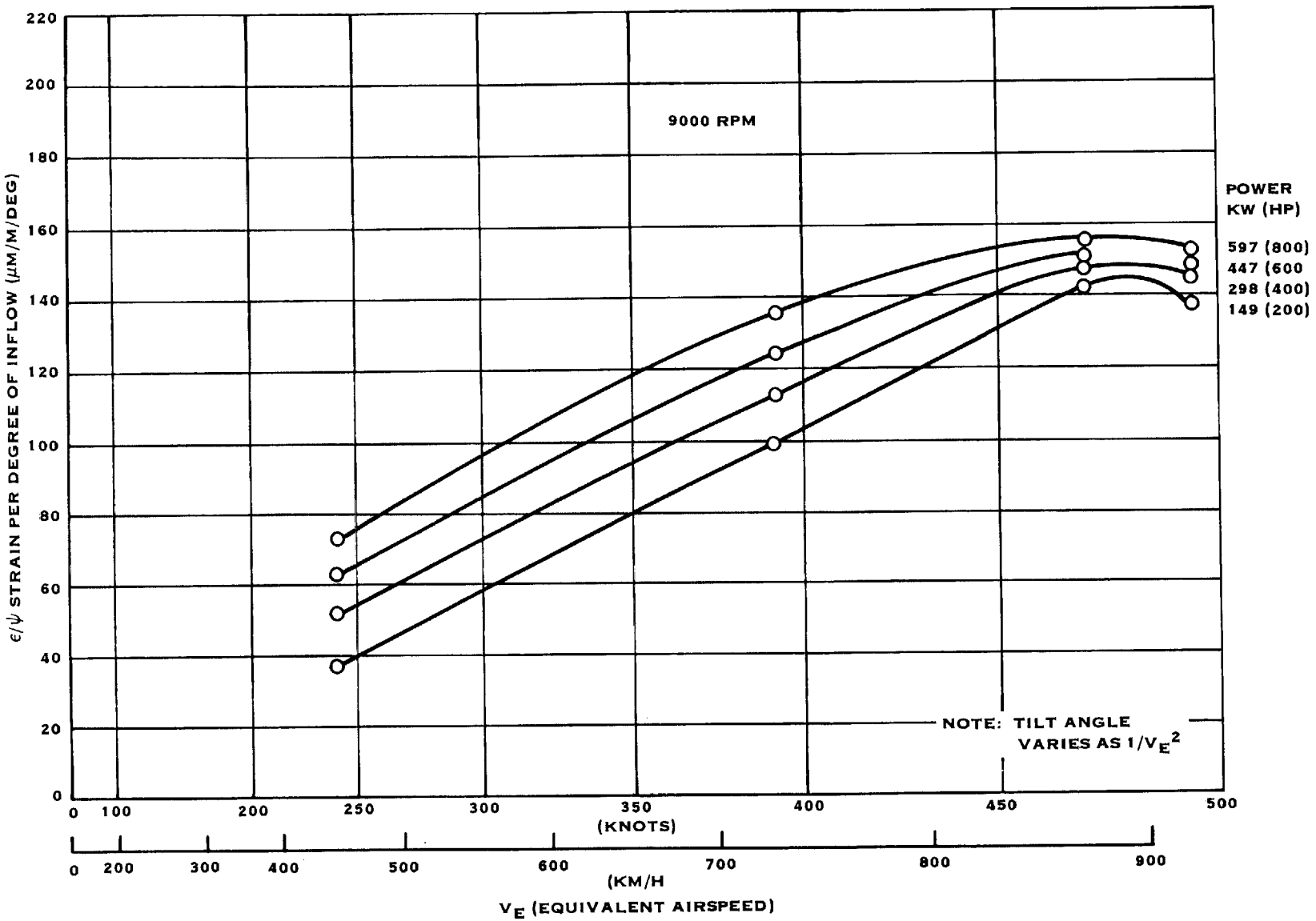

FIGURE 3-11 SR-2C MODEL PROP-FAN 1P CALCULATIONS, STRAIN GAGE 1 (ISOLATED NACELLE) USING HS CODES HS/H444, HS/H026 (9000 RPM)

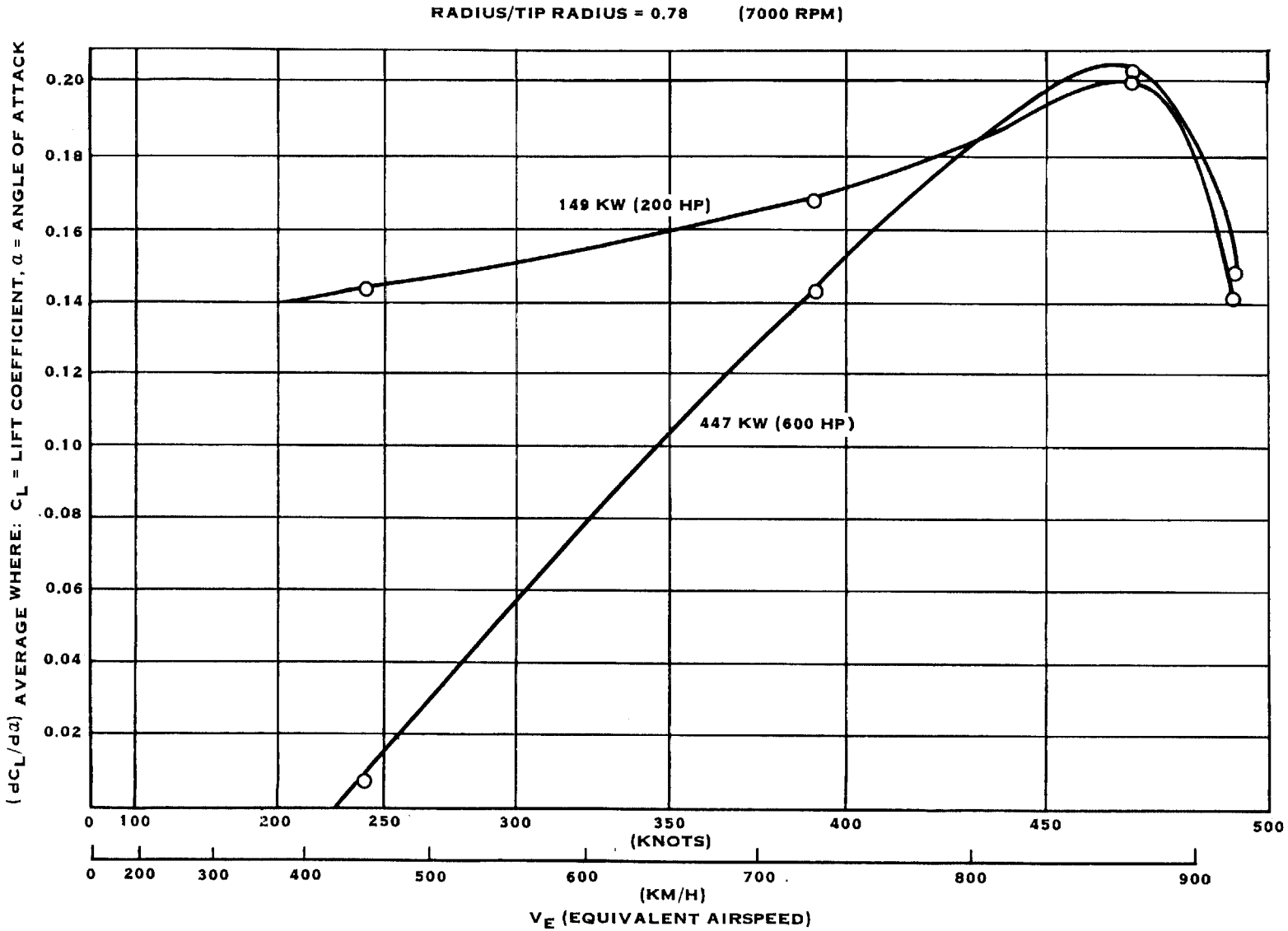

FIGURE 3-12 SR-2C PROP-FAN MODEL BLADE 1P CALCULATIONS (ISOLATED NACELLE) USING HS CODE HS/H444 - LIFT CURVE SLOPE VARIATION

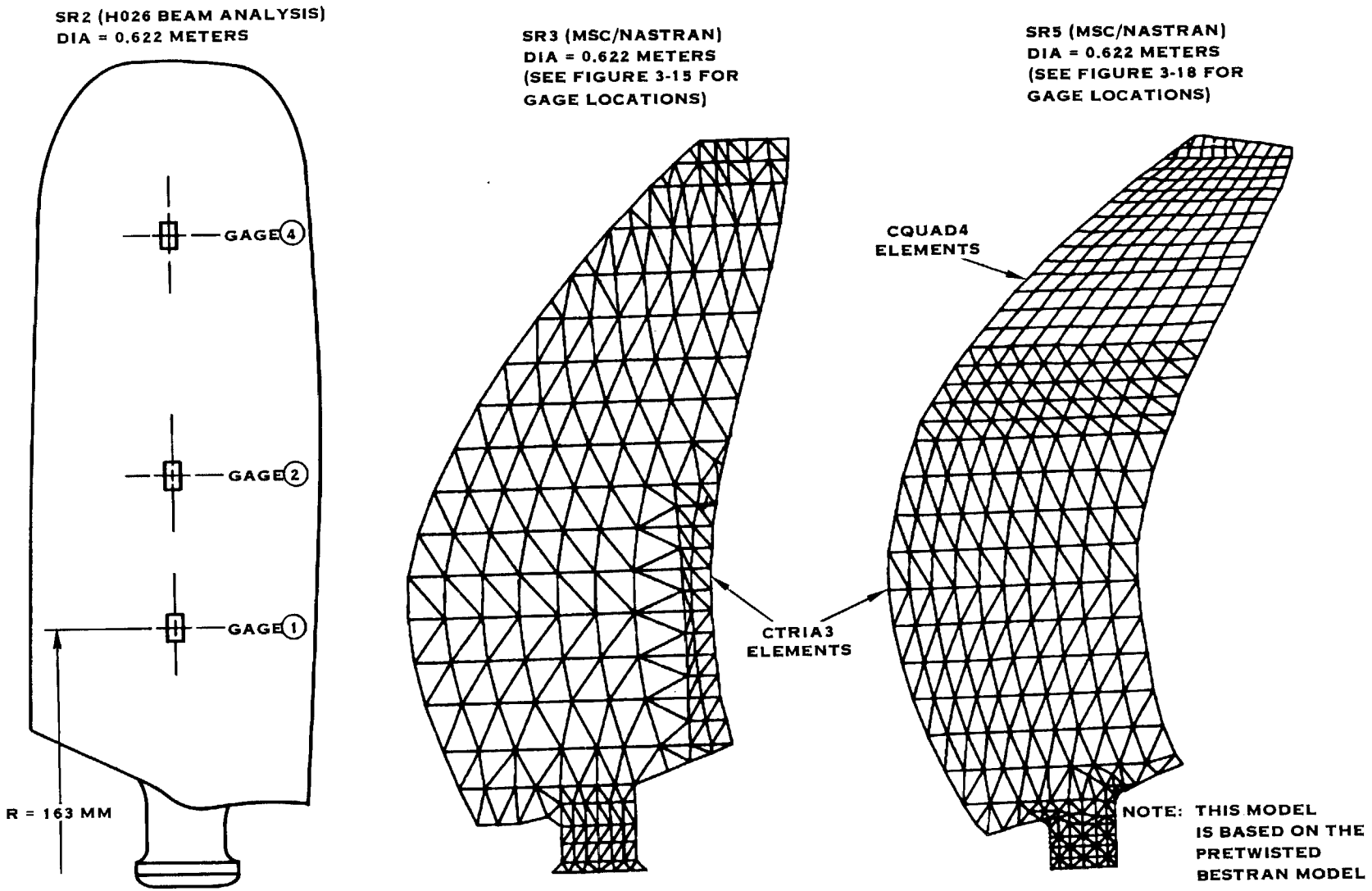

FIGURE 3-13 PROP-FAN ANALYTICAL MODELS USED FOR 1P RESPONSE PREDICTIONS

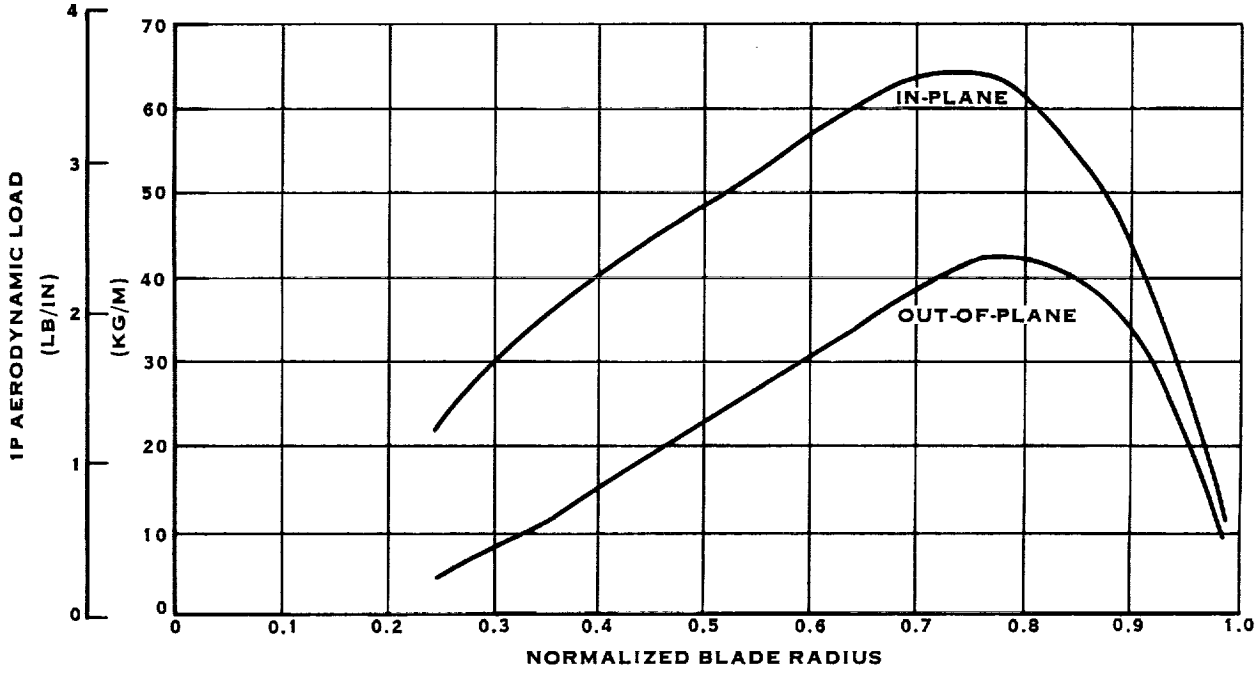

FIGURE 3-14 SR-3 MODEL PROP-FAN 1P AERODYNAMIC LOAD SPANWISE DISTRIBUTION (CASE 6)

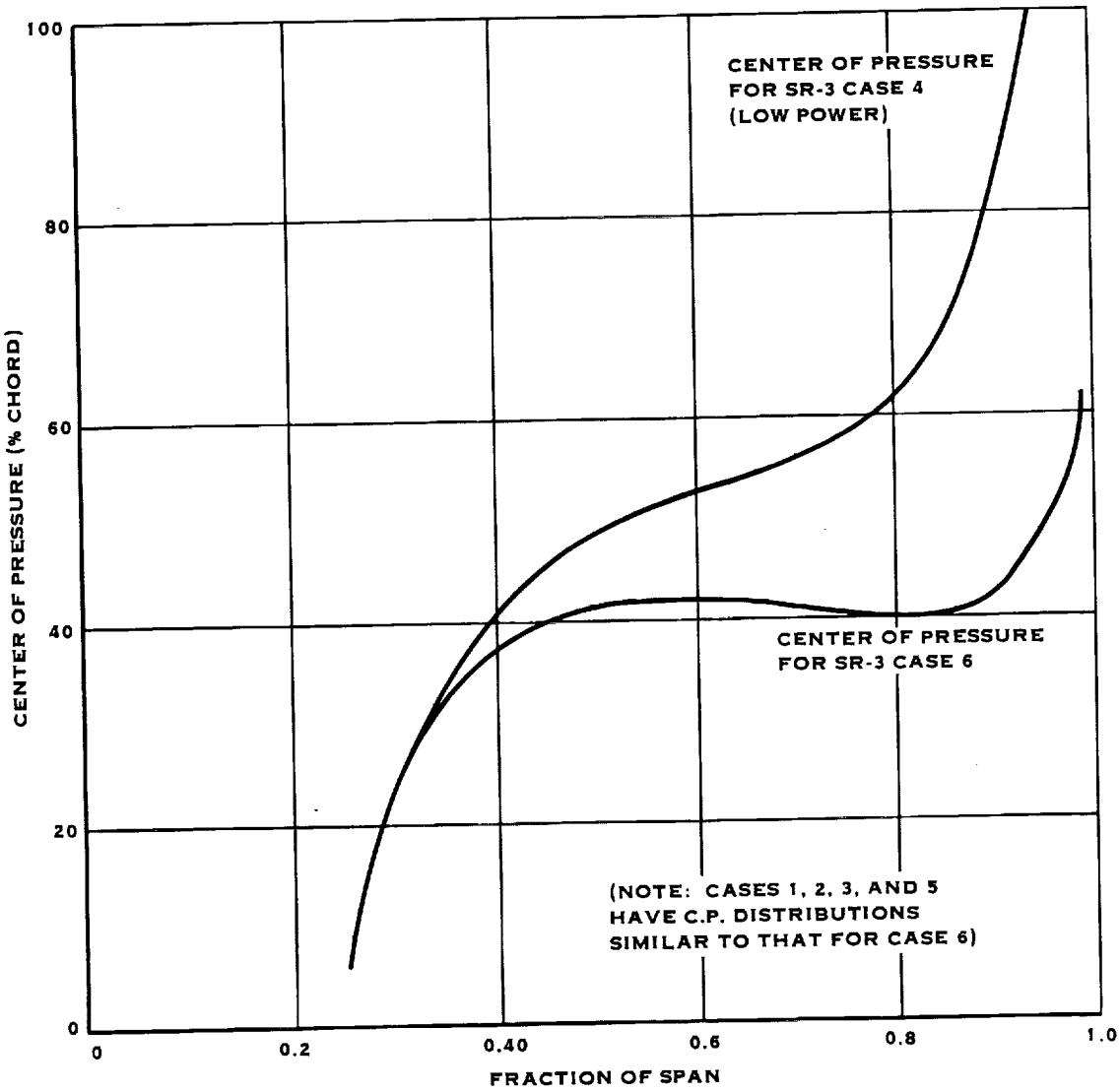

FIGURE 3-15 SR-3 MODEL PROP-FAN 1P ANALYSIS CALCULATED SPANWISE DISTRIBUTION OF CENTER OF PRESSURE (ASSUMED TO BE INDEPENDENT OF AZIMUTH)

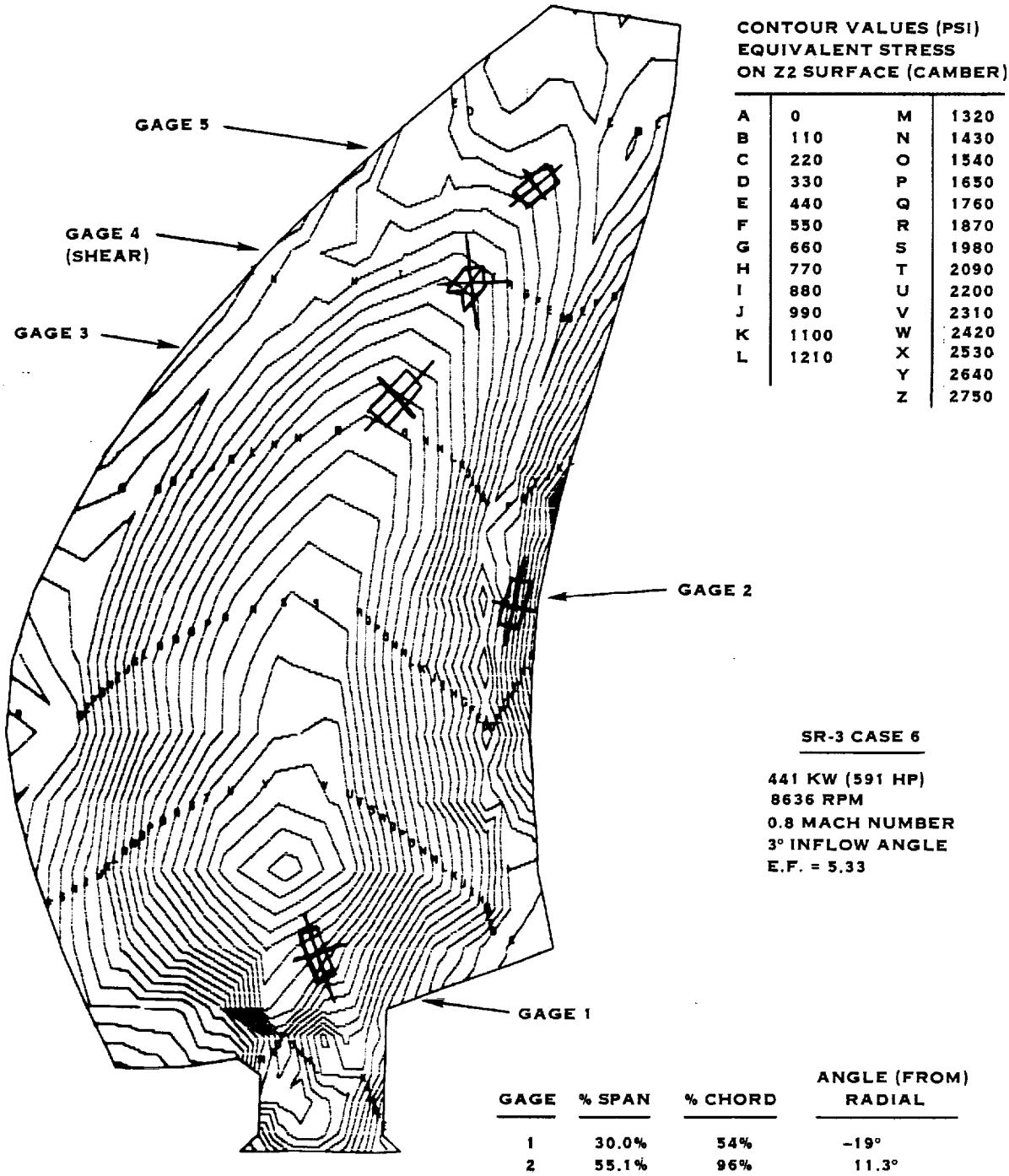

GAGE	% SPAN	% CHORD	ANGLE (FROM) RADIAL
1	30.0%	54%	-19°
2	55.1%	96%	11.3°
3	69.9%	56%	42°
4	78.4%	59%	-6.5°
5	86.3%	61%	49°

FIGURE 3-16 CONTOUR PLOT OF SR-3 EFFECTIVE SURFACE STRESS FOR 1P DYNAMIC RESPONSE

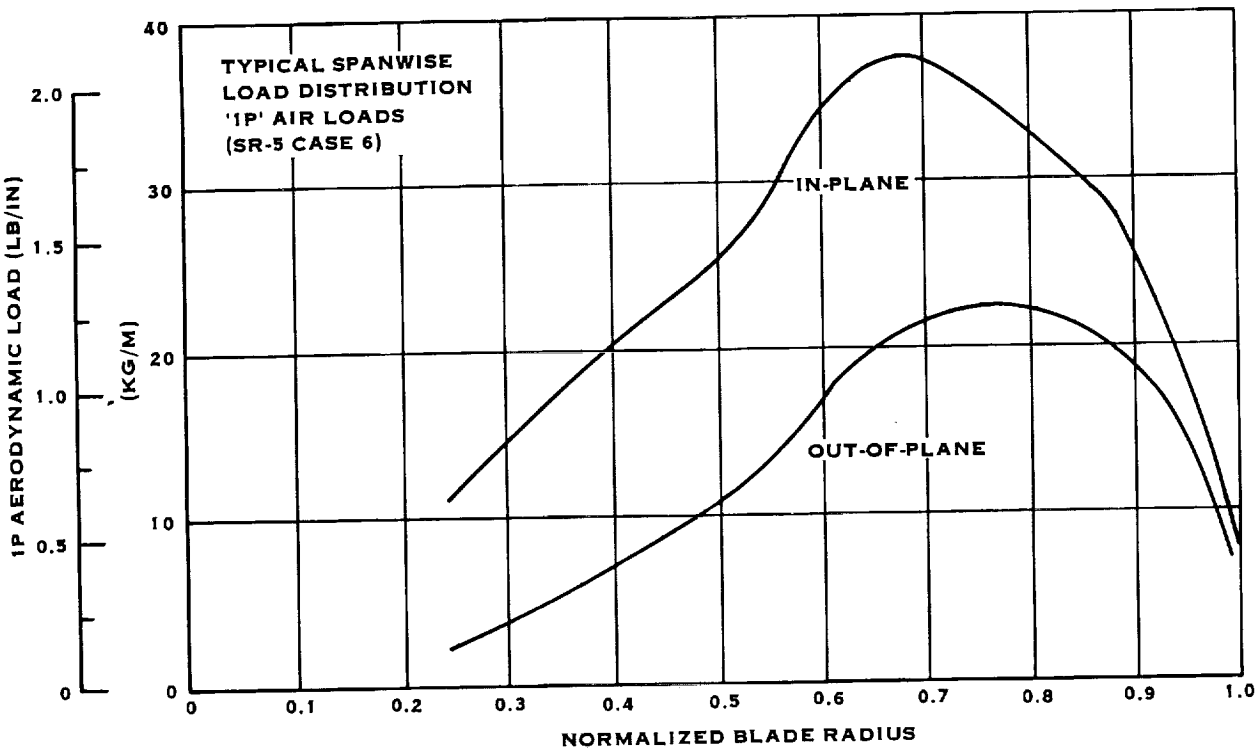

FIGURE 3-17 SR-5 MODEL PROP-FAN 1P AERODYNAMIC LOAD SPANWISE DISTRIBUTION

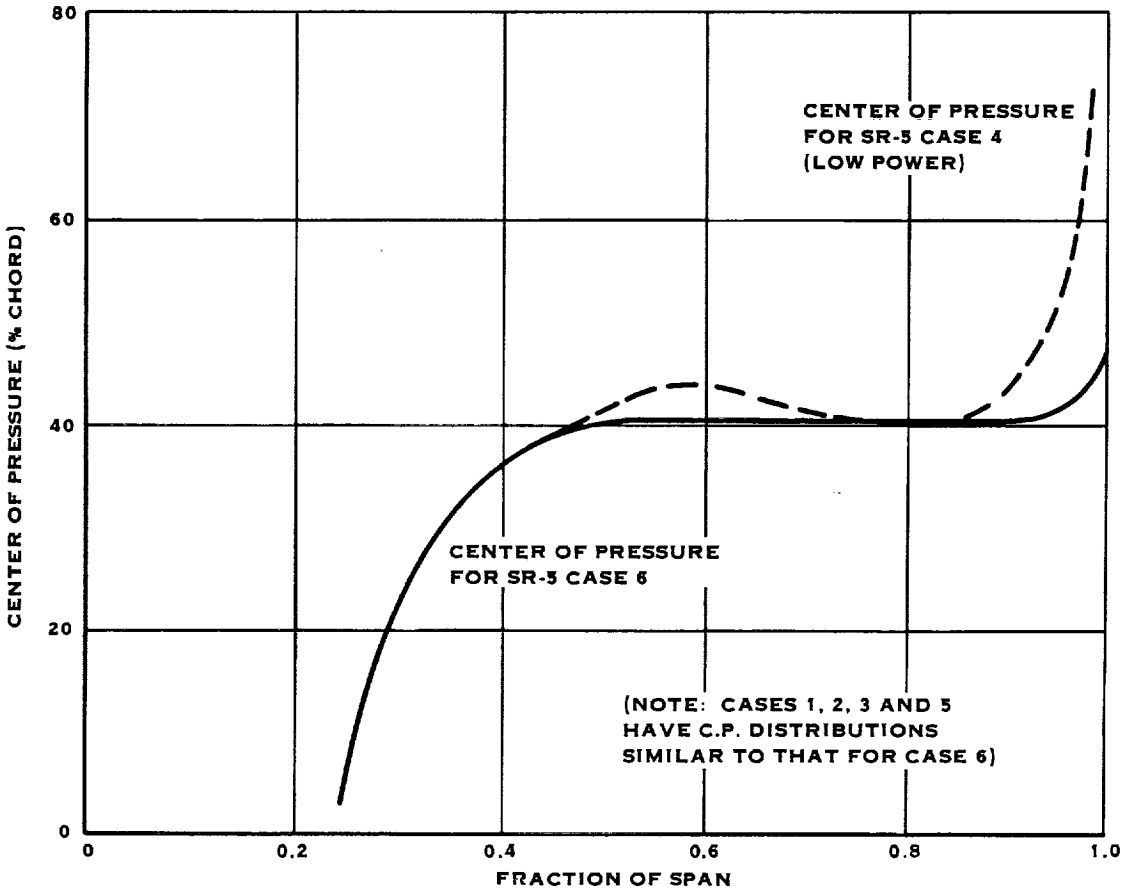

FIGURE 3-18 SR-5 MODEL PROP-FAN 1P ANALYSIS CALCULATED SPANWISE DISTRIBUTION OF CENTER OF PRESSURE (ASSUMED TO BE INDEPENDENT OF AZIMUTH)

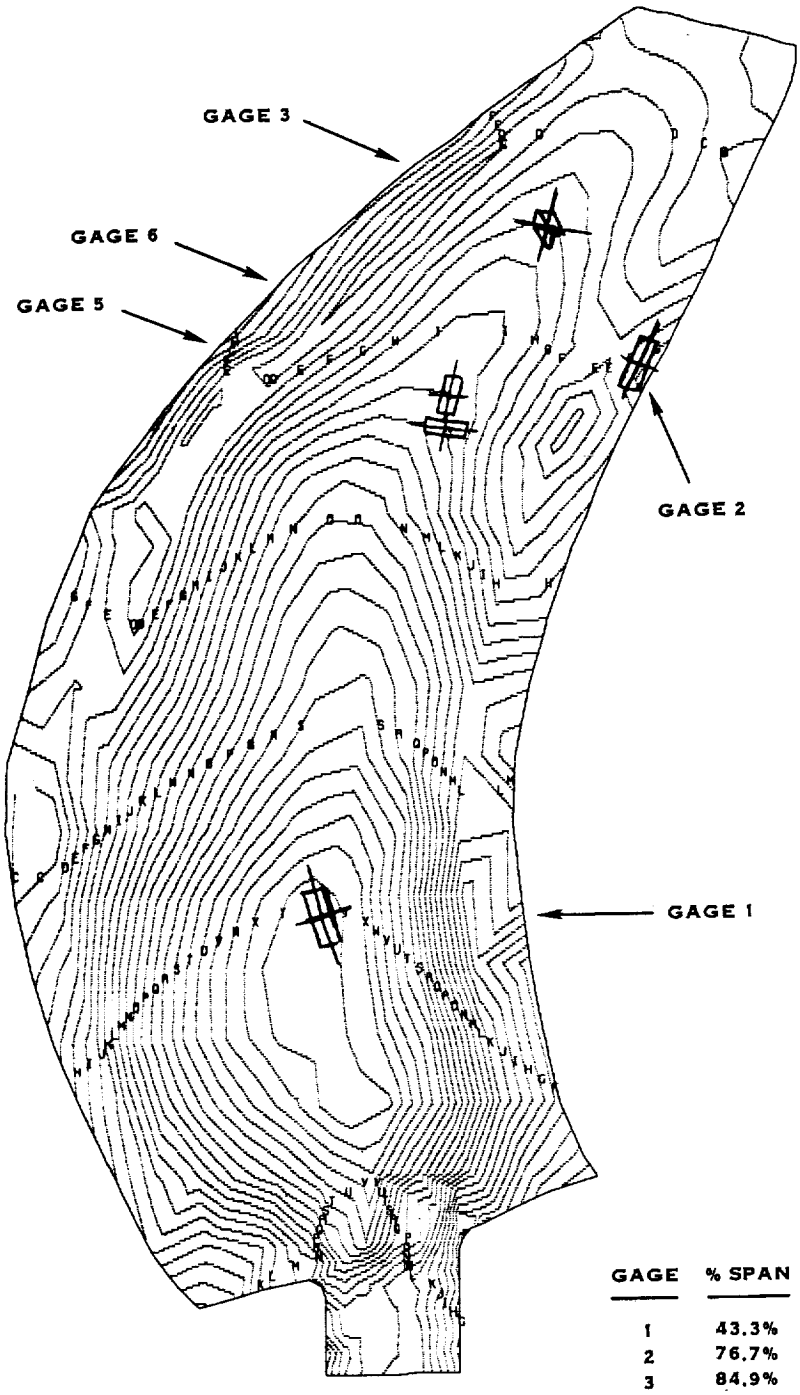

CONTOUR VALUES
EQUIVALENT STRESS (PSI)
ON Z2 SURFACE (CAMBER)

A	0	M	1380
B	115	N	1495
C	230	O	1610
D	345	P	1725
E	460	Q	1840
F	575	R	1955
G	690	S	2070
H	805	T	2185
I	920	U	2300
J	1035	V	2415
K	1150	W	2530
L	1265	X	2645
		Y	2760
		Z	2875

SR-5 CASE 6

387 KW (520 HP)
7950 RPM
0.8 MACH NUMBER
2° INFLOW ANGLE
E.F. = 3.49

GAGE	% SPAN	% CHORD	ANGLE (FROM RADIAL)
1	43.3%	60%	-10°
2	76.7%	96%	35.5°
3	84.9%	50%	6°, -84°
5	72.7%	63%	-80°
6	74.3%	60%	10°

FIGURE 3-19 CONTOUR PLOT OF SR-5 EFFECTIVE SURFACE STRESS FOR 1P DYNAMIC RESPONSE

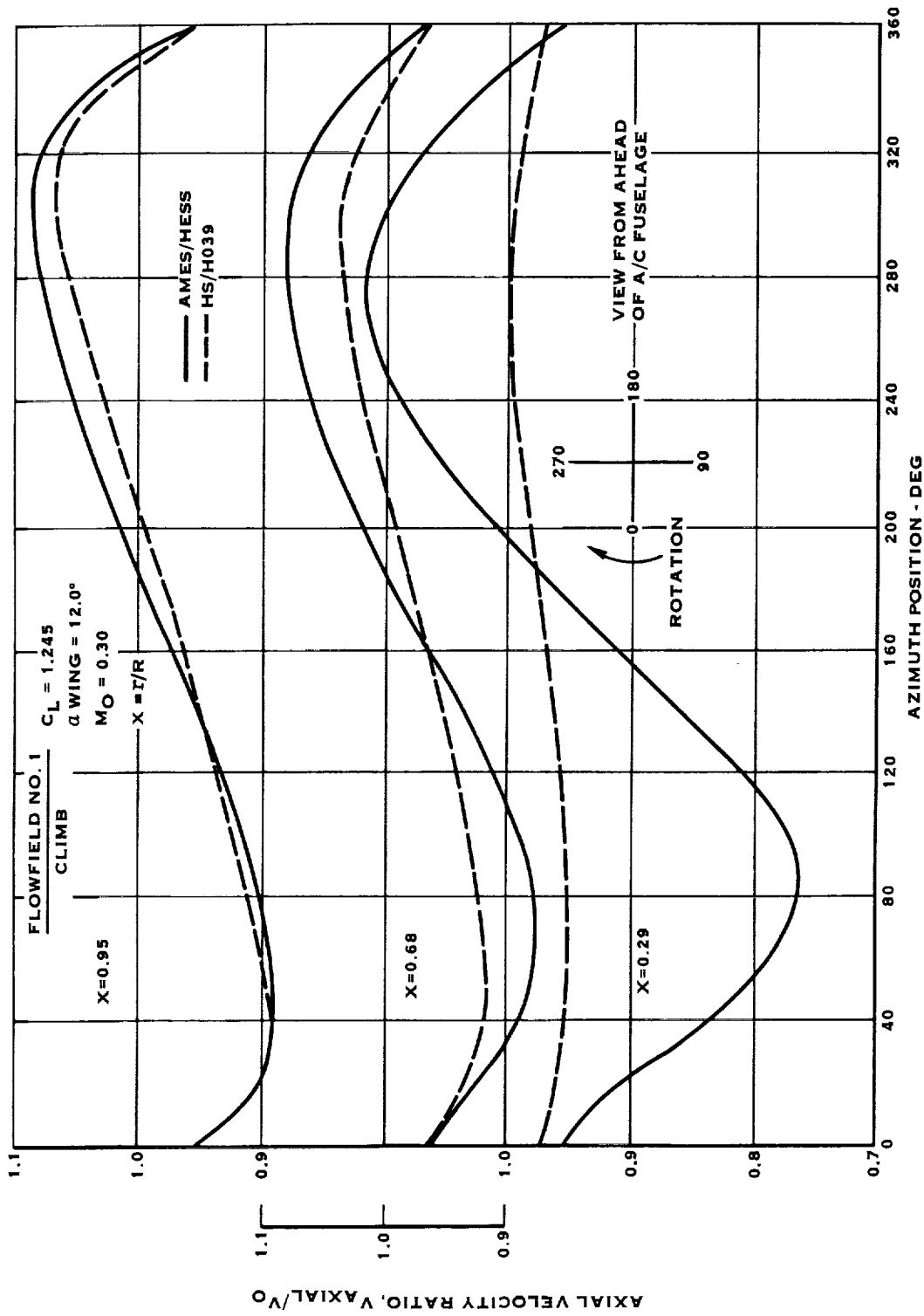

FIGURE 3-20. FLOWFIELD PREDICTIONS FOR THE NASA-AMES SEMI-SPAN AIRCRAFT MODEL AXIAL VELOCITIES, CASES NO. 1 THROUGH 4 (VELOCITIES DEFINED IN PLANE OF THE PROPELLER)

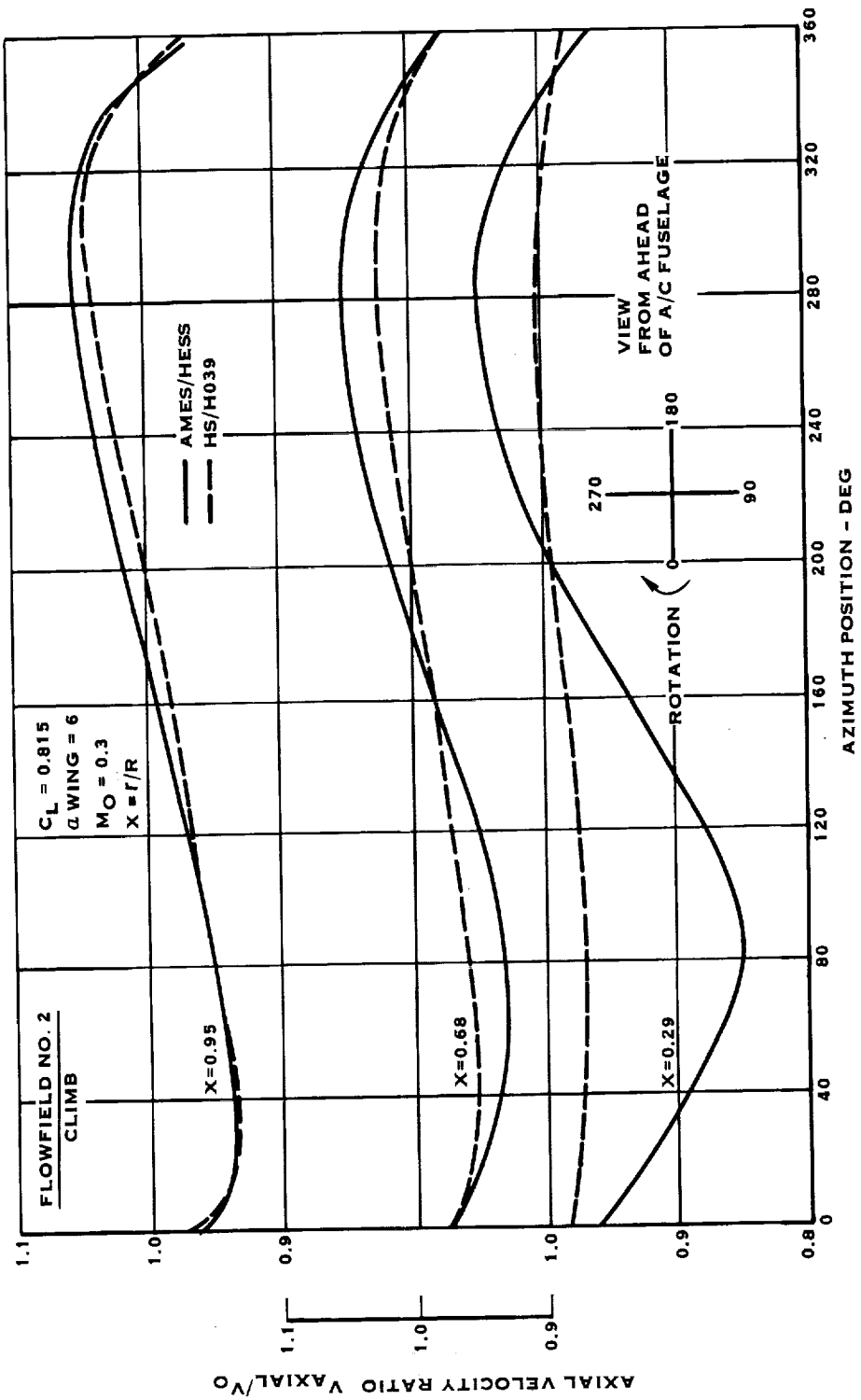

FIGURE 3-21. FLOWFIELD PREDICTIONS FOR THE NASA-AMES SEMI-SPAN AIRCRAFT MODEL AXIAL VELOCITIES, CASE NO. 5 (VELOCITIES DEFINED IN PLANE OF THE PROPELLER)

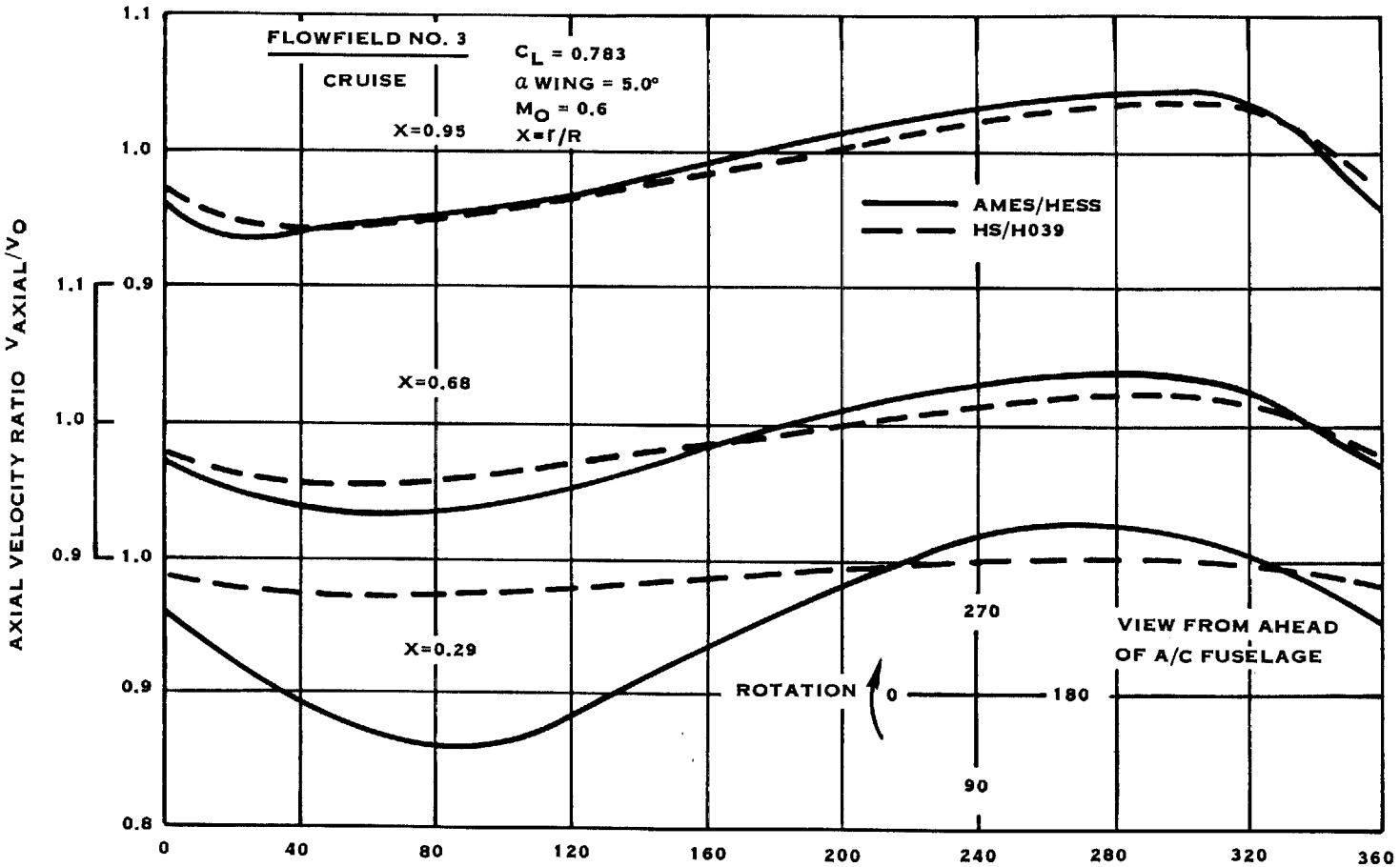

FIGURE 3-22. FLOWFIELD PREDICTIONS FOR THE NASA-AMES SEMI-SPAN AIRCRAFT MODEL AXIAL VELOCITIES, CASES NO. 6 AND 7 (VELOCITIES DEFINED IN PLANE OF THE PROPELLER)

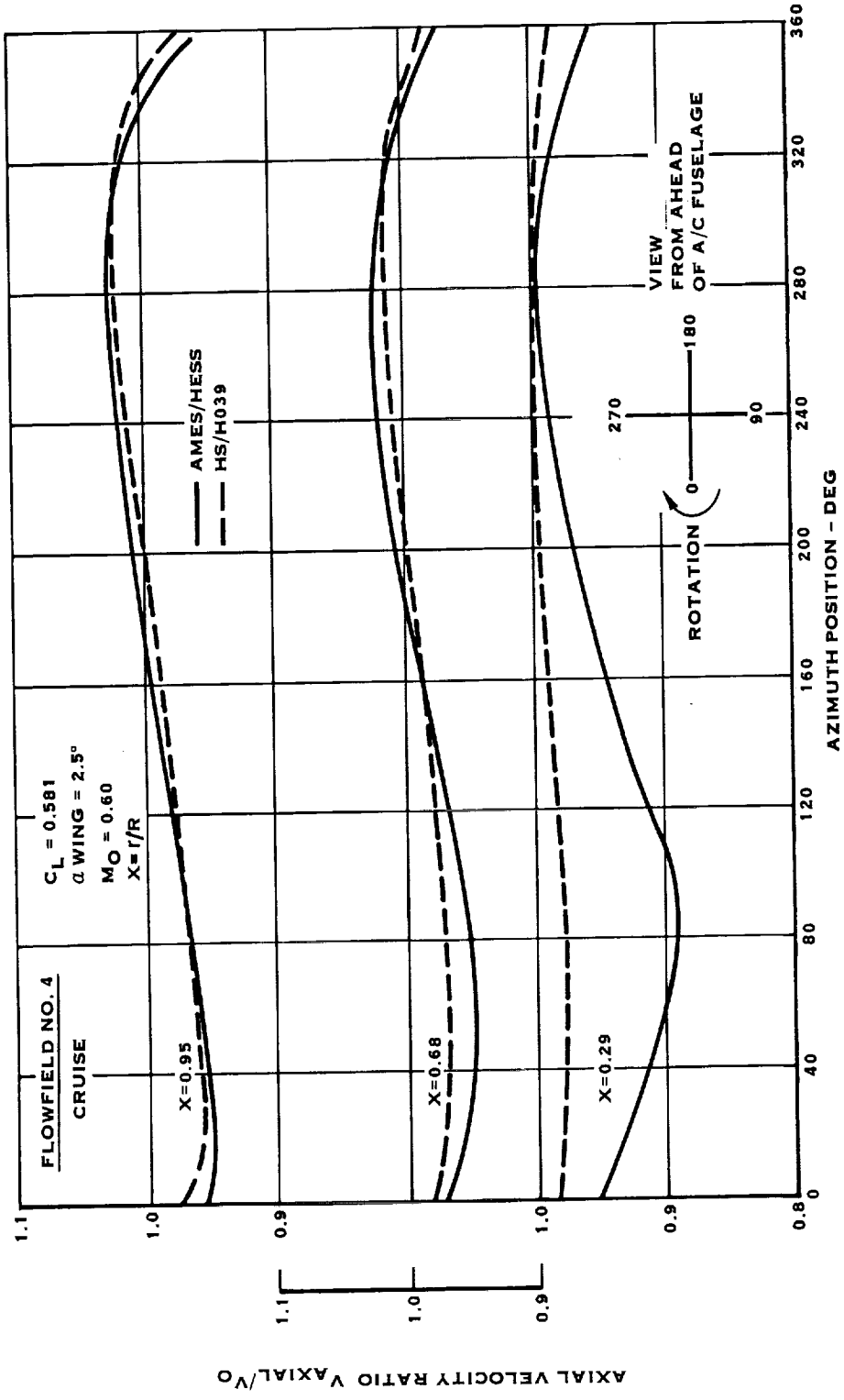

FIGURE 3-23. FLOWFIELD PREDICTIONS FOR THE NASA-AMES SEMI-SPAN AIRCRAFT MODEL AXIAL VELOCITIES, CASE NO. 8 (VELOCITIES DEFINED IN PLANE OF THE PROPELLER)

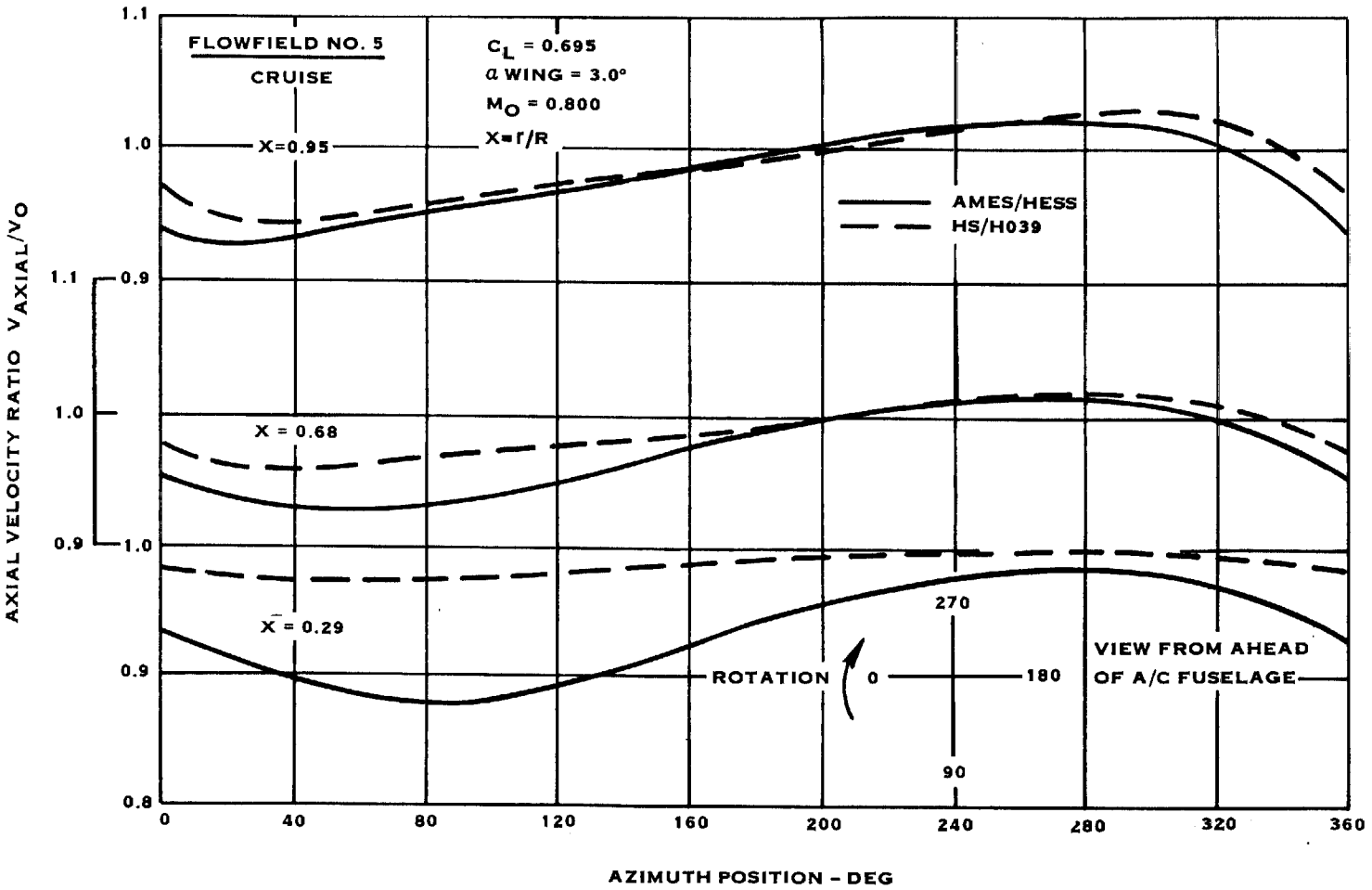

FIGURE 3-24. FLOWFIELD PREDICTIONS FOR THE NASA-AMES SEMI-SPAN AIRCRAFT MODEL AXIAL VELOCITIES, CASE NO. 9
(VELOCITIES DEFINED IN PLANE OF THE PROPELLER)

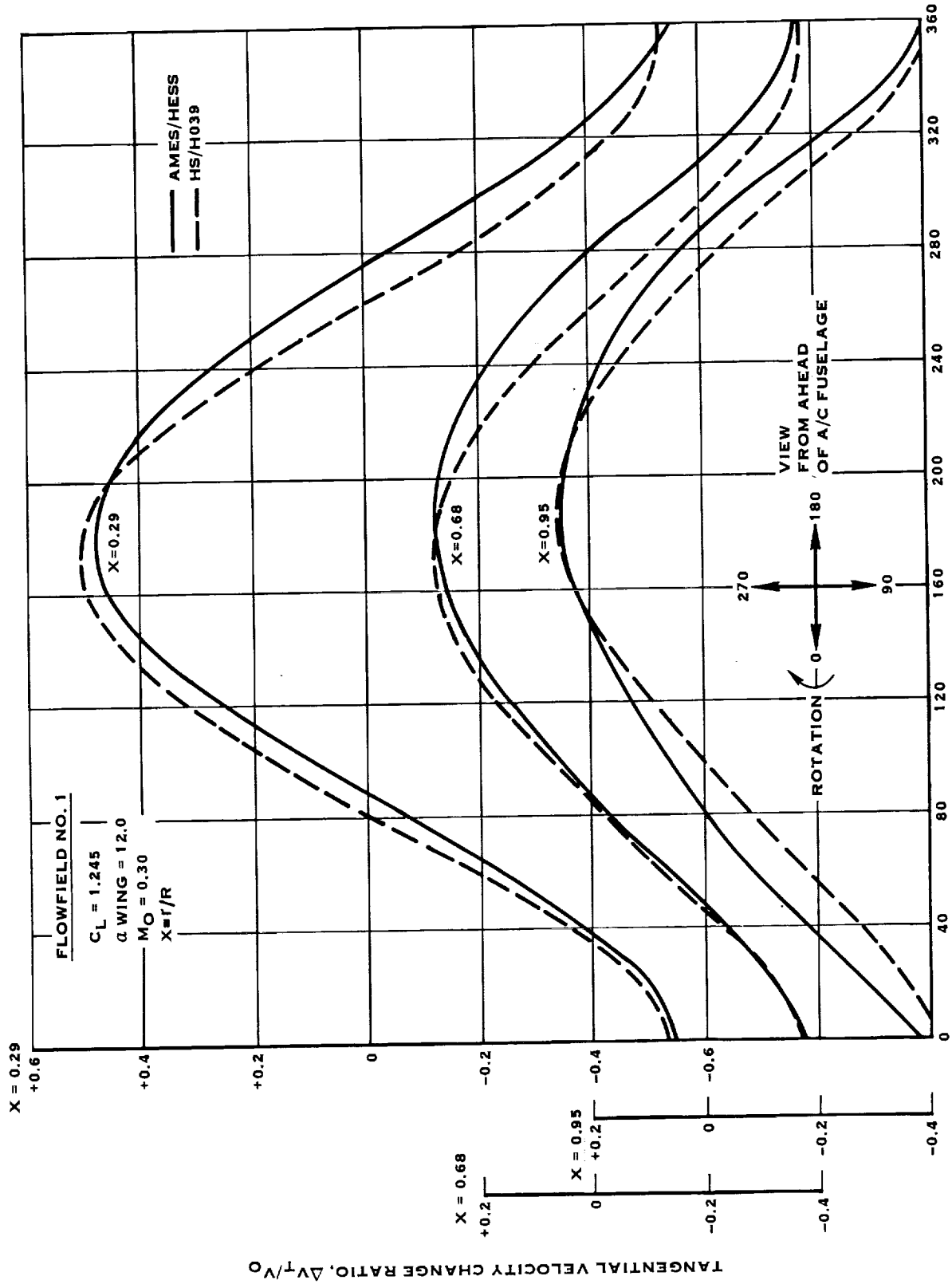

FIGURE 3-25. FLOWFIELD PREDICTIONS FOR THE NASA-AMES SEMI-SPAN AIRCRAFT MODEL TANGENTIAL VELOCITIES, CASES 1 THROUGH 4 (VELOCITIES DEFINED IN PLANE OF THE PROPELLER)

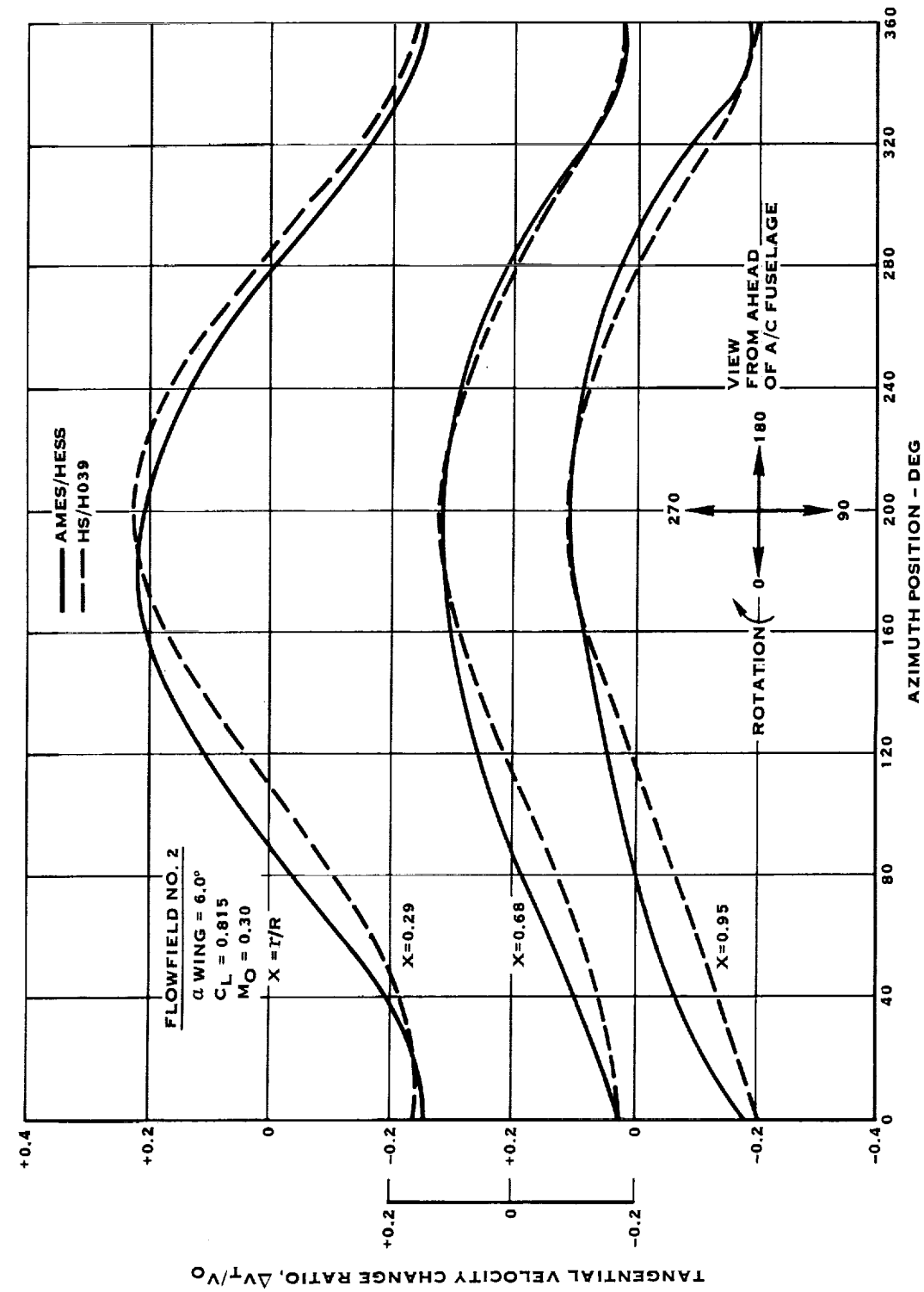

FIGURE 3-26. FLOWFIELD PREDICTIONS FOR THE NASA-AMES SEMI-SPAN AIRCRAFT MODEL TANGENTIAL VELOCITIES, CASE NO. 5 (VELOCITIES DEFINED IN PLANE OF THE PROPELLER)

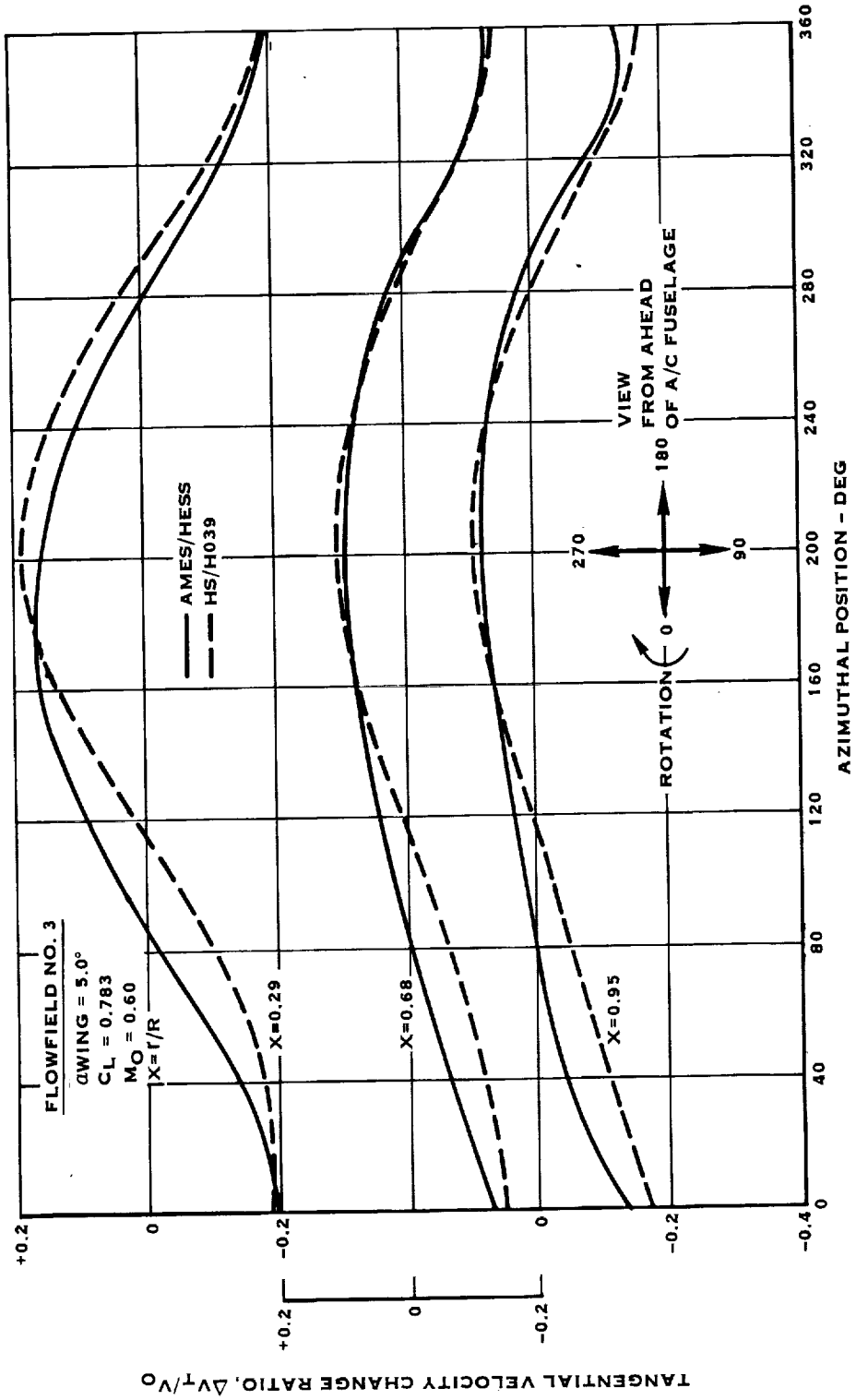

FIGURE 3-27. FLOWFIELD PREDICTIONS FOR THE NASA-AMES SEMI-SPAN AIRCRAFT MODEL TANGENTIAL VELOCITIES, CASES NO. 6 AND 7 (VELOCITIES DEFINED IN PLANE OF THE PROPELLER)

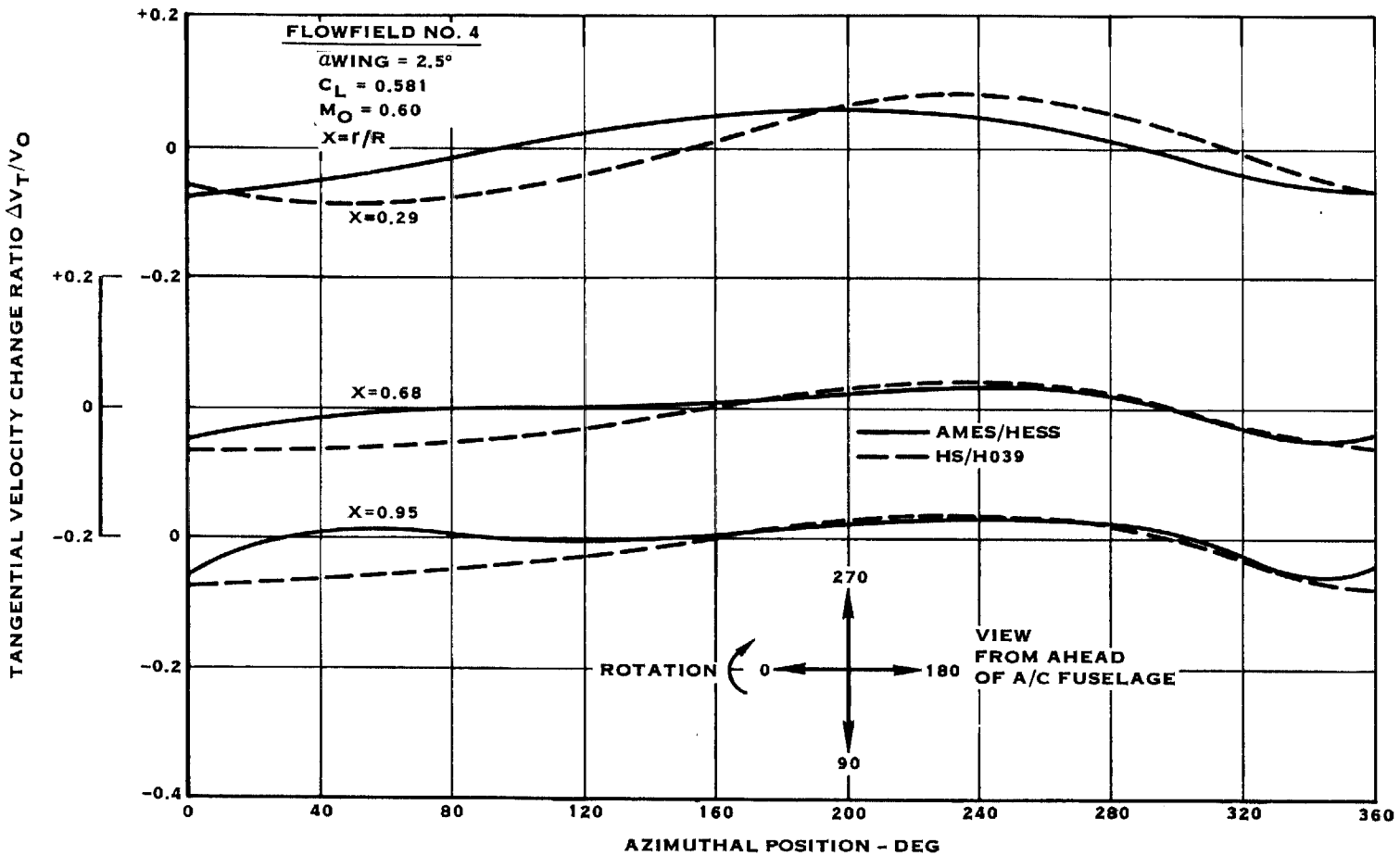

FIGURE 3-28. FLOWFIELD PREDICTIONS FOR THE NASA-AMES SEMI-SPAN AIRCRAFT MODEL TANGENTIAL VELOCITIES, CASE NO. 8 (VELOCITIES DEFINED IN PLANE OF THE PROPELLER)

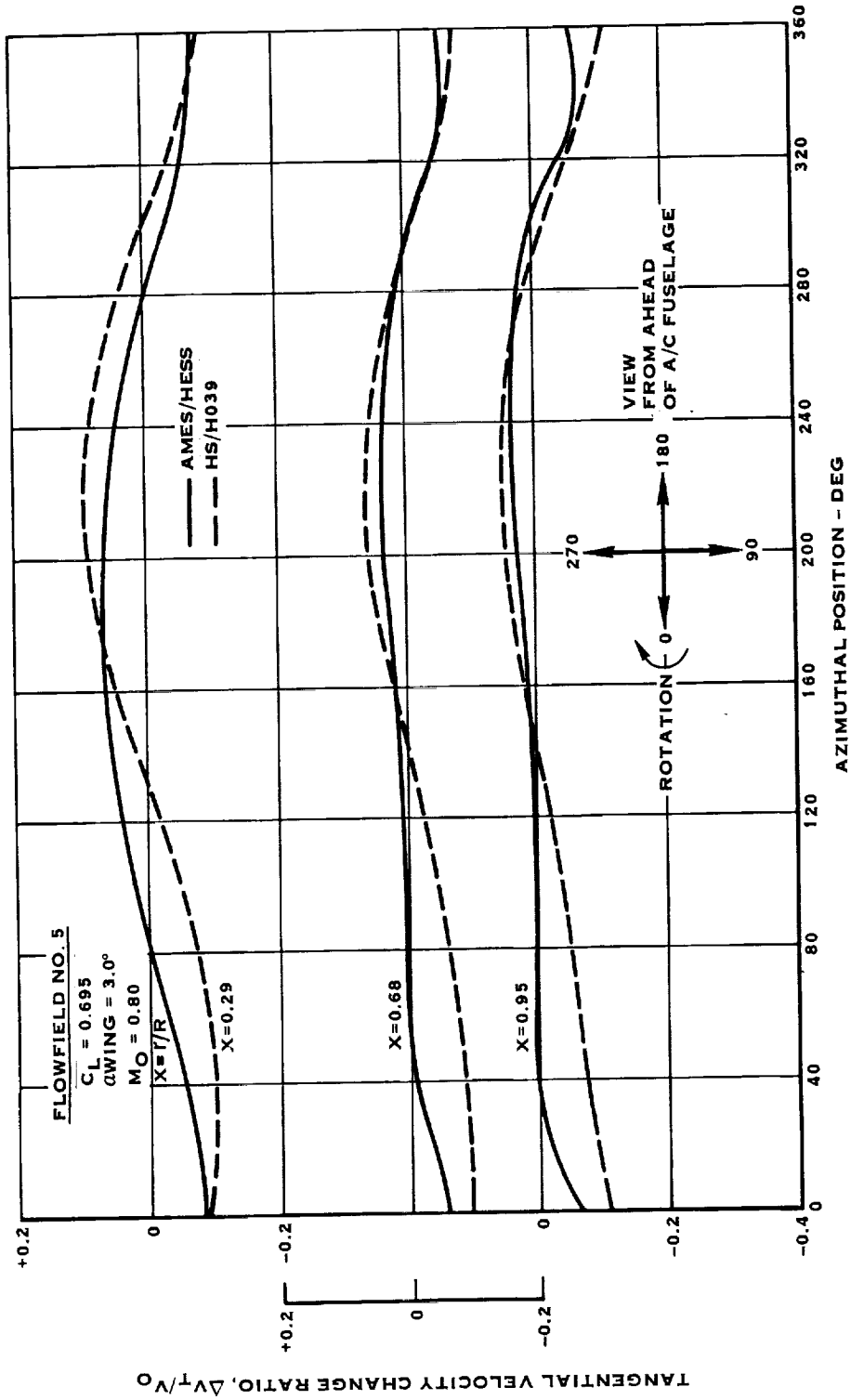

FIGURE 3-29 FLOWFIELD PREDICTIONS FOR THE NASA-AMES SEMI-SPAN AIRCRAFT MODEL TANGENTIAL VELOCITIES, CASE NO. 9 (VELOCITIES DEFINED IN PLANE OF THE PROPELLER)

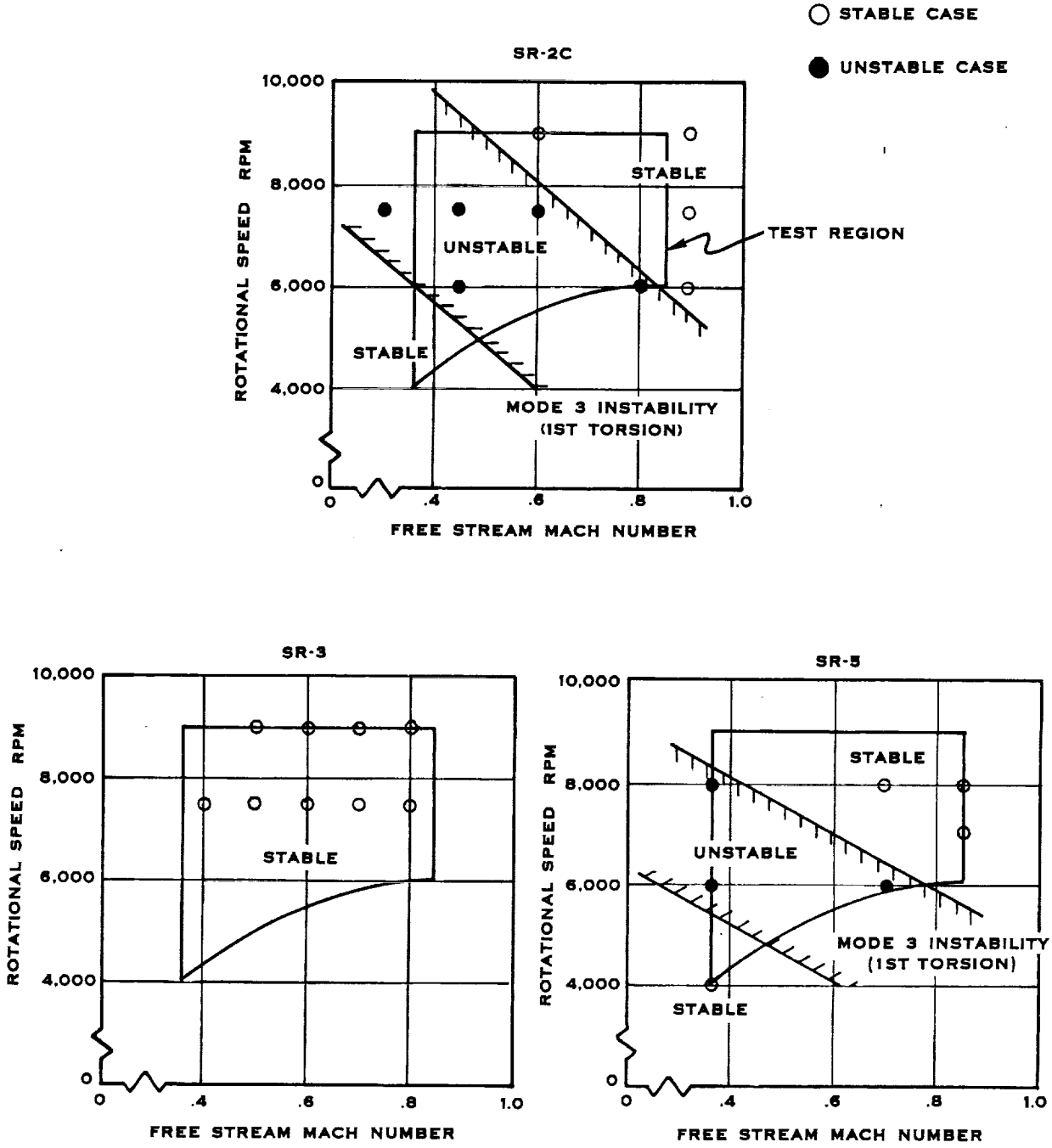

FIGURE 3-30. CALCULATED MODEL PROP-FAN CLASSICAL FLUTTER STABILITY BOUNDARIES USING THE G400T2 AEROELASTIC RESPONSE ANALYSIS

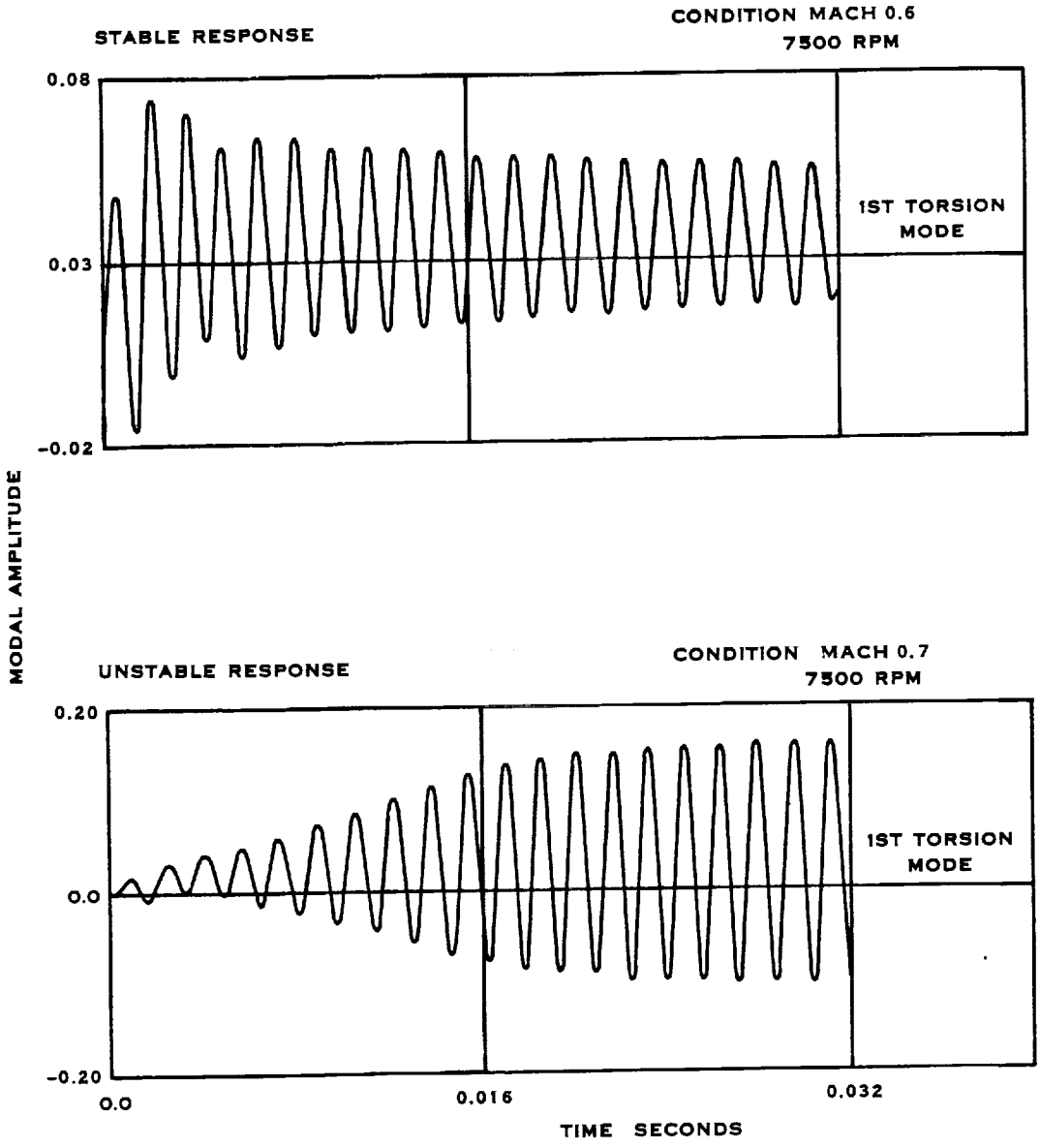

FIGURE 3-31. SR-2C MODEL PROP-FAN RESPONSE DUE TO AN INITIAL DISTURBANCE CALCULATED USING THE G400T2 AEROELASTIC STABILITY ANALYSIS

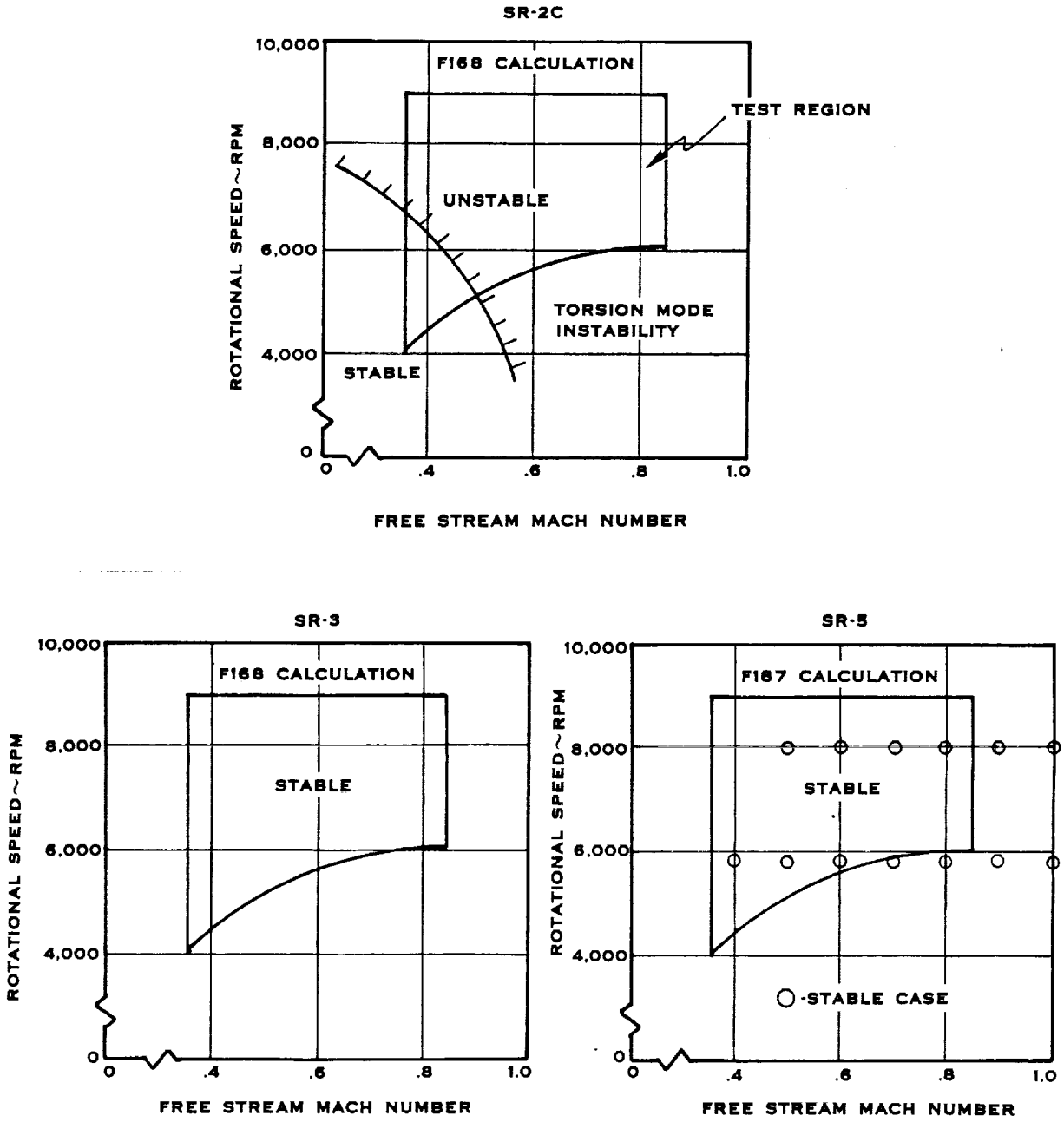

FIGURE 3-32. CALCULATED MODEL PROP-FAN CLASSICAL FLUTTER BOUNDARIES USING THE F168 OR F187 AEROELASTIC STABILITY ANALYSIS

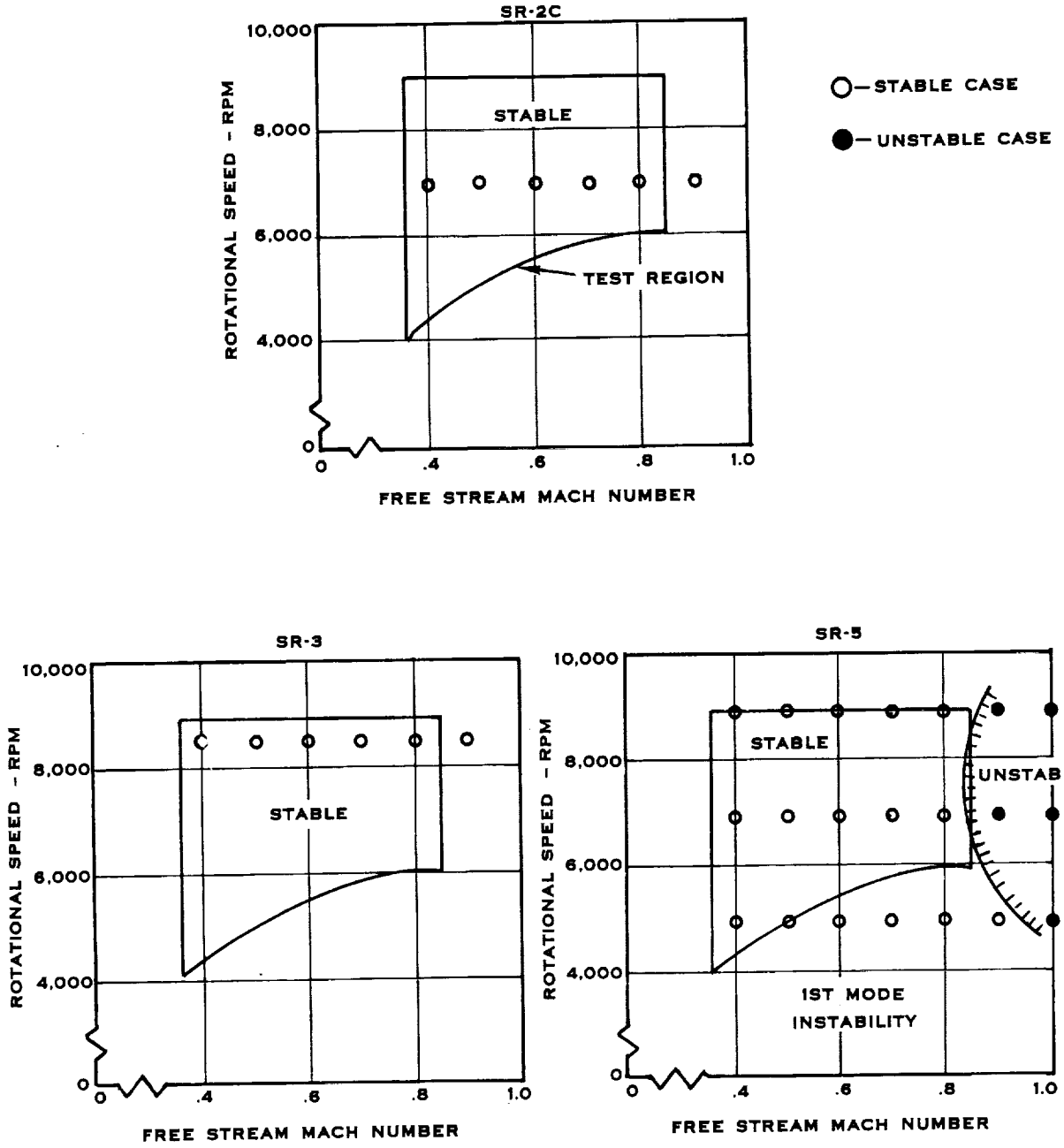

FIGURE 3-33. CALCULATED MODEL PROP-FAN CLASSICAL FLUTTER STABILITY USING THE F203 AEROELASTIC STABILITY ANALYSIS ASSUMING NO CASCADE EFFECTS.

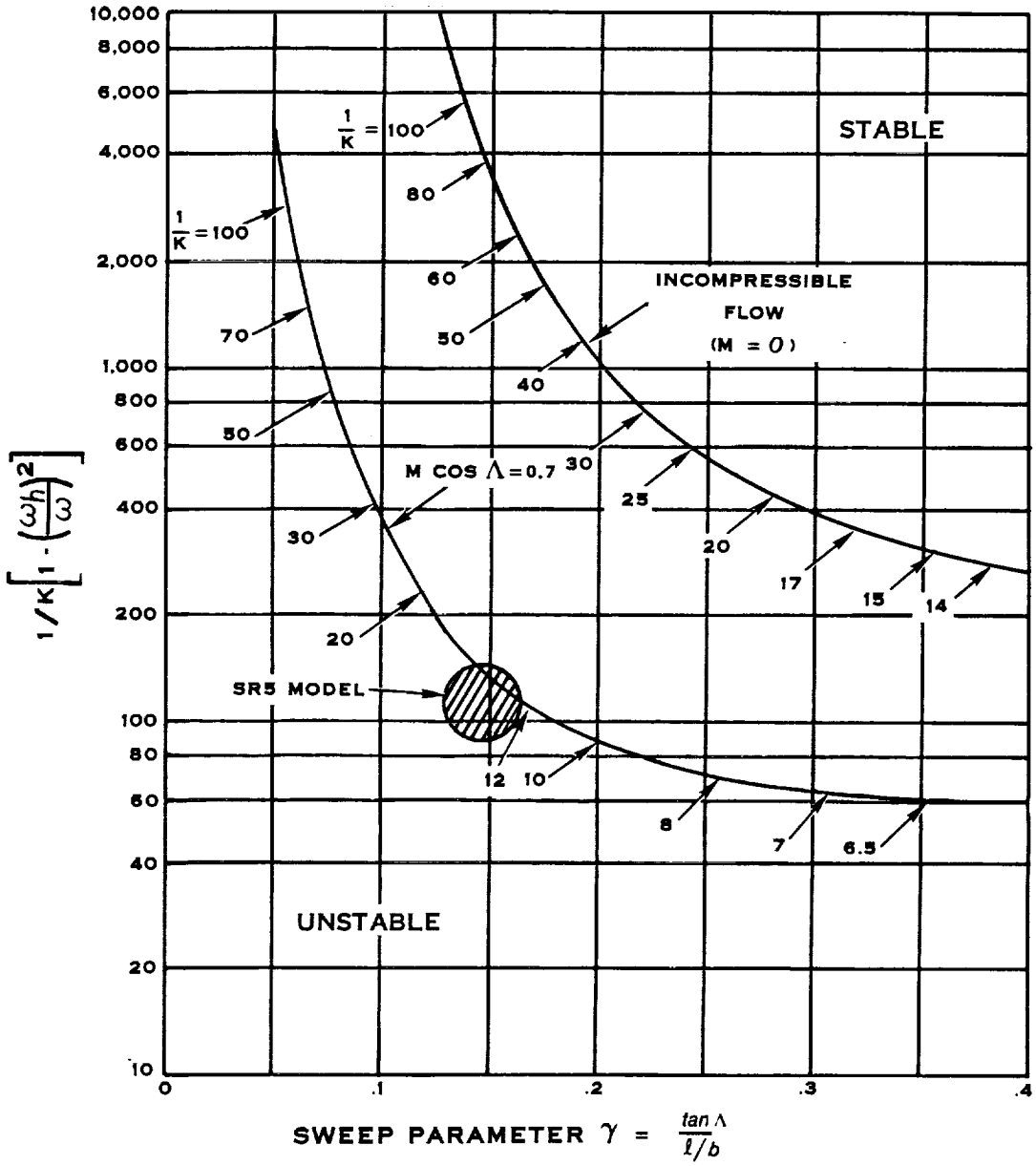

FIGURE 3-34. CURVES WHICH GIVE $1/K\left[1-\left(\frac{\omega_h}{\omega}\right)^2\right]$ AS FUNCTIONS OF THE SWEEP PARAMETER γ FOR SINGLE-DEGREE BENDING FLUTTER OF UNIFORM CANTILEVER SWEPT WINGS IN INCOMPRESSIBLE FLOW AND IN THE COMPRESSIBLE FLOW M COS Λ = 0.7. (REFERENCE 16)

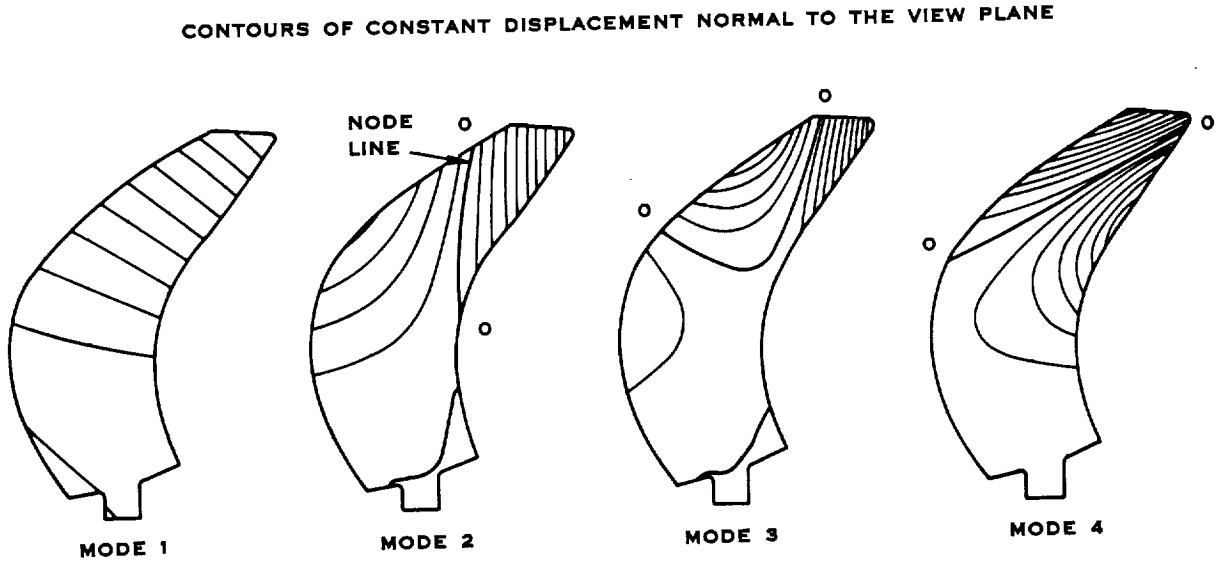

FIGURE 3-35. SR-5 MODEL PROP-FAN MODE SHAPE PREDICTIONS AT 7000 RPM WITH A BLADE ANGLE β3/4 OF 55°

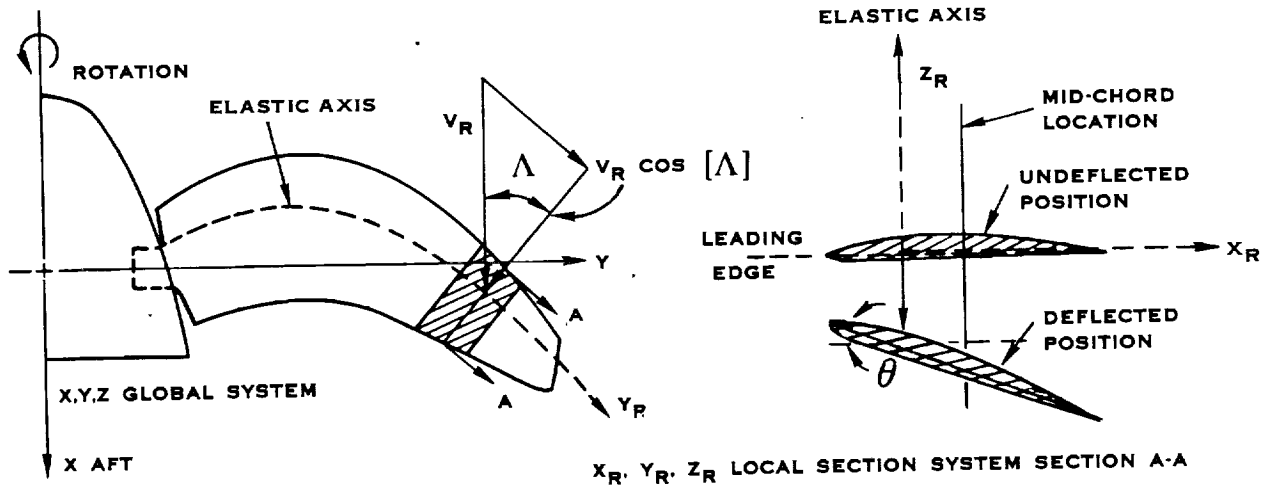

FIGURE 3-36. SWEPT COORDINATE SYSTEM DEFINITION USED IN THE F203 AEROELASTIC STABILITY ANALYSIS

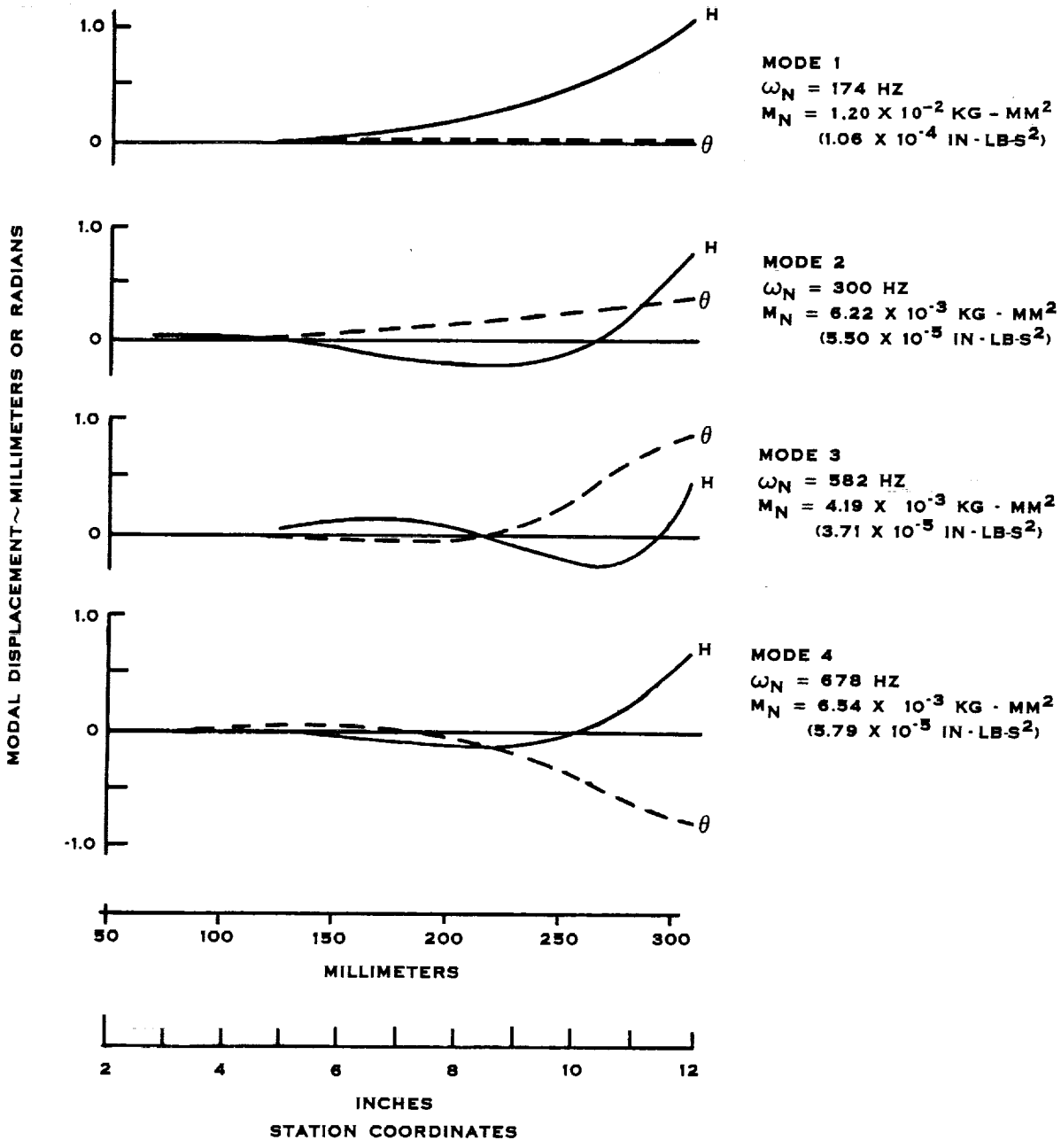

FIGURE 3-37. BENDING TORSION COUPLED MODE SHAPES FOR THE SR-5 MODEL PROP-FAN AT 7000 RPM WITH A BLADE ANGLE OF $\beta_{3/4} = 55°$

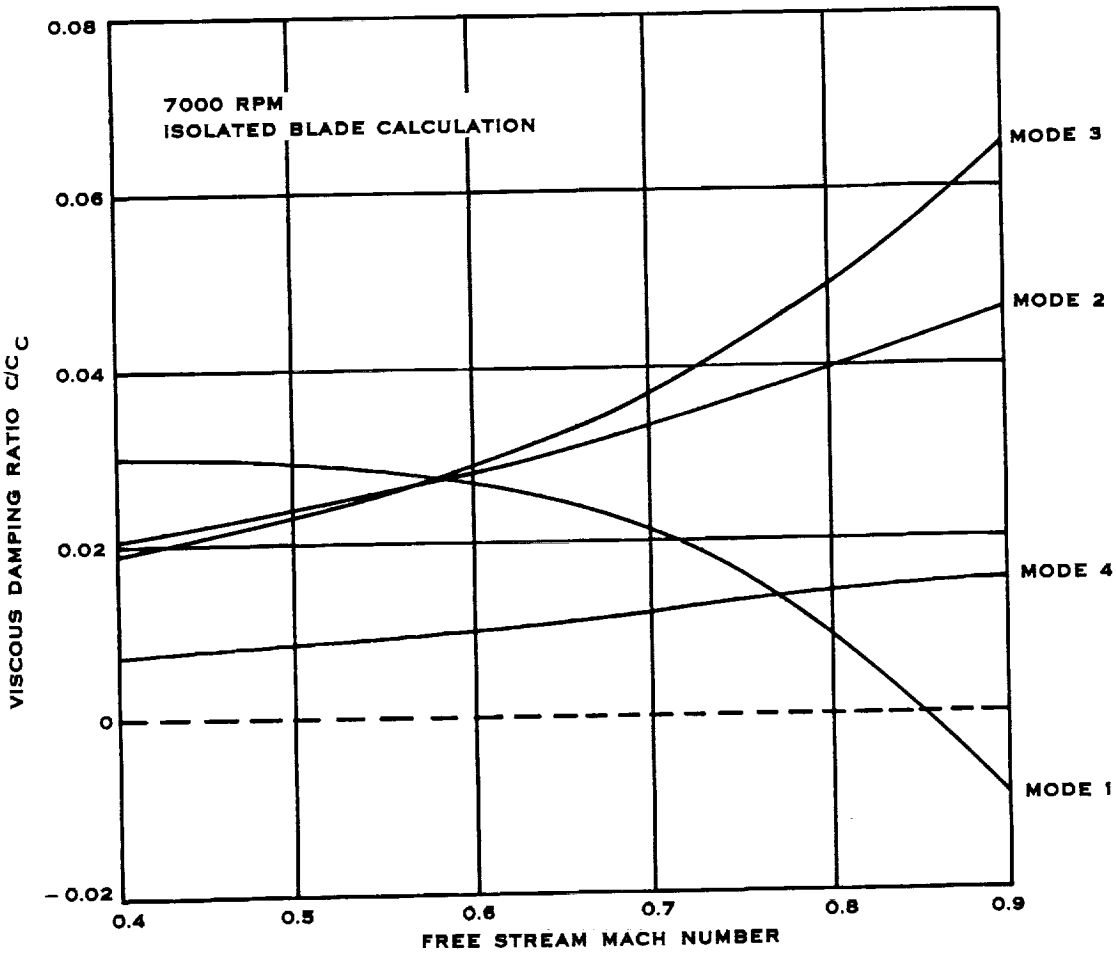

FIGURE 3-38. VISCOUS DAMPING RATIO PREDICTION FOR THE SR-5 MODEL PROP-FAN USING THE F203 AEROELASTIC STABILITY ANALYSIS AND ASSUMING AN ISOLATED BLADE SYSTEM $\beta_{3/4} = 55°$

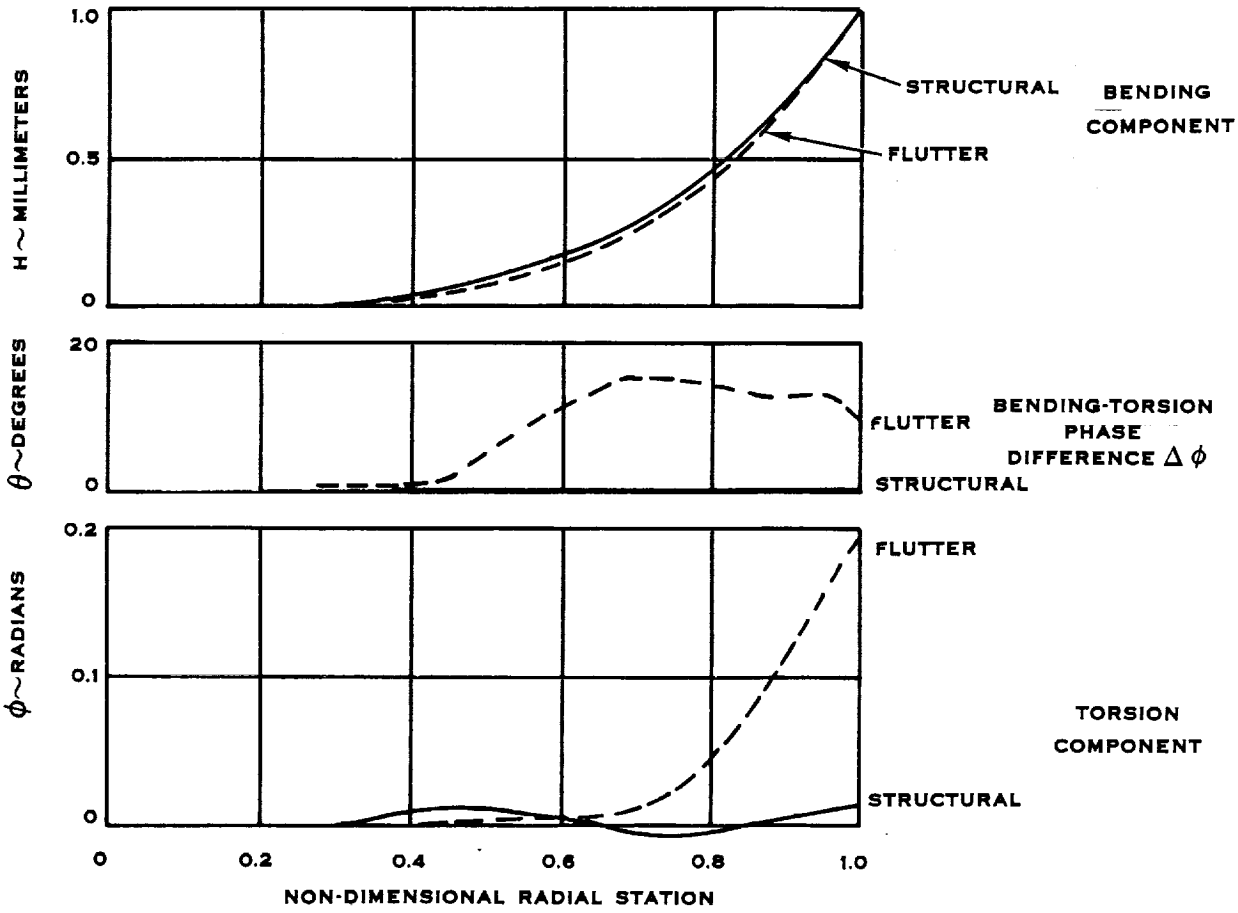

FIGURE 3-39. COMPARISON OF THE PREDICTED FLUTTER MODE SHAPE FOR THE SR-5 MODEL PROP-FAN TO THE FIRST STRUCTURAL MODE SHAPE OF THE BLADE: PREDICTED USING F203

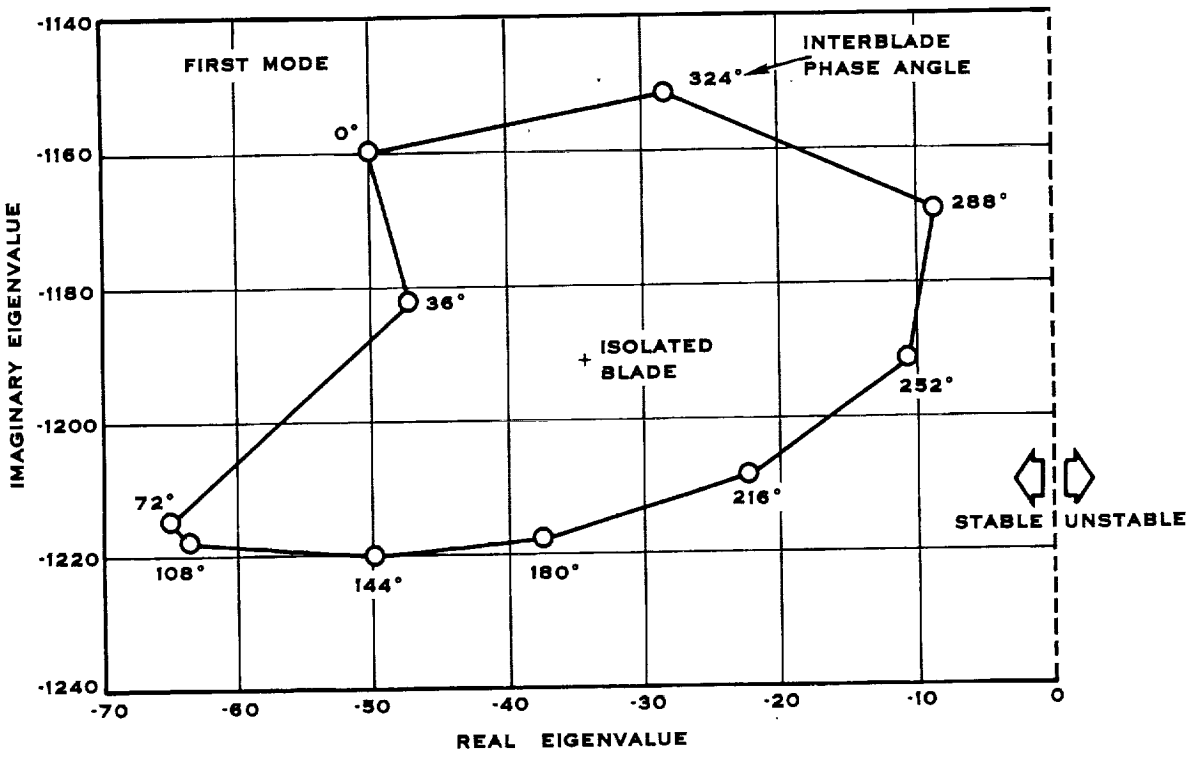

FIGURE 3-40. ROOT LOCUS PLOT OF SR-5 MODEL PROP-FAN STABILITY AT MACH 0.4 AND 7000 RPM FOR TEN INTERBLADE PHASE ANGLES: PREDICTED USING F203

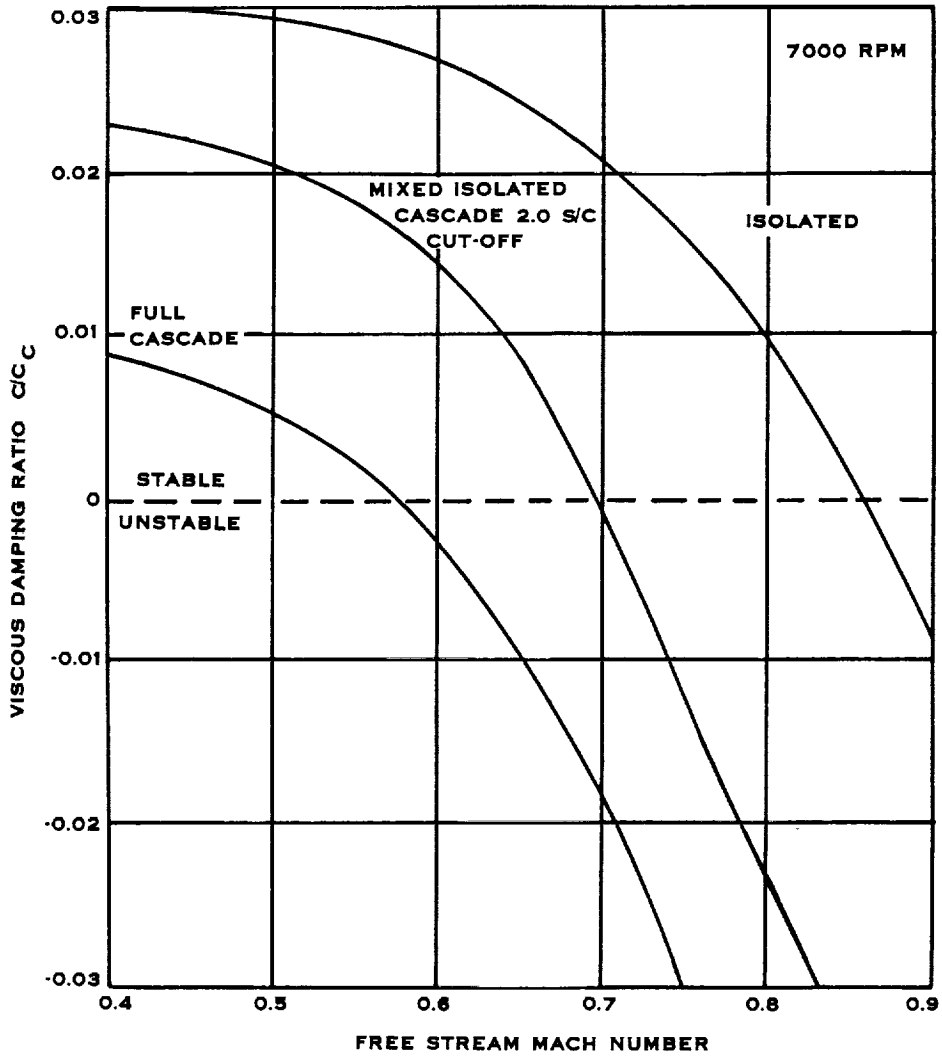

FIGURE 3-41. FIRST MODE DAMPING COMPARISON FOR THE SR-5 MODEL PROP-FAN FOR THREE SPANWISE AERODYNAMIC ASSUMPTIONS ISOLATED DATA, CASCADE DATA, AND MIXED ISOLATED AND CASCADE DATA. PREDICTED USING F203.

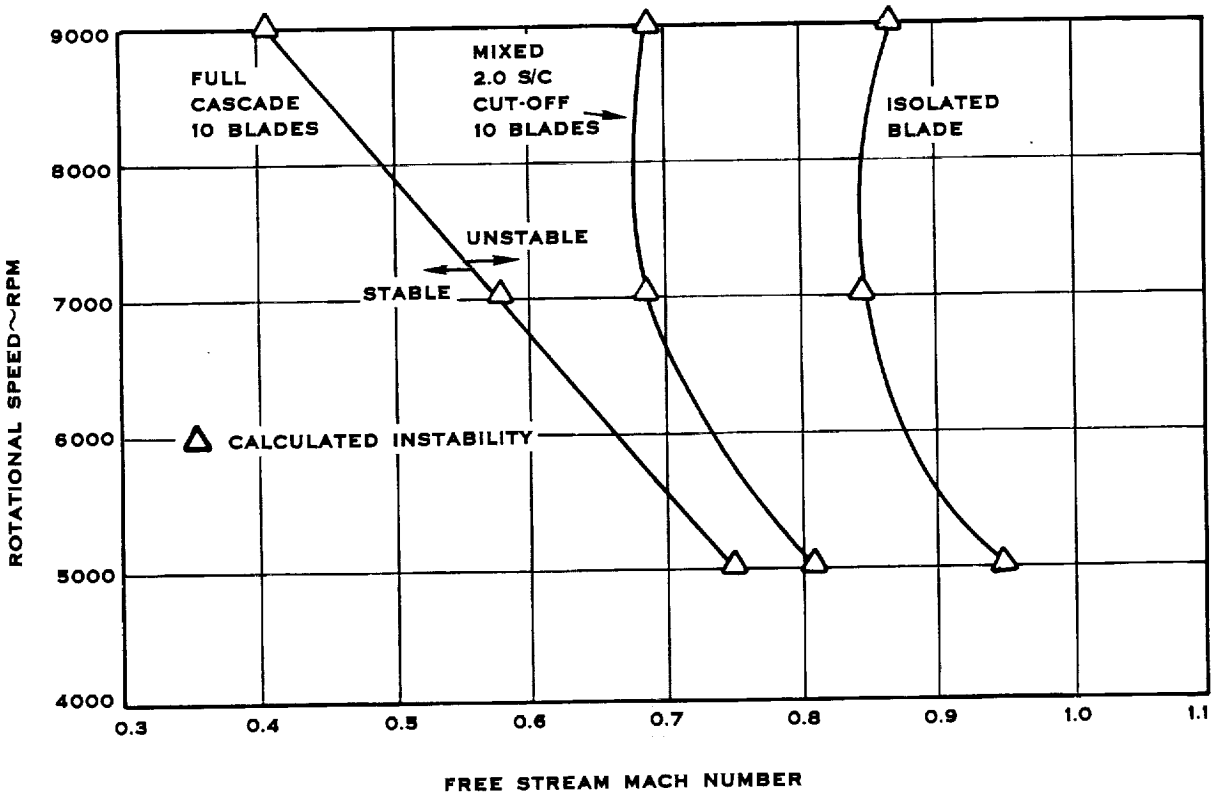

FIGURE 3-42. PREDICTED SR-5 MODEL PROP-FAN STABILITY BOUNDARIES FOR THREE AERODYNAMIC ASSUMPTIONS, ISOLATED DATA, CASCADE DATA, AND MIXED ISOLATED AND CASCADE DATA. CALCULATIONS MADE WITH F203.

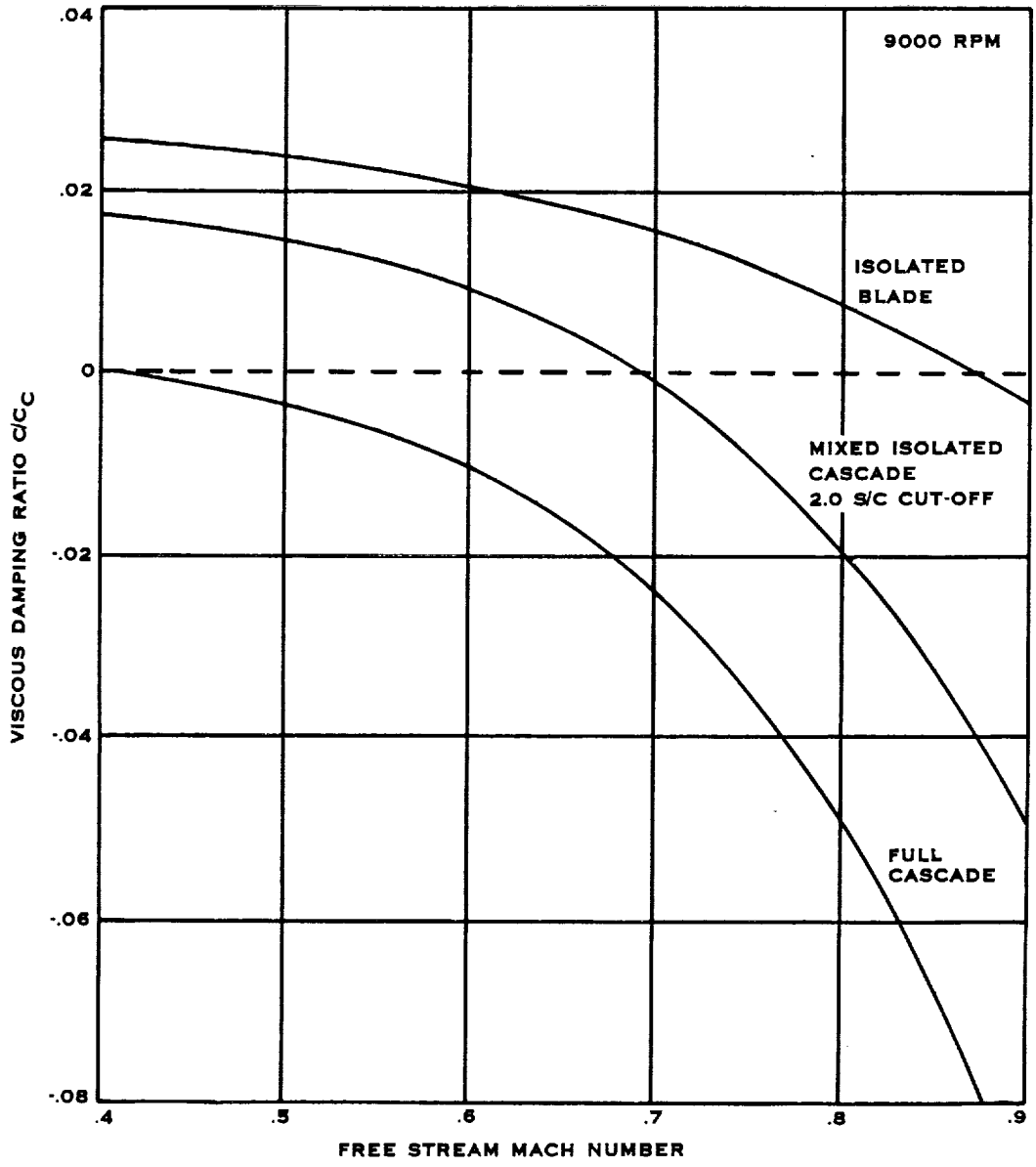

FIGURE 3-43. FIRST MODE DAMPING COMPARISON FOR THE SR-5 MODEL PROP-FAN FOR THREE SPANWISE AERODYNAMIC ASSUMPTIONS ISOLATED DATA, CASCADE DATA, AND MIXED ISOLATED AND CASCADE DATA. PREDICTED USING F203.

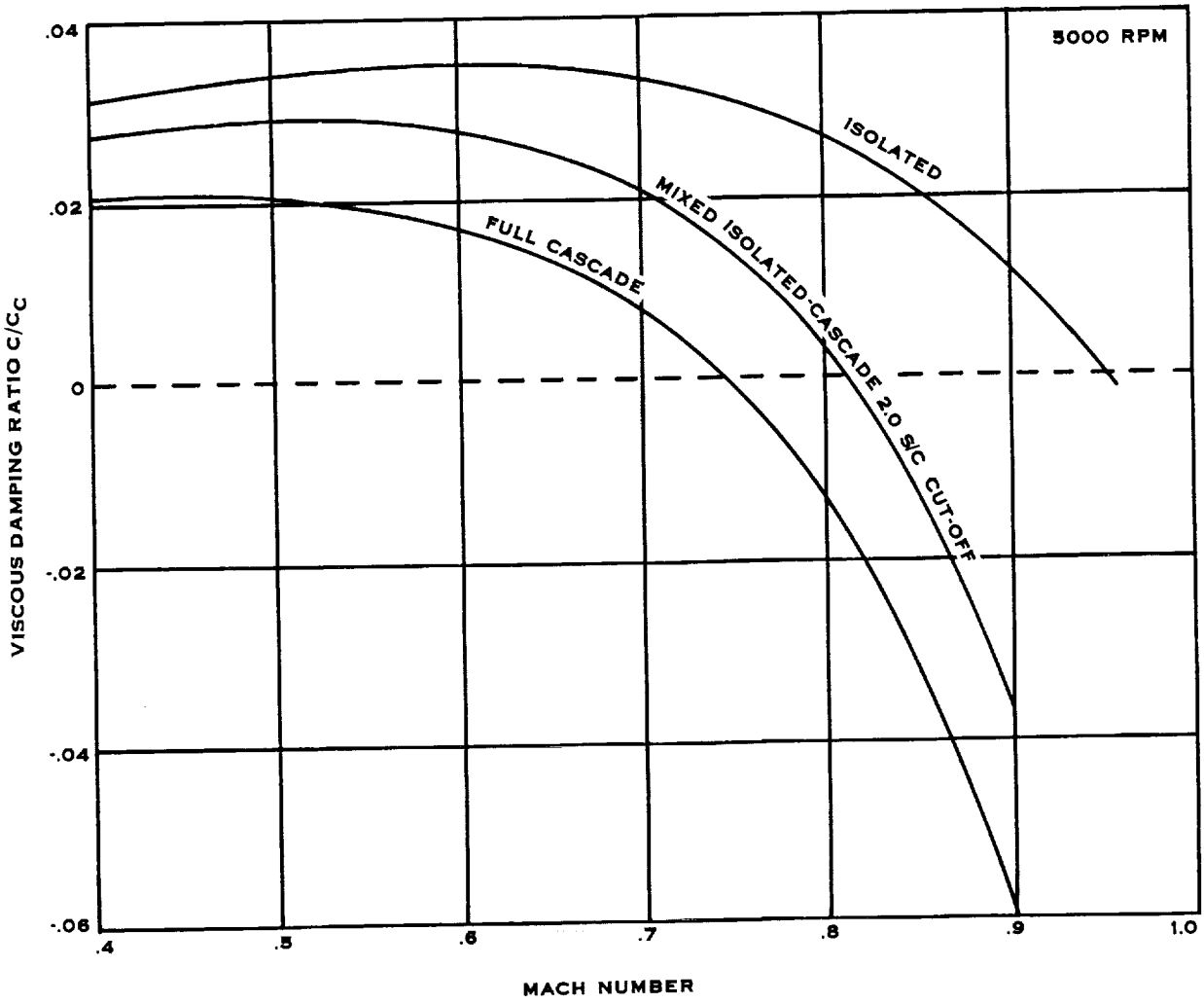

FIGURE 3-44. FIRST MODE DAMPING COMPARISON FOR THE SR-5 MODEL PROP-FAN FOR THREE SPANWISE AERODYNAMIC ASSUMPTIONS ISOLATED DATA, CASCADE DATA, AND MIXED ISOLATED AND CASCADE DATA. PREDICTED USING F203.

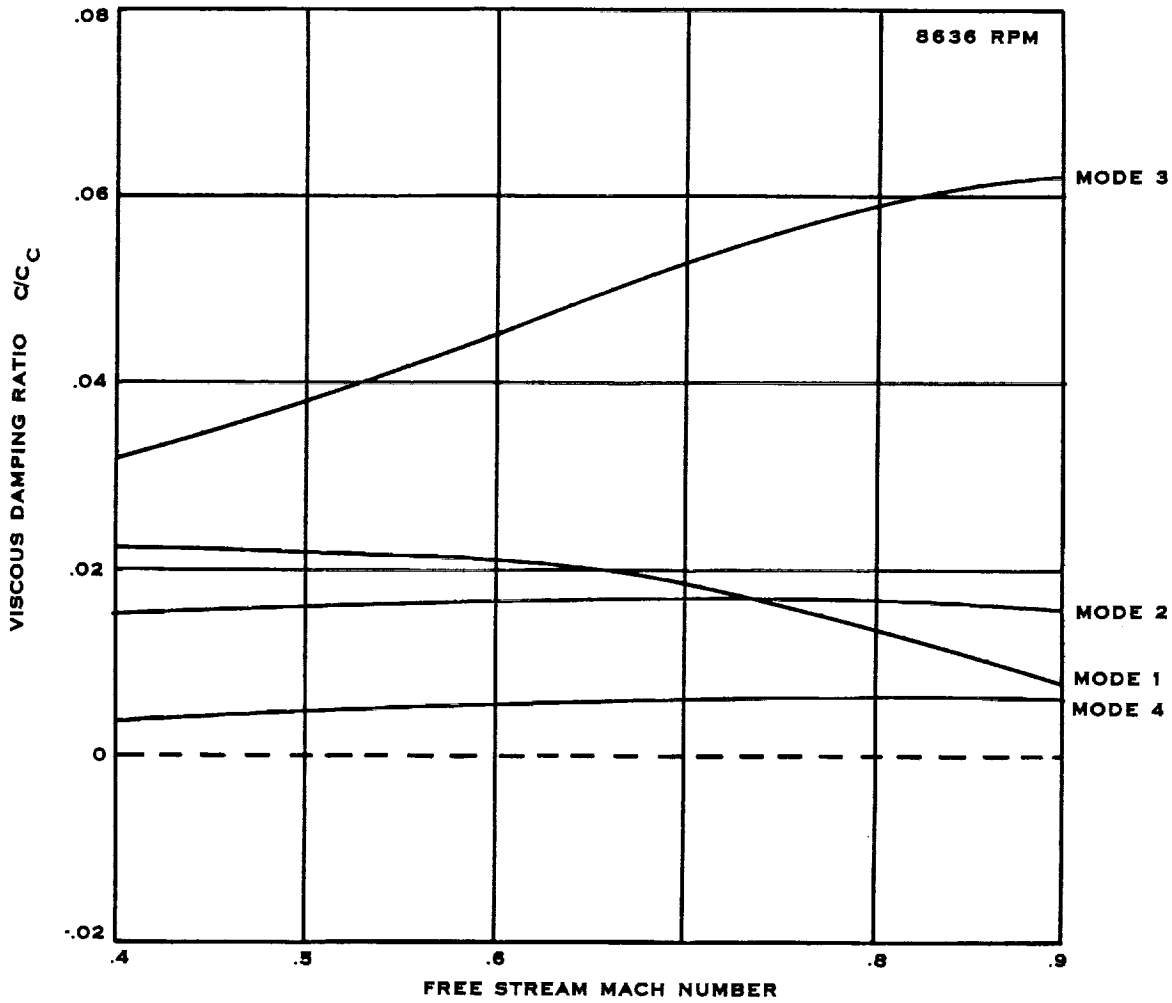

FIGURE 3-45. VISCOUS DAMPING RATIO PREDICTION FOR THE SR-3 MODEL PROP-FAN USING THE F203 AEROELASTIC STABILITY ANALYSIS AND AN ISOLATED BLADE ASSUMPTION.

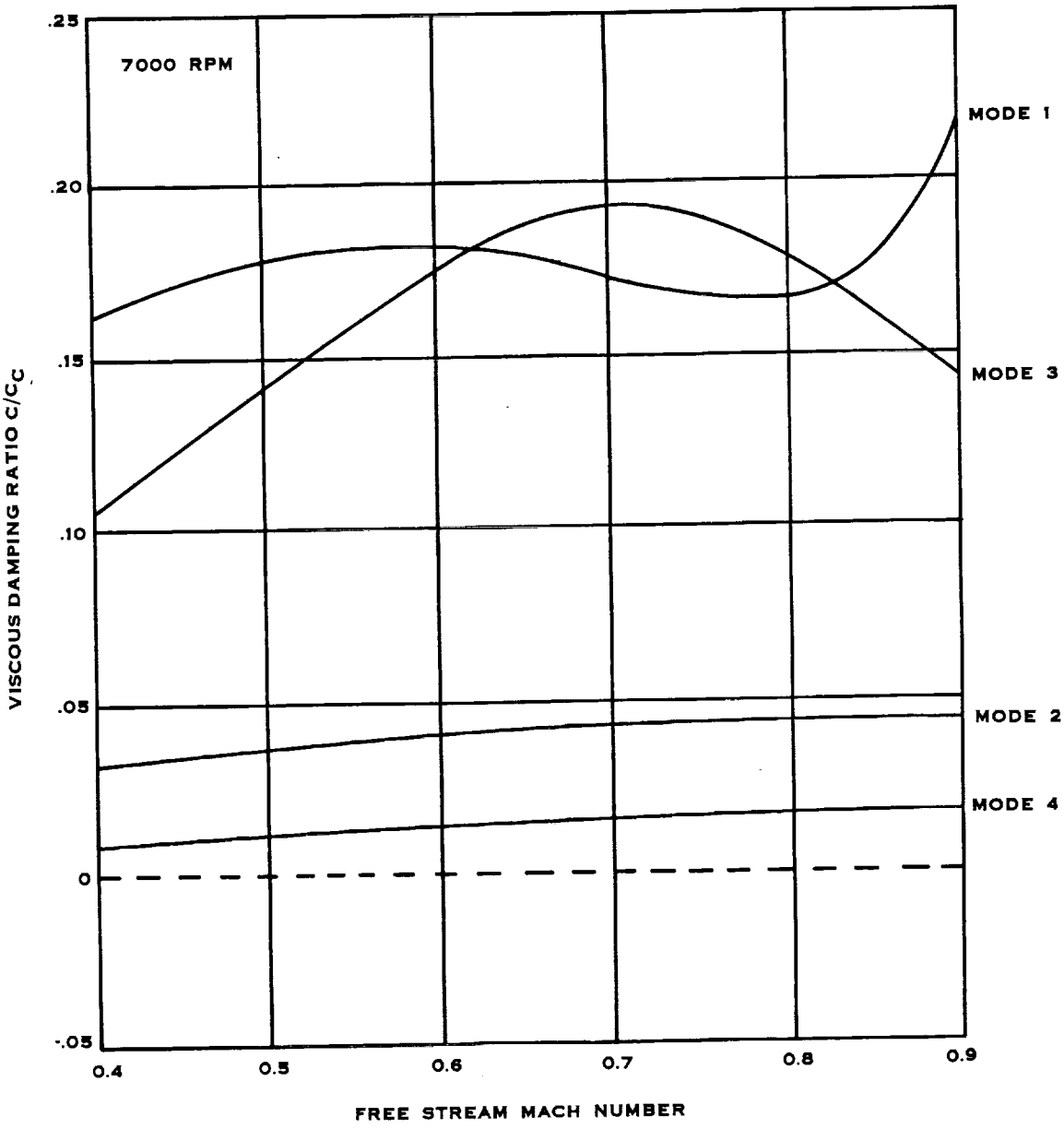

FIGURE 3-46. VISCOUS DAMPING RATIO PREDICTION FOR THE SR-2C MODEL PROP-FAN USING THE F203 AEROELASTIC STABILITY ANALYSIS AND AN ISOLATED BLADE ASSUMPTION

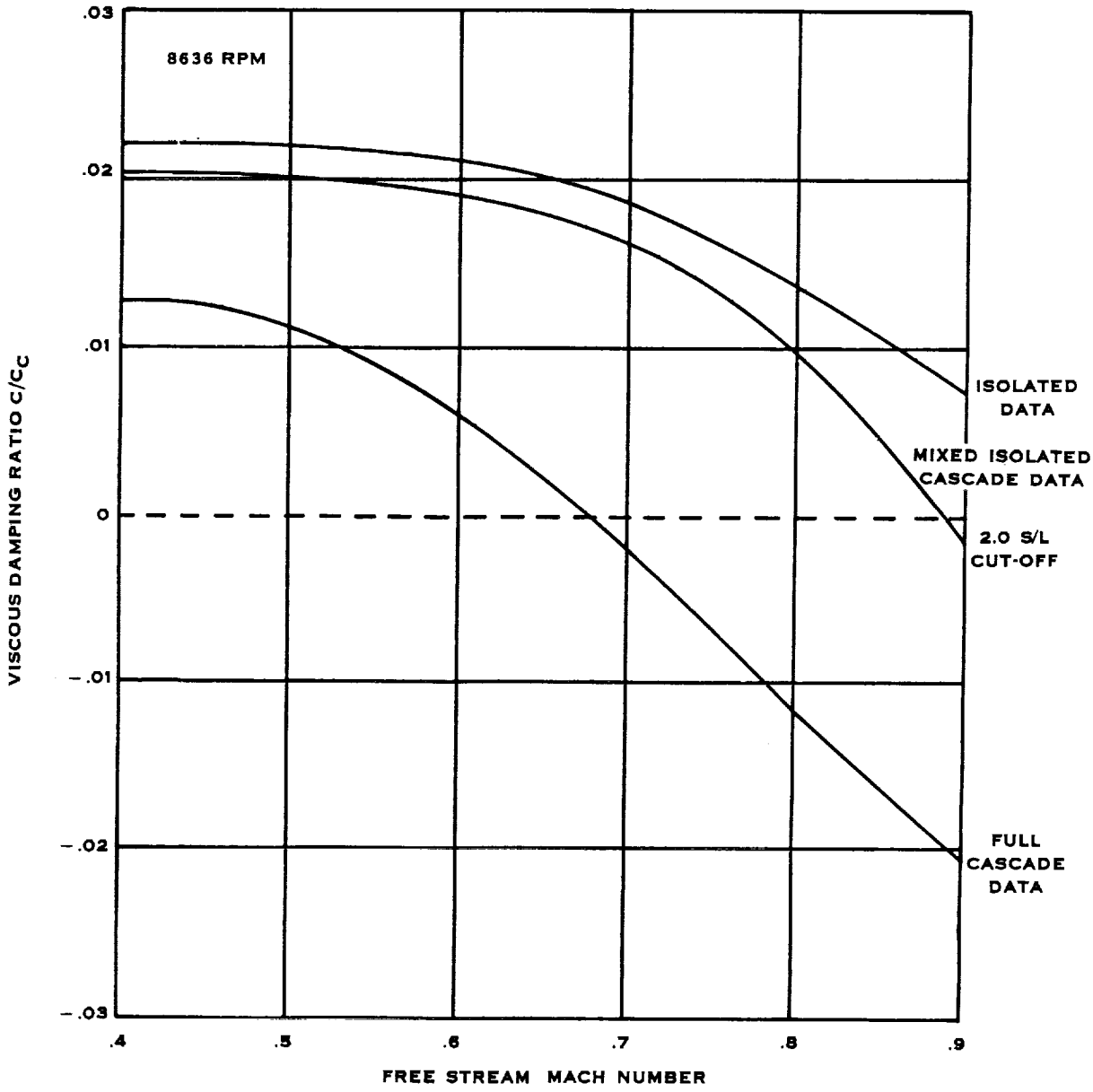

FIGURE 3-47. FIRST MODE DAMPING COMPARISON FOR THE SR-3 MODEL PROP-FAN FOR THREE SPANWISE AERODYNAMIC ASSUMPTIONS ISOLATED DATA, CASCADE DATA, AND MIXED ISOLATED AND CASCADE DATA. PREDICTED USING F203

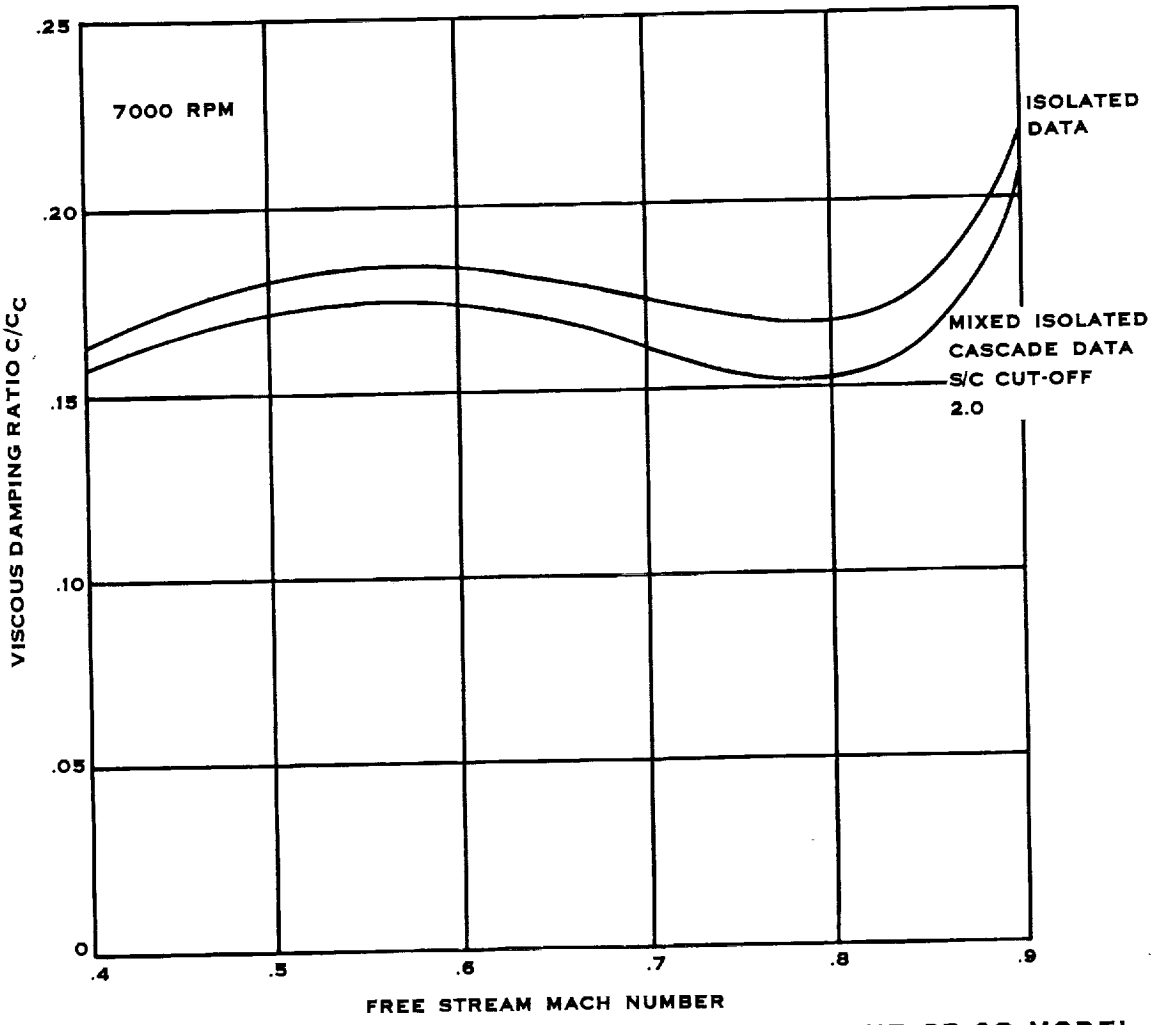

FIGURE 3-48. FIRST MODE DAMPING COMPARISON FOR THE SR-2C MODEL PROP-FAN FOR TWO SPANWISE AERODYNAMIC ASSUMPTIONS ISOLATED DATA AND MIXED ISOLATED AND CASCADE DATA. PREDICTED USING F203.

SECTION 4.0
EXPERIMENTAL DATA EVALUATION AND COMPARISON

4.1 NASA/LEWIS 8 x 6 WIND TUNNEL DYNAMIC RESPONSE AND VIBRATORY STRESS TEST DATA ANALYSIS

Critical Speeds

The theoretical critical speed maps (Campbell diagrams) of the SR-2C, SR-3 and SR-5 Prop-Fan models were presented and discussed in Section 3.1. The experimental critical speeds were obtained from the transient response data via the Fast Fourier Transform (FFT) method. A detailed discussion of the procedure will be presented in Section 4.2.

Figures 4-1, 4-2 and 4-3 show a comparison of the wind tunnel test and in-vacuum predicted critical speeds for the SR-2C, SR-3 and SR-5 models, respectively. It is clear from these figures that the correlation between the test results and theory is good for all the three models.

1P Vibratory Stresses

The test procedure and the location of various strain gages for measuring the vibratory stresses of the SR-2C, SR-3 and SR-5 models were discussed in Section 2, and the analytic results of the vibratory stresses were presented and discussed in Section 3.1. In this section, a comparison of the test and calculated stresses will be presented.

SR-2C Vibratory Strain Data Evaluation and Results - The SR-2C 8-way model was operated in the wind tunnel at various free stream Mach numbers, blade angles, inflow angles and rotational speeds. The resulting 1P vibratory strain is shown for the various strain gages as defined in Figure 2-3. The magnitude of the 1P strain was obtained by spectral analysis techniques. Figure 4-4 is a graphic summary of the operating conditions for the test conducted in the NASA/Lewis 8 x 6 wind tunnel. Here the reference blade angle is plotted as a function of rotational speed and Mach number. The ranges of propeller shaft tilt angles (ψ) used are indicated. The operating conditions generally ranged between windmilling and the torque limit.

The mid-blade vibratory strain results are shown in Figure 4-5 where the 1P strain is plotted as a function of propeller shaft tilt angle and rotational speed. In this curve, it is observed that the strain, generally, has a linear relationship with inflow angle and is close to zero at zero tilt angle. This is consistent with previous analytical and test results for propellers.

C-2

4.1 (Continued)

Figure 4-6 shows the Lewis test data plotted in the form of 1P strain per degree of inflow as a function of equivalent airspeed. The airspeed is plotted on a squared scale. The horizontal axis is equal to a constant times velocity squared. Since the effect of inflow angle is divided into the strain, it is expected that these curves would develop as straight lines. Inflow angle is assumed to be linear with the 1P excitation for small angles. However, the data in Figure 4-6 show substantial scatter indicating some effects of rotational speed.

As previously discussed in Section 3.1, the vibratory strains and excitation for the SR-2C model were calculated via computer programs HS/H444 and HS/H026. Comparisons of calculated and measured strains are presented in Figures 4-7 through 4-10. The strain per degree of inflow is plotted as a function of the equivalent airspeed on a squared scale. Rotational speed is held constant for each plot with values of 6000, 7000, 8000 and 9000 rpm, respectively. The test data show trends of increasing strain per degree of inflow with less scatter since they have been grouped by rotational speed. The calculations using HS/H444 and HS/H026 show reasonable correlation with the test data with the worst correlation occurring at 7000 rpm. It should be noted that the test data as well as the calculations show that the strain per degree of inflow does not remain linear with equivalent air speed squared, but falls off at the higher speeds. This is attributed to the effects of compressibility on the blade section lift curve slope. A more detailed explanation of the causes of fall off in the curve is given in Section 3.1.

SR-3 Vibratory Stress Test Data Evaluation and Results - During May, June, and July of 1980, tests were conducted at NASA/Lewis on the SR-3 8-way Prop-Fan model to evaluate the vibratory stress levels which are induced in a blade due to angular inflow. To measure strains at several locations, two blades (#1 and #5) were strain gaged. Five strain gages, as shown in Figure 3-16 were positioned on Blade 1. These were: inboard (BG-1), trailing edge (BG-2), mid-blade (BG-3), VEE (BG-4), and tip gage (BG-5). However, there were only three gages on Blade 5. These were: inboard (BG-6), mid-blade (BG-7), and VEE (BG-8). The recorded signals were analog.

Digitized data for 135 test points, in the form of peak stress amplitudes were received from NASA/Lewis in March 1981. The parameters which were varied during the tests, and the ranges of these variables are: rotational speed (N = 4000 to 9000 rpm), Mach number (M = 0.36 to 0.85), inflow angle (ψ = 0° to 15°) and power (0 to 671 kw (900 shp)).

The 1P stress, as shown in Figure 4-11, varies linearly with the inflow angle. To eliminate the effect of inflow angle and equivalent airspeed, the stress per excitation factor, as a function of the shaft power and propeller speed, is plotted in Figures 4-12 and 4-13 respectively. The 1P stress data are from the inboard gage of blade 1.

4.1 (Continued)

Figure 4-12 shows the variations in (σ/EF) versus shaft power. The vibratory stress increases with increased shaft power. However, it should be noticed that the rotational speed also increased as the shaft power was increased, therefore, the increased stresses are not due to increased shaft power only. At the higher Mach numbers (M), the (σ/EF) values were lower for a fixed value of shaft power and rotational speed.

Figure 4-13 shows the effect of increased rotational speed on the (σ/EF) of the inboard strain gage. But it should be noted that the shaft power was not kept constant as the rotational speed was increased. However, the effect of the rotational speed on the (σ/EF) appears to be greater than the shaft power effect, as is evidenced from the slopes of the curves of Figures 4-12 and 4-13. At higher Mach numbers, the (σ/EF) values were lower.

The theoretical vibratory stresses, as discussed previously in Section 3.1, were calculated for six test operating conditions (see Table 4-1), assuming a non-linear finite element model of the SR-3 Prop-Fan, via MSC NASTRAN.

To compare test results with theory, the calculated stresses for the six points are superimposed on the experimental stress plots of Figures 4-12 and 4-13. The experimental stresses are about 60% to 77% higher than the predicted stresses indicating poor correlation between test and theory. A point for point comparison, for the five strain gages of blade 1, is also shown in Table 4-I. The cause of these differences is not known at this time.

The next consideration in the evaluation of the stress data was to examine the intergage stress ratios of blade 1. Since, the inboard gage of blade 1 had the highest stress, all stress ratios are calculated with respect to this gage. The results are plotted in Figures 4-14 through 4-17.

The stress ratio (BG-3/BG-1) plot for the mid-blade is shown in Figure 4-14. In spite of considerable data scatter, a curve was fitted through the data to provide a best estimate of the trend. As the speed was increased from 4000 rpm to 9000 rpm, the stress ratio reduced from 0.95 to 0.7. The predicted stress ratio at 7016 rpm is about 1.1 to 1.28 times of the corresponding experimental data and almost equal to the experimental value at the higher propeller speeds of 8836 rpm and 8800 rpm. These values are superimposed on Figure 4-14.

The stress ratios for the Vee gage (BG-4/BG-1) are plotted in Figure 4-15. As expected the Vee gage stresses are quite low (8% to 18% of inboard gage). However the calculated stresses are about 0.5-times to 3-times higher than the experimental values.

The plot of the tip gage ratio (BG-5/BG-1) is shown in Figure 4-16. The trend is similar to that of the mid-blade and Vee gages. With increased speed (4000 rpm to 9000 rpm), the ratio drops (from 60% to 35%). The predicted values show a considerable scatter.

4.1 (Continued)

The trend for the trailing edge gage (BG-2/BG-1), as shown in Figure 4-17, is contrary to the other strain gages. Here, the stress ratio increases with speed. Also, the predicted values are very high as compared to the test values.

SR-3 Summary - The foregoing discussion of the 1P vibratory stressing of the SR-3 model Prop-Fan blades has shown that the correlation between test and calculated stresses is poor. The causes of the poor correlation, as yet, are not clearly understood.

The relationship between the 1P vibratory stresses and the inflow angle is linear and hence, for comparisons, the effects of inflow angle are eliminated by the use of excitation factors. The effects of rotational speed and shaft power on stressing are significant, but the effect of rotational speed is more predominant. The highest stresses were measured by the inboard gage. The measured intergage stress ratios, with respect to the inboard gage, decrease with increased propeller speed except for the trailing edge gage.

SR-5 Vibratory Stress Test Data Evaluation and Results - A 10-bladed SR-5 model Prop-Fan was tested at NASA/Lewis during 1981, to evaluate its vibratory stress response due to angular inflow. The test setup was previously discussed in Section 2 and the location of the strain gages on blade 1 is shown in Figure 2-5. Three blades (1, 2 and 6) were strain gaged, and the effects of varying inflow angle (ψ), tunnel Mach number (M), the rotational speed (N) and power were investigated. The range of the test variables was: Inflow angle (ψ = 0 to 15°), blade angle ($\beta_{.75}$ = 49.1° to 72.8°), propeller rotational speed (N = windmilling to 9000 rpm) and shaft power (0 to 522 kW (700 shp)).

One hundred eighty-two test points were analyzed to evaluate the trends in 1P vibratory stresses, and the test results were compared with analytic results which, as already discussed in section 3.1, were calculated using the MSC NASTRAN program. 1P vibratory stresses, from six strain gages were measured: inboard (BG1-1), Vee (BG1-3), tip crosswise (BG1-5) and tip span wise (BG1-6)) of blade 1, and inboard (BG2-1, BG6-1) gages of blades 2 and 6, respectively.

Discussion of SR-5 results - The 1P vibratory stresses, measured by the inboard gage, were found to be the highest. The largest value of the tested 1P stress was ± 73,632 kPa (10,679 psi) at M = 0.36, ψ = 15 degrees, and N = 7000 rpm.

The 1P stresses were found to vary linearly with the propeller shaft tilt angle. This is clearly demonstrated in Figure 4-18 where plots of the inboard gage stresses, as a function of the inflow angle, are shown. The 1P stresses, corresponding to two test conditions, ie., M = 0.36 and M = 0.8, are plotted. For both cases, negative propeller shaft tilt angle data are shown.

4.1 (Continued)

Included on Figure 4-18 is a plot of the total stresses for the 0.8 Mach number condition. The 1P stresses are shown to be within 15% of the peak total stresses at 0.8 Mach number. Accordingly, only the 1P stresses were used to study the data trends. Since the 1P stresses were found to vary linearly with the inflow angle, the results are presented in the form of stress per excitation factor (σ/EF) to eliminate the effects of different inflow angles and airspeeds.

The effect of varying the tunnel Mach number on (σ/EF) was minimal, as shown in Figure 4-19. The test values plotted are from four strain gages of blade 1, and also include some effect of change in the power. The effect of varying power on (σ/EF) of the inboard gage is shown in Figure 4-20 for 0.6 Mach number and constant rpm conditions. However, for each rpm only two test points were available, except at 6000 rpm. The effect of increasing power produces a significant increase in (σ/EF). One test point, at 6000 rpm and 312.5 kW (419 shp), is out of line as shown on the graph. In the absence of more data points at other rpm's, it is difficult to say whether this data point represents scatter or an actual condition.

The effect on stress of propeller rpm at constant shaft horsepower is shown in Figure 4-21. Increasing rpm results in considerably reduced (σ/EF). The plotted data are for the inboard gage at constant power and 0.6 Mach number.

To compare the interblade stresses, results for the inboard gage are shown in Table 4-II. The data are from blades 1, 2, and 6. The stresses, as shown in the last three columns of Table 4-III, are normalized with respect to blade 1. Generally, stresses of blades 1 and 6, are of the same order, however, stresses of blade 2 are about 10% lower than blade 1.

As previously discussed in Section 3.1, five test cases, shown in Table 4-III, were selected to compare test results with theory. Calculations were done at two Mach numbers (M = 0.6 and 0.8), two propeller speeds (6000 and 7950 rpm) and three power conditions (186 kW (250 shp), 336 kW (450 shp), 388 kW (520 shp)). The analysis accounted for the centrifugal stiffening of the blade, the center of pressure variation, and the gage thickness (assumed 3 mils). However, the effect of gage thickness was considered to be important only for the tip gages.

It should, however, be noted that the test data were interpreted using the nominal inflow angles which were set during the test. Upwash effects could increase the actual inflow angle and thus reduce the experimental values of (σ/EF). This effect is estimated at 10 percent. The test conditions were slightly different from those assumed for analysis. The test results were extrapolated/interpolated as required to obtain a comparison with the analysis.

4.1 (Continued)

A detailed comparison, of the predicted and test stresses, is shown in Table 4-III. However, to examine the trends of 1P stresses as a function of the shaft power and rotational speed, the data are plotted in Figures 4-22 to 4-25. Figure 4-22 shows a comparison of the test and calculated stresses for the inboard gage. The experimental stresses are about 30% to 50% higher than the NASTRAN predictions. The differences appear to increase at the higher shaft powers.

The Vee gage comparison is shown in Figure 4-23. Here, the predicted stresses are higher than the experimental stresses. At lower power levels, the test values are about 60% of the predicted, and at higher power and Mach number (case 5, table 4-III), the experimental stress is only about 36% of the predicted stress.

The experimental stresses for the tip spanwise gage, as shown in Figure 4-24, are about twice of the calculated stresses. This gage is considered to be far more susceptable to orientation errors. Consequently significant errors in measured stresses, and hence large discrepancy between test and theory, may be partly attributed to orientation errors.

As compared to other gages, the comparison for the tip crosswise gage (see Figure 4-25), is very peculiar. The experimental stresses are lower than the calculated stresses (12% to 36% lower) at lower power, but are higher at higher power (5% to 48% higher) for both Mach numbers (M = 0.6 and M = 0.8). The behavior may be due to the center of pressure and chordwise load distribution effects, as previously discussed in Section 3.1.

SR-5 Summary - The foregoing discussion of the SR-5 model Prop-Fan test and theoretical vibratory stress results has shown widely differing comparisons for each of the strain gages. No consistent correlation trend was observed. Generally, the correlation between test and theory, similar to the SR-3 model, was poor.

The experimental 1P vibratory stresses were found to vary linearly with the inflow angle. The effect of increased shaft power and propeller speed on (σ/EF) was significant. However, the effect of Mach number appeared to be small. The interblade stress ratios for the inboard gage of blades 2 and 6, relative to the inboard gage of blade 1, were 0.9 and 1.0, respectively.

4.2 SR-2C, SR-3, AND SR-5 MODEL PROP-FAN STABILITY TESTS

Summary

The SR-2C, SR-3 (4-way and 8-way) and SR-5 (2-way, 5-way and 10-way) model Prop-Fan blades were tested in the NASA/Lewis 8 x 6 foot wind tunnel to determine the modal damping and frequencies of these models. The SR-2C model was excited by the natural turbulence of the wind tunnel, and SR-3 and SR-5 models were excited by a jet pulse. The resulting transient response data were recorded and analyzed. Thus, the frequency predictions could be verified by comparison with the test frequencies, and the damping values could be used to compare the predicted stability boundaries with those of the test models.

During testing, the effects of the tunnel Mach number (M), the rotational speed (N) and the shaft power on the flutter boundaries of the test models were investigated. No flutter was encountered with the SR-2C and SR-3 models, but was encountered with the SR-5 model. The SR-5 flutter points were determined from the tests for a 10 blade configuration, a 5 blade configuration and a 2 blade configuration. These results are discussed in Reference 15.

The Fast Fourier Transform (FFT) method was applied to the test data to determine the damped natural frequencies of interest. The SR-2C response frequencies were discussed in Section 4.1. The Randomdec method was used to analyze the SR-2C data and it was determined that the natural wind-tunnel turbulence was insufficient to give a decay clear enough for damping analysis. No discussion of damping will therefore be made on the SR-2C model.

The modal damping of the SR-3 model was calculated by the moving-block analysis (MBA). However, the SR-5 modal damping was determined by both moving-block and time-domain-technique (ITD) analyses.

For both the SR-3 and SR-5 models, the predicted frequencies were in good agreement with the test frequencies, and the lower modes were better damped than the higher modes. The effect of increased Mach number (M) and rpm on the modal damping of the SR-3 model was small. However, the effect of increased M on the SR-5 model was to lower its instability threshold speed.

The 4-way configuration of the SR-3 model was better damped than the 8-way configuration. For example, in some cases, the modal damping of the 4-way model was about twice that of the 8-way model. Generally, the modal damping values for the 8-way model were about 0.25 to 1.8 percent of the critical damping.

The test data, in general, were not freely decaying vibration signals, and appeared to be influenced by several unknown forcing functions. Hence, the jet pulse configuration used, was evaluated to be inadequate for proper excitation of the Prop-Fan blades.

4.2 (Continued)

Damping Trends

Review of Moving-Block Analysis - The moving-block analysis is a digital technique for analyzing a transient response time history to determine modal damping and frequency. The method has been primarily used in the rotorcraft industry and has been described in references 18 and 19. The method has been shown to give reliable results in applications wherein the modal frequencies are well separated. However, when the modal frequencies are closely spaced, the damping values obtained by the moving-block analysis may be unreliable. A solution to the problem of closely spaced frequencies has been discussed in reference 20.

The following description of the moving-block analysis is taken from reference 20. A single mode's transient response is that of a damped sinusoid

$$f(t) = Ae^{\sigma\tau}\sin(\omega\tau + \phi) \tag{1}$$

The finite Fourier transform of this function from τ to $\tau + T$ is

$$F(\omega,\tau) = \int_{\tau}^{\tau + T} Ae^{\sigma\tau} \sin(\omega\tau + \phi)\, e^{-i\omega\tau}\phi t \tag{2}$$

where the function $F(\omega,\tau)$ is a function of τ at the frequency of analysis ω. The amplitude of the function $F(\omega,\tau)$ is referred to as the moving-block function, known as $\bar{F}(\omega,\tau)$. For small damping, $\zeta << 1$, the natural logarithm of the moving-block function is

$$\ln \bar{F}(\omega,\tau) = -\zeta\omega\tau + 1/2 \sin 2(\omega\tau + \phi) + \text{constant} \tag{3}$$

where $\sigma = -\zeta\omega$. Thus a plot of $\ln \bar{F}(\omega,\tau)$ as a function of τ will give a straight line with a slope of $-\zeta\omega$ and an additional oscillating component at twice the analysis frequency.

For sampled data the method is applied by first determining the frequency of interest, using a Fast Fourier Transform (FFT) algorithm on the entire data signal. A block length N_b is then selected, which must be less than the sample size N, and the natural logarithm of the moving-block function is calculated for $\tau = 0$. The block is then shifted one sample point at a time, and $\ln \bar{F}(\omega,\tau)$ recomputed where $\tau = n\Delta t$ for $n = 0,1,2,\ldots, N - N_b$. A slope is fitted to the resulting curve, usually with a least-squares fit, and a damping estimate is thereby obtained.

4.2 (Continued)

Review of ITD Method - The ITD method is a time domain technique to determine the modal damping and frequencies from the free vibration response of a test model. The method was developed by Ibrahim and Mikulcik (see reference 21), but was not available at UTRC until the SR-5 investigation.

The advantage of the ITD method over the moving-block method is that it can be used to simultaneously analyze data from several strain gages, whereas the moving-block method can analyze only one strain gage at a time. However, in the analysis of data from the SR-5 model tests the ITD method results were found to be unreliable, as will be discussed in the section entitled "Discussion of SR-5 Model Results", to follow.

Data Analysis - The test data were digitized at NASA/Lewis. Each test reading consists of several channels of data. These were strain gage and speed pickup signals. For the SR-3 model, each strain gage data block consisted of 100 revolutions of transient response and there were 512 digitized points per revolution. For the SR-5, on the other hand, each data block consisted of 50 revolutions of response and 256 digitized points per revolution. Approximately 20 revolutions of the SR-5 data occurred before the jet pulse was cut off and the remaining 30 revolutions after the jet cut off (see Figure 4-26).

Before applying the moving-block analysis, it was necessary to review a given sample of amplitude versus time trace to determine where the jet pulse was cut off and whether the decay signal was smooth or not. In many instances, however, the decay was observed to be erratic. The irregular decay of the vibration signal was considered to be either due to the presence of the unsteady aerodynamic flow field or because the jet pulse didn't have adequate energy. In general, a block of 16 revolutions after the jet pulse cut off was selected for the moving-block analysis. A typical transient response trace from a strain gage is shown in Figure 4-26.

Discussion of SR-3 Damping Measurements - Eleven readings of the SR-3 test were analyzed. These readings covered Mach numbers from M = 0.8 to 0.85 and propeller speeds of 7000, 8000 and 9000 rpm. Five cases (reading numbers 181, 182, 183, 191 and 192, shown in Table 4-IV) were used to compare the frequency and modal damping test results of the first mode, obtained from oscillograph traces, with those calculated by the moving-block analysis. Readings 306, 312 and 373 pertain to the 4-way configuration and readings 221, 231 and 283 are for the 8-way configuration, as shown in Table 4-V.

A comparison of the modal damping and frequency results for the first mode, obtained from the oscillograph traces and the moving-block analysis (MBA), is shown in Table 4-IV. For all five test readings the frequencies match very well. The modal damping values, except at 8000 rpm and M = 0.8, also show good agreement. This comparison shows that the results obtained from the moving block analysis should be considered reliable except when the decay signal is not smooth.

4.2 (Continued)

Additional results of modal damping and natural frequencies for the 4-way and 8-way configurations of the SR-3 model are listed in Table 4-V. The calculated frequencies are in reasonable agreement with the test frequencies of readings 231, 312 and 373. However, the calculated frequencies of the third and fourth modes are about 5% to 8% higher than those obtained from readings 221, 283 and 306.

The modal damping values listed in the table are given as a percentage of the critical damping. The range of modal damping for the 8-way configuration is of the order of 0.23% to 3.7%, and 0.03% to 8.46% for the 4-way configuration. Also, the 4-way configuration has about twice the damping of the 8-way configuration, for some cases.

Discussion of SR-5 Damping Measurements - The SR-5 model proved during test to be unstable at certain conditions, However, over the stable portion of the test, the jet pulse technique was used to evaluate modal damping and frequency. These results were extrapolated for comparison to actual flutter data.

Twelve readings (see Table 4-VI) for the SR-5 model test were selected for analysis. These points covered a range of Mach number (M = 0.75, 0.80, 0.85) and propeller speeds from 5100 to 5800 rpm. Four readings (8252, 8254, 8261 and 8271) were also analyzed via the ITD method for comparison with the results of the moving-block analysis (MBA).

The instability threshold rotational speed of the test model was found to be dependent upon the tunnel Mach number. The threshold speed was reduced with increased Mach number. For example, whereas at M = 0.75 the instability was encountered at 5970 rpm, at M = 0.85 the model could not be run beyond 5400 rpm. These results, for the SR-5, ten bladed, five bladed and two bladed models, will be discussed in the section entitled "Flutter boundaries", to follow.

The decay signals were not properly defined near the instability zone. Consequently, the results for these points have a low confidence factor. On the other hand, away from instability the data appeared to behave better and the results should have a higher confidence factor. A typical data signal is shown in Figure 4-26.

The test results are summarized in Table 4-VI. The table includes the test conditions, the test frequencies and the corresponding values of modal damping. The test results for some of the strain gages are missing from the table. For these gages either the data were of poor quality or the decay curve was not properly defined.

4.2 (Continued)

It is apparent from Table 4-VI that at M = 0.75 and a propeller speed of 5300 rpm (Reading 8249), the first bending frequency of the test model was determined to be about 151 Hz. The intergage relationship for blade 1 for the first bending frequency is very close. Even the frequency measured from the data of blade 2 is very close to blade 1 measurements. However, the same modal frequency as measured by a strain gage on blade 6 was 156 Hz. The modal damping values as a percent of critical damping ratio showed a large scatter ranging from 2.5% to 9.2%. For the same operating conditions, the frequencies for the 2nd, 3rd and 4th modes, respectively, were 314 Hz, 600 Hz and 654 Hz. The modal damping values decreased with increased modal order and again show a wide scatter (3.98% to 0.66%). The results also show that lower modes were better damped than the higher modes.

As the test model was driven into the instability region (5800 rpm), the first bending frequency increased to 161 Hz from 151 Hz showing the stiffening effect of increased propeller speed. This is consistent with theoretical expectations. It is also obvious from Table 4-VI that near the instability region the damping was considerably lower than when the model was operating away from the instability region.

The theoretical natural frequencies of the test model, as previously discussed in Section 3.1, were calculated using the computer program BESTRAN. The predicted and test frequencies are plotted in Figure 4-27. For the first two modes the correlation between the test and theory is excellent. However, for the third and fourth modes the agreement is within five percent.

It should be noted that the damping values obtained by the moving-block analysis are greatly affected by the quality of the test data. If the decay curve is not smooth and clearly defined, the results may be considerably in error. This is due to the subjective nature of the analysis. The analyst has to select a block of test data to apply the moving-block analysis and then a curve is fitted through the amplitude versus time data. The slope of this curve gives the damping value.

ITD Analysis and Comparison with Moving-Block Analysis - Four readings (8259, 8254, 8261 and 8271) were analyzed by R.A. Arnoldi at the United Technologies Research Center using the ITD method. Data from all nine gages were used to determine the modal damping and frequencies of the test model. The results of the analysis are discussed in Reference 22.

The results, which are taken from Reference 22, are shown in Table 4-VII. A comparison of these results with those of moving-block analysis is shown in table 4-VIII. The frequencies for the first bending mode are in good agreement, however, the damping values calculated by the ITD method are an order of magnitude higher than those calculated by the moving-block analysis. The ITD results are less realistic.

4.2 (Continued)

An attempt was made to analyze data from a single strain gage (Reading 8271 BG#1-1) by the ITD method. This procedure is similar to the moving-block analysis. The first bending frequency was 154.6 Hz and modal damping was 0.73%. The corresponding values from the moving-block analysis were 155 Hz and 0.562%. The foregoing discussion indicates that the advantages of ITD analysis over the moving-block analysis were not demonstrated.

Another comment about the ITD analysis is in order. Two bending modes at 155 and 165 Hz were found to persist, but the higher frequency predominates initially. Later in the decay, the 155 Hz mode emerged as the predominant mode which is the same mode used in the moving-block analysis. Only the predominant mode was found to give reasonable damping values by the ITD method, which were still considerably higher than the values obtained by the moving-block analysis. Hence, it was concluded that the damping of the first mode could not be accurately established from the available positions of the strain gages.

Flutter Boundaries - The predicted trends of the stability boundaries of the SR-2C, SR-3 and SR-5 models were previously discussed in Section 3.2. During testing, only the SR-5 fluttered. Figure 4-28 shows some of the actual flutter points obtained in the SR-5 tests given as Prop-Fan rotational speed vs. free stream Mach number. These data were obtained from Reference 15. The reference blade angle setting is shown next to each point. Data are shown for the ten bladed model, the five bladed model and the two bladed model. It is seen that flutter occured at lower rotational speeds as the free-stream Mach number was increased, and as the reference blade angle was increased. Also, as the number of blades was increased from two to ten, the flutter rotational speed was reduced. This shows that cascade effects have a strong destabilizing influence on the flutter boundary.

Comparison of Measured and Predicted Damping - Comparisons of experimentally determined, and calculated viscous damping ratios (C/C_c) plotted as a function of rotational speed are shown for the SR-3 and SR-5 models in figures 4-29 through 4-32. For the SR-3 model, results of isolated, mixed, and full cascade analyses are discussed. For the SR-5, the results of mixed and full cascade analyses are shown.

Figure 4-29 shows the stability margin plot, from analysis and test data using the MBA, for the 1st mode of the SR-3 8-way model at M = 0.8 and blade angle of 60.1 degrees. Only two test points were available at 9000 rpm, which show considerable scatter. However, if an average value of damping is assumed, and the damping trend line is plotted as shown, the mixed cascade analysis results nearly fall on the data derived trend line. On the other hand, the results of the full cascade analysis appear to be quite out of line.

Figure 4-30 shows the stability margin plot for the 1st and 2nd modes of the SR-3 4-way model at M = 0.8 and blade angle of 59 degrees. Again there is considerable data scatter at 9000 rpm. Average damping values indicate increased damping with increased propeller speed, which appears to be inconsistent with physical reasoning. The test data for the first mode, therefore,

4.2 (Continued)

appear to be of low quality. The results of the isolated blade analysis show reasonable agreement for the second mode. A similar conclusion is shown for M = 0.85 in Figure 4-31.

A comparison of the predicted and measured damping values of the first mode of the SR-5 model Prop-Fan is shown in Figure 4-32. The test results shown are at propeller speeds of 5100 rpm and 5300 rpm, 0.85 tunnel Mach number, and blade angle of 73 degrees. The predicted results are at 5000 rpm.

At 5000 rpm, the predicted equivalent viscous damping ratio (C/C_c) by the "Mixed Flutter Analysis" is negative (-0.013), and the corresponding experimental value obtained by extrapolating the test results, as shown in Figure 4-32, is positive (0.047). The corresponding comparison for the full cascade analysis is even worse (-0.033 Versus +0.047). This comparison therefore, shows that for the first mode, for the single point only, the test results do not agree with the predictions.

It should also be noted from Figure 4-32, that the jet excitation test instability threshold speed (extrapolated from the MBA at damping equal to zero), is about 5350 rpm. This is very close to the actual 5400 rpm threshold instability speed observed during the wind tunnel test (See Figure 4-28). This observation indicates that the damping results of the moving-block analysis, for well defined data signals, may be considered reliable.

Evaluation of Deviations From Predicted Values - The foregoing discussion of the analysis of the stability data of the SR-2C, SR-3 and SR-5 models has shown that the results of the moving-block analysis can be considered reliable only if the decay signal is sufficiently smooth. It was observed that the natural wind tunnel turbulence and the jet pulse excitations were inadequate to properly excite the test models. Also, comparisons of the predicted and measured stability margins of the test models were inconsistent. For example, whereas the analysis predicted the SR-5 blade to go unstable at 5000 rpm at M = 0.85, the model was stable up to 5300 rpm. These deviations strongly suggest the need for followup work to develop and evaluate alternate excitation techniques and improvements to the unstalled flutter analysis.

4.3 NASA/AMES INSTALLED SR-2C RESPONSE TEST

The SR-2C Prop-Fan wing/nacelle and fuselage test model has been discussed in Section 2 along with the blade strain gage locations. The calculations for these tests were discussed in Section 3.1 and a summary of the conditions calculated is shown in Table 4-IX. The operating conditions of the tests are summarized in Table 4-X, where for each Mach number, blade angle and fuselage angle, a series of propeller rpm's were run. These were usually in 500 rpm increments, ranging from 5000 to 9000 rpm. The following ranges of variables were covered: Mach number from 0.6 to 0.85, blade angle from 50.69 to 57 deg., and fuselage angle from -3 to 5 deg.

In comparing Table 4-IX to Table 4-X it is seen that none of the tests were conducted at a Mach number of 0.3. Also, none of the other prediction points in Table 4-IX were run at exactly the same condition as were tested.

Specific data analyses were made using a real time analyzer. A sample carpet plot is shown in Figure 4-33. These results show some higher P-order (PER-REV) content. Unfortunately, excitation at the natural blade response frequencies is comparatively low, such that only the first and second flat-wise frequencies can be observed. The placement of these modes has been transposed to a Campbell diagram in Figure 4-34 for a typical run. Here the observed values are compared with the calculated beam theory values and the correlation is good. The cross-hatched areas indicate that the aerodynamics can change the response frequency. The calculated frequencies do not include the effects of the air.

Stress data were obtained at steady state conditions during the wind tunnel tests and recorded on analog tapes. These tapes were processed using a real time analyzer and observed on a CRT display terminal. Spectral analyses were produced for three channels of data for all runs. This output was transmitted to a digital computer for processing. Some sample spectral plots of vibratory stress vs. frequency are found in Figures 4-35 through 4-38.

Automatic plotting capability was added to the data reduction precedure such that the NP peak stresses were plotted vs. reference angle (fuselage angle of attack). Figures 4-39 through 4-42 are sample computer plots for a blade angle of β = 50.69 deg. and a Mach number of M = 0.6. Each plot contains curves for various rpm's and represents the vibratory 1P, 2P, 3P and 4P stresses, respectively. These sample plots are for the mid-blade bending stress on blade number 5 (6.4 inch station). The vibratory stresses represented in Figures 4-39 though 4-42 show substantial 1P and 2P response, but neglible 3P and 4P response for the mid-blade bending gage. The tip bending gage shows similar but lower values of 1P, 2P and 3P but shows a little more 4P at the higher rpm's. Figure 4-43 is a typical example of the 4P vibratory stress measured using the tip bending gage on blade 8. Again, the 4P response remains at a constant low amplitude level over the range of propeller attitude and rpm. Since the 3P and 4P response stress levels are low, they were not included in the correlation to be discussed in the following paragraphs.

4.3 (Continued)

As previously mentioned, Table 3-VII shows the results of the analytical computations for the NP vibratory stresses of the Ames model. Only cases No. 6, 7, 8, and 9 can be compared to data, since all the other cases were calculated at a Mach number of M = 0.3 (see Table 4-IX), for which no wind tunnel data are available. However, even for cases 6, 7, 8 and 9 no experimental data were obtained at exactly the conditions analyzed. It was, therefore, necessary to interpolate the data outlined in Table 4-X in order to match the conditions of the calculations. Values of 1P and 2P vibratory stresses were linearly interpolated from the test runs such that fuselage reference angle, rpm, Cp, blade angle and Mach number matched those of the calculated conditions.

The comparisons between the calculations and the interpolated test results are shown in Table 4-XI. For cases 6, 8 and 9 the HS/H039 flow field results produce 1P vibratory stresses that are almost twice the test values and 2P vibratory stresses that vary between 0.9 and 2.8 times the test values. The values of calculated stress that resulted from the use of the Hess code flow field are also generally higher than the interpolated values. Comparisons with the Hess code results indicate that the calculated 1P stresses are 0.8 to 1.8 times the test values and the 2P stress values are 1.6 to 4.8 times the test values.

The correlation shown in Table 4-XI seems poor. However, it is difficult to make comparisons because, 1) the calculations were not made at the identical conditions at which test data were taken, and 2) there are not enough calculated points to show trends. It is also noted that the variations in vibratory stress may not be linear. Thus, linear interpolations may give erroneous results. It is recommended that more calculations be made for conditions that coincide with the test conditions.

Output vibratory signals from the analog tapes were also recorded on brush charts to give time histories of the vibratory stress amplitudes. These signals were recorded for six channels of data. These data were read from the charts and tabulated in the form of average total vibratory stress. Total stress is defined as a summation of all stress amplitudes at all frequencies. Figure 4-44 is a sample of these data plotted with stress as a function of fuselage reference angle. These curves are shown for Mach numbers of 0.6 and 0.7, for various rpm's. Also plotted on these curves are the calculated stress points for cases 6 and 9. The calculated points at a fuselage reference angle of 5 degrees were computed at 8700 rpm, which is 200 rpm higher than the other points on this curve. This discrepancy is not considered important in view of the fact that the test data show little effect of rpm at this attitude. The predictions of total stress compare reasonably with tested values at lower fuselage angle, but are high at higher angles. The Hamilton Standard code predicts up to 250% higher stresses than the measured values and the Hess code predicts up to 195% higher stress. The cause of these differences is not known.

4.3 (Continued)

Figure 4-45 is a curve showing some of the results of the NASA/Ames SR-2C semi-span model tests for a wind tunnel Mach number of 0.78 and a reference blade angle of 55.0 degrees. Also shown on this curve are some of the results of the NASA/Lewis response tests on the SR-2C for a Mach number of 0.8 and a reference blade angle of 55.7 deg. The once-per-rev vibratory stress is shown as a function of propeller tilt angle or aircraft reference angle at 8000 rpm.

Both curves show a minimum stress, and because of symmetry, the Lewis tests show the minimum occurring at 0.0 degrees propeller tilt angle as is expected. The Ames tests show the minimum occurring at a 2 degrees aircraft reference angle, which is what might be expected since the propeller down-tilt is 3.5 degrees (See Section 2, the discussion of the model.). This would indicate that the upwash is approximately 1.75 degrees. Generally the slopes of both curves are similar on either side of the minimum point. Note that the minimum stress for the Ames test is not near zero. This excitation floor is due to the 2 degree toe-in of the nacelle. It is expected that these curves should have similar slopes except that some modification might occur due to wing lift nonlinearities. There are not enough points to determine this from this curve.

TABLE 4-I. COMPARISON OF PREDICTED AND TEST 1P VIBRATORY STRESSES FOR THE SR-3 MODEL PROP-FAN

TEST POINT	CASE	RPM	MACH NO.	INFLOW ANGLE DEG	EXCITATION FACTOR (EF)	DENSITY RATIO ρ/ρ_O	POWER KW (SHP)	σ/EF – KPA PER EF – PREDICTED/TEST INBOARD GAGE BG1-1	TRAILING EDGE GAGE BG1-2	MID-BLADE GAGE BG1-3	VEE GAGE BG1-4	TIP GAGE BG1-5
215	1	7016	0.596	4	4.86	0.9377	225 (301.8)	2006	1407	1751	455	745
								3551	1434	2730	524	1655
217	2	8802	0.596	4	4.79	0.9440	650 (871.8)	2799	1696	1917	690	324
								4923	2144	3489	407	2289
245	3	7006	0.695	3	4.60	0.9046	195 (261.4)	2027	1717	2000	255	1248
								3420	1400	2593	407	1710
272	4	7017	0.799	2	3.54	0.8000	148 (198.6)	2055	2627	2799	545	3324
								3268	1172	2331	372	1214
296	5	7012	0.792	4	7.06	0.8134	224 (300.5)	2158	1889	2186	200	1517
								3585	1379	2572	400	1607
NA	6	8636	0.80	3	5.33	0.7602	441 (591)	2296	1552	1551	310	593
								4047	1710	2689	359	1434

TABLE 4-II. INTERBLADE STRESS RATIO FOR THE INBOARD GAGE LOCATED ON BLADES 1, 2, AND 6 OF SR-5 PROP-FAN TEST MODEL

READING NUMBER	TUNNEL MACH NUMBER (M)	BLADE ANGLE $\beta_{3/4}$	INFLOW ANGLE ψ	PROPELLER ROTATIONAL SPEED (RPM)	POWER COEFFICIENT (C_P)	SHAFT POWER KW (SHP)	INTERBLADE STRESS RATIO		
							NORMALIZED STRESS PER EXCITATION FACTOR (σ/EF)		
							BG1-1/BG1-1	BG2-1/BG1-1	BG6-1/BG1-1
8606	0.36	60.8	15	6000	2.020	278 (373)	1.0	0.88	0.97
8607	0.36	60.8	12	6000	2.014	275 (369)	1.0	0.89	0.97
8608	0.36	60.8	9	6000	2.014	274 (367)	1.0	0.91	1.00
8609	0.36	60.8	6	6000	2.013	271 (363)	1.0	0.91	0.99
8610	0.36	60.8	3	6000	2.014	269 (360)	1.0	0.85	0.97
8611	0.36	60.8	0	6000	2.013	269 (360)	1.0		
8450	0.7	68.9	5	4000	0	0 (0)	1.0	1.00	0.99
8451	0.7	68.9	5	4500	1.081	44 (59)	1.0	0.93	1.01
8452	0.7	68.9	5	5000	1.769	98 (131)	1.0	1.00	0.94
8453	0.7	68.9	5	5500	2.214	163 (218)	1.0	0.92	1.01
8454	0.7	68.9	5	6000	2.501	239 (321)	1.0	0.90	1.01
8455	0.7	68.9	5	6500	2.664	324 (434)	1.0	0.90	1.02
8456	0.7	68.9	5	6910	2.755	402 (539)	1.0	0.92	1.03
8490	0.7	70.8	5	3412	0	0 (0)	1.0	0.90	0.97
8491	0.7	70.8	5	4000	1.675	48 (64)	1.0	0.92	1.00
8492	0.7	70.8	5	4500	2.497	101 (135)	1.0	0.93	0.99
8493	0.7	70.8	5	5000	2.979	165 (221)	1.0	0.91	1.00
8494	0.7	70.8	5	5500	3.283	242 (325)	1.0	0.91	1.02
8495	0.7	70.8	5	6000	3.456	331 (444)	1.0	0.77	1.01
8496	0.7	70.8	5	6500	3.543	430 (577)	1.0	0.89	1.02
8497	0.7	70.8	5	6700	3.561	473 (634)	1.0	0.88	1.01
8383	0.7	72.9	5	2998	0	0 (0)	1.0	0.90	0.98
8384	0.7	72.9	5	3500	1.966	37 (49)	1.0	0.91	1.00
8385	0.7	72.9	5	4000	3.063	85 (114)	1.0	0.89	0.97
8386	0.7	72.9	5	4500	3.682	145 (195)	1.0	0.90	1.00
8387	0.7	72.9	5	5000	4.005	218 (292)	1.0	0.92	1.02
8388	0.7	72.9	5	5500	4.189	303 (406)	1.0	0.88	1.00
8389	0.7	72.9	5	6000	4.276	400 (536)	1.0	0.89	1.01
8390	0.7	72.9	5	6500	4.282	510 (684)	1.0	0.89	1.01
8507	0.8	70.8	1	5500	2.626	178 (238)	1.0	0.80	0.96
8508	0.8	70.8	2	5500	2.645	179 (240)	1.0	0.92	1.02
8509	0.8	70.8	3	5500	2.686	182 (244)	1.0	0.93	1.02
8510	0.8	70.8	4	5500	2.723	186 (249)	1.0	0.97	1.00
8511	0.8	70.8	5	5500	2.750	187 (251)	1.0	0.96	0.98

TABLE 4-III. COMPARISON OF PREDICTED AND TEST 1P VIBRATORY STRESSES FOR THE SR-5 MODEL PROP-FAN

CASE	RPM	MACH NO.	INFLOW ANGLE DEG	EXCITATION FACTOR (EF)	DENSITY RATIO ρ/ρ_o	POWER KW (SHP)	σ/EF ~ KPA PER EF (PREDICTED/TEST) INBOARD GAGE BG1-1	VEE GAGE BG1-3	TIP CROSSWISE BG1-5	TIP SPANWISE BG1-6
1	6000	0.6	7	7.86	0.8889	186 (250)	4599	593	883	1455
							6033	359	779	2779
2	6000	0.6	7	7.86	0.8889	336 (450)	5033	662	1000	1620
							7571	414	1282	3075
3	7950	0.6	7	7.86	0.8889	388 (520)	4695	524	600	1282
							6371	228	1145	2496
4	6000	0.8	2	3.49	0.7976	186 (250)	4930	510	1393	1351
							6936	303	876	2965
5	6000	0.8	2	3.49	0.7976	336 (450)	5337	572	1076	1538
							7909	207	1145	3296

TABLE 4-IV. PULSE EXCITED FREQUENCIES AND DAMPING FOR SR-3/8-WAY PROP-FAN FOR THE FIRST MODE USING MOVING BLOCK ANALYSIS AND VISICORDER DATA GAGE BG1-1, $\beta = 57.7°$, TEST DATE 1-22-81

READING NO.	ROTATIONAL SPEED (RPM)	TUNNEL MACH NUMBER (M)	POWER COEFFICIENT (C_P)	FREQUENCY (HZ) MBA	FREQUENCY (HZ) VISICORDER	PERCENT OF CRITICAL DAMPING MBA	PERCENT OF CRITICAL DAMPING VISICORDER
181	7000	0.8	0.315	214	214	1.90	1.90
182	8000	0.8	0.970	225	225	1.05	1.66
183	9000	0.8	1.379	234	232	0	≈ 0
191	8000	0.85	0.436	224	231	2.01	1.86
192	9000	0.85	0.947	240	245	0	≈ 0

TABLE 4-V. MODAL DAMPING AND FREQUENCIES OF THE SR-3 MODEL PROP-FAN OBTAINED FROM TEST DATA BY MOVING-BLOCK ANALYSIS

NASA READING #	TYPE OF MODEL	M	$\beta_{3/4}$	C_P	N	STRAIN GAGE	MODE	FREQUENCIES (HZ) PREDICTED	FREQUENCIES (HZ) TEST	MODAL DAMPING % OF C/C_C
221	8-WAY	0.8	60.1	1.199	7000	BG1-1	1	220	216.0	1.696
						BG1-3	2	430	428.0	0.758
						BG1-5	3	685	625.0	0.376
						BG1-4	4	770	741.0	0.231
231	8-WAY	0.8	60.1	2.074	9000	BG1-1	1	245	237.0	1.595
						BG1-3	2	445	445.0	0.946
						BG1-5	3	688	691.0	0.544
						BG1-4	4	787	783.0	0.393
283	8-WAY	0.85	61.0	2.142	9000	BG1-1	1	235	227.0	1.750
							2	445	443.2	0.800
							4	775	739.2	0.370
						BG1-3	1	235	227.0	3.700
							2	445	443.2	1.410
							4	775	739.2	0.820
306	4-WAY	0.80	59.0	0.489	7000	BG1-1	1	220	216.0	2.265
						BG1-3	2	430	422.0	1.182
						BG1-5	3	685	628.0	0.635
						BG1-4	4	770	722.0	0.606
312	4-WAY	0.80	59.0	1.141	9000	BG1-1	1	245	237.2	25.70
							2	445	446.4	8.60
							3	688	682.2	1.45
							4	787	790.2	3.00
						BG1-3	1	245	237.2	7.20
							2	445	446.4	2.54
							3	688	682.2	1.51
							4	787	790.2	0.95
						BG1-5	1	245	237.2	5.20
							2	445	446.4	1.28
							3	688	682.2	1.03
							4	787	790.2	0.64
						BG1-4	1	245	237.2	1.07
							2	445	446.4	1.80
							3	688	682.2	1.55
							4	787	790.2	1.05
373	4-WAY	0.85	60.0	1.369	9000	BG1-1	1	245	235.9	3.10
							2	445	444.8	2.50
							3	688	688.3	0.97
							4	787	784.4	0.466
						BG1-3	1	245	235.9	5.74
							2	445	444.8	0.97
							3	688	688.3	0.03
							4	787	784.4	0.35
						BG1-5	1	245	235.9	2.82
							2	445	444.8	1.78
							3	688	688.3	0.72
							4	787	784.4	1.10
						BG1-4	1	245	235.9	2.33
							2	445	444.8	3.50
							3	688	688.3	4.60
							4	787	784.3	2.84

TABLE 4-VI. NATURAL FREQUENCIES AND MODAL DAMPING VALUES OF THE SR-5 PROP-FAN TEST MODEL OBTAINED BY FFT AND MOVING BLOCK ANALYSES FROM NASA-LEWIS TEST DATA

TEST RDG.	M	PROP SPEED (RPM)	SHAFT POWER KW	POWER COEFFICIENT (C_P)	ADVANCE RATIO (J)	BLADE ANGLE β	STRAIN GAGE NUMBER	TEST FREQUENCIES OF MODEL (HZ)	MODAL DAMPING PERCENT OF C/C_C	COMMENTS
8249	0.75	5300	248	3.92	4.622	73	BG1-1	150.7	4.53	
								313.9	2.18	
								604.8	1.68	
							BG1-3	150.8	4.90	
								313.9	1.68	
								599.4	0.80	
								654.4	0.66	
							BG1-5	150.8	9.16	DAMPING ABOUT TWICE OF GAGES 1 & 3
								313.9	3.98	
								599.0	2.49	
								615.4	1.99	
								654.3	0.80	
							BG1-6	150.8	8.60	VERY WEAK SIGNAL. IT APPEARS THAT THE JET PULSE DIDN'T HAVE SUFFICIENT ENERGY.
								316.0	4.20	
								599.2	3.53	
								700.6	--	DECAY SIGNAL WASN'T CLEARLY DEFINED
							BG2-1	151.0	4.16	
								166.0	3.24	
								308.0	2.95	
								316.0	2.88	
								603.0	1.70	
								615.5	1.32	
							BG6-1	156.0	2.46	FIRST BENDING FREQUENCY FROM 6TH BLADE DATA WAS HIGHER THAN FROM EITHER BLADE 1 OR 2
								161.5	1.62	
								308.3	0.59	
								612.0	0.38	
								625.0	0.37	
								645.0	0.40	

TABLE 4-VI. NATURAL FREQUENCIES AND MODAL DAMPING VALUES OF THE SR-5 PROP-FAN TEST MODEL OBTAINED BY FFT AND MOVING BLOCK ANALYSES FROM NASA-LEWIS TEST DATA (CONT'D)

TEST RDG.	M	PROP SPEED (RPM)	SHAFT POWER KW	POWER COEFFICIENT (C_P)	ADVANCE RATIO (J)	BLADE ANGLE β	STRAIN GAGE NUMBER	TEST FREQUENCIES OF MODEL (HZ)	MODAL DAMPING PERCENT OF C/C_C	COMMENTS
8250	0.75	5500	283	4.01	4.46	73	BG1-1	160.3 308.0 322.0 602.0	0.80 0.35 0.51 0.25	
							BG1-3	160.3 317.0 598.0 632.0 665.0	0.93 0.44 0.05 0.04 0.02	DECAY WASN'T CLEARLY DEFINED
							BG1-5	160.3 305.8 316.8 322.0 611.5 626.0	0.90 0.70 0.38 0.38 0.21 0.21	
							BG1-6	160.2 318.0 615.0 626.0	1.34 0.26 0.07 0.11	
8252	0.75	5600	302.6	4.05	4.38	73	BG1-1	161.0 309.0 609.0 615.0 629.8	0.95 0.40 0.28 0.30 0.26	
							BG1-3 BG1-5			NO ANALYSIS WAS PERFORMED BECAUSE THE SIGNAL WASN'T CLEAR ENOUGH
8253	0.75	5700	323	4.09	4.30	73	BG1-1	162.0 324.0 410.3 615.0	2.78 1.41 1.04 0.47	SIGNAL WAS AMPLIFIED AFTER DECAY

TABLE 4-VI. NATURAL FREQUENCIES AND MODAL DAMPING VALUES OF THE SR-5 PROP-FAN TEST MODEL OBTAINED BY FFT AND MOVING BLOCK ANALYSES FROM NASA-LEWIS TEST DATA (CONT'D)

TEST RDG.	M	PROP SPEED (RPM)	SHAFT POWER KW	POWER COEFFICIENT (C_P)	ADVANCE RATIO (J)	BLADE ANGLE β	STRAIN GAGE NUMBER	TEST FREQUENCIES OF MODEL (HZ)	MODAL DAMPING PERCENT OF C/C_C	COMMENTS
8254	0.75	5800	342	4.13	4.22	73	BG1-1	161.0	0.90	
								309.0	0.40	
								609.0	0.28	
								615.0	0.30	
								629.0	0.26	
							BG1-3			NEAR INSTABILITY. DECAY WAS ERRATIC
							BG1-5			
8260	0.80	5400	255	3.72	4.83	73	BG1-1	154.0	0.45	
								311.0	0.56	
								599.0	0.102	
								605.0	0.104	
								613.0	0.104	
								621.0	0.092	
							BG1-5	668.0	0.113	
							BG1-6	154.3	0.51	VERY LOW DECAY. ONLY A PORTION OF THE GRAPH WAS VISIBLE
								654.7	0.21	
8261	0.80	5400	255	3.72	4.83	73	BG1-1	154.9	0.354	BEATS IN DATA; DECAY WAS SUDDEN; HIGHER AMPLITUDE AFTER THE DECAY THAN BEFORE THE JET WAS CUT OFF.
								171.2	0.291	
								176.7	0.253	
								267.0	0.145	
								304.3	0.116	
								313.0	0.142	
								587.2	0.061	
								601.8	0.059	
								613.7	0.619	
							BG1-3	155.0	4.926	
								160.5	4.643	
								306.5	0.410	
								502.6	0.044	
								508.0	0.046	
								513.3	0.046	
								517.3	0.060	
								605.8	0.310	
								614.2	0.060	
								661.3	0.043	

TABLE 4-VI. NATURAL FREQUENCIES AND MODAL DAMPING VALUES OF THE SR-5 PROP-FAN TEST MODEL OBTAINED BY FFT AND MOVING BLOCK ANALYSES FROM NASA-LEWIS TEST DATA (CONCLUDED)

TEST RDG.	M	PROF SPEED (RPM)	SHAFT POWER KW	POWER COEFFICIENT (C_P)	ADVANCE RATIO (J)	BLADE ANGLE β	STRAIN GAGE NUMBER	TEST FREQUENCIES OF MODEL (HZ)	MODAL DAMPING PERCENT OF C/C_C	COMMENTS
8262	0.8	5500	255	3.77	4.74	73	BG1-1	159.6 316.5 407.0 480.4 480.6 616.0	2.40 0.50 0.38 0.51 0.41 0.41	BEATS WERE PRESENT IN RESPONSE
8263	0.8	5600	257	3.81	4.65	73	BG1-1	162.0 315.0 619.2	2.46 0.77 0.31	
							BG1-5	162.4 306.2 602.0 619.5	3.093 1.547 0.066 0.029	
							BG1-6	162.4 321.0 619.8 694.0	1.48 0.55 0.19 0.14	DECAY WAS NOT CLEARLY SHOWN
8269	0.85	5100	177	3.41	5.35	73	BG1-1	154.0 154.0 308.0 480.8 618.0	3.86 3.20 2.05 1.01 0.94	BEATS IN DATA AND WEAK SIGNAL
8270	0.85	5200	190	3.46	5.25	73	BG1-1			SUDDEN DROPOFF IN SIGNAL, RESULTS QUESTIONABLE, NOT TABULATED
8271	0.85	5300	203	3.50	5.15	73	BG1-1	155.0 480.8 615.6	0.562 0.209 0.161	
							BG1-3	154.2 262.5 319.0 583.5 647.4 672.0	0.835 0.498 0.409 0.322 0.264 0.233	
							BG1-5	155.0 262.5 299.7 672.2	0.845 0.555 0.489 0.213	
							BG1-6	154.5 262.5 291.0 315.5	0.604 0.375 0.326 0.287	

TABLE 4-VII. MODAL DAMPING AND FREQUENCIES OF THE SR-5 MODEL PROP-FAN OBTAINED FROM TEST DATA VIA ITD ANALYSIS

RDG.	RPM	FREQ.	DAMPING*	MODAL CONFIDENCE FACTOR (APPROX. AVG)	
8254	5800	82.4	91.0%	60%	
		160.3	11.0	95%	1ST BENDING
		186.8	24.5	90%	
		636.1	34.7	30%	
8252	5600	130.5	41.5	80%	1ST BENDING
		154.4	6.2	90%	1ST BENDING
		187.6	86.2	25%	
		228.0	67.9	40%	
		270.5	33.5	60%	
8261	5400	88.1	80.4	70%	
		159.0	4.7	95%	1ST BENDING
		167.4	19.6	85%	1ST BENDING
		258.1	23.6	80%	
8271	5300	93.9	10.7	95%	
		155.9	59.4	80%	1ST BENDING
		168.5	1.5	98%	1ST BENDING
		260.6	3.2	97%	
		266.0	40.4	70%	
		588.8	16.2	70%	

*DAMPING IS GIVEN AS PERCENT OF CRITICAL.
POSITIVE VALUES INDICATE STABILITY.

TABLE 4-VIII. COMPARISON OF THE SR-5 RESULTS OF MOVING-BLOCK AND ITD ANALYSIS

RDG.	RPM	FREQ. (HZ)		DAMPING *		MODAL CONFIDENCE FACTOR (APPROX. AVG.)	
		ITD	MBA	ITD	MBA		
8254	5800	82.4		91.0%		60%	
		160.3	161.0	11.0	0.90%	95%	1ST BENDING
		186.8		24.5		90%	
		636.1	629.0	34.7	0.26	30%	
8252	5600	130.5		41.5		80%	1ST BENDING
		154.4	161.0	6.2	0.95	90%	1ST BENDING
		187.6		86.2		25%	
		228.0		67.9		40%	
		270.5		33.5		60%	
8261	5400	88.1		80.4		70%	
		159.0	154.9	4.7	0.354	95%	1ST BENDING
		167.4	171.2	19.6	0.291	85%	1ST BENDING
		258.1	267.0	23.6	0.145	80%	
8271	5300	93.9		10.7		95%	
		155.9	154.2	59.4	0.83	80%	1ST BENDING
		168.5		1.5		98%	1ST BENDING
		260.6	262.5	3.2	0.50	97%	
		266.0		40.4		70%	
		588.8	583.51	16.2	0.32	70%	

*DAMPING IS GIVEN AS PERCENT OF CRITICAL.
POSITIVE VALUES INDICATE STABILITY.

TABLE 4-IX. SR-2C OPERATING CONDITIONS FOR CALCULATIONS

	CASE NO.	MACH NO.*	WING ZERO LIFT ANGLE	RPM	POWER KW/M^2	ALT (M)
CLIMB	1	0.3	12°	7846	580	SL
	2	0.3	12°	7846	290	SL
	3	0.3	12°	5883	580	SL
	4	0.3	12°	5883	290	SL
	5	0.3	6°	7846	580	SL
CRUISE	6	0.6	5°	8771	302	10668
	7	0.6	5°	8771	151	10668
	8	0.6	2.5°	8771	302	10688
	9	0.8	3°	8549	302	10668

*NO TEST RUNS WERE MADE AT MACH=0.3 DUE TO POWER LIMITATION

TABLE 4-X. SR-2C OPERATING CONDITIONS - TEST

	RANGE	
	MIN.	MAX.
PROP-FAN RPM	5000 RPM	9000 RPM
AIRCRAFT REFERENCE ANGLE (FRL)	-3 DEG.	+5 DEG.
WING ZERO LIFT ANGLE	0 DEG.	8 DEG.
TUNNEL MACH NO.	0.6	0.85
REF. BLADE ANGLE	50.69 DEG.	57.0 DEG.

TABLE 4-XI. SR2C PROP-FAN SEMI-SPAN MODEL WIND TUNNEL TEST AT AMES EXPERIMENTAL AND PREDICTED STRESS*

				1P VIBRATORY STRESS – KPA			2P VIBRATORY STRESS – KPA		
CASE NO.	MACH NO.	FUSELAGE REF. ANGLE DEGREE	RPM	TEST** INTERPOLATION	CALCULATED HESS	CALCULATED H039	TEST** INTERPOLATION	CALCULATED HESS	CALCULATED H039
6	0.6	5.0	8771	22216	41163	52678	1203	8136	4764
7	0.6	5.0	8771	N/A***	35302	43025	N/A***	7998	5254
8	0.6	2.5	8771	12135	10067	20961	4013	6343	3751
9	0.8	3.0	8549	13576	16824	30269	3992	7791	5102

*GAGE RADIAL LOCATION=0.163M (6.4")

**LINEAR INTERPOLATION

***THIS CASE IS TOO FAR FROM TEST CASE FOR INTERPOLATION – C_p=0.846 CALCULATED

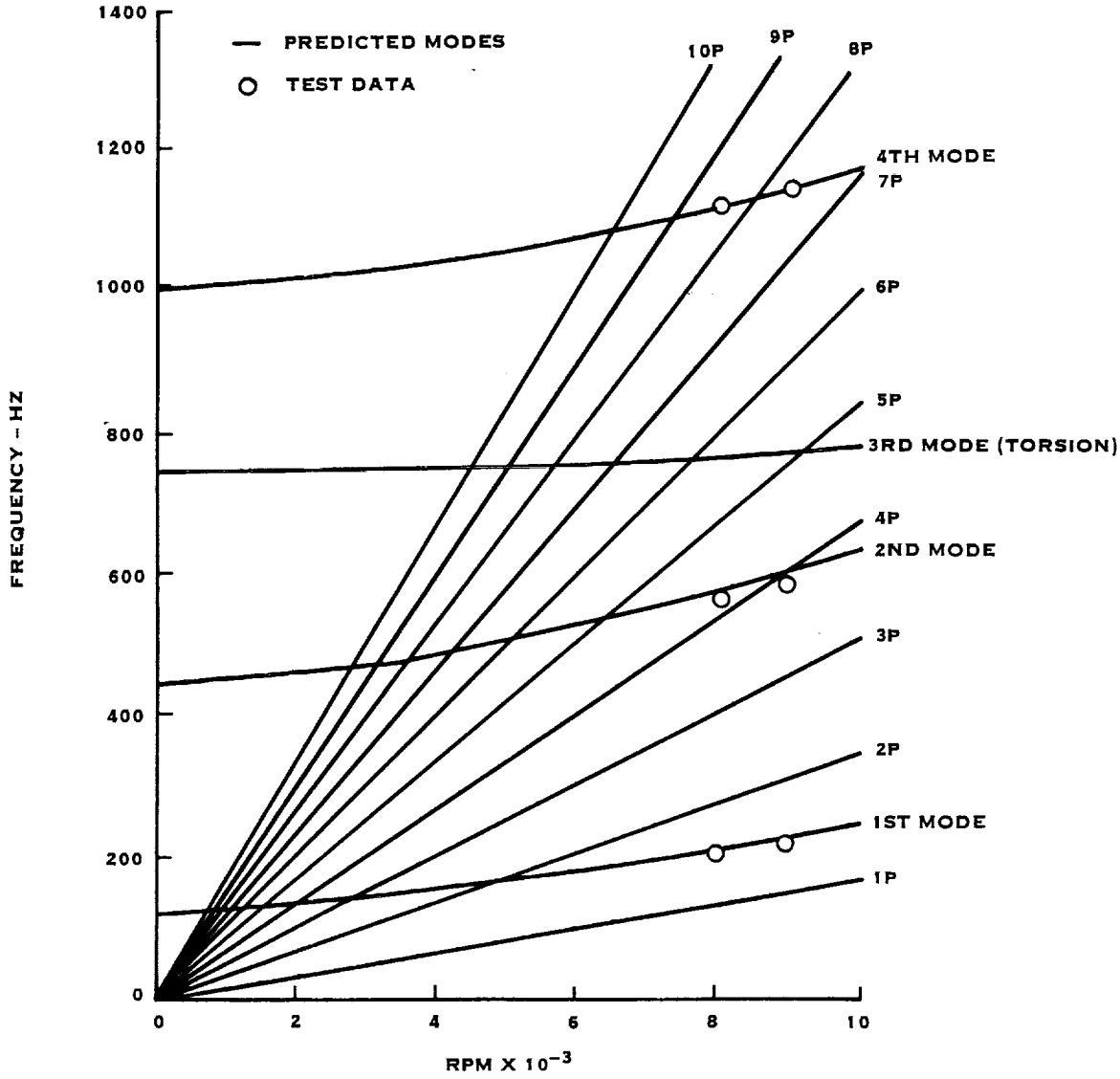

FIGURE 4-1. COMPARISON OF TEST & PREDICTED CRITICAL SPEEDS SR-2C PROP-FAN MODEL CAMPBELL DIAGRAM DIA = 622.3MM (24.5 IN.), $\beta_{.75}$ = 55° (CALCULATIONS WITH HS/H025, HS/H027)

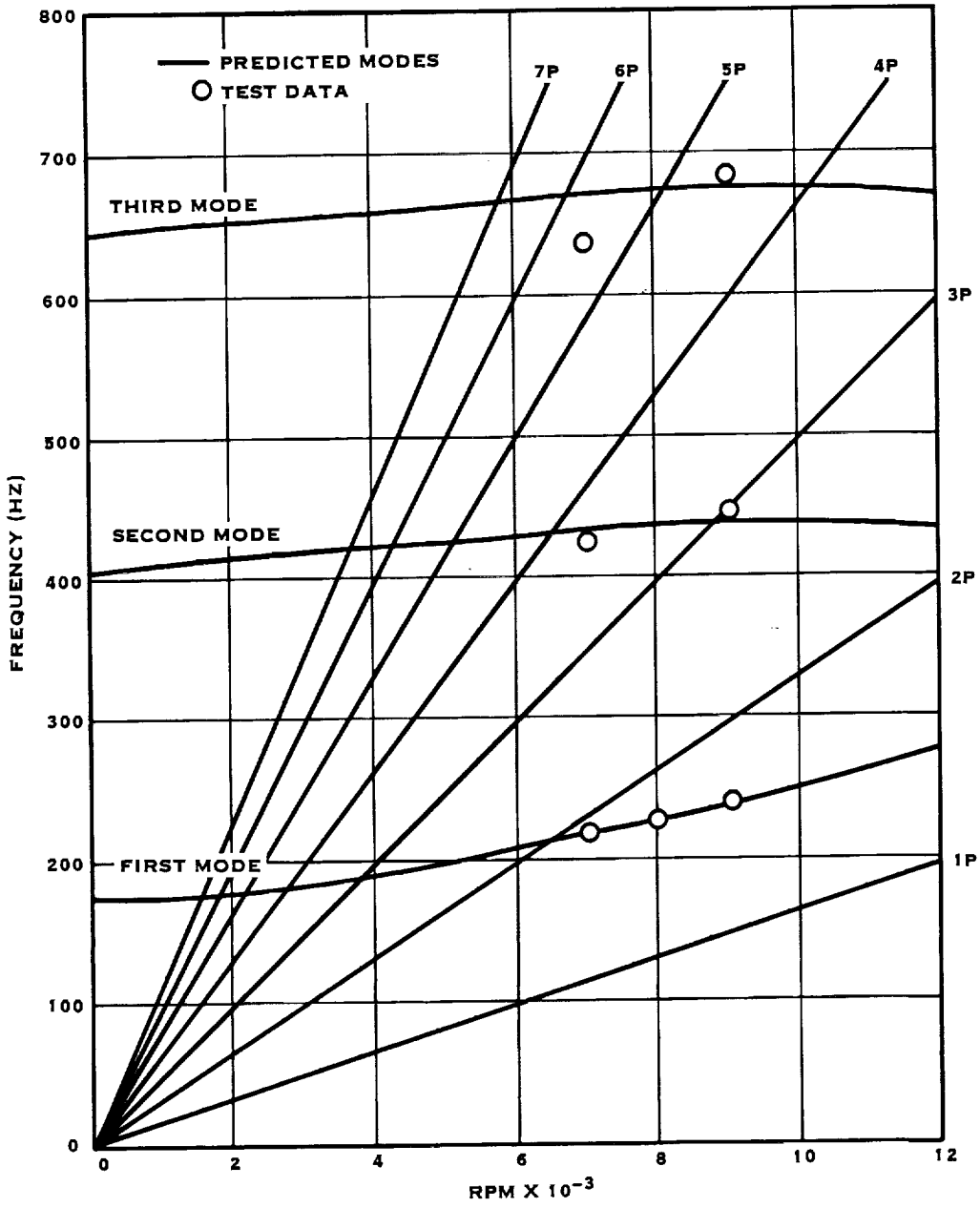

FIGURE 4-2. COMPARISON OF TEST AND PREDICTED CRITICAL SPEEDS (SR-3 PROP-FAN MODEL CAMPBELL DIAGRAM $\beta_{3/4} = 57°$)

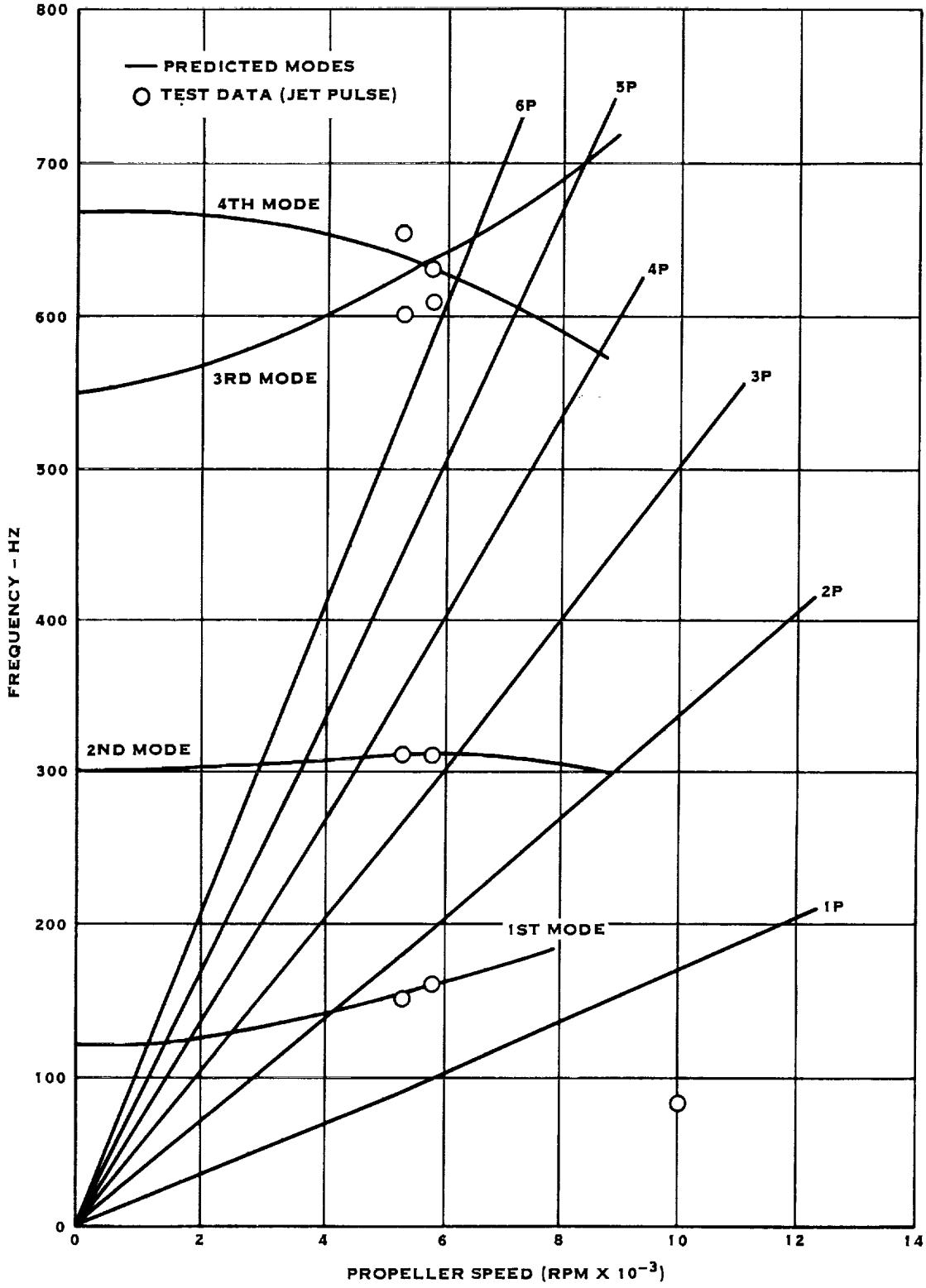

FIGURE 4-3. COMPARISON OF TEST AND PREDICTED CRITICAL SPEEDS OF SR-5 MODEL PROP-FAN ($\beta_{.75}$ = 61.1°) PRETWISTED $\beta_{3/4}$ = 66.7° STATIC

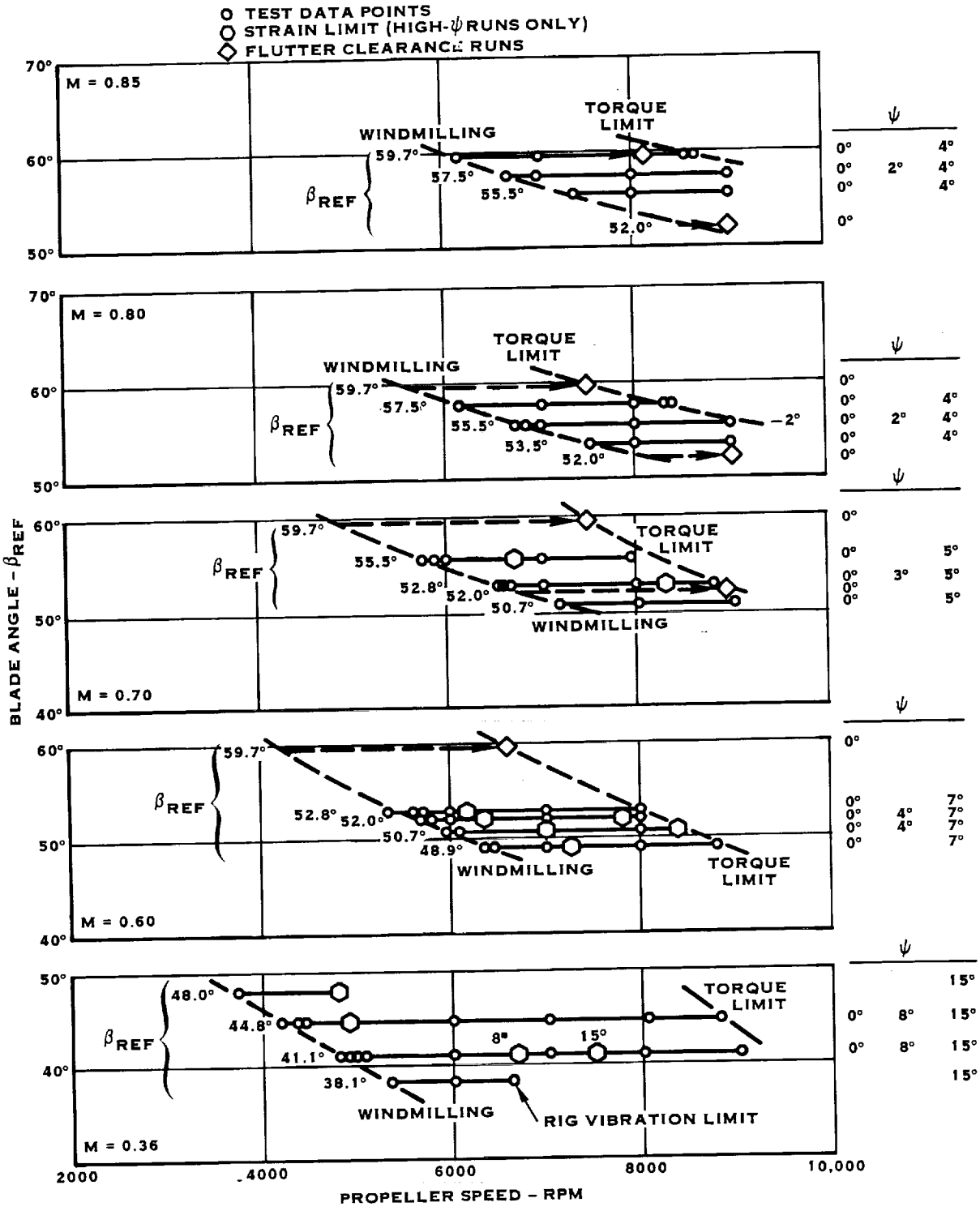

FIGURE 4-4. SUMMARY OF OPERATING CONDITIONS SR-2C 8-WAY MODEL PROP-FAN TESTS AT NASA-LEWIS, APRIL 1980

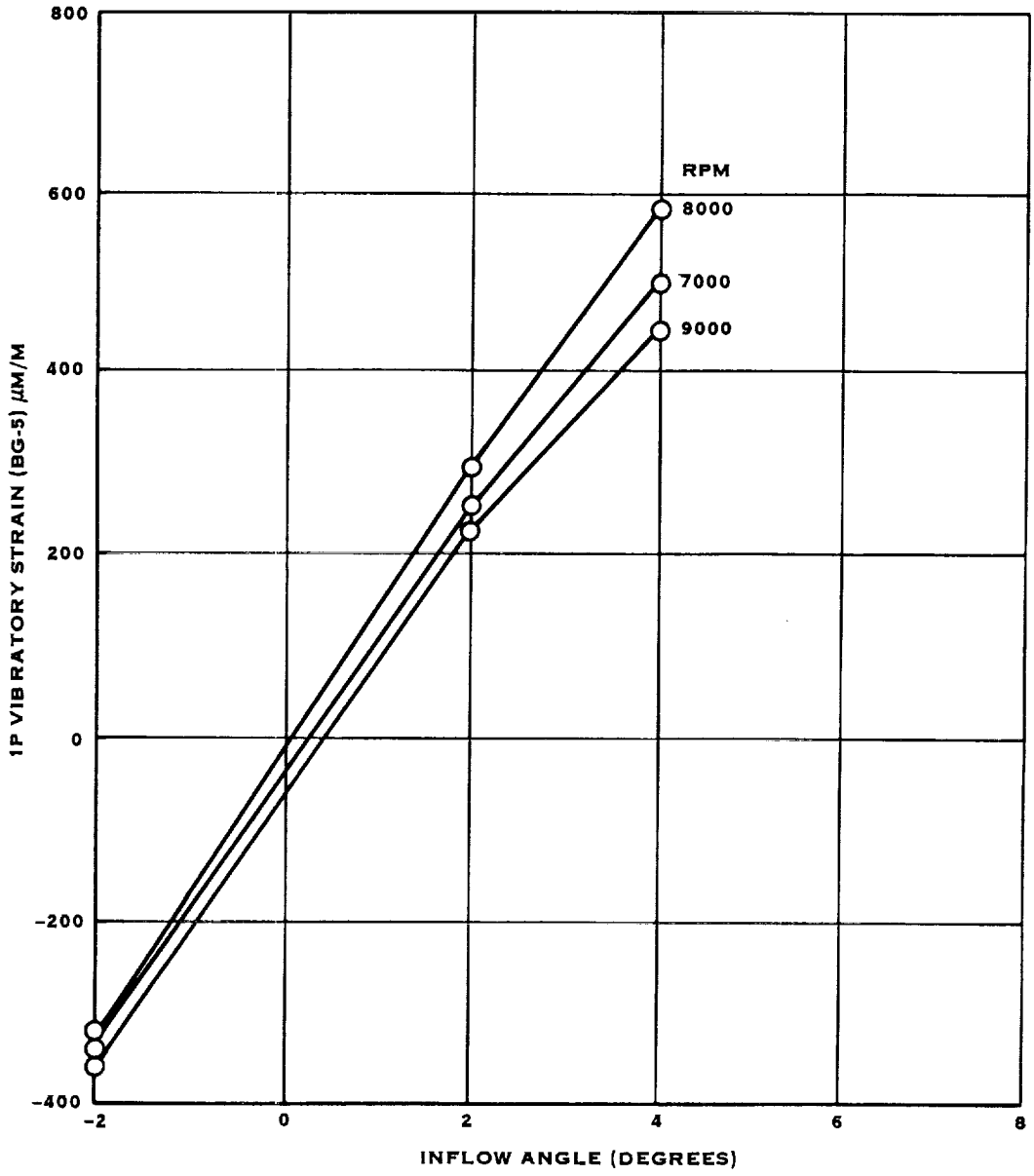

FIGURE 4-5. SR-2C PROP-FAN BLADE MODEL WIND TUNNEL TEST AT NASA-LEWIS, APRIL, 1980 - 1P VIBRATORY STRAIN (BG-5) VS. INFLOW ANGLE, β = 55.5, M = 0.8

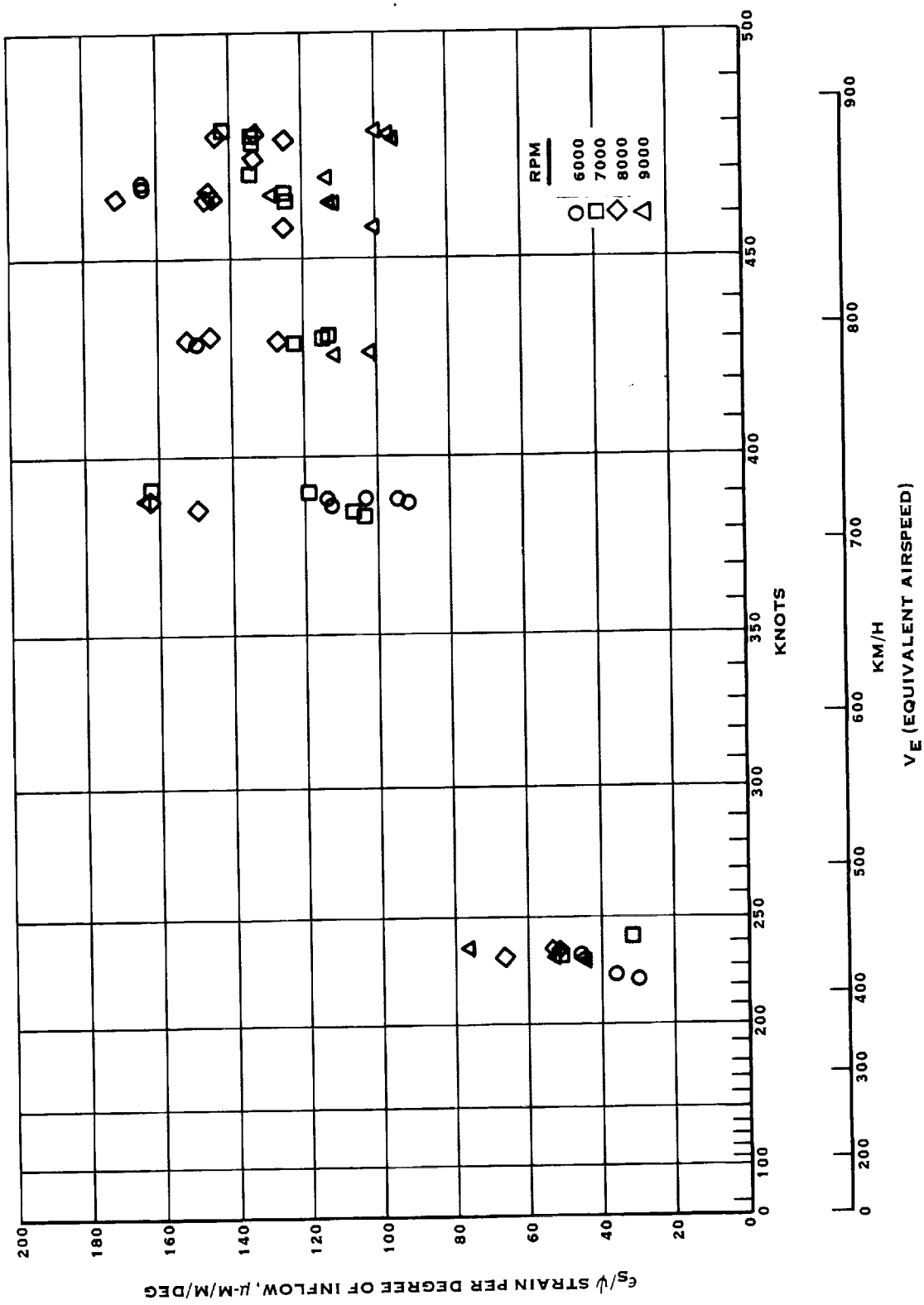

FIGURE 4-6. NASA-LEWIS SR-2C MODEL PROP-FAN TESTS

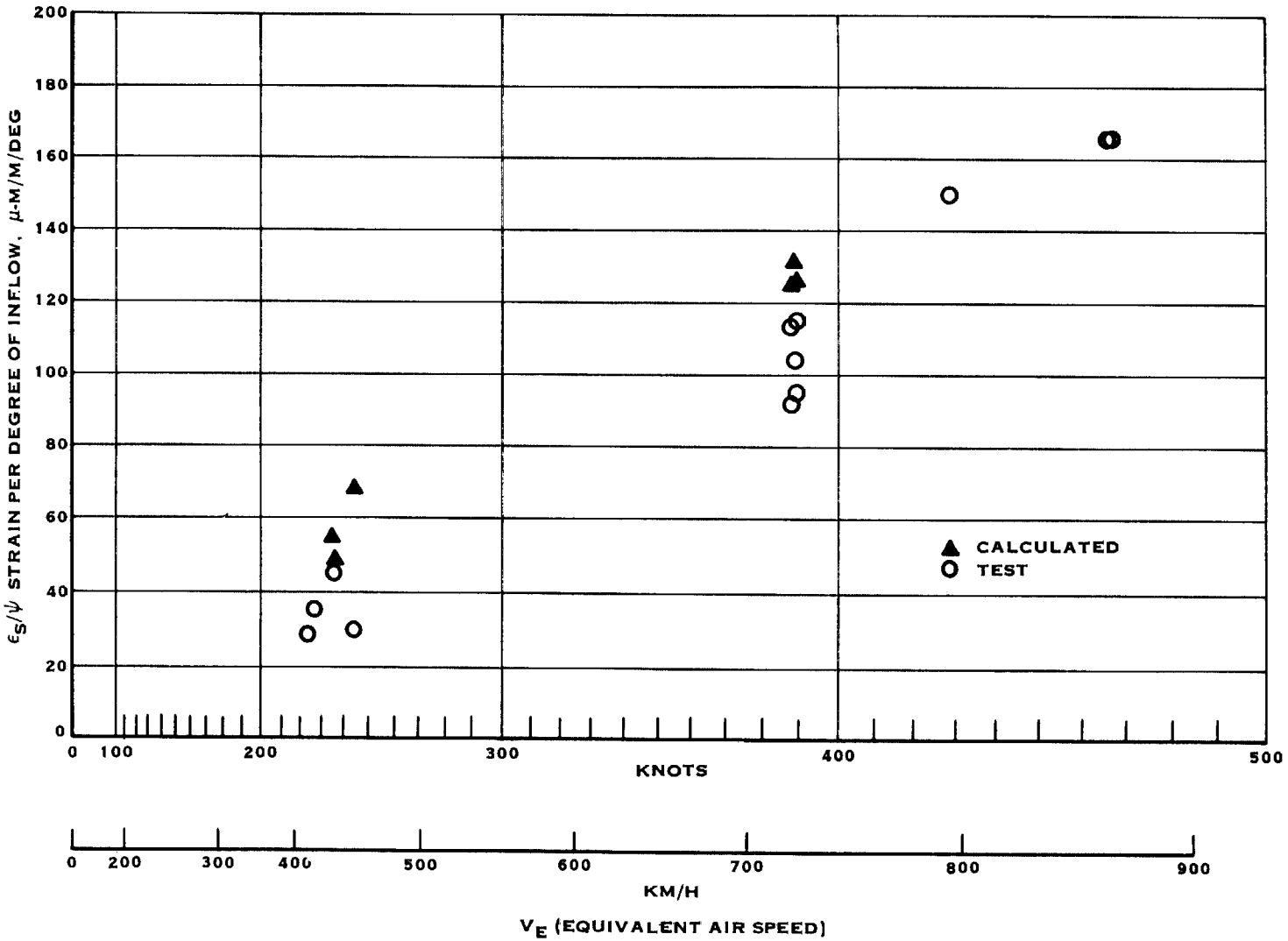

FIGURE 4-7. NASA-LEWIS SR-2C MODEL PROP-FAN TESTS, N = 6000 RPM

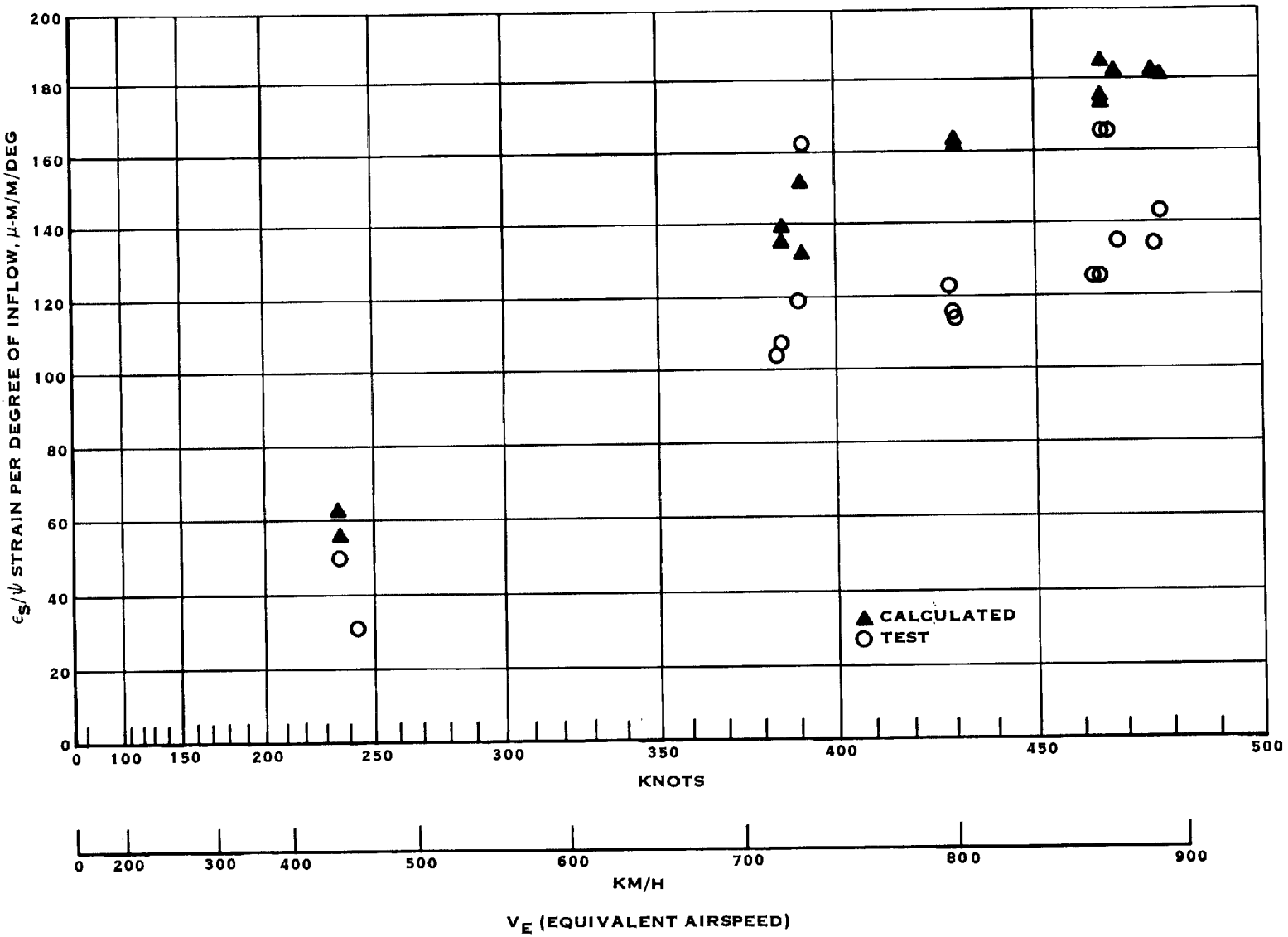

FIGURE 4-8. NASA-LEWIS SR-2C MODEL PROP-FAN TESTS, N = 7000 RPM

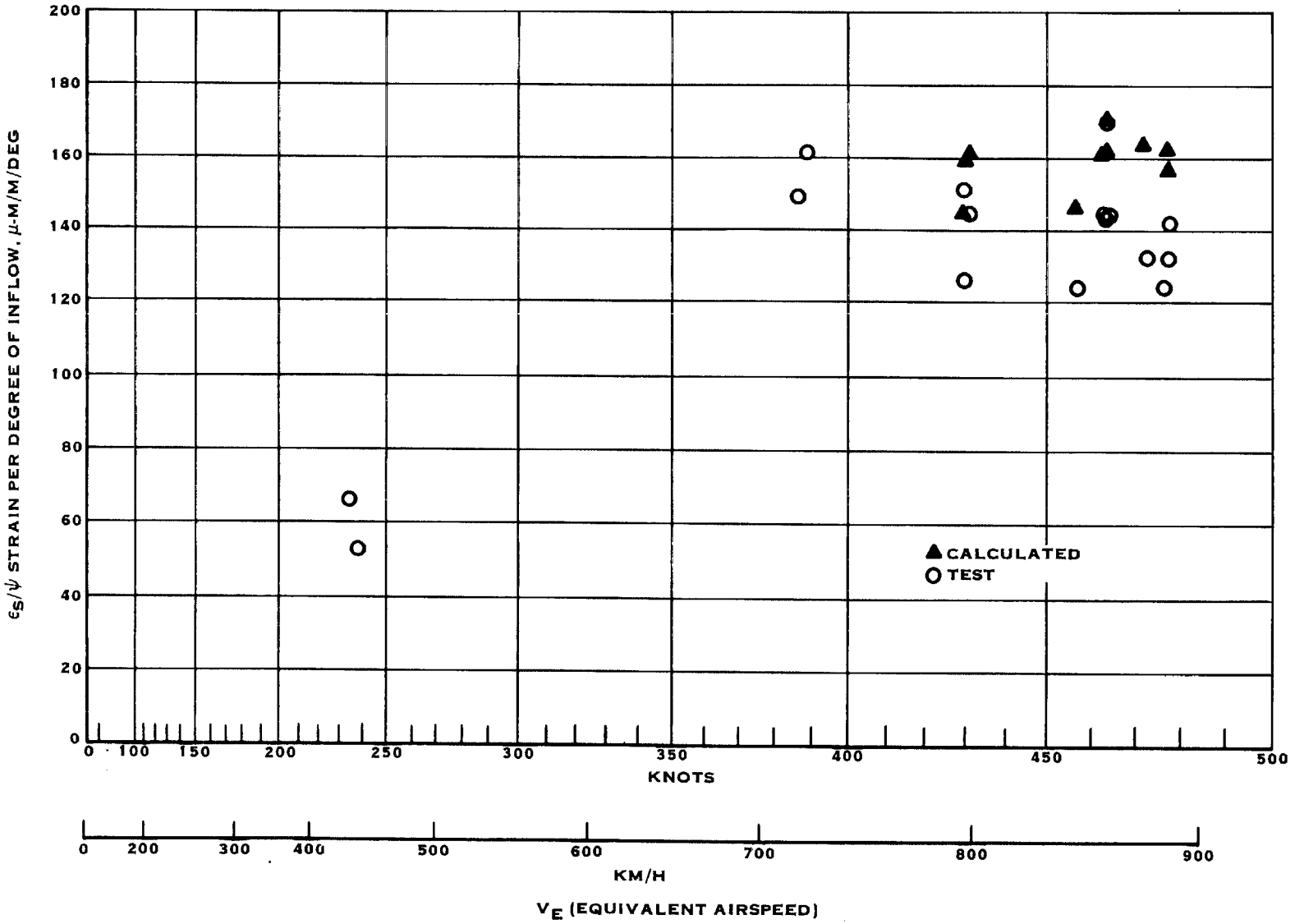

FIGURE 4-9. NASA-LEWIS SR-2C MODEL PROP-FAN TESTS, N = 8000 RPM

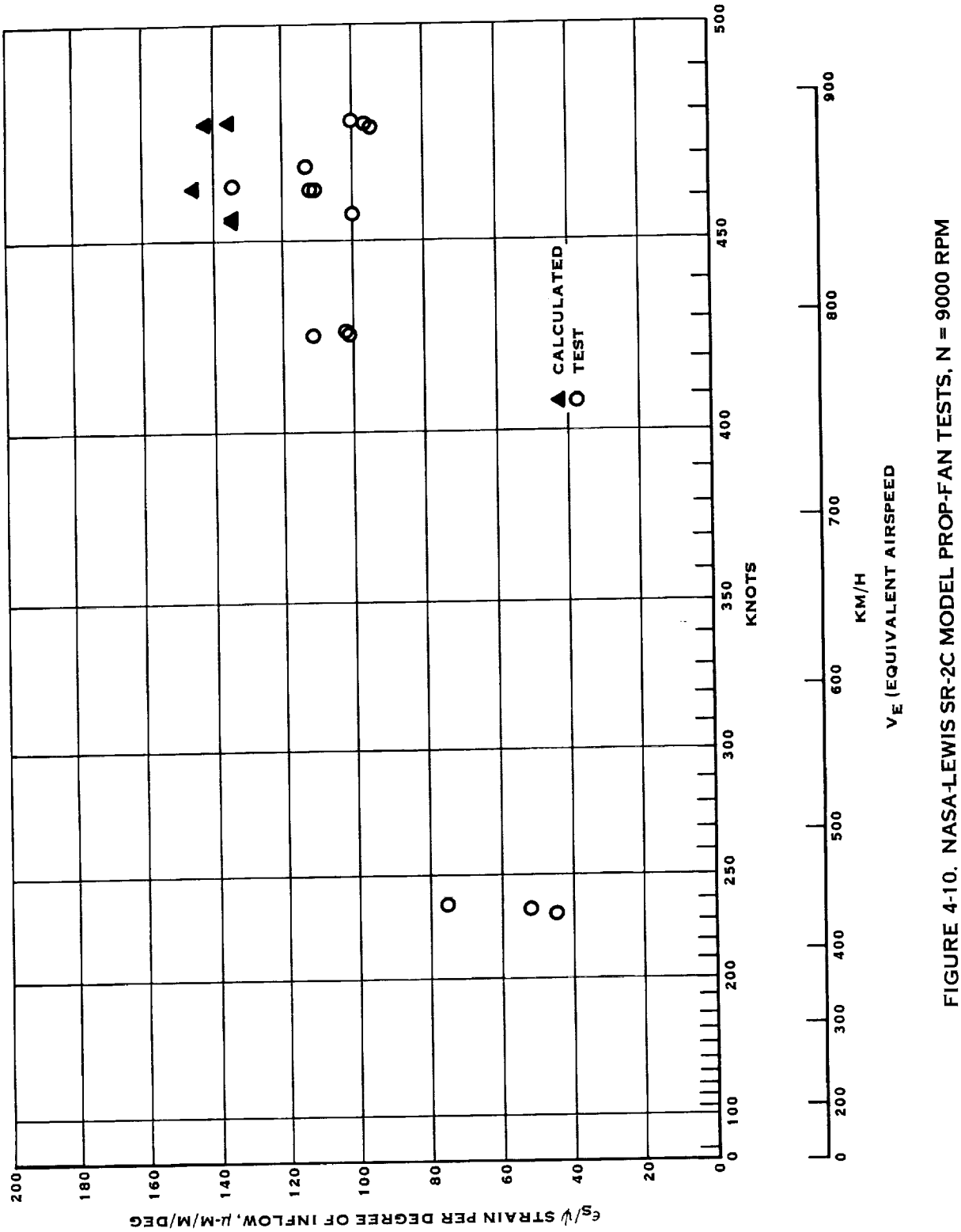

FIGURE 4-10. NASA-LEWIS SR-2C MODEL PROP-FAN TESTS, N = 9000 RPM

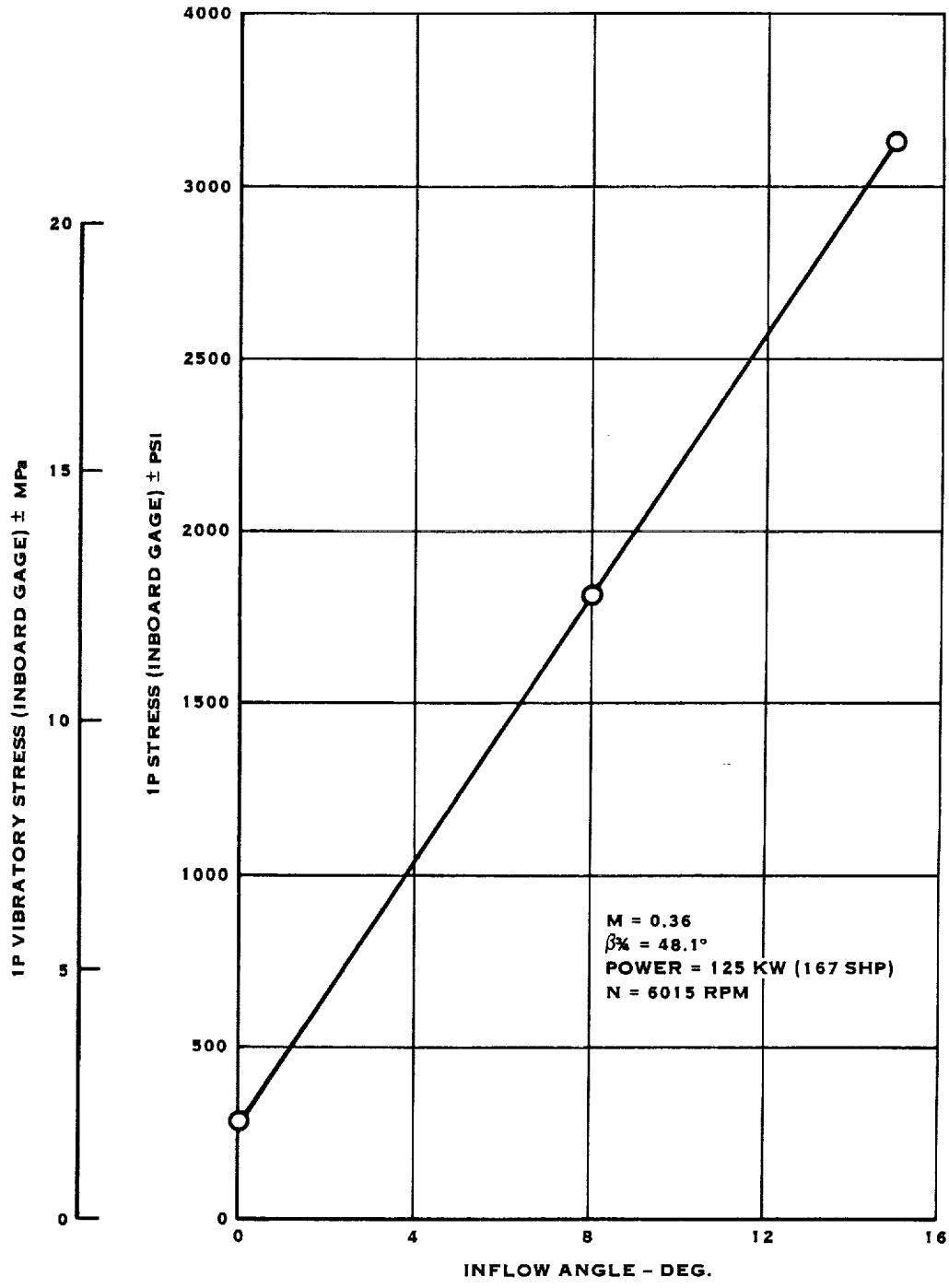

FIGURE 4-11. SR-3 PROP-FAN MODEL 1P STRESS VS. INFLOW ANGLE

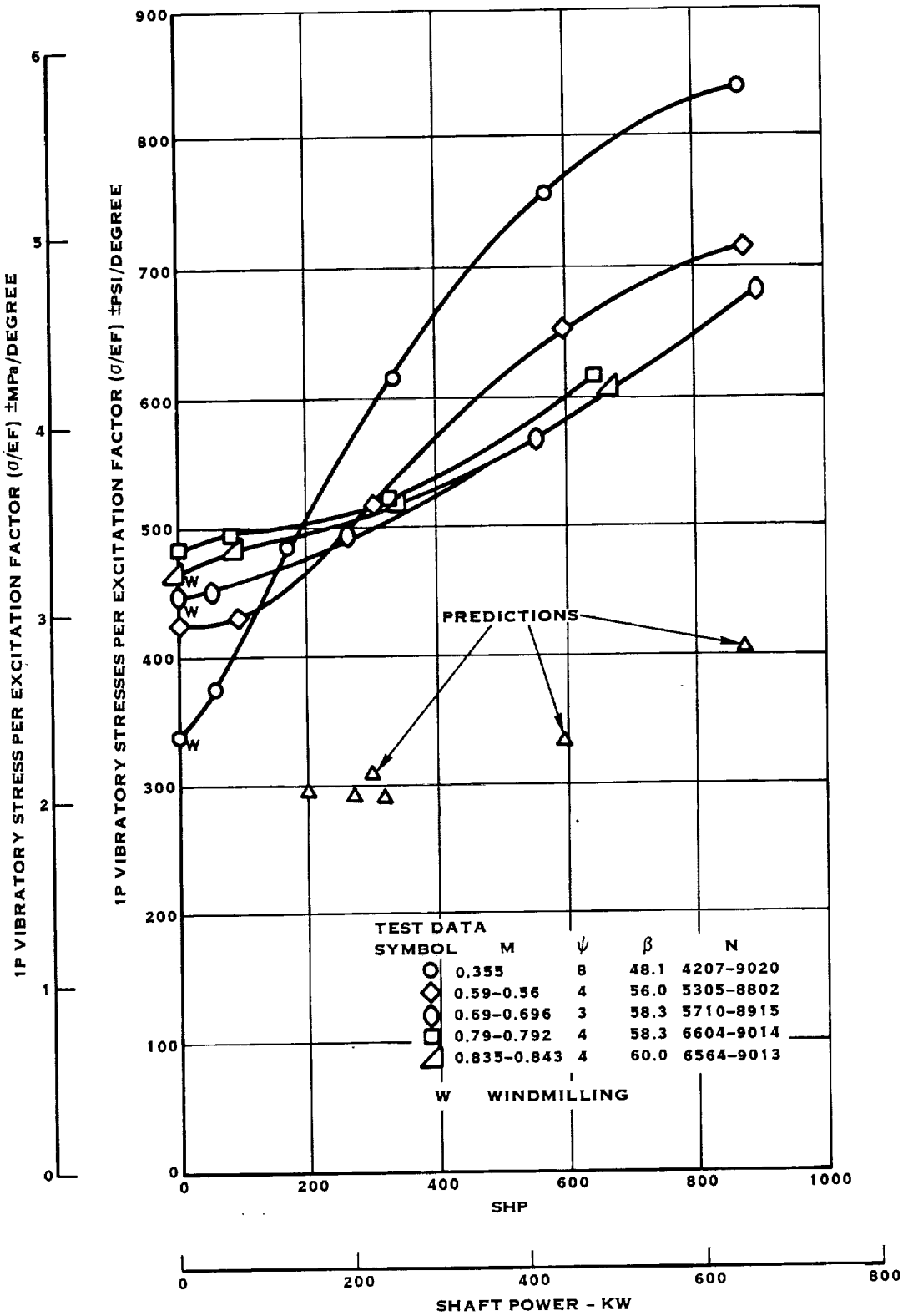

FIGURE 4-12. SR-3 (BG-1) 1P STRESS TEST DATA

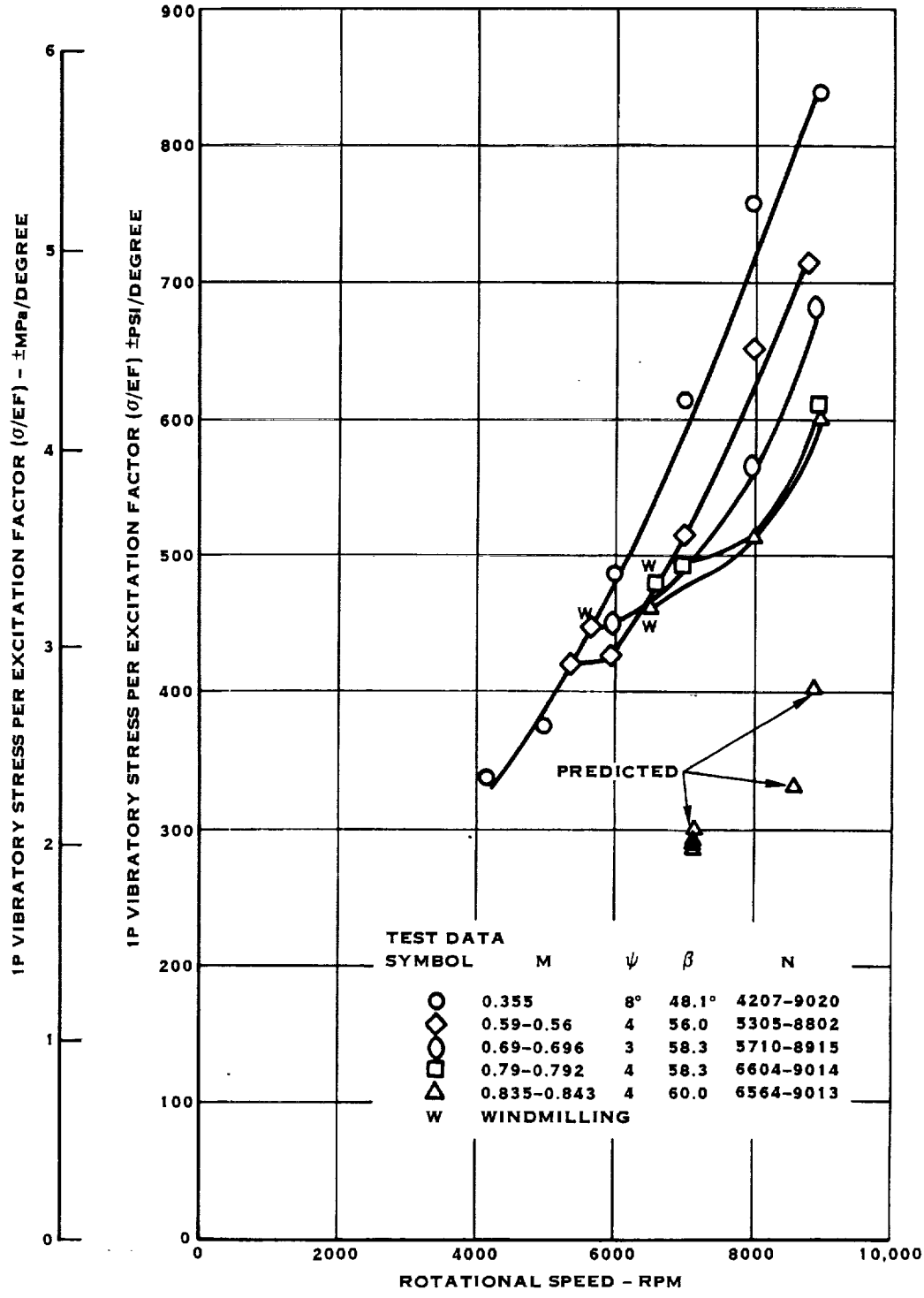

FIGURE 4-13. SR-3 (BG-1) 1P STRESS TEST DATA

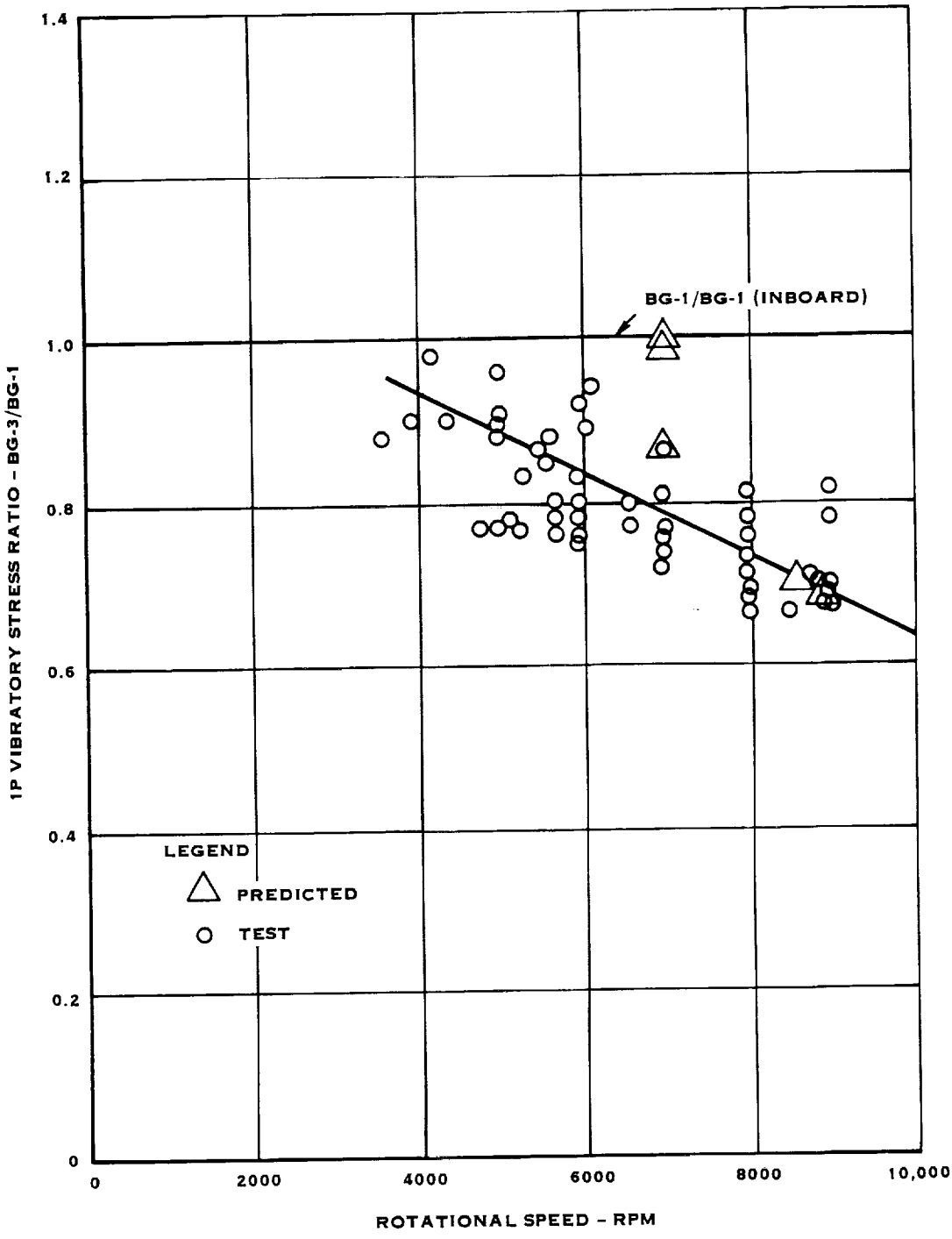

FIGURE 4-14. SR-3 1P STRESS TEST DATA INTERGAGE RELATIONSHIP (MID BLADE)

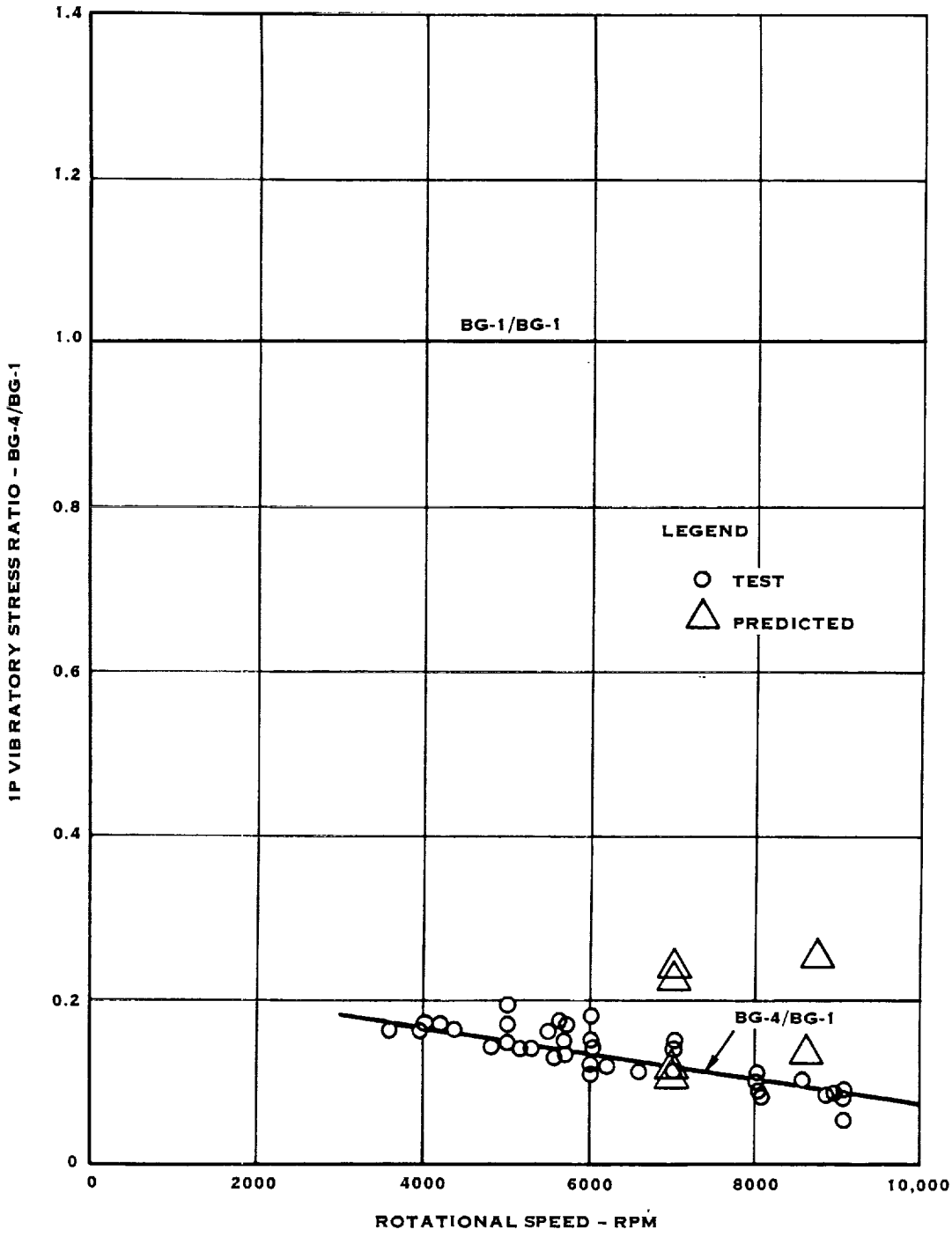

FIGURE 4-15. SR-3 1P STRESS TEST DATA INTERGAGE RELATIONSHIP (VEE GAGE)

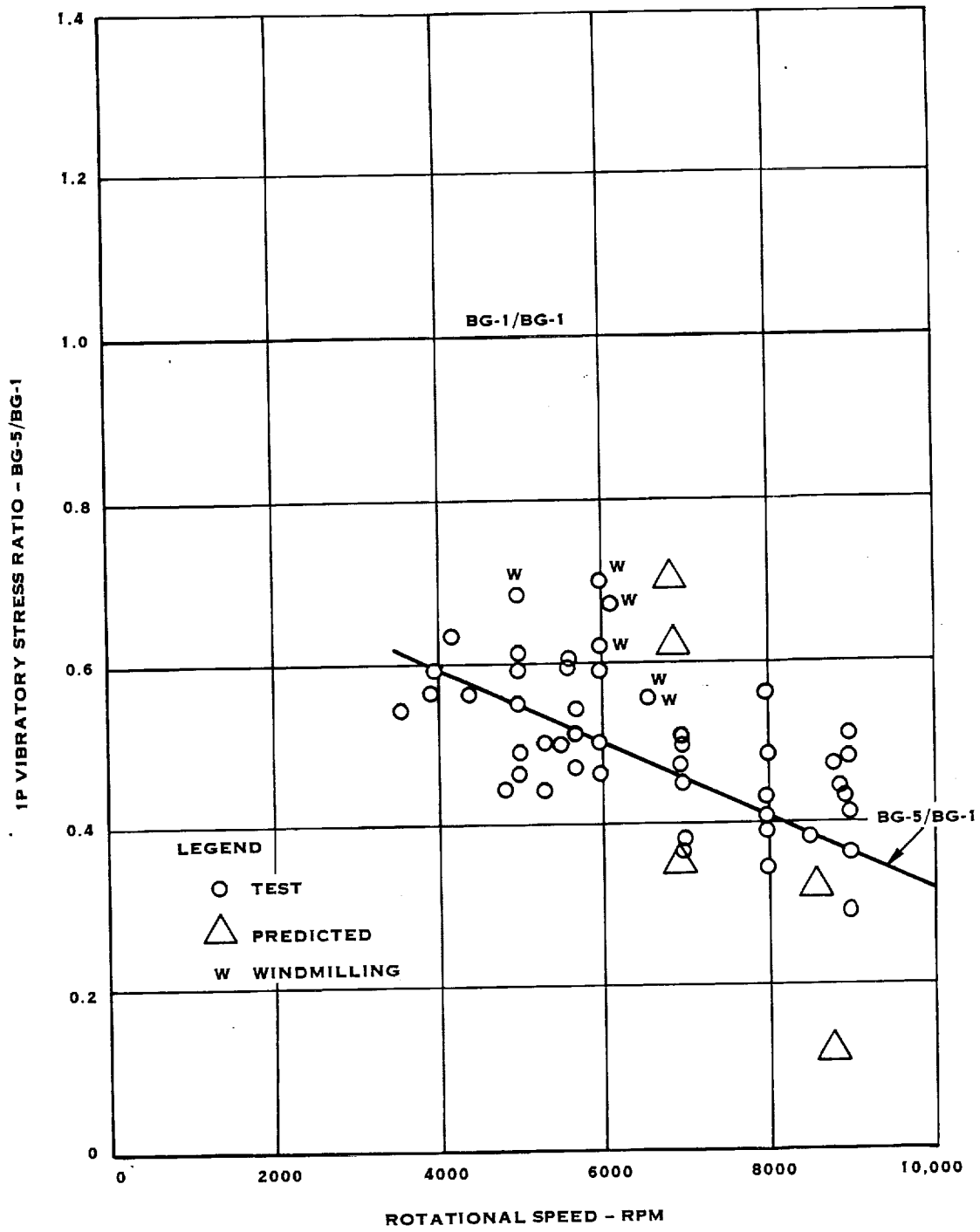

FIGURE 4-16. SR-3 1P STRESS TEST DATA INTERGAGE RELATIONSHIP (TIP GAGE)

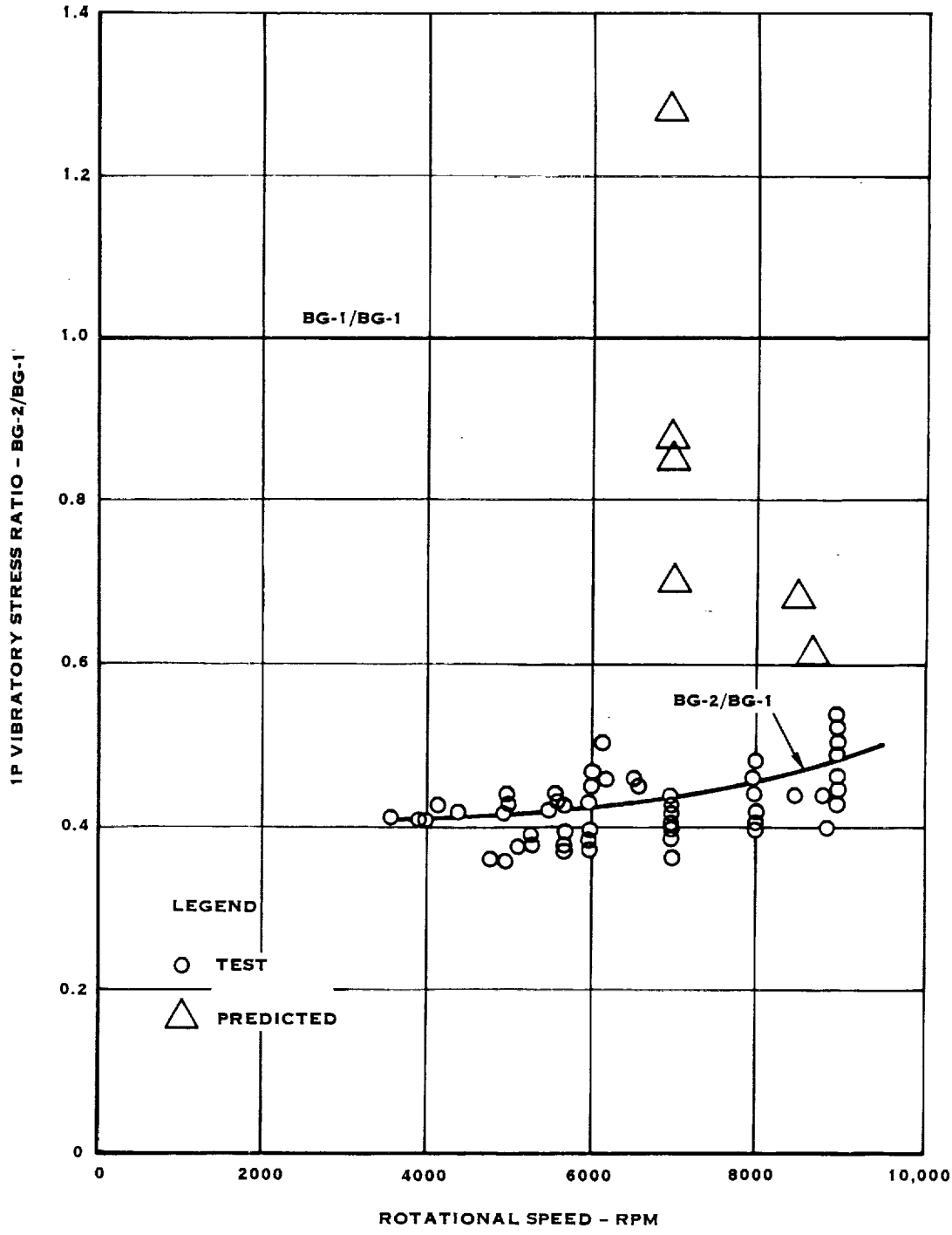

FIGURE 4-17. SR-3 1P STRESS TEST DATA INTERGAGE RELATIONSHIP (T.E.GAGE)

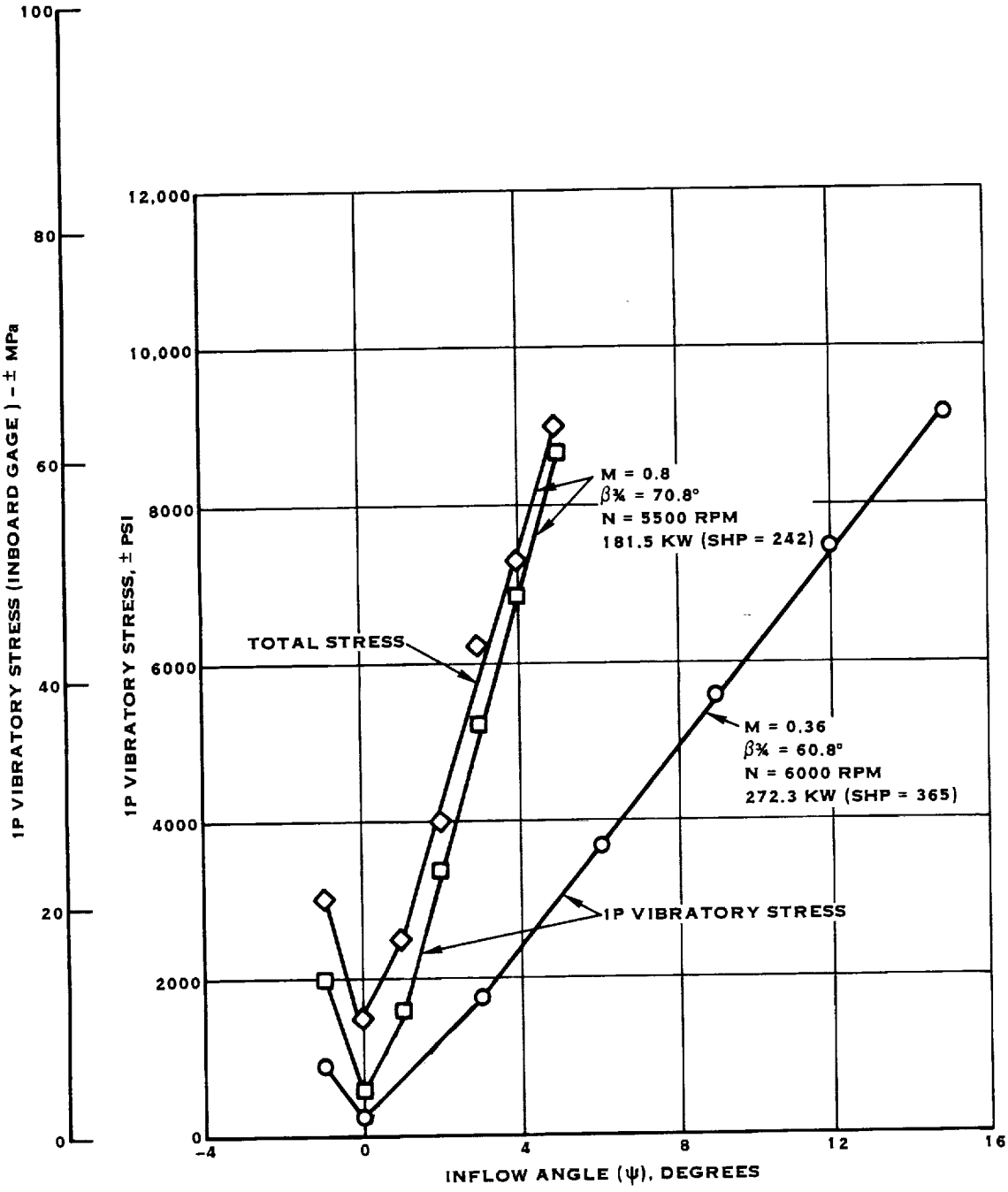

FIGURE 4-18. INBOARD GAGE 1P VIBRATORY STRESS VS. INFLOW ANGLE
SR-5 PROP-FAN TEST MODEL NASA-LEWIS

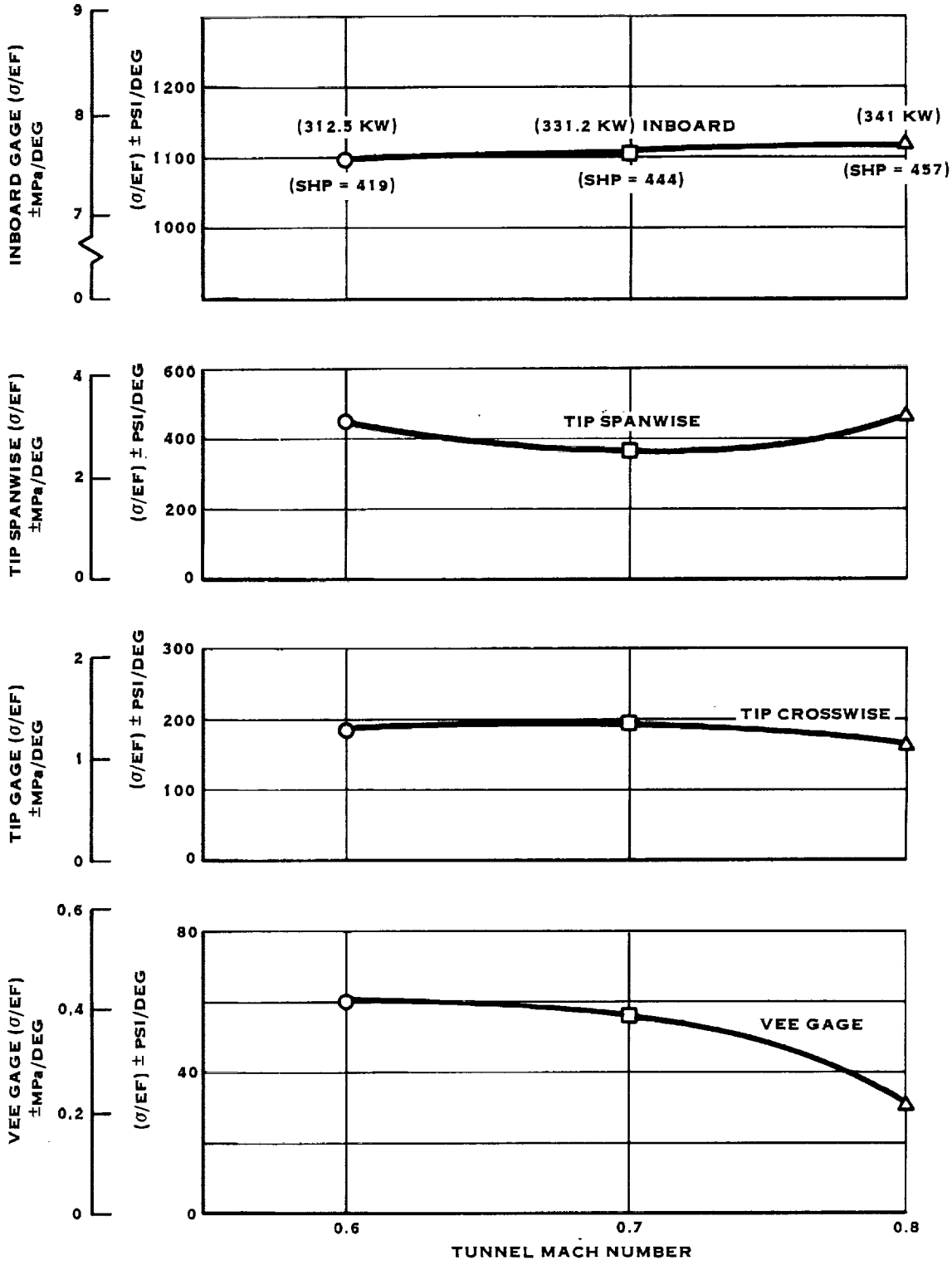

FIGURE 4-19. EFFECT OF TUNNEL MACH NUMBER ON σ/EF VALUES FOR BLADE 1 OF SR-5 PROP-FAN MODEL AT 6000 RPM AND SHAFT POWER AS MARKED

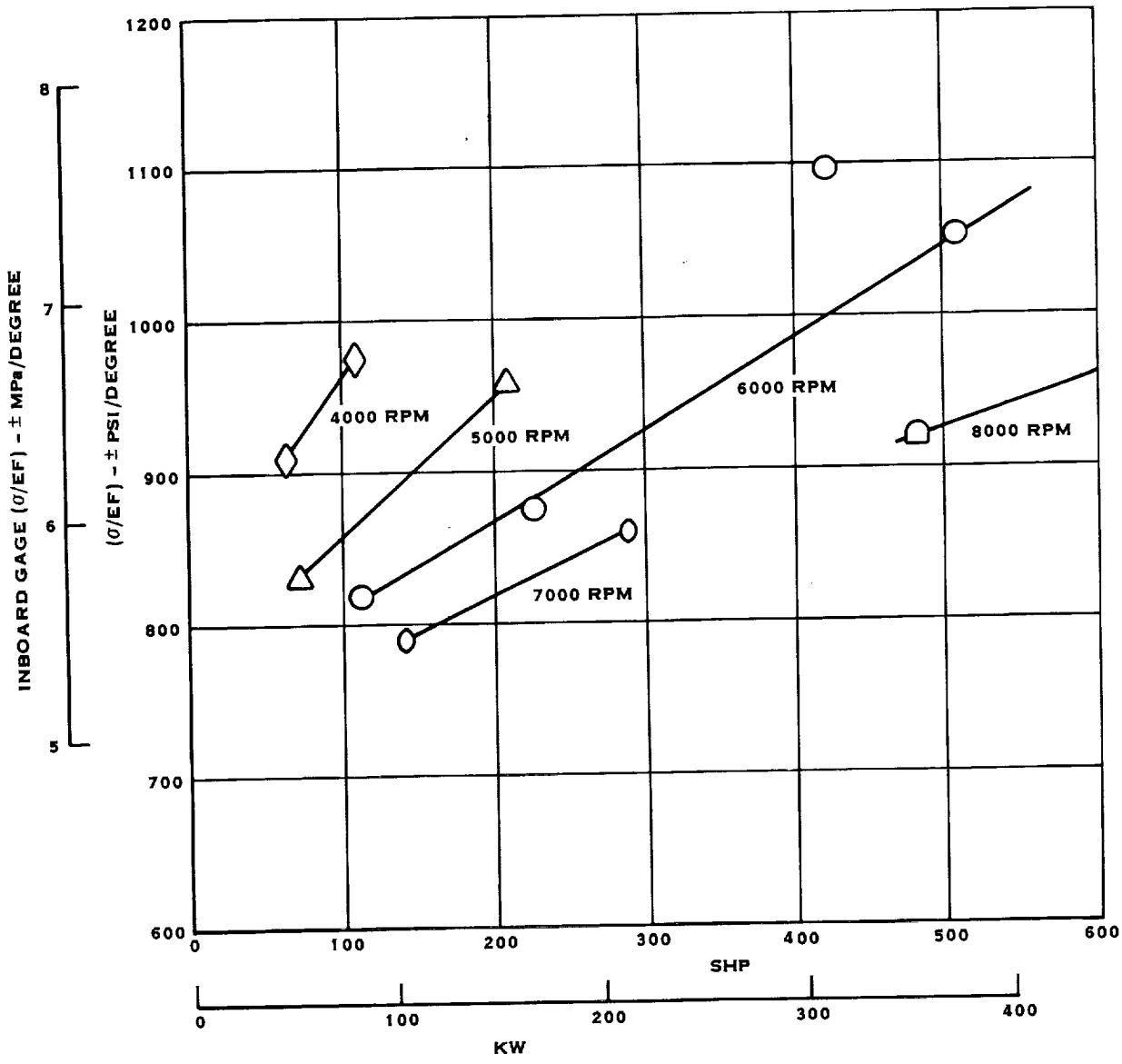

FIGURE 4-20. EFFECT OF SHAFT POWER ON σ/EF AT CONSTANT RPM
INBOARD GAGE DATA AT M = 0.6 FOR SR-5 PROP-FAN MODEL

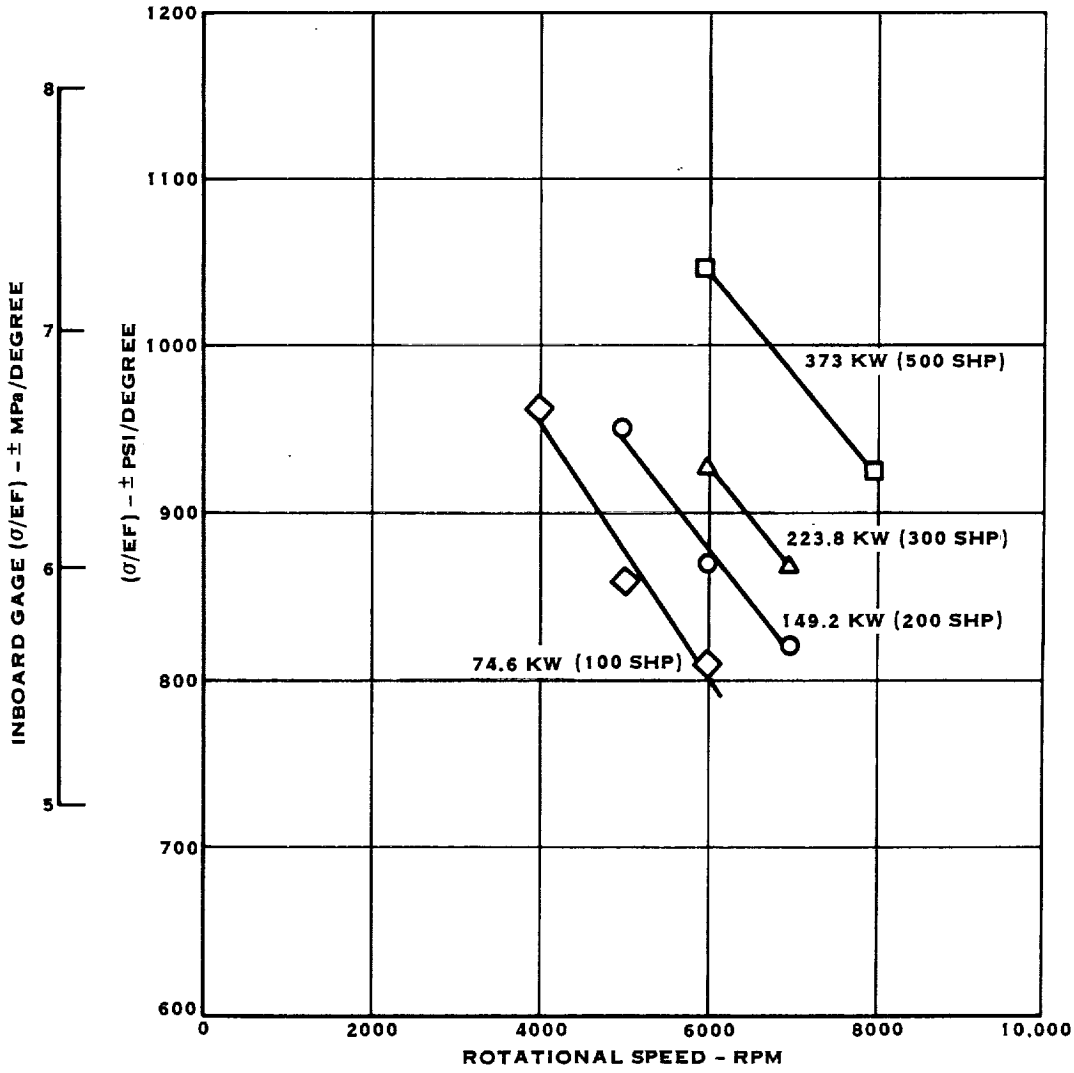

FIGURE 4-21. EFFECT OF RPM ON σ/EF AT CONSTANT SHP - INBOARD GAGE DATA AT M = 0.6 FOR SR-5 PROP-FAN MODEL

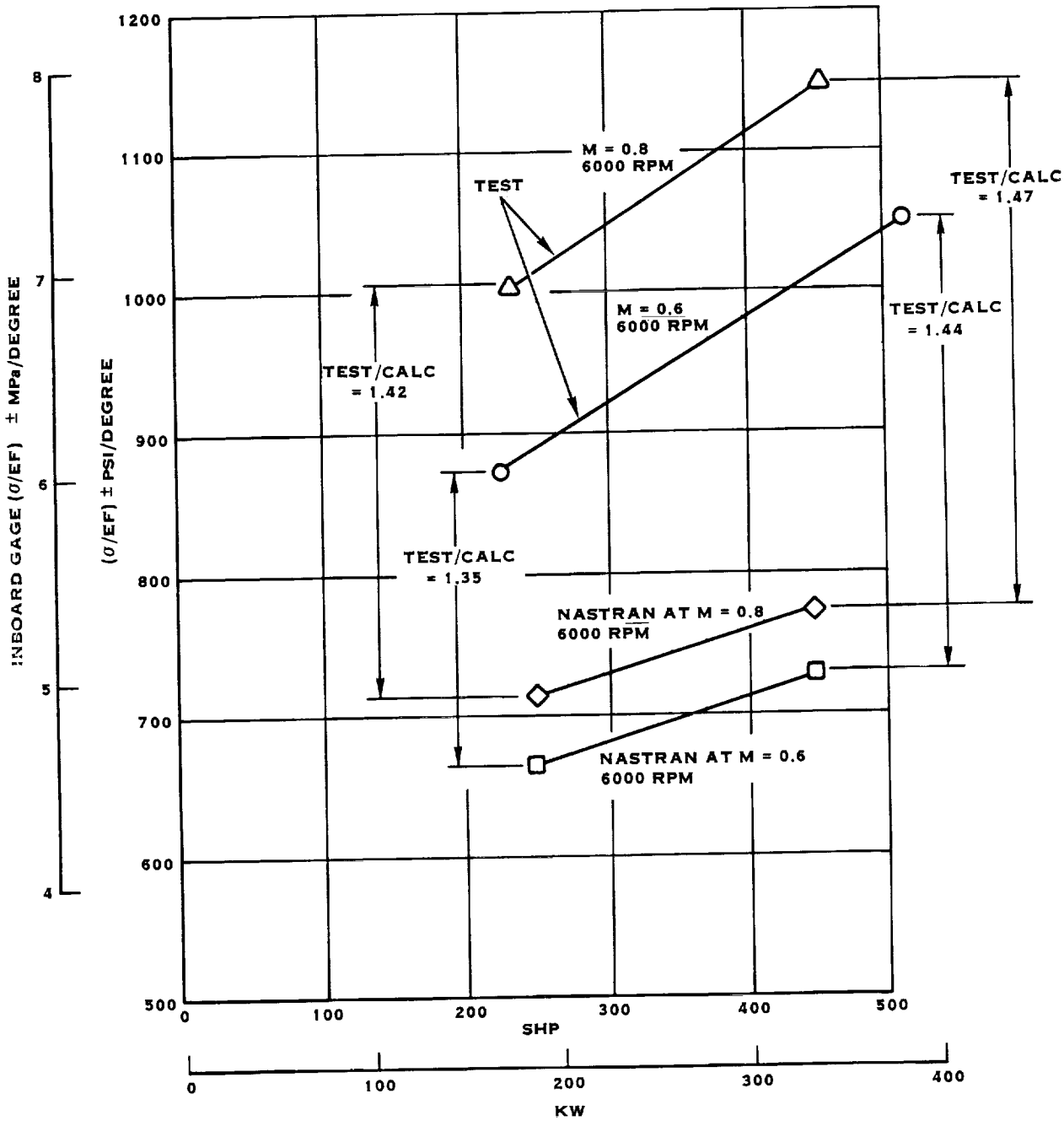

FIGURE 4-22. SR-5 IN-BOARD GAGE σ/EF TEST VS. MSC/NASTRAN

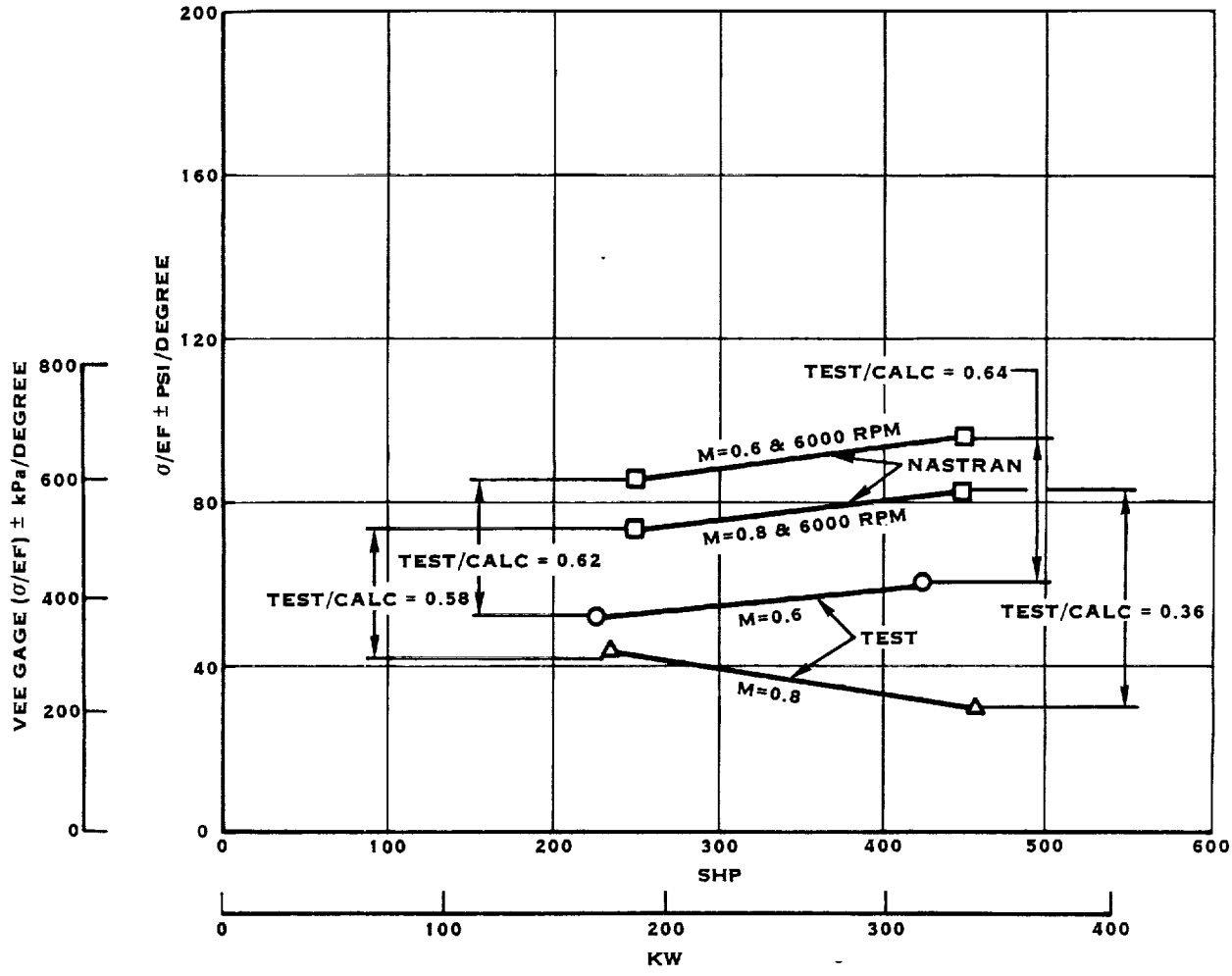

FIGURE 4-23. SR-5 VEE GAGE σ/EF TEST VS. MSC/NASTRAN

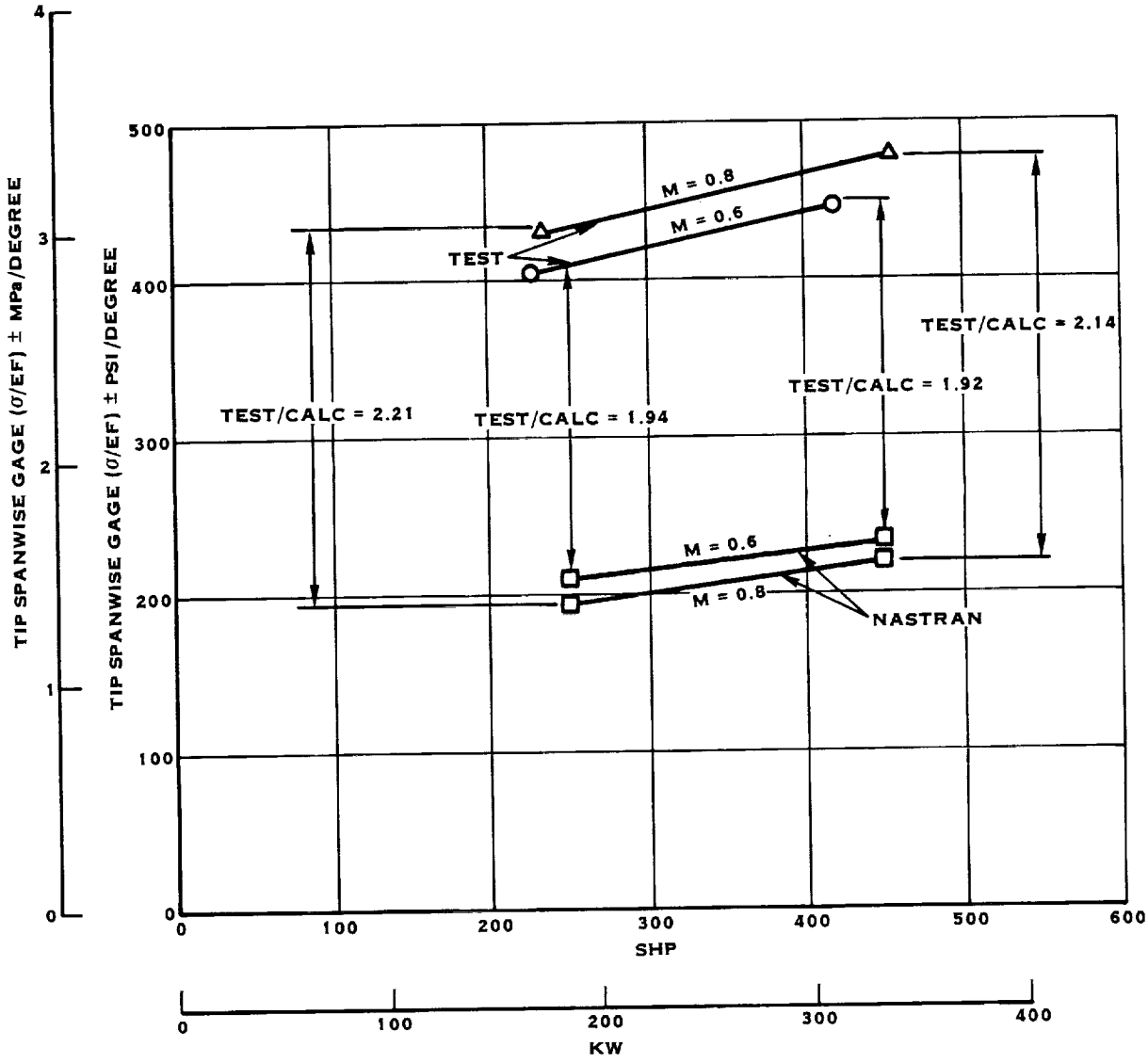

FIGURE 4-24. SR-5 TIP SPANWISE GAGE σ/EF TEST VS. MSC/NASTRAN
PROPELLER RPM = 6000

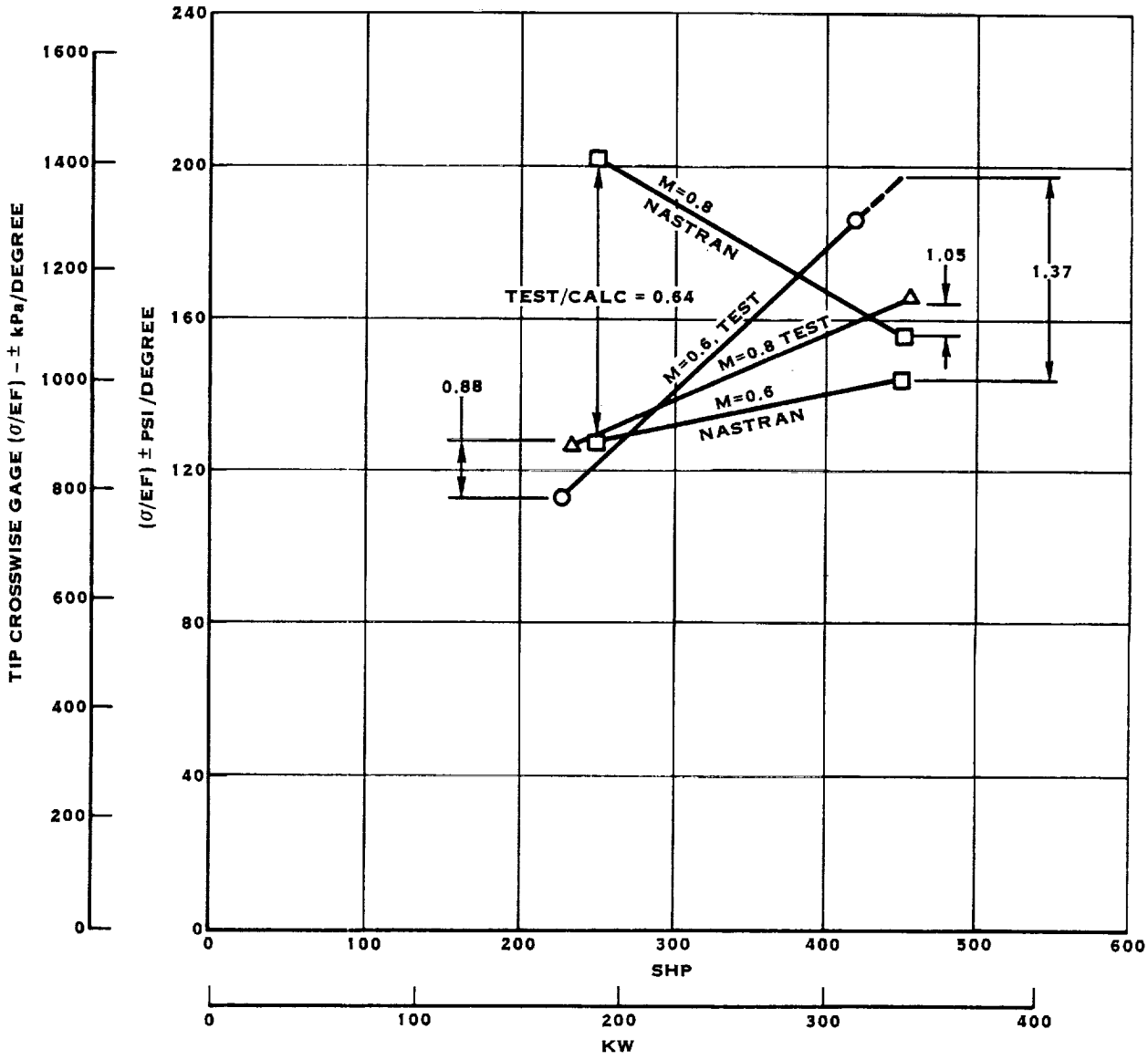

FIGURE 4-25. SR-5 TIP CROSSWISE GAGE σ/EF TEST VS. MSC/NASTRAN PROPELLER RPM = 6000

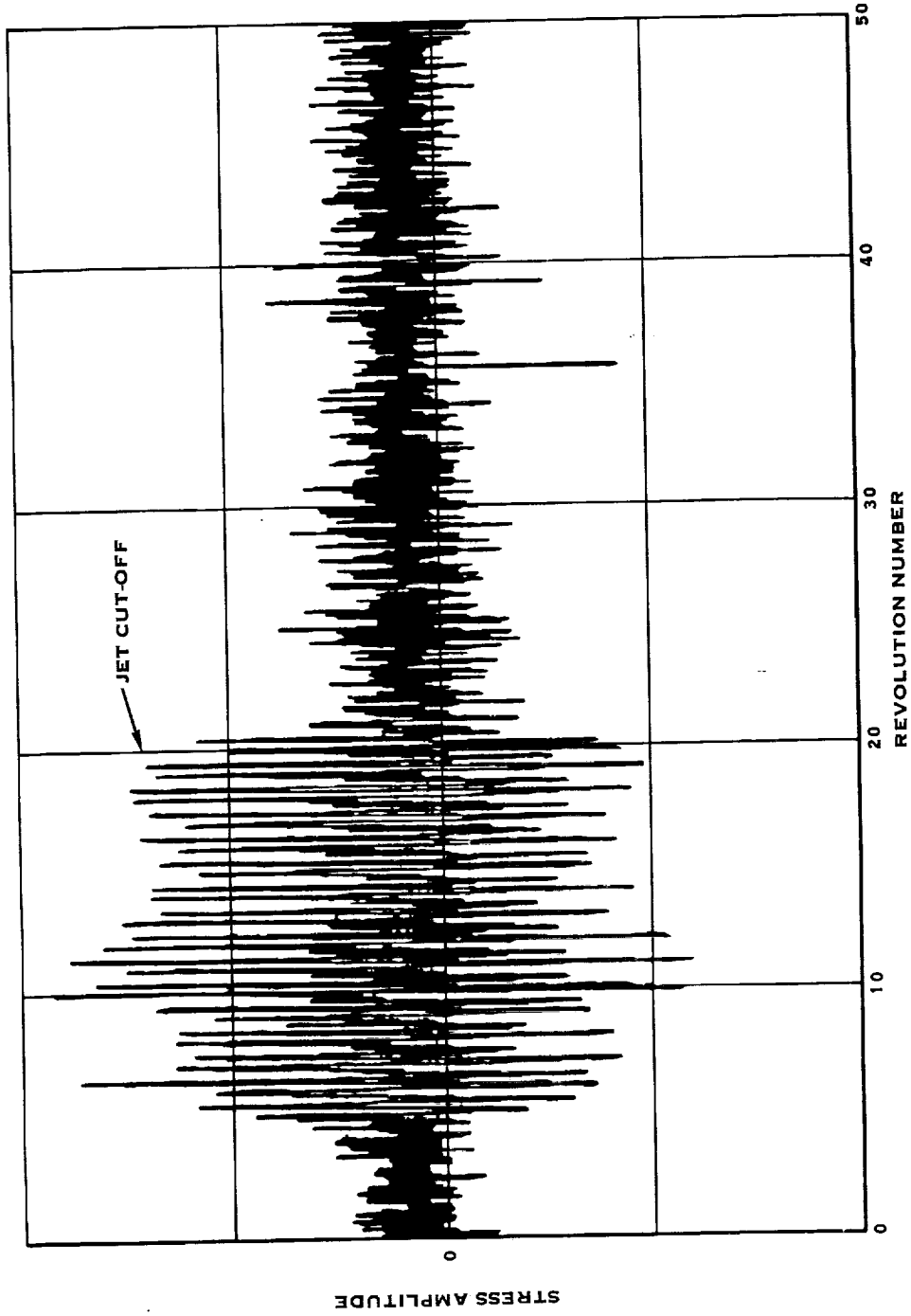

FIGURE 4-26. SR-5 PROP-FAN JET PULSE TEST DATA SHOWING THE JET CUT-OFF POINT

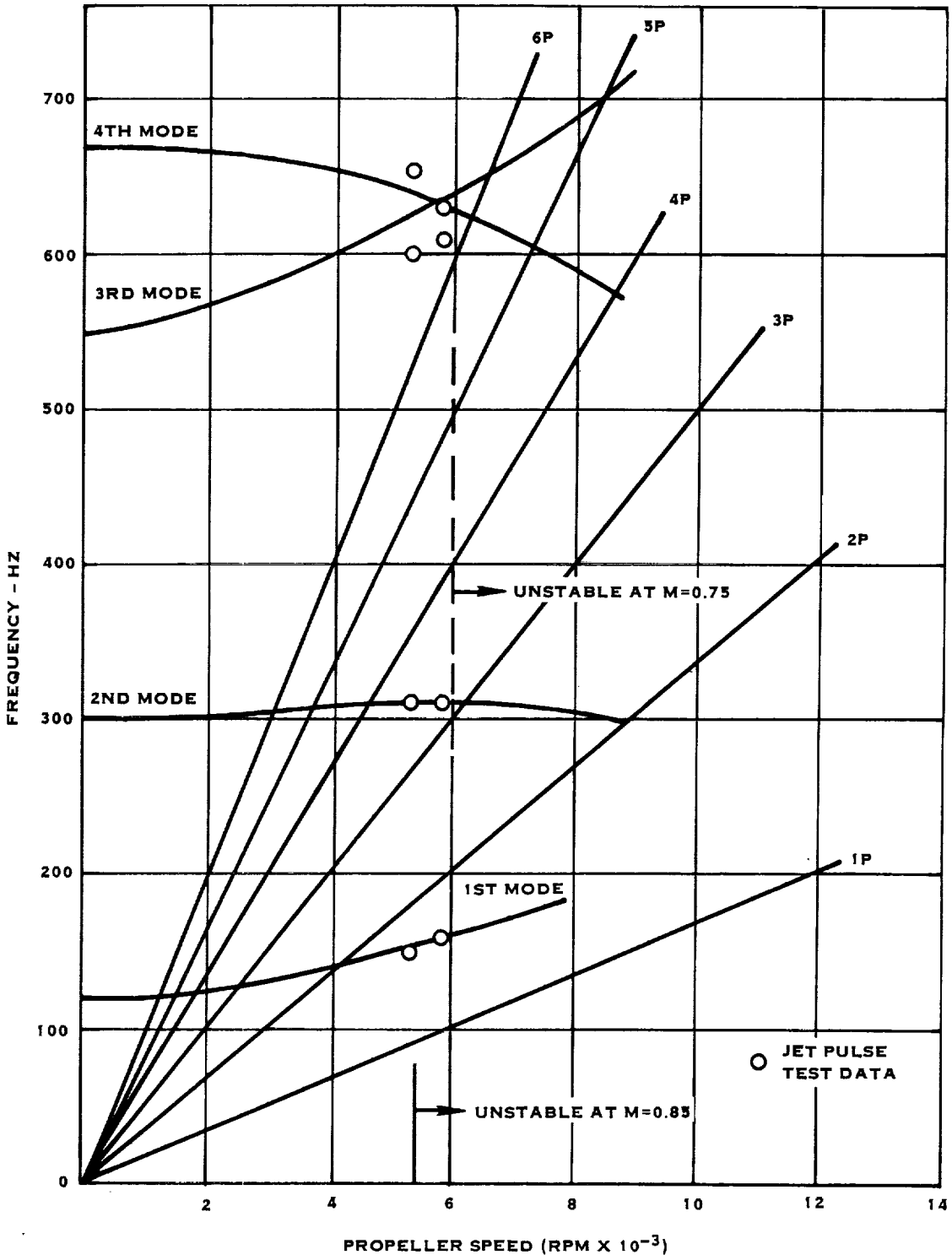

FIGURE 4-27. COMPARISON OF PREDICTED AND MEASURED CRITICAL SPEEDS OF THE SR-5 MODEL PROP-FAN

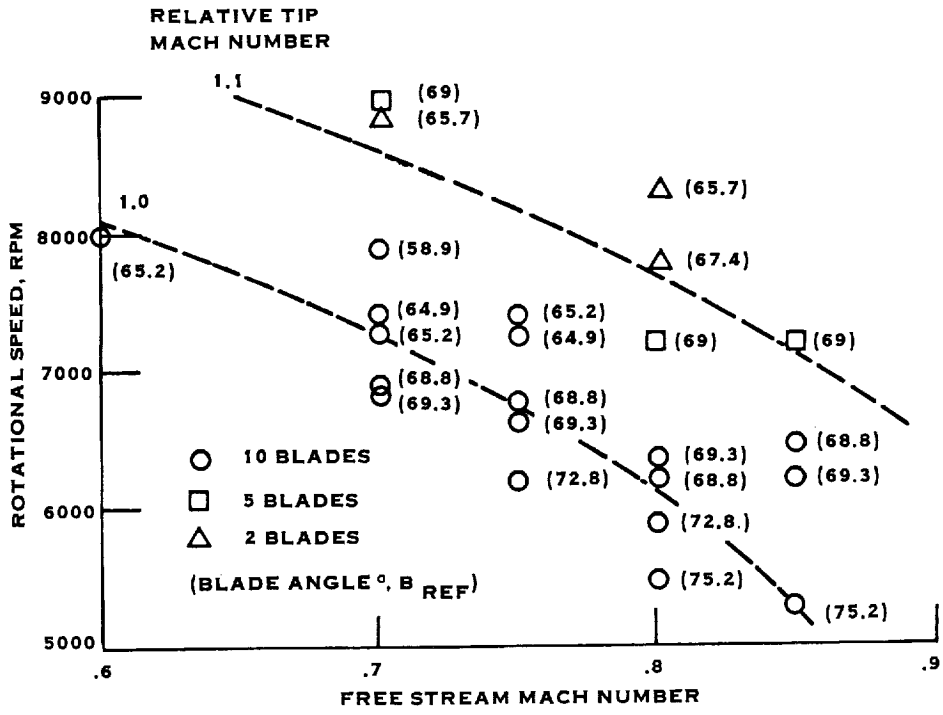

FIGURE 4-28. FLUTTER POINTS AS A FUNCTION OF ROTATIONAL SPEED, FREE STREAM MACH NUMBER AND BLADE ANGLE, (FROM MEHMED, ET. AL., REFERENCE 15)

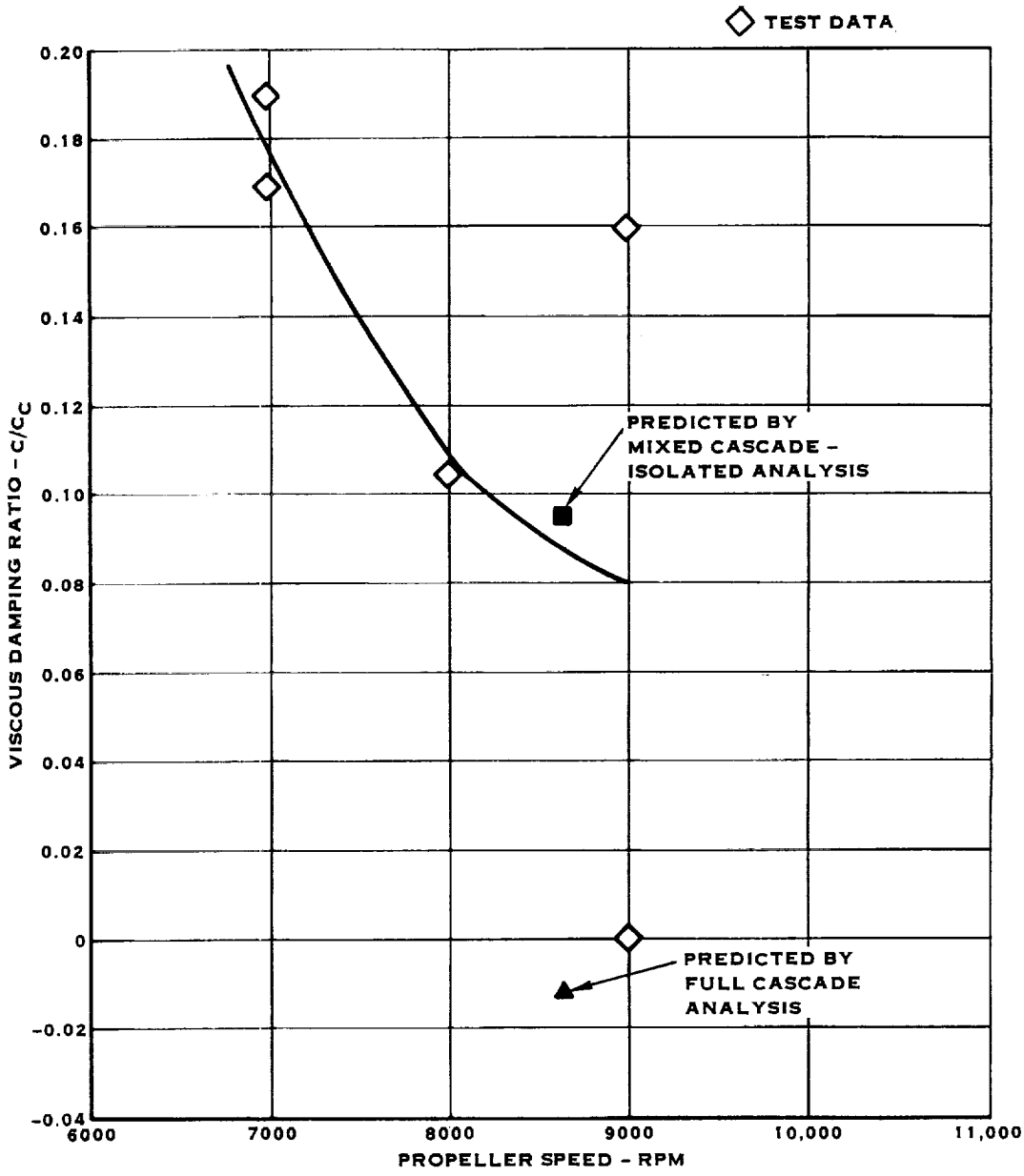

FIGURE 4-29. COMPARISON OF TEST AND PREDICTED STABILITY MARGINS FOR THE FIRST MODE OF THE SR-3 8-WAY MODEL PROP-FAN AT M = 0.8, $\beta_{3/4}$ = 60.1°

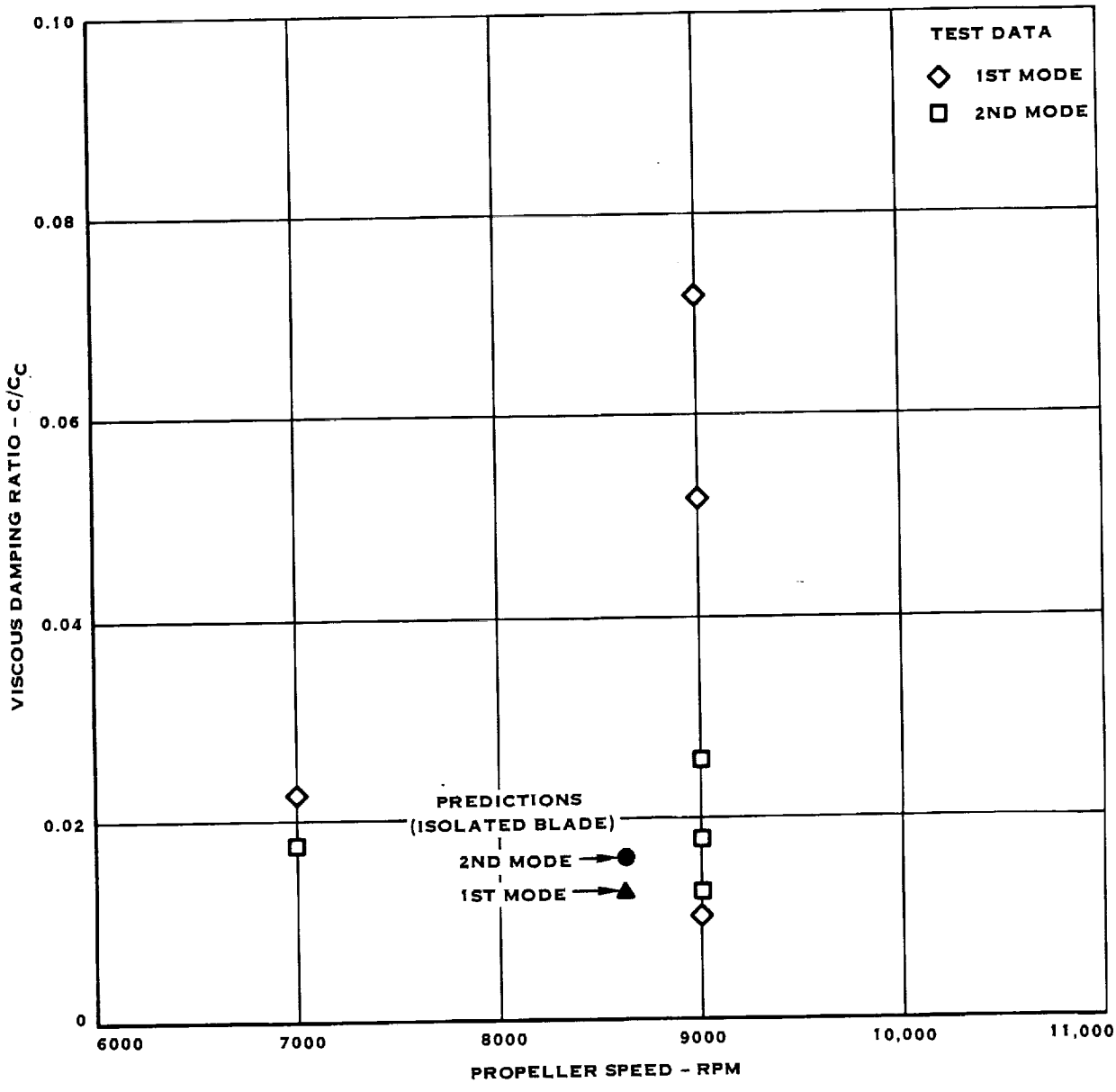

FIGURE 4-30. COMPARISON OF TEST & PREDICTED STABILITY MARGINS FOR THE FIRST AND SECOND MODES OF THE SR-3 4-WAY MODEL PROP-FAN AT M = 0.8, $\beta_{3/4}$ = 59°

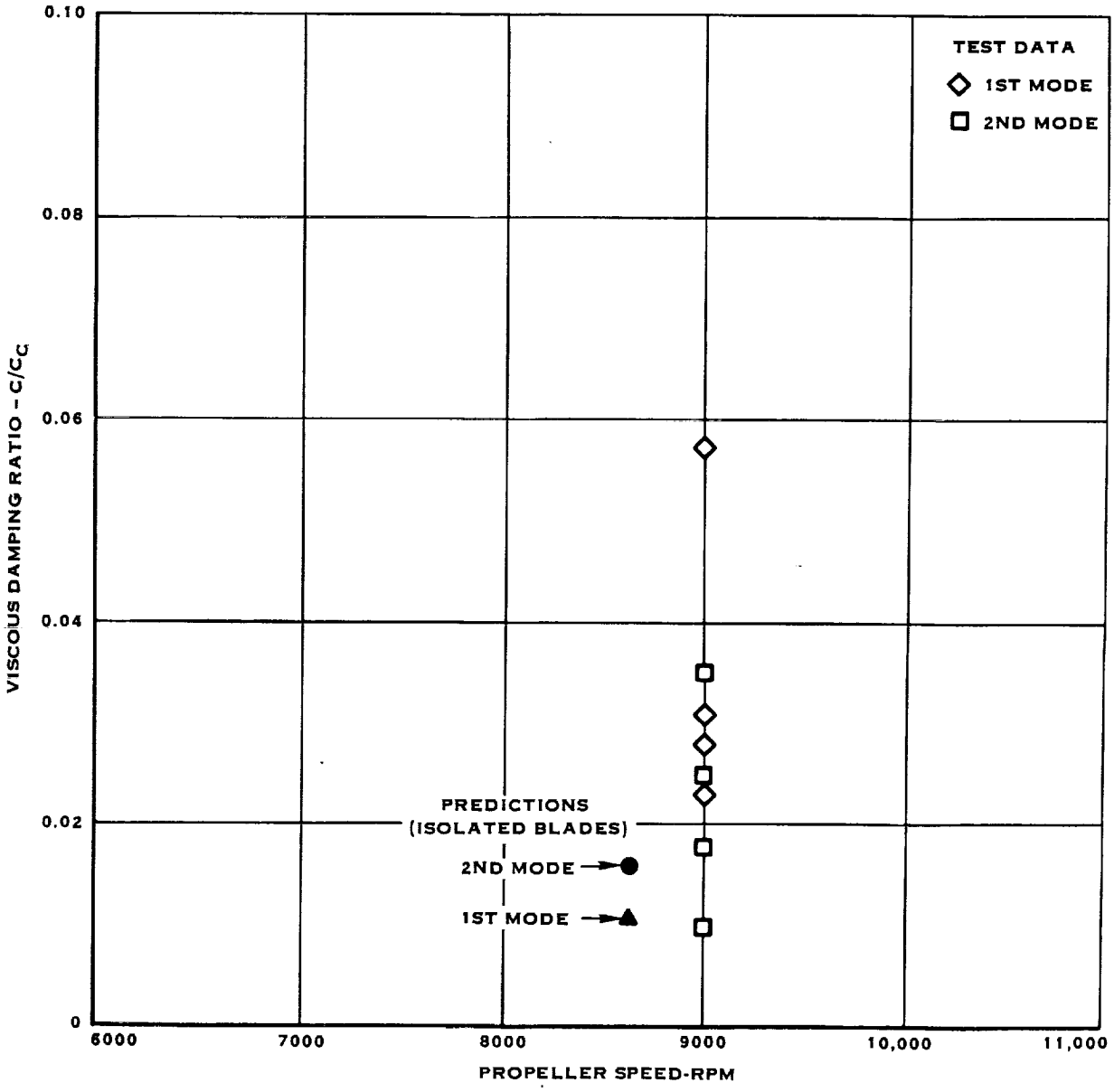

FIGURE 4-31. COMPARISON OF TEST & PREDICTED STABILITY MARGINS FOR THE FIRST AND SECOND MODES OF THE SR-3 4-WAY MODEL PROP-FAN AT M = 0.85, $\beta_{3/4}$ = 60°

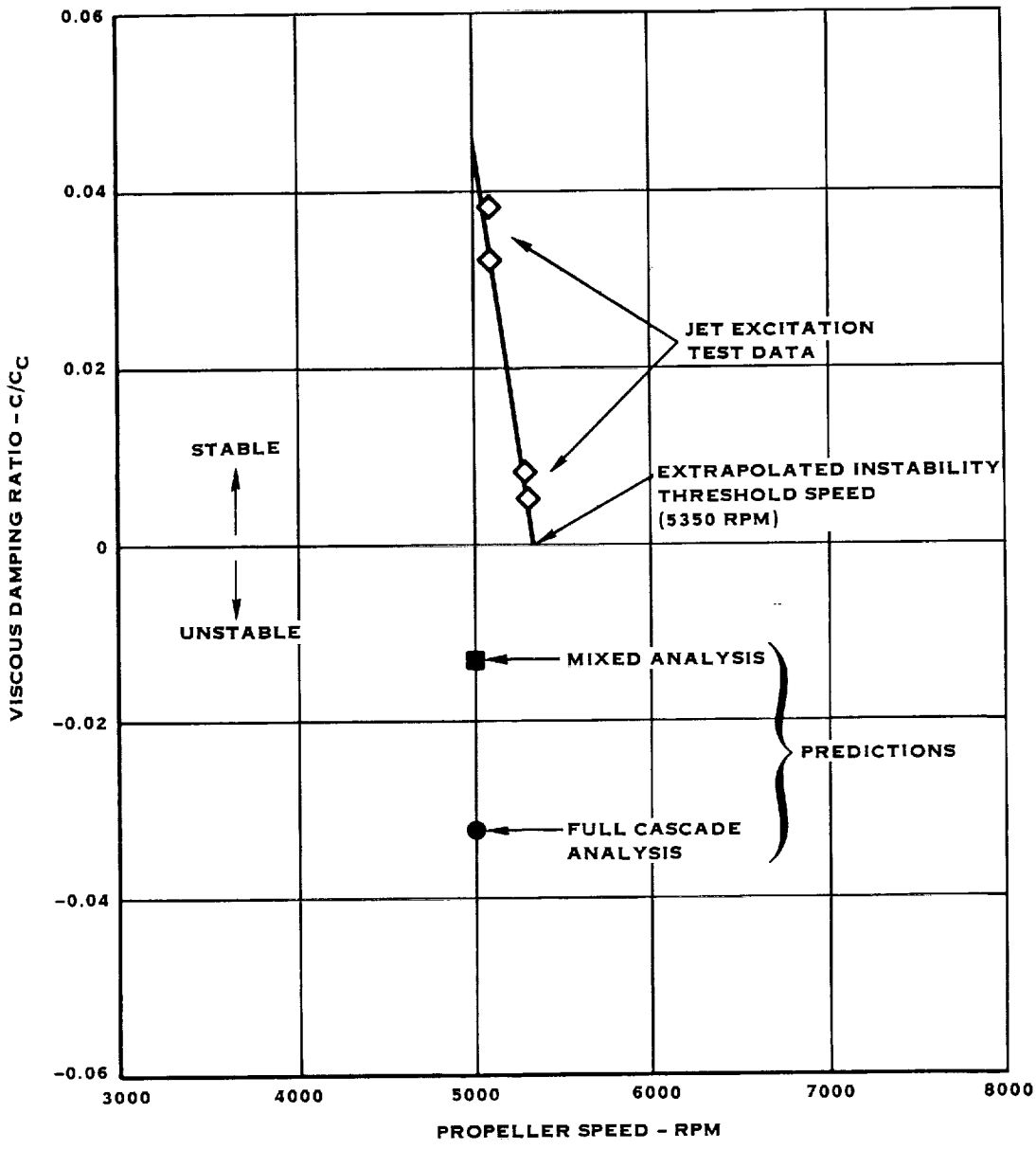

FIGURE 4-32. COMPARISON OF TEST & PREDICTED STABILITY MARGINS FOR THE FIRST MODE OF THE SR-5 MODEL PROP-FAN AT M = 0.85, $\beta_{3/4}$ = 73°

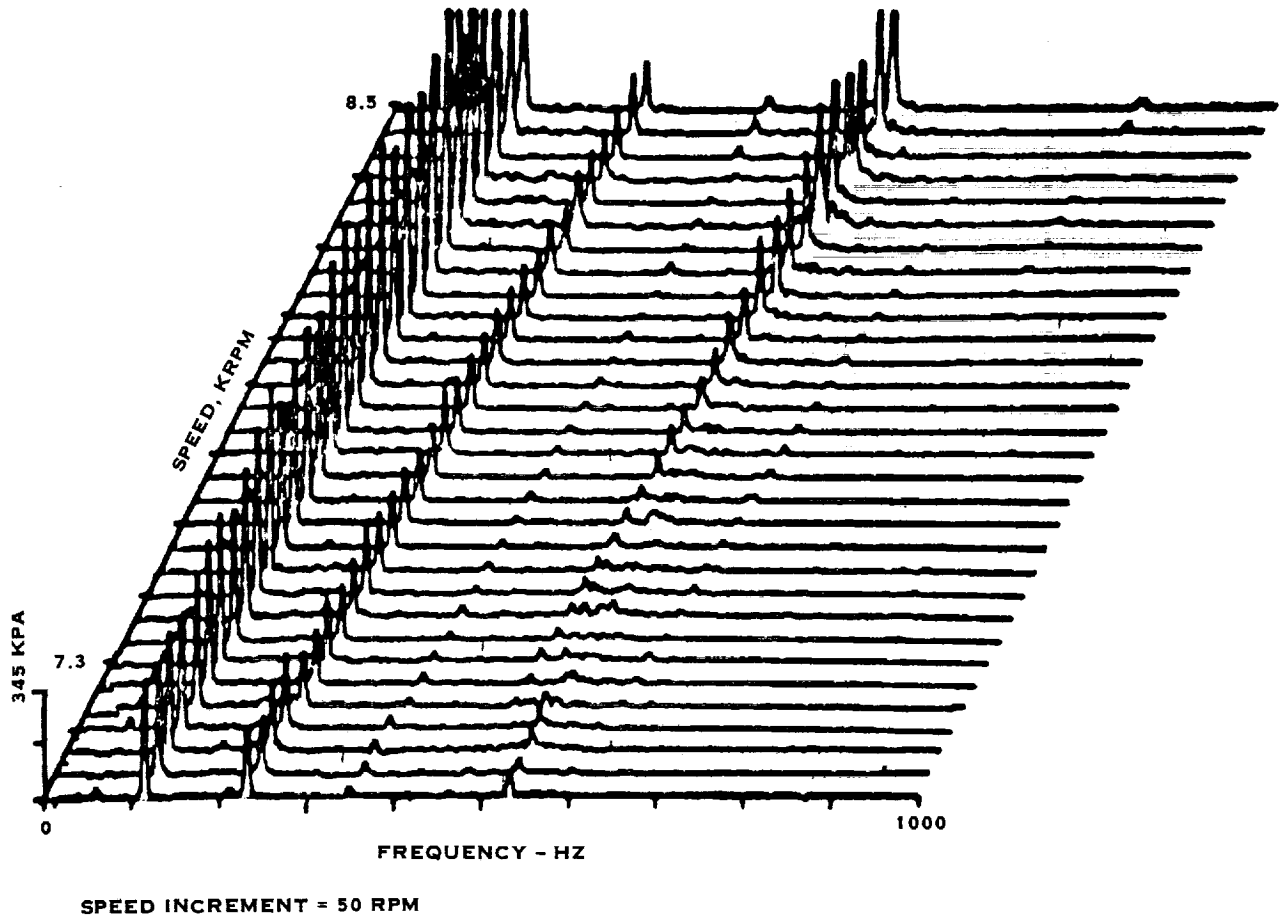

FIGURE 4-33. CARPET PLOT OF VIBRATORY STRESS VS. FREQUENCY AND ROTATIONAL SPEED, RPM SWEEP, TIP BENDING STRESS, BLADE NO. 8 (SR-2C PROP-FAN MODEL)

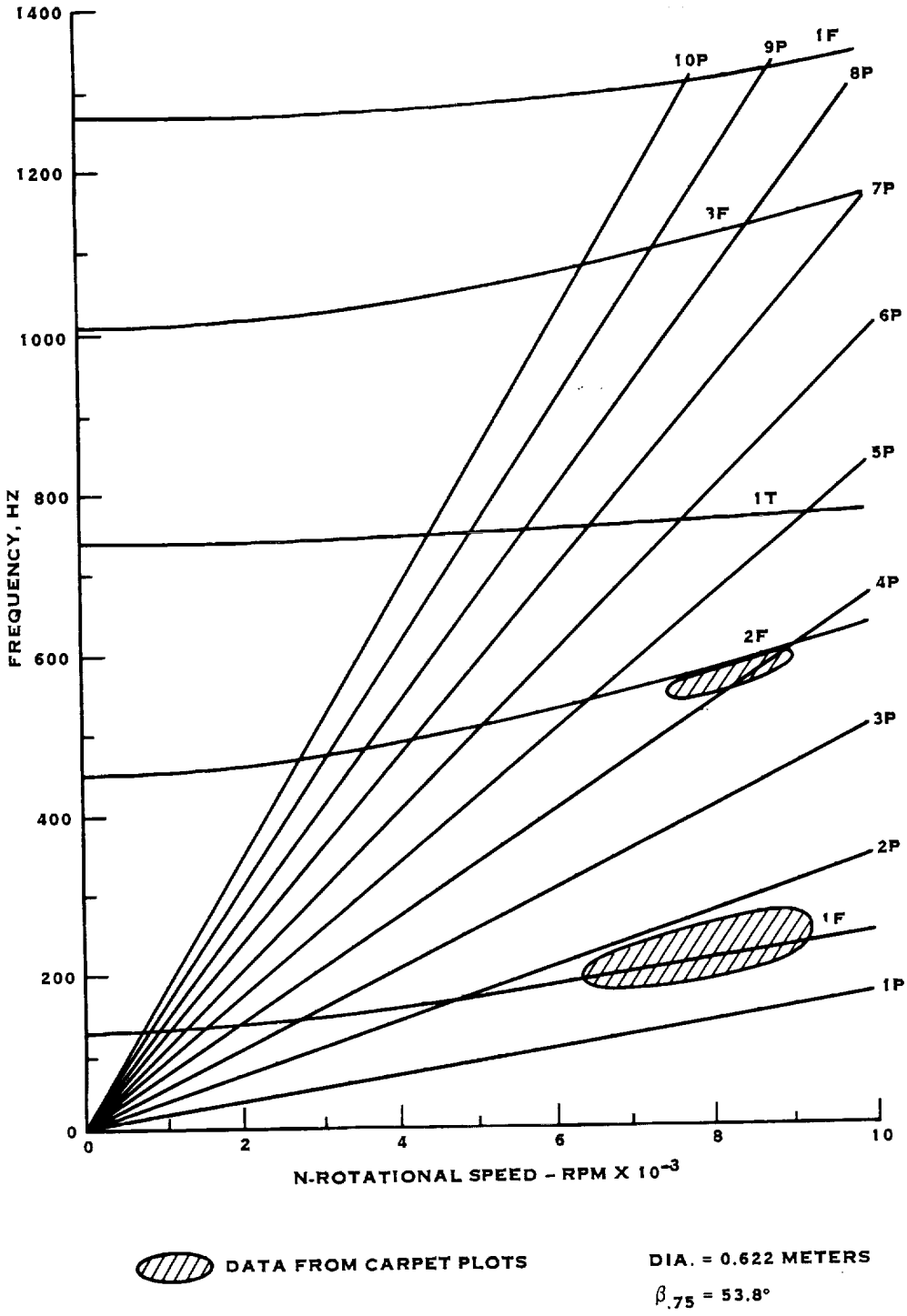

FIGURE 4-34. SR-2C MODEL PROP-FAN BLADE

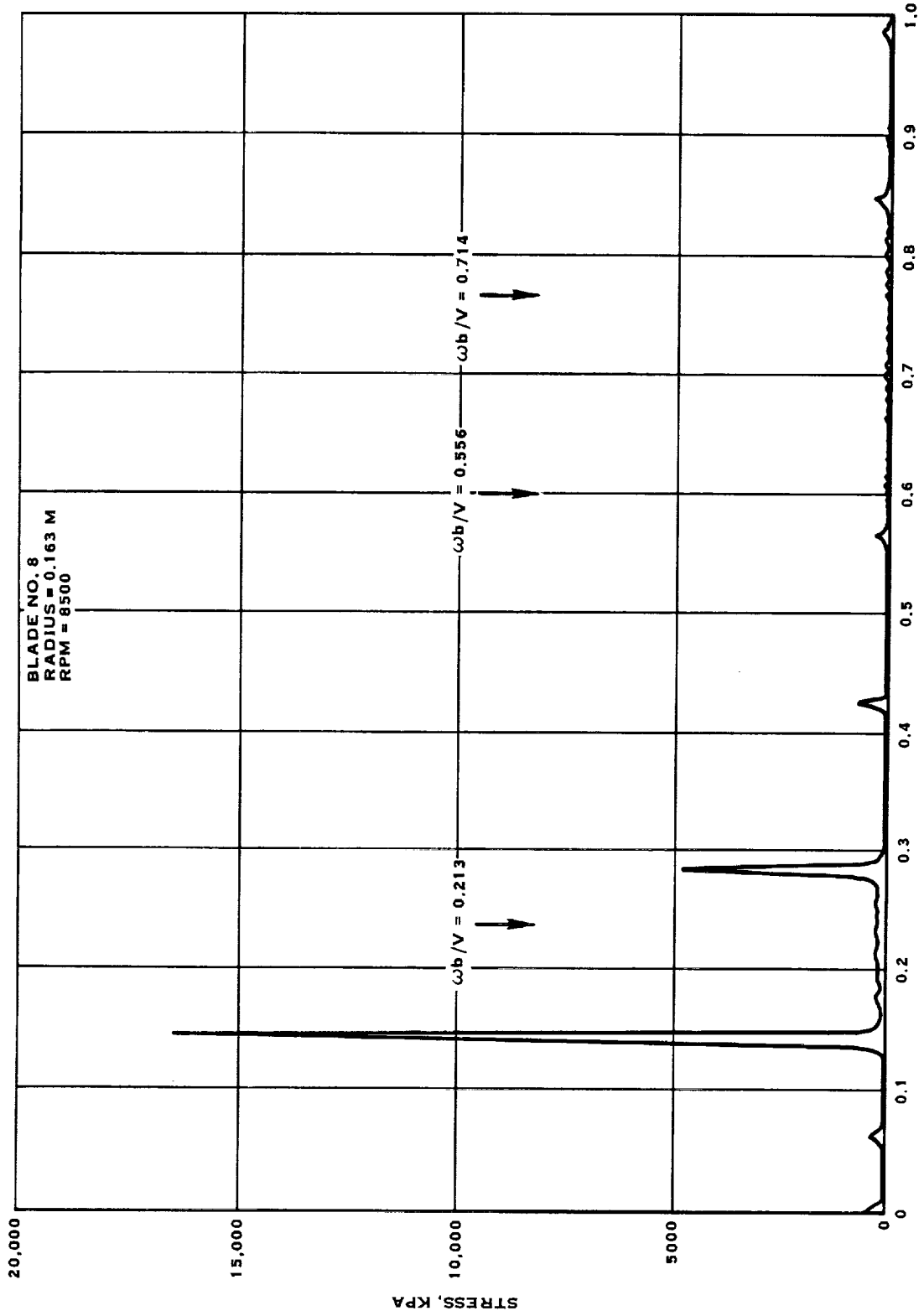

FIGURE 4-35. SPECTRAL ANALYSIS - SR-2C MODEL PROP-FAN - NASA/AMES WIND TUNNEL TEST, RUN 23, INBOARD BENDING STRESS, BLADE NO. 8

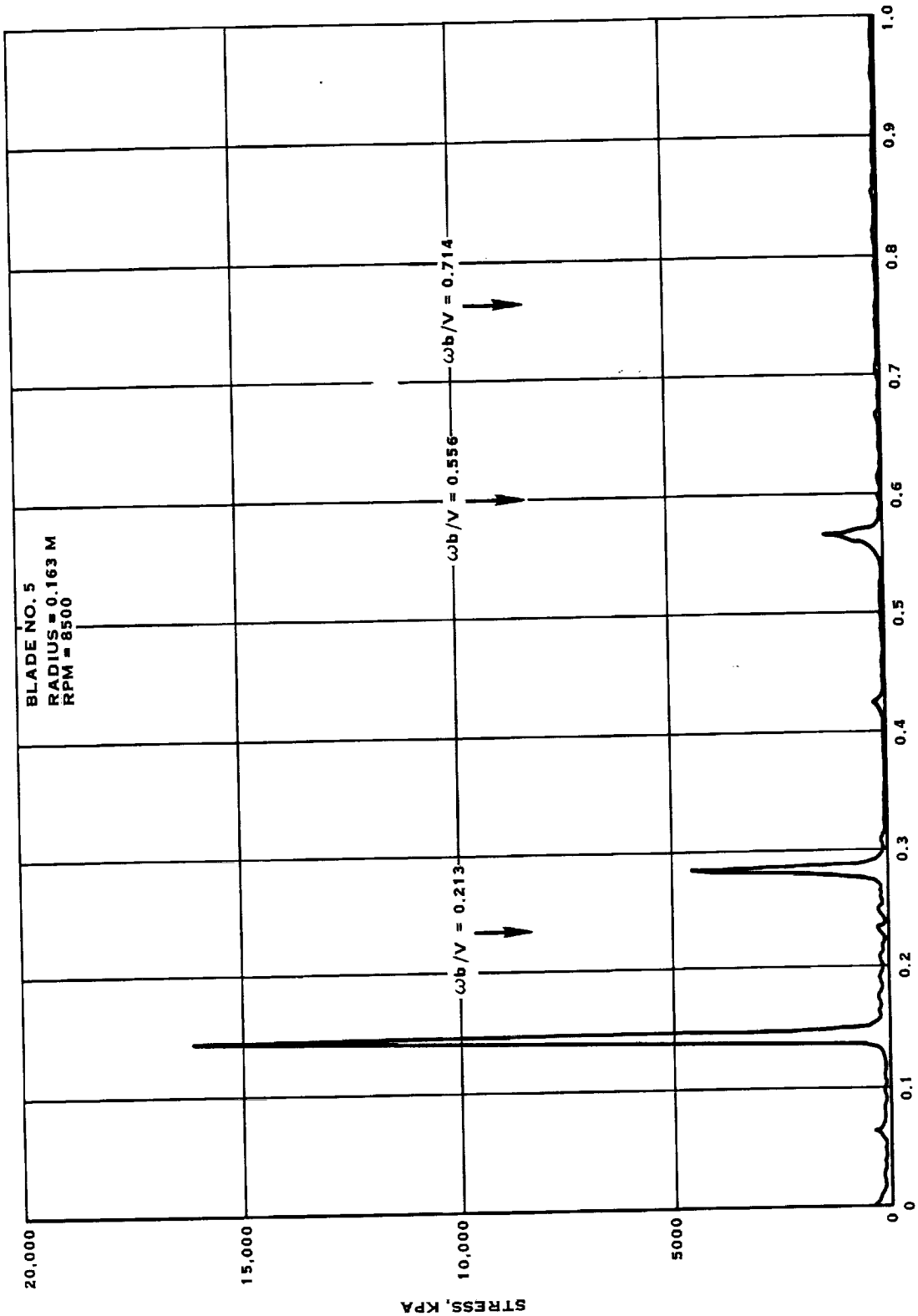

FIGURE 4-36. SPECTRAL ANALYSIS - SR-2C MODEL PROP-FAN - NASA/AMES WIND TUNNEL TEST, RUN #23, MID-BLADE BENDING STRESS, BLADE NO. 5

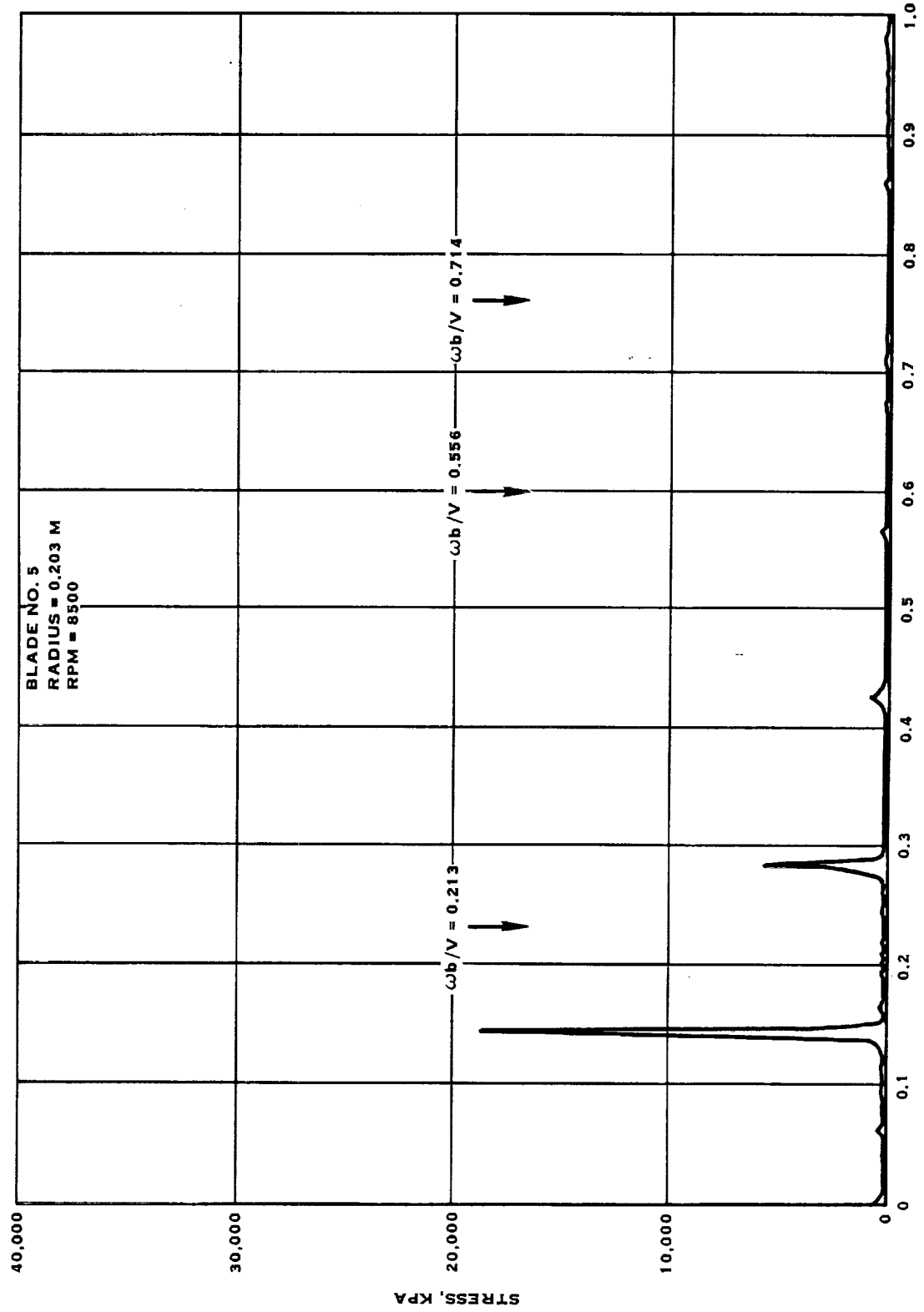

FIGURE 4-37. SPECTRAL ANALYSIS - SR-2C MODEL PROP-FAN, NASA/AMES WIND TUNNEL TEST, RUN #23, INBOARD BLADE BENDING STRESS, BLADE NO. 5

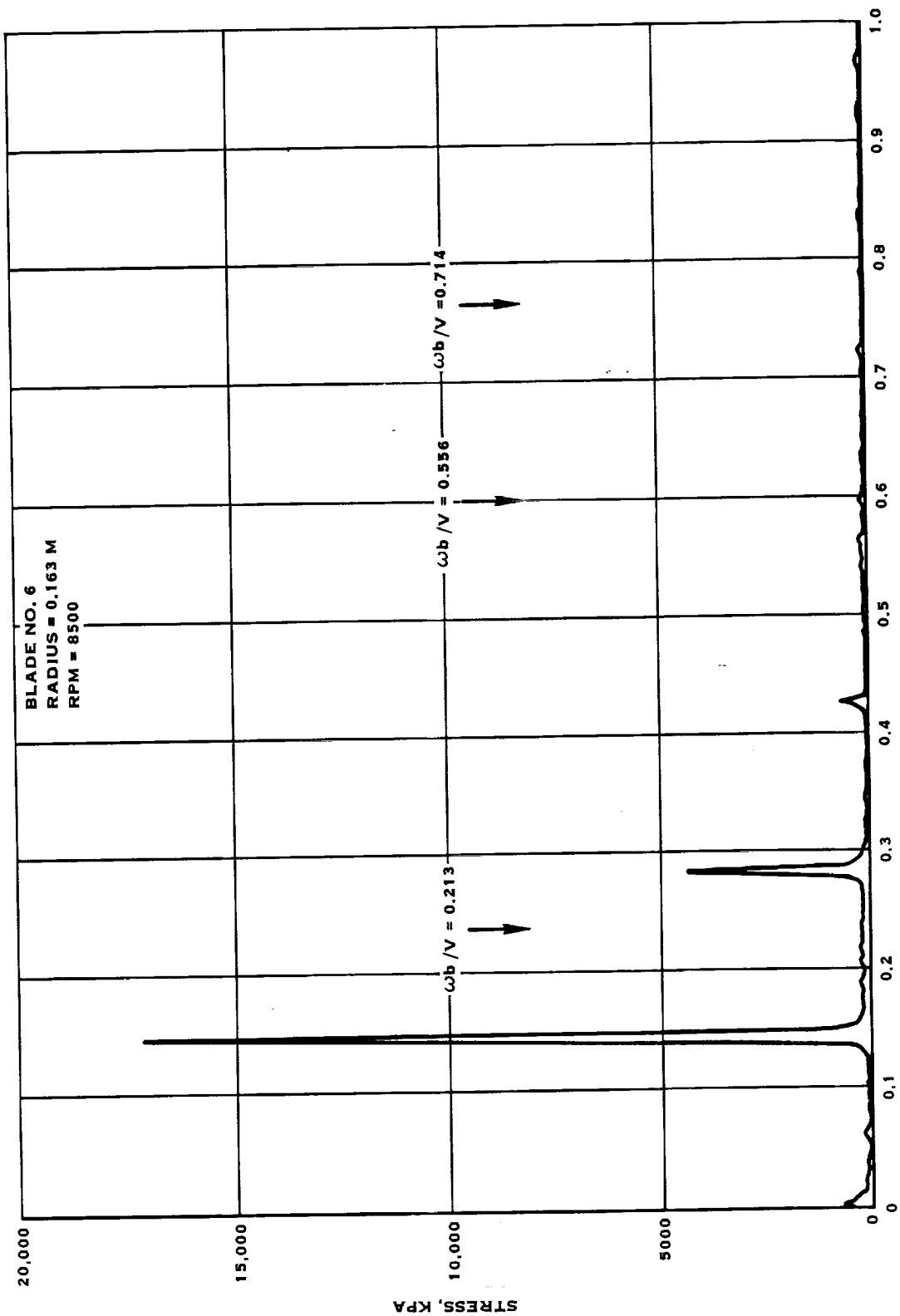

FIGURE 4-38. SPECTRAL ANALYSIS - SR-2C MODEL PROP-FAN
NASA/AMES WIND TUNNEL TEST - INBOARD BENDING STRESS, BLADE NO. 6

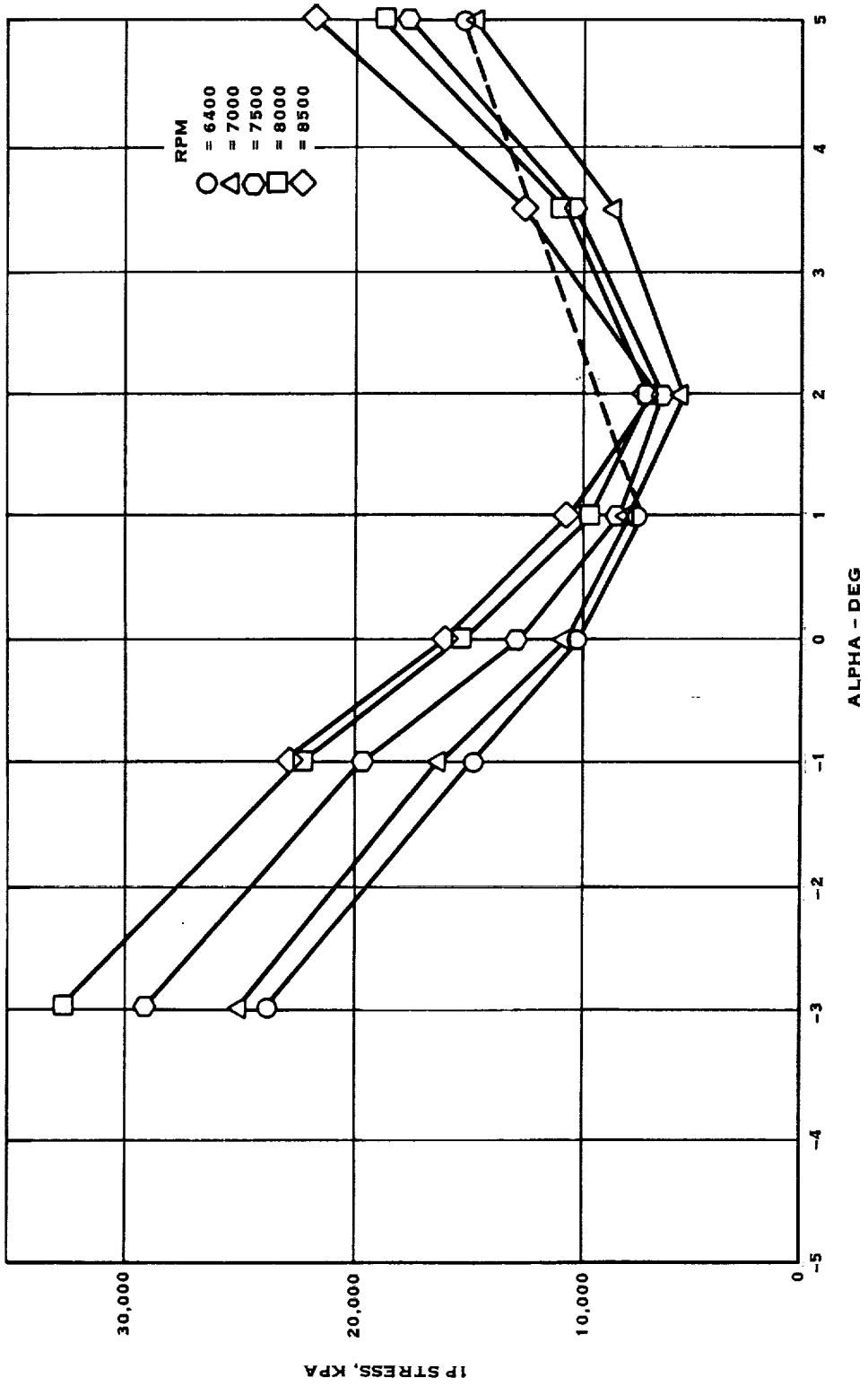

FIGURE 4-39. 1P STRESS FOR SR-2C PROP-FAN SEMI-SPAN MODEL EXCITATION TESTS NASA/AMES 14 FT TRANSONIC TUNNEL, BETA 50.69, MACH=0.6, INBOARD BENDING STRESS, BLADE NO. 5

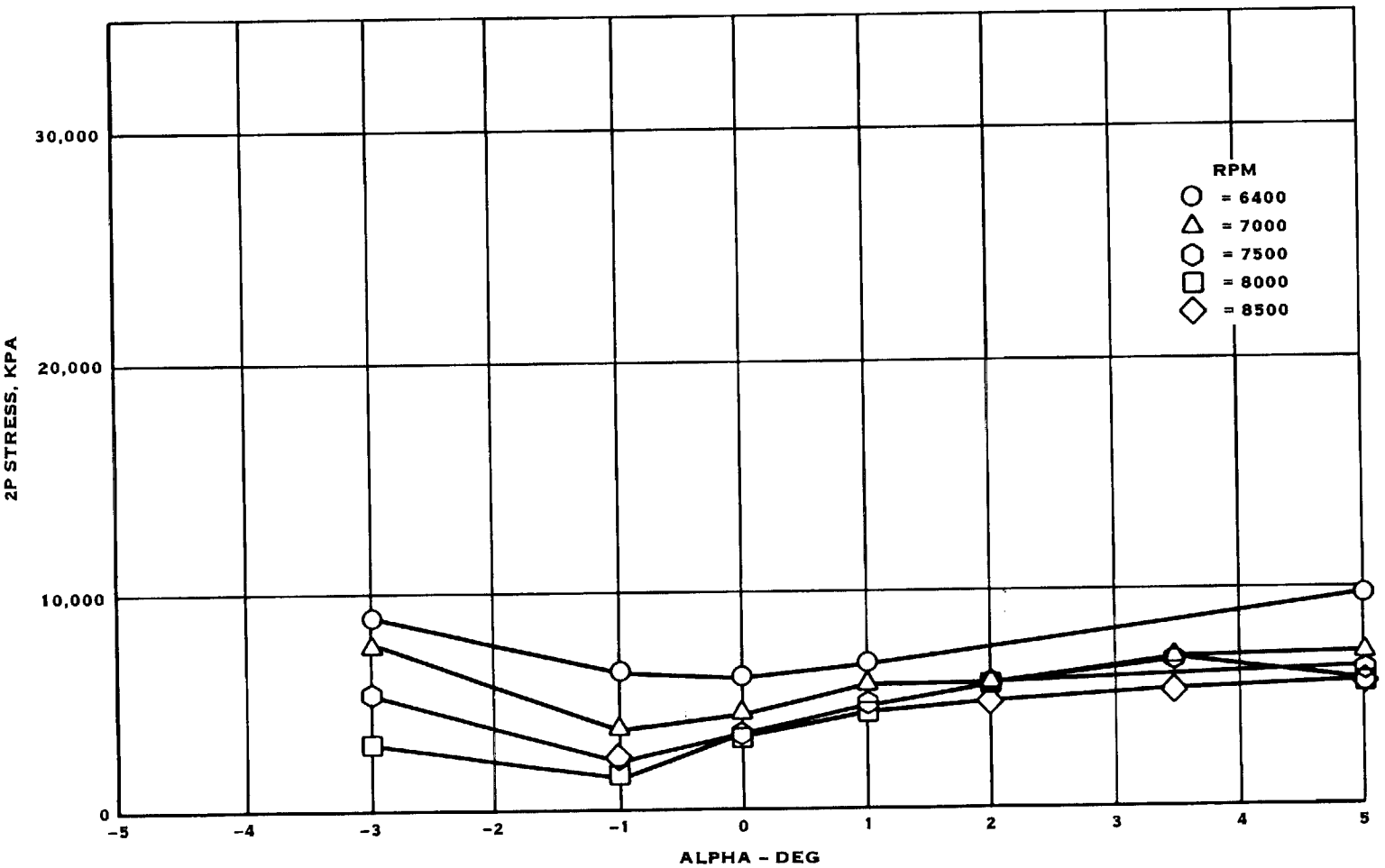

FIGURE 4-40. 2P STRESS FOR SR-2C PROP-FAN SEMI-SPAN MODEL EXCITATION TESTS NASA/AMES 14 FT TRANSONIC TUNNEL, GAGE #5/6.4, BETA = 50.69, MACH=0.6, INBOARD BENDING STRESS, BLADE NO. 5

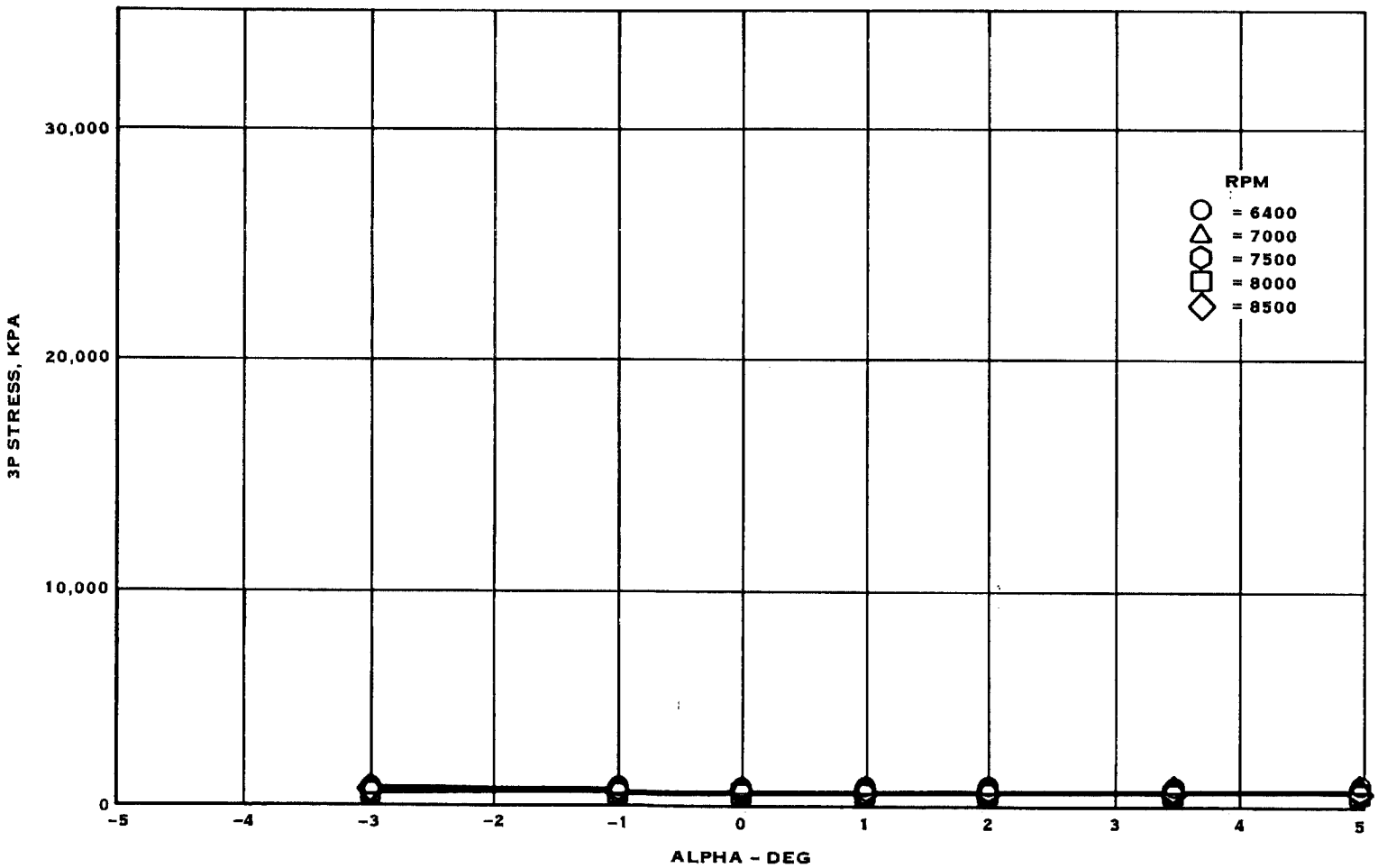

FIGURE 4-41. 3P STRESS FOR SR-2C PROP-FAN SEMI-SPAN MODEL EXCITATION TESTS NASA/AMES 14 FT TRANSONIC TUNNEL, BETA = 50.69, MACH=0.6, INBOARD BENDING STRESS, BLADE NO. 5

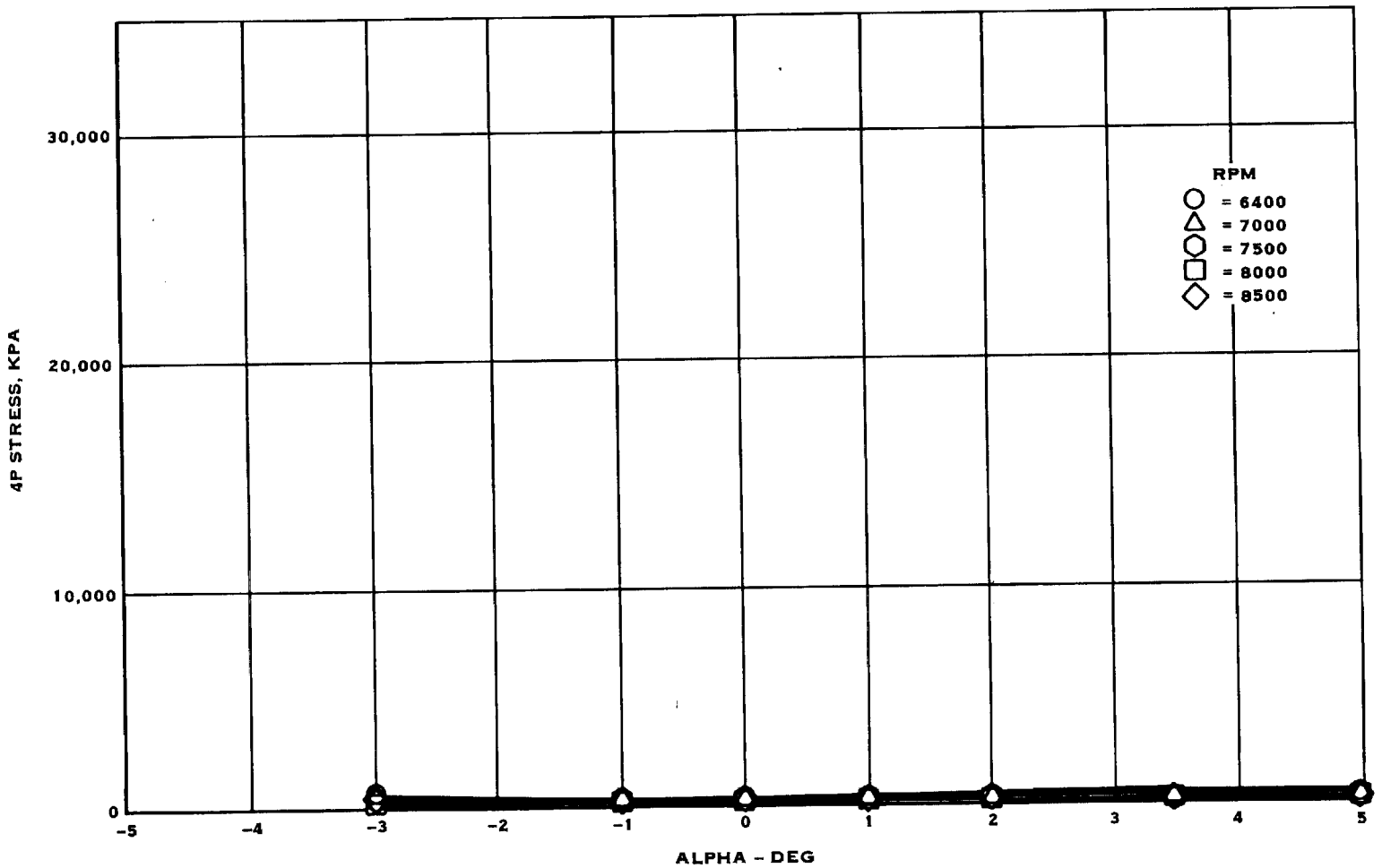

FIGURE 4-42. 4P STRESS FOR SR-2C PROP-FAN SEMI-SPAN MODEL EXCITATION TESTS NASA/AMES 14 FT TRANSONIC TUNNEL, BETA=50.69, MACH=0.6, INBOARD BENDING STRESS, BLADE NO. 5

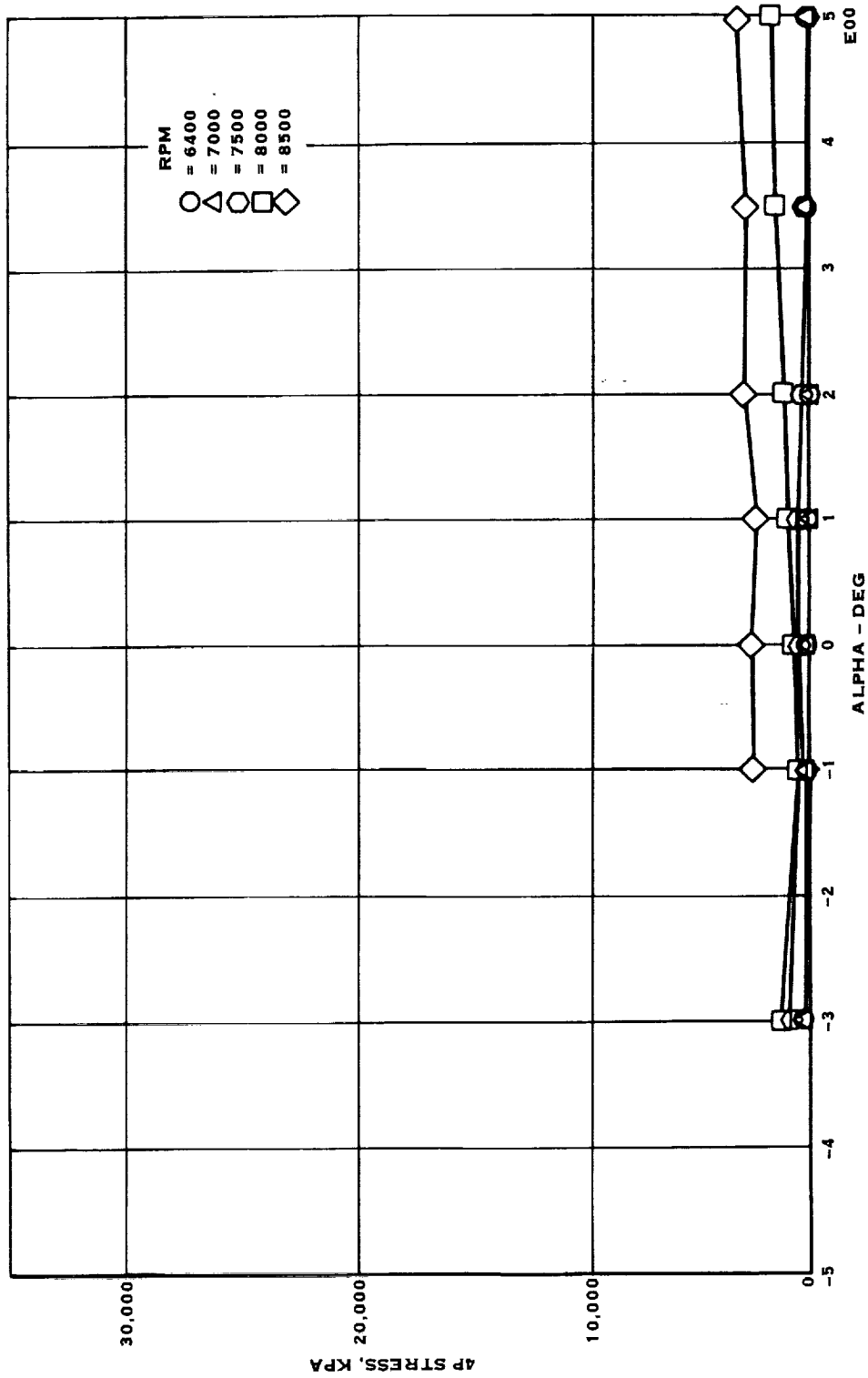

FIGURE 4-43. 4P STRESS SR-2C PROP-FAN SEMI-SPAN MODEL EXCITATION TESTS NASA/AMES 14 FT TRANSONIC TUNNEL, BETA=50.69, MACH=0.6, TIP-BENDING STRESS, BLADE NO. 8

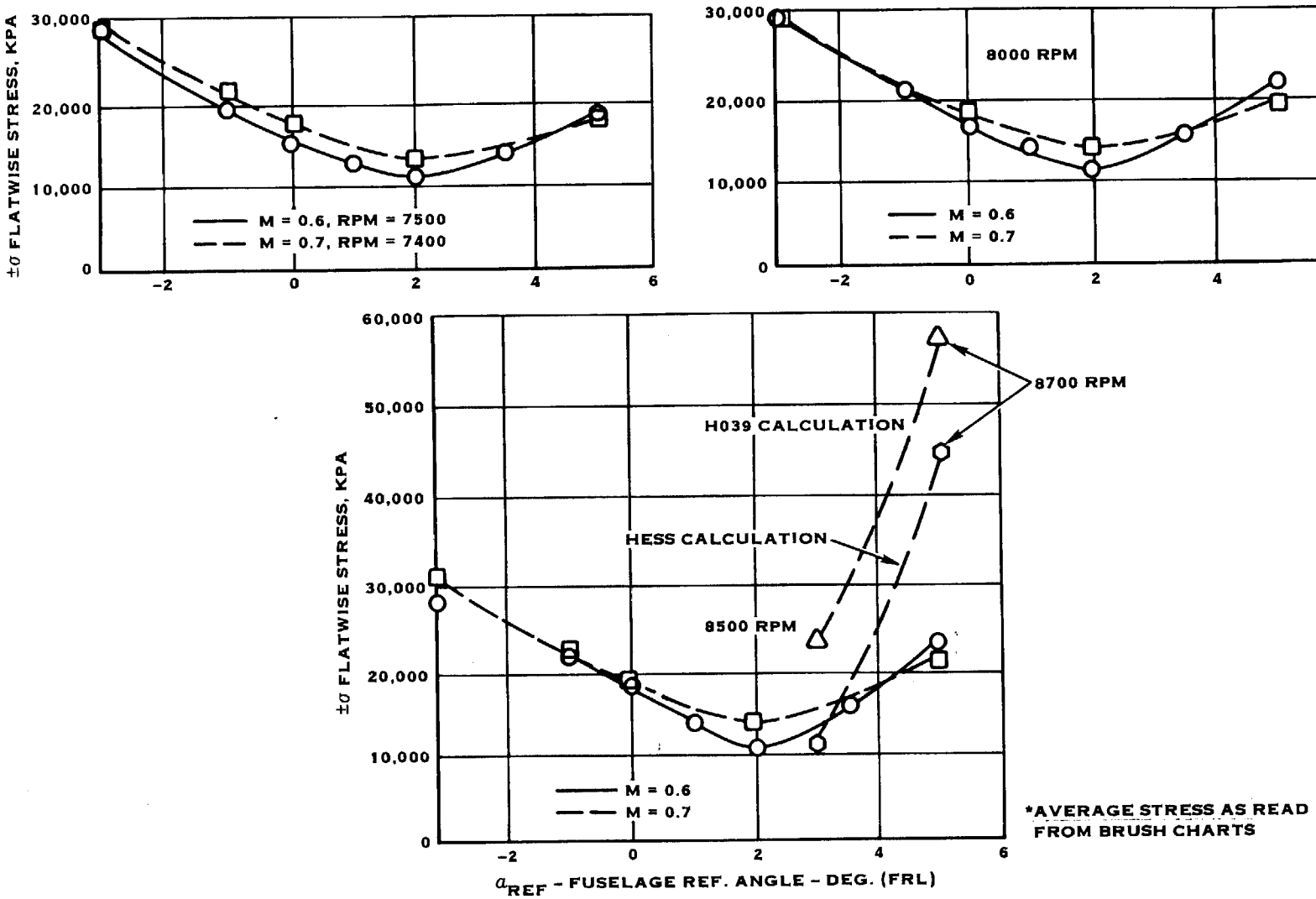

FIGURE 4-44. SR-2C PROP-FAN TOTAL STRESS* - NASA/AMES EXCITATION TESTS, SEMI-SPAN MODEL WING & NACELLE

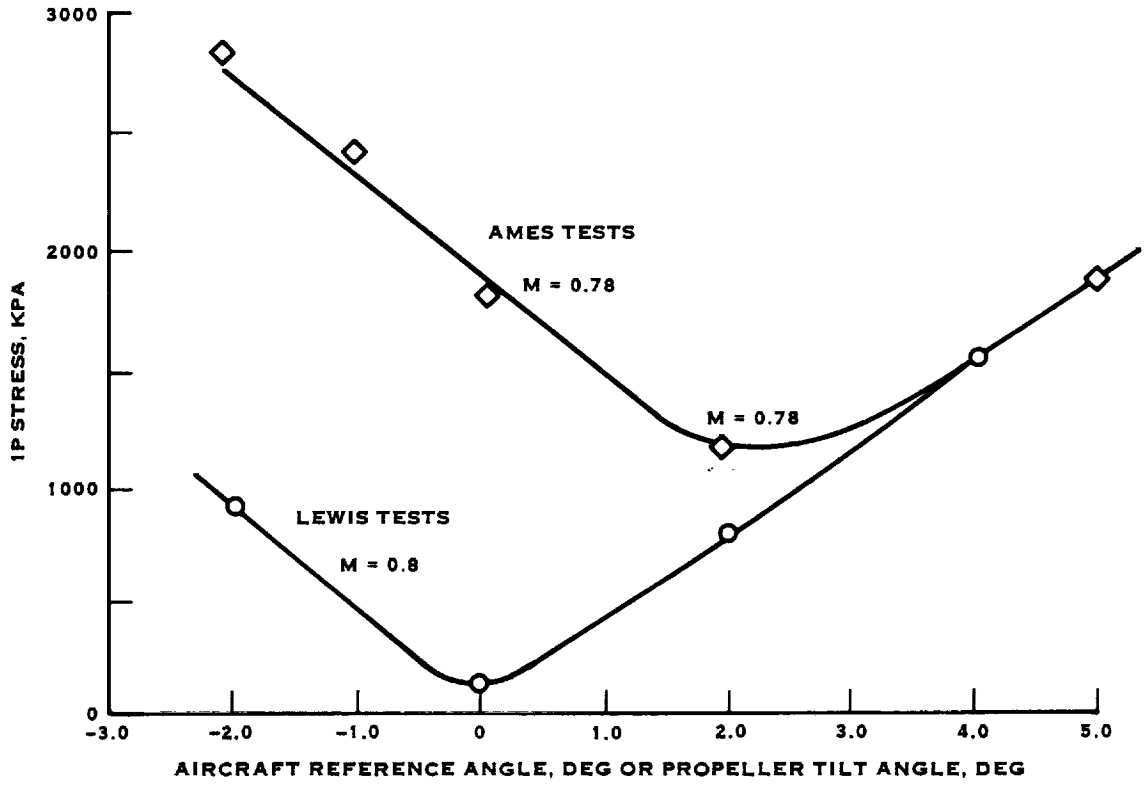

FIGURE 4-45. SR-2C MODEL PROP-FAN RESPONSE TESTS
MID BLADE BENDING STRESS BLADE NO. 5,
REF BLADE ANGLE ≈ 55.7 DEG, 8000 RPM

SECTION 5.0

DISCUSSION OF RESULTS

In the spring of 1980 and fall of 1981 the analysis and testing of the structural response and stability of the Prop-Fan models was conducted, and was subsequently followed by an organized evaluation. The work was done on three Prop-Fan models tested in the NASA/Lewis 8 x 6 wind tunnel. The model Prop-Fan designations are the SR-2C eight way, SR-3 eight way and the SR-5 ten way. Also, the SR-2C model Prop-Fan mounted on a semi-span wing, nacelle and fuselage combination was tested in the NASA/Ames 14 foot wind tunnel. Discussions of the test configuration and models can be found in Section 2. A detailed discussion of the tests analysis and results can be found in Sections 3 and 4. The following section will summarize the results of these efforts.

5-1. ANALYSIS METHODS

Many computer analyses were used to predict blade loads, stability and response of the Prop-Fan configurations at conditions determined by the tests. The initial studies require the use of a flow field analysis. Two flow field analyses were used. One was supplied by Hamilton Standard, and the other known as the Hess Code, was supplied by NASA/Ames. Extensive use was made of the Hamilton Standard analyses to determine blade loads. These analyses use blade element theory for vectoring the local air velocities. Real airfoil data are approximated by equations and/or table look-up and account for sweep, thickness, camber and compressibility effects. For an isolated propeller, the loads due to angular inflow are calculated at locations 180 degrees apart. For a propeller installed on a aircraft the loads are calculated at many azimuthal locations. The stability analyses are linear perturbation type analyses that use the load slopes calculated at the operating conditions.

The structural response and stresses were determined by several analyses that cover different categories of the calculation. Some of these categories are as follows; critical speed and modal characteristics determination, blade stability, blade stress and retention loads. Additional categories are due to the differences between the SR-2C straight blade and the SR-3 and SR-5 swept blades. Beam type solutions are sufficient and were used for the SR-2C but finite element solutions were necessary for the swept blades.

For the SR-2C, a Hamilton Standard beam type critical speed analysis provided the blade frequencies and modal properties for all calculations, while a Hamilton Standard beam type 1P response analysis was used for the isolated nacelle calculations. Because the excitation of the wing/nacelle combination is comprised of higher order loading, a Hamilton Standard n-p response analysis was used to describe the NASA/Ames wind tunnel model.

5.1 (Continued)

For the SR-3 and SR-5 model blades the critical speeds and model properties were determined by two finite element methods, a Hamilton Standard method called "BESTRAN" and "MSC NASTRAN". These analyses were also used to calculate the response and stresses on the SR-3 and SR-5 models using the loading described above.

The modal properties generated with the above NASTRAN analysis were used to provide modal masses and frequencies for the Hamilton Standard stability analyses. A Hamilton Standard computer code is used to make transformations of the modal properties obtained from NASTRAN, to the blade section co-ordinate system. This must be done because high blade angles are required at design operating conditions due to the high inflow angles encountered. If the co-ordinate system is in the blade section then small angle assumptions can be made, allowing linear solutions to be used. The equations of motion are solved by eigen-value solution methods to provide damping and response frequencies for each mode. Flutter boundaries can be established when the analysis shows zero or negative damping for various operating conditions. Detailed discussions and the results of the analyses are presented in Section 3.

5.2 TEST RESULTS

The Prop-Fan Model blade tests were accomplished during the period of spring 1980 to summer 1981. The tests were accomplished in three phases, 1) the 1P response tests, 2) the stability tests and 3) the SR-2C installed Prop-Fan tests. The first two were conducted in the NASA Lewis 8 x 6 wind tunnel and the last was conducted in the NASA/Ames 14 foot wind tunnel. Table 2-I indicates this information along with the ranges of test parameters, which are shown for each test and each blade combination.

1P Response Tests

The purpose of the 1P response isolated nacelle tests was to measure 1P stresses and to determine the variation in stress with tilt angle, reference blade angle, horsepower and Mach number and to correlate these variations with current analyses.

For the 1P response test the blade angle and the tilt-angle were fixed for each run and the Mach number and propeller rpm were varied. Usually the test points were made between windmilling and the maximum power available and/or stress limit. The results of these tests are the output of strain gages generally reported in stress units, except for the SR-2C model which was reported in strain units. This is because a proper stress based on a local material modulus was difficult to establish due to the composite construction.

5.2 (Continued)

Significant trends were observed from the results of the isolated nacelle tests. The effect of inflow or tilt angle on the 1P vibratory stress for the SR-3 and SR-5, and 1P vibratory strain for the SR-2C was very linear. The effect of equivalent airspeed on the SR-2C model vibratory strain was linear with airspeed squared, indicating that strain divided by excitation factor would be constant with airspeed. Stress per excitation factor is constant with Mach number for the other models. On the SR-2C, however, the strain seems to fall off at high Mach number and high rotational speed. This is probably due to compressibility effects. This effect is less pronounced for the SR-5 because sweep was designed to reduce compressibility effects. Other trends show that 1P vibratory stress per excitation factor increases with power, either holding blade angle constant or holding rotational speed constant.

Stability Tests

The purpose of the stability tests was to determine the blade flutter boundaries, or the degree of stability if instability was not encountered. The effects of tunnel Mach number, rotational speed and shaft power were investigated for all models. No flutter boundaries were encountered for both the SR-2C and the SR-3 within the entire test envelope. However the SR-5 model did encounter instabilities over a range of operating conditions. These instabilities were determined to be predominantly first-mode coupled bending/torsion unstalled flutter.

For the case of no instability, two methods were used to excite the blades. Blade damping and frequencies were observed from 1) random excitations from the tunnel stream and/or 2) from excitations caused by a gas jet located behind the propeller. This jet was pointing upstream such that the jet was cut by the propeller and the response would decay when the jet was stopped. The resulting transient response data were recorded and analyzed.

The first test method was used for the SR-2C and subsequent analysis using the Pratt and Whitney Aircraft 'Randomdec' technique showed that there was not enough natural turbulence in the wind tunnel to cause sufficient excitation to properly measure damping. The second test method was used for the SR-3 and SR-5 models and a moving-block analysis technique was used to determine the damping.

Generally for the SR-3 and SR-5 models, the lower modes were better damped than the higher modes in areas of good stability. The effect of Mach number and rotational speed on the modal damping for the SR-3 was small. However the modal damping for the SR-5 was reduced when the point of instability was approached.

The effect of the number of blades was investigated for the SR-3 model and it was found that the 4-way configuration generally had higher damping than the 8-way configuration. This shows the importance of cascade effects.

5.2 (Continued)

From the test data it was determined that the blade response was not a freely decaying signal, as it appeared to contain some unknown forcing functions. It was therefore concluded that additional work is required to improve this test procedure, to better determine blade damping characteristics.

SR-2C Installed Prop-Fan Tests

The purpose of the SR-2C Prop-Fan model tests on a semi-span aircraft model was to show the trends of vibratory stress resulting from realistic flow field excitation and to compare the results to the various computations that were made. The tests were conducted in the NASA/Ames 14 x 14 foot transonic wind tunnel. The tests were run at steady state conditions in which the blade reference angle and fuselage angle of attack (reference angle) were set and variations in tunnel Mach number and propeller rotational speed were made. Also, tunnel density was varied.

Before discussing the results of this test, it should be recalled from Section 2 that the propeller and nacelle have some toe-in. Therefore the variation in 1P excitation will never reach zero as the wing angle of attack goes from negative to positive. The results of these tests show that the 1P inboard blade stresses exhibit a parabolic variation with fuselage reference angle. Other results show that the 1P vibratory stresses increase with increasing rpm, however this effect is diminished at higher Mach number, probably due to compressibility effects. Otherwise Mach number has little effect on the overall 1P stress value. The 2P vibratory stresses show little variation with angle of attack and represent 20% of the high 1P stress values. The 2P stresses seem to decrease with increasing Mach number and propeller rotational speed. The 2P vibratory stress seems to increase slightly with propeller blade angle while the 1P vibratory stresses show little effects of blade angle. Comparisons of some of the data between the NASA/Ames (semi-span) test and the NASA/Lewis (isolated nacelle) tests on the SR-2C Prop-Fan blade show similar trends in stress magnitude and slopes. Differences are attributed to wing circulation and nacelle toe-in on the NASA/Ames model.

5.3 DATA EVATUATION AND COMPARISON

This Section deals with the correlation between the calculated results and the test results. The correlation for these tests are primarily involved with 1) critical speed placement, 2) 1P response stresses and/or strains (higher order for the installed Prop-Fan), and 3) blade stability. A more detailed description of these comparisons can be found in Section 4.

5.3 (Continued)

Critical Speeds

For the Prop-Fan models, the critical speeds correlation is very good. For the SR-2C model Prop-Fan the calculations were made with the Hamilton Standard beam analyses and the test points are within 3 percent for the bending modes. The correlation of blade frequencies for the SR-3 Prop-Fan blade shows the test frequencies to be within 6 percent for the first three modes. The test frequencies for the SR-5 Prop-Fan blades are within 4 percent. Figures 4-1 through 4-3 show these results.

1P Stress Versus Angle of Inflow

The 1P vibratory strain due to angular inflow was measured on the SR-2C model Prop-Fan and the results show the same trends that were observed in the calculations. The tested strain per degree of inflow increases with the square of equivalent airspeed, as do the calculations, and exhibits the same fall-off due to compressibility effects. The data show a great deal of scatter, since trends with propeller blade angle could not be determined. The results are therefore within 40 percent of the calculated values for all rotational speeds. Generally, the calculated strains are higher than the test results.

For the SR-3 Prop-Fan the relationship between 1P vibratory blade stress and inflow angle is quite linear. This eliminates the inflow angle variation if stress per EF is used instead of stress. The measured values for 1P vibratory response stress per EF, for the SR-3 Prop-Fan blades, are 60 to 77 percent higher than the predicted values. In spite of these differences, the intergage relationships between the stresses of the various gages show fair correlation between the test results and the predictions. As an example, the measured stress ratio of the mid-blade gage to the inboard gage varies between 0.96 to 0.7 for rotational speeds of 4000 rpm to 9000 rpm. At 7000 rpm the predicted intergage stress ratios are 10 to 20 percent greater than the test ratios. The difference between predicted and measured values can not be explained.

The test data for the SR-5 Prop-Fan model also show linear relationships between inflow angle and 1P vibratory stress. Stress per EF can therefore be used to eliminate the effects of inflow angle. The test data for the inboard gage show stress per EF to vary from 35 to 55 percent higher than the predicted values. For the shear gages the test results are lower than the calculations and are 36 to 64 percent of the predicted values. For the tip gage the test values are 92 to 120 percent higher than the predicted values. These differences cannot be explained. The decrepancies mentioned above show large percentages but do not necessarily reflect high stresses. One should therefore review the lack of correlation with caution.

5.3 (Continued)

Stability

The results of the SR-2C stability tests were invalidated because there was not enough excitation generated by natural wind tunnel turbulence.

Analytical results using several flutter prediction methods were obtained for the SR-3 and SR-5 Prop-Fan models. Of the four aeroelastic stability analyses applied to the model Prop-Fan blades, the F203 analysis gave the best correlation with test data. The F203 analysis shows the SR-5 instability to be a coupled bending/torsion classical flutter dominated by the first mode. For calculations that assume a mixture between the full cascade analysis and the single blade analysis, the damping ratio falls in the middle of the values measured using the Moving-Block techniques. This correlation is for the first bending mode on the SR-3 8-way model at a Mach number of 0.8 and a blade angle of 60.1 degrees. For the SR-3 4-way model test, measured damping ratios are from 0.01 to 0.07, while the predictions for an isolated blade are 0.013 for the first mode and 0.016 for the second mode, at 0.8 Mach number. Similar results are shown for 0.85 Mach number. The results from the SR-5 test show that the blade has an instability in the first mode at about 5300 rpm. The predictions, using mixed cascade effects show first mode instabilities just below 5000 rpm. This is for a Mach number of 0.85 and a blade angle of 75 degrees. With just one calculated point for the SR-3 it is difficult to make a judgement on the degree of correlation. However, the correlation for the SR-5 seems reasonable.

Further detailed study should be performed on the model Prop-Fan blades to resolve discrepancies between the predicted and measured stability. These studies should be carried out using more refined finite element analyses of the model Prop-Fan blades. Also, a study should be undertaken to refine understanding of the unsteady aerodynamics, to account for transonic conditions and the three-dimensional characteristics of the flow.

NASA/Ames Installed SR-2C Response Tests

The test points for these cases were not run exactly at the conditions used for the predictions. It is therefore difficult to make one-to-one comparisons. However, the experimental data were extrapolated to the proper conditions. It was found that the 1P predictions can be 237 percent higher than the test values and the 2P predictions can be 480 percent higher than the test values. The predicted total vibratory strain can be 2.5 times the measured values. No explanation is available for the low measured strains with respect to predictions with the model wing at Ames. This is in contrast to the better correlation between prediction and test with the isolated nacelle at Lewis.

SECTION 6.0
CONCLUSIONS

The following conclusions were reached as a result of the program summarized in this report:

1) The Hamilton Standard aerodynamic strip analyses (HS/H444 and HS/ H045) and beam dynamic response analyses (HS/H026 and HS/F094) were satisfactory to predict the vibratory stresses of long, slender, beamlike blades, such as the SR-2C.

2) Finite element representations were needed to model the wide, swept blades of the SR-3 and SR-5 configurations. The beam analysis did not adequately predict the complex coupling between the flatwise bending, edgewise bending and torsion modes.

3) Trends for 1P vibratory response (stress and/or strain) for the model rotors, as measured during the isolated nacelle tests, showed a conventional linear increase with airspeed squared (excitation factor). At high Mach number the SR-2C 1P response fell off, due to compressibility effects.

4) Correlations between 1P stress predictions and isolated nacelle measurements for the SR-2C model were reasonable. For the SR-3 and SR-5 models, 1P stress predictions using the MSC/NASTRAN code were considerably lower than measured values. Calculated 1P stresses for the SR-3 and SR-5 blades were a strong function of the assumed chordwise and spanwise distributions of aerodynamic loading, particularly in the tip region.

5) Calculations of 1P and 2P vibratory stresses for the SR-2C installed wing/fuselage tests, using both the Hamilton Standard flow field code and the Ames Hess code, were found to be several times the values measured, although the absolute stresses were not high. This may be due in part to the extrapolations necessary to match measurements with earlier predictions accomplished at different operating conditions. Higher order (3P and 4P) stresses were not significant.

6) The measured stresses for the Ames wing/fuselage test show similar magnitudes and trends with the data measured in the Lewis isolated nacelle test. Differences are due to wing upwash and nacelle toe-in effects present in the Ames test.

7) Test values for critical speeds showed good correlation to the predicted values for all the rotor models.

6.0 (Continued)

8) The SR-2C and SR-3 models did not flutter during wind tunnel testing. However, the more highly swept SR-5 model was unstable over a range of operating conditions. Flutter occurred at lower rotational speeds as the free-stream Mach number, reference blade angle, or the number of blades was increased.

9) The natural turbulence of the wind tunnel did not excite the SR-2C blades sufficiently to obtain modal damping data.

10) The excitation jet was marginally acceptable for exciting the SR-3 and SR-5 models. Measured modal damping values obtained by the moving-block analysis were more realistic than the ITD (time-domain-technique) results. Therefore superiority of the ITD method was not demonstrated. Intergage and interblade damping values showed considerable data scatter. Lower modes were better damped than higher order modes, as expected.

11) The stability predictions for the SR-3 model showed good correlation with measured damping values from jet excitation made during wind tunnel tests. However, the SR-5 model was stable to higher rpm values than predicted, showing the predictions to be conservative.

SECTION 7.0
RECOMMENDATIONS

Based on the results and conclusions of the program summarized in this program, the following recommendations are offered:

1) For wide, swept Prop-Fan blades, beam analyses are inadequate and finite element representations are required. Work should continue to improve the modeling and analysis techniques. In particular, element sizing and type studies should be performed. It is recommended that MSC/NASTRAN quadrilateral elements be employed.

2) Since the measured 1P stresses for the SR-3 and SR-5 model blades are underpredicted by the analytical methodology, correction factors based on the test correlation should be derived for application to future vibratory stress predictions for Prop-Fan blades.

3) Future studies should be undertaken to resolve the descrepancies between test and analysis. The emphasis of these studies should be placed on proper aerodynamic modeling of the nacelle effects, blade induction effects, aeroelastic effects and the effects of chordwise, spanwise and azimuthal variations in 1P load distribution on the blade.

4) Procedures should be developed for analyzing composite blade structures using MSC/NASTRAN. Pre- and post-processors will be required for the generation of the models and extraction and analysis of ply stresses from the NASTRAN results.

5) For blade stability testing, an alternate excitation technique should be evaluated for future test programs.

6) Further work should be done to improve the analytical stability model by including the effects of airloads in calculating the mode shapes and natural frequencies and the tip loss factors used in the flutter analysis.

7) In order to better evaluate the installed fuselage/wing model, more calculations of model response should be made at actual test conditions. Also, testing of a swept blade model installed on a wing should be performed.

SECTION 8.0
REFERENCES

1. C. Rohrbach and F.B. Metzger, "The Prop-Fan - A New Look in Propulsors",. AIAA Paper 75-1208 AIAA/SAE 11th Propulsion Conference, Anaheim, California, September 29, 1975.

2. D. Black, R.W. Menthe and H.S. Wainauski, "Design and Performance Testing of an Advanced 30° Swept, Eight Bladed Propeller at Mach Numbers from 0.2 to 0.85", NASA Lewis Contract NAS3-20219, NASA CR-3047, September 1978.

3. Jeracki, R.J.; Mikkelson, D.C.; and Blaha, B.J., "Wind Tunnel Performance of Four Energy Efficient Propellers Designed for Mach 0.8 Cruise", NASA TM 79124 and SAE Paper 790573, April, 1979.

4. Metzger, F.B.; and Rohrbach, C., "Aero-Acoustic Design of the Prop-Fan", AIAA Paper 79-0610, March 1979.

5. Rohrbach, C.; Metzger, F.B.; Black, D.M. and Ladden, R.M., "Evaluation of Wind Tunnel Performance Testing of An Advanced 45° Swept Eight-Bladed Propeller At Mach Numbers From 0.45 to 0.85", NASA Lewis Contract NAS3-20769, NASA CR-3505, March 1982.

6. Black, D.M.; Ladden, R.M.; Leishman, D.; Metzger, F.B. and Rohrbach, C., "Aerodynamic And Acoustic Design Report: 10 Bladed Highly Swept Prop-Fan For Cruise At 0.80 Mach Number", NASA CR To Be Published, Submitted April, 1983.

7. R.J. Swallow and R.A. Aiello "NASA Lewis 8-by 6- foot Supersonic Wind Tunnel", NASA Lewis Research Center, NASA TMX-71542, May 1974.

8. Anon., "Ames Research Facilities Summary - 1974", Brochure Available From Technical Information Division, NASA/AMES Research Center.

9. Seely, M.B., Smith, J.O., "Advanced Mechanics of Materials", copyright 1952, John Wiley & Sons, New York.

10. Bielawa, R.L., "Aeroelastic Analysis for Helicopter Rotor Blades with Time-Variable, Nonlinear Structural Twist and Multiple Structural Redundancy," NASA CR-2638, October 1976.

11. Turnberg, J.E., "Classical Flutter Stability of Swept Propellers," Proceedings of the 24th AIAA/ASME/ASCE/AHS Structures, Structural Dynamics and Materials Conference, May, 1983.

REFERENCES (Continued)

12. Barmby, J.G., Cunningham, H.J., and Garrick, I.E., "Study of Effects of Sweep on the Flutter of Cantilever Wings," NACA TN 2121, June, 1950.

13. Jordan, P.F., "Aerodynamic Flutter Coefficients for Subsonic, Sonic, and Supersonic Flow (Linear-Two-Dimensional Theory). Rep. No. Structures 141, British R.A.E., ARC. R&M 2932-1953, April 1953.

14. Smith, S.N., "Discrete Frequency Sound Generation in Axial Flow Turbomachines", British A.R.C. reports and memoranda 3709, 1971.

15. Mehmed, O., Kaza, K.R.V., Lubomski, J.F., and Kielb, R.E., "Bending-Torsion Flutter of a Highly Swept Advanced Turboprop," NASA Technical Memorandum 82975, 1982.

16. Cunningham, H.J., "Analysis of Pure-Bending Flutter of a Cantilever Swept Wing and Its Relation to Bending-Torsion Flutter," NASA TN 2461, September, 1951.

17. Bisplinghoff, R.L., Ashley, H., and Halfman, R.L., "Aeroelasticity," Addison-Wesley Publishing Company, Cambridge, Mass., 1955.

18. Hammond, Charles E. and Dogget, Robert V., Jr., "Determination of Subscritical Damping by Moving-Block/Randomdec Applications," NASA Symposium on Flutter Testing Techniques, NASA SP-415, PP 59-76, October 1975.

19. Kuczynski, William A., "Inflight Rotor Stability Monitor," NASA Symposium on Flutter testing techniques, NASA SP-415, PP 457-472, October 1975.

20. Bousman, W. G. and Winkler, D. J., "Application of the Moving-Block Analysis", AIAA, 81-0653, 1981.

21. Ibrahim, S. R. and Mikulcik E. C., "A Method for The Direct Identification Of Vibration Parameters From The Free Response," Shock and Vibration Bulletin, No. 47, PP 183-198, September, 1977.

22. UTRC Memorandum from R. A. Arnoldi to A. V. Srinivasan, "ITD Analysis of SR-5 Prop-Fan Data (Rdgs 8254, 8252, 8261, 8271)", dated March 16, 1982.